KU-13-7

Skewed Steel Bridges, Part II: Cross-Frame and Connection Design to Ensure Brace Effectiveness

By

James Zhou

Caroline Bennett

Adolfo Matamoros

Jian Li

A Report on Research Sponsored by
The Kansas Department of Transportation

Structural Engineering and Engineering Materials
SM Report No. 118
March 2017

THE UNIVERSITY OF KANSAS CENTER FOR RESEARCH, INC.

2385 Irving Hill Road – Campus West, Lawrence, Kansas 66045

Executive Summary

Skewed bridges in Kansas are often designed such that the cross-frames are carried parallel to the skew angle up to 40°, while many other states place cross-frames perpendicular to the girder for skew angles greater than 20°. Skewed-parallel cross-frames are longer and require different connections than cross-frames oriented perpendicular to the girder. As cross-frames lengthen, they become less stiff and less effective at distributing forces between girders if the same connecting elements are used. For the cross-frame / diaphragm elements to be able to brace the bridge girders, the brace elements must possess both sufficient strength and stiffness to restrain the girder from instability. While strength can be addressed by increasing the cross-sectional properties of the brace elements, providing sufficient stiffness is a more significant challenge. Stiffness of the brace system is dependent on both the brace elements and the type of connection made (Yura et al. 1992; Yura 2001). Therefore it is important to determine whether the cross-frames and their corresponding connecting elements placed in a parallel-to-skew configuration are sufficiently designed to resist lateral torsional buckling demands using current KDOT practices.

The authors have performed a study to investigate the effect of cross-frame orientation, skew angle, and cross-frame connection upon bridge system behavior and cross-frame stresses. In a suite of detailed 3D, solid finite element analyses models of skewed bridge systems, cross-frame layout, connection thickness and type, and skew angle were varied. Skewed bridge systems with cross-frames placed parallel to the skew angle as well as systems with cross-frames arranged in a staggered configuration were considered. Varying bent plate connection thicknesses and a half-pipe connection were also analyzed. Cross-frame spacing of 4.6 m [15 ft] and 9.14 [30 ft] were examined; severe cross-frame spacing of 13.7 m [45 ft] was also considered to examine behavior at very long unbraced lengths. The models include geometric nonlinearities to assess the lateral deflection and lateral flange bending stresses in different bridge systems. Material nonlinearities were found to produce insignificant differences in the results and were not included in the full parametric analysis.

The findings of this study showed that skew angle, skew configuration, and connection type all influenced the strength and stiffness of system. The skewed-staggered configuration produced higher lateral deflections in the girders compared to the skewed-parallel configuration.

With a couple of exceptions, the skewed-staggered configuration also produced higher cross-frame stresses compared to the skewed-parallel configuration. Larger skew angles resulted in lower lateral deflections. As the skew angles increased, cross-frame compression stresses generally remained the same or increased while maximum cross-frame tension stresses generally decreased. Thicker bent plates produced higher lateral displacements, with the 12.7 mm [1/2 in.] and 25.4 mm [1.0 in.] thick bent plates producing similar lateral displacement values. For skewed configurations, cross-frame stress generally increased with thicker bent plates, with 12.7 mm [1/2 in.] and 25.4 mm [1.0 in.] thick bent plates producing similar cross-frame tension stresses. For the non-skewed configuration, cross-frame stresses decreased with thicker bent plates. The half-pipe connection was shown to correspond with smaller magnitudes of lateral deflections than bent plate connections.

Finally, the data showed that cross-frame placed parallel to skew up to an angle of 40° performed similar or better than cross-frames oriented perpendicular to skew for every given skew angle and connection type.

Acknowledgements

The authors of this report would like to gratefully acknowledge the Kansas DOT, for their support of the work performed under this project, and for knowledgeable guidance and input provided by Mr. John Jones throughout the project activities.

Table of Contents

List of Figures

List of Tables

1. Introduction and Background

The American Association of State Highway and Transportation Officials (AASHTO) provisions for lateral flange bending stresses are based on the assumption that cross-frames are oriented perpendicular to the girder line whenever the skew angle is greater than 20°. Current Kansas Department of Transportation (KDOT) design practice is to align cross-frames parallel to the skew angle for bridges with skew angles up to 40°. This approach avoids problems associated with fit-up during erection and deck placement, and limits the potential for distortion-induced fatigue. However, there is a potentially significant discrepancy between assumptions implicit in the AASHTO-LRFD Bridge Design Specifications (AASHTO 2010) and bridges that are designed to be skewed between 20 and 40° when cross-frames are placed parallel to the skew.

AASHTO (2010) defines a cross-frame as a transverse truss framework connecting adjacent longitudinal flexural components. In non-skewed (right) bridges under dead loads, only tensile forces develop in the intermediate cross-frame chords and only compressive forces develop in the cross-frame diagonals. However, in skewed bridges, most members of the intermediate cross-frames develop both compressive and tensile forces, depending on the loading condition. Skewed bearing lines subject the bridge to torsion by developing transverse load paths between the girders through the cross-frames. Furthermore, girder vertical displacements, major-axis bending stresses, and lateral flange bending stresses can be significantly influenced by large skew effects if the transverse load transfer is large (Ozgur 2011). On the other hand, it has been suggested that the effects of skew on forces induced in the cross-frame members may be neglected for skew angles 20° or less (Bishara and Elmir 1990).

Intermediate cross-frames in multi-beam steel bridges are used predominantly for lateral-load resistance, live load distribution, and reducing the unbraced length of the girder's compression flange, providing support against lateral-torsional buckling. Cross-frames also provide support against lateral bending and torsional buckling, particularly in skewed and curved bridges. In traditional designs for skewed and curved girders, gravity loads are assumed to be resisted by the girders and transverse loads are presumed to be resisted by the intermediate cross-frames. In actuality, the whole bridge acts as a system, with gravity loads producing stresses in the cross-

frames as well as the girders, and girders also resisting lateral bending loads transmitted through the cross-frames.

Stability of the overall bridge system depends on cross-frames and diaphragms placed at discrete locations along the bridge to resist buckling loads. For these cross-frame and diaphragm elements to effectively brace the bridge girders, both sufficient strength and stiffness are required to restrain the girder from instability. These dual criteria for bracing systems were first presented for column-buckling behavior (Winter 1958). While the buckling behavior of beams is more complicated, dual bracing criteria (strength and stiffness) still apply to beam bracing systems.

When the cross-frame/diaphragm elements are placed at any angle other than 90° against the girder line, their efficiency in transferring lateral loads is reduced due to a smaller lateral force component that is developed in the brace. Wang and Helwig (2008) note that although cross-frames placed parallel to skew can be effective at skew angles greater than 20°, the effects of connection flexibility and lowered brace stiffness due to longer braces becomes an issue that must be considered. This can be easily addressed from a strength perspective by increasing the cross-sectional properties of the brace elements such that the cross-frame/diaphragm has sufficient strength in the skewed position to transfer lateral forces from one girder to another. However, increasing the cross-frame member section properties results in an increase in their internal forces and vice versa (Bishara and Elmir 1990). The greater the skew angle, the larger the maximum forces induced in the cross-frame members (Bishara and Elmir 1990). While greater cross-frame forces would suggest greater bridge transverse stiffness and lower girder lateral deflection, research have found that moments, rotations, and deflections increased with an increase in skew angle (Gupta and Kumar 1983).

Previous research has also shown that the larger the bridge skew, the larger the lateral load transfer becomes, influencing bottom flange lateral bending stress (Ozgur 2011). In skewed bridges, torsional moments created in the girders by the lateral deflection of their bottom flanges, while low in magnitude, were higher than in right bridges (Bishara and Elmir 1990). McConnell et al. (2014) found that bridge skew and cross-frame placement significantly influenced bottom flange lateral bending stress and indicated that placing cross-frames in the staggered configuration reduced a bridge's transverse stiffness. In the staggered configuration, cross-frame forces cannot

be directly balanced by a cross-frame on the opposite side of the girder section. This leads to a decrease in cross-frame forces, but an increase in flange lateral bending stresses and girder lateral deflection (McConnell et. al 2014).

Ensuring that cross-frame and brace elements have sufficient stiffness can be a more difficult task than ensuring sufficient strength. If the stiffness of the cross-frames approaches or exceeds that necessitated to restrain the girders, they can provide "nuisance stiffness" that increase stresses in the bottom flange that are not typically accounted for in design (Ozgur 2011). Increases in undesirable stiffness of the girders due to the location and stiffness of cross-frames/diaphragms often occur near skewed supports as well (Krupicka and Poellot 1993). Simply increasing the cross-sectional properties of the cross-frame members can increase both the unwanted stiffness of the cross-frames and induce greater internal forces in its members. These forces can be significantly greater than girder stresses in highly-skewed bridges (McConnell et al. 2013).

As a result, cross-frames are required by AASHTO to be oriented perpendicular to the girder line for skew angles greater than 20°, due to lower cross-frame forces and lower demand-to-capacity ratios for cross-frame stresses compared to cross-frames oriented parallel to the girder line. While this decreased stiffness would lead to greater lateral bending stresses in girders with cross-frames in the staggered configuration, studies showed that these lateral bending stresses were of low magnitudes (McConnell and Radovic 2014). Therefore, small increases in girder lateral stresses is seen as an efficient tradeoff for reduced cross-frame stresses afforded by placing cross-frames perpendicular to the girder. This is especially significant since cross-frames stresses are generally closer in magnitude to their limiting stresses than the girder stresses are to their yielding stresses (McConnell and Radovic 2014).

By orienting cross-frames perpendicular to the girder line, cross-frame forces are reduced at the expense of increased lateral bending stresses in flanges. However, the vertical displacements at the opposite ends of a given brace can differ substantially in a skewed-staggered bracing layout. This can result in large live load induced forces and distortion induced fatigue, with stiffer braces attracting larger forces (Hassel et al. 2012). While the influence of skew had little effect on the strength and stiffness requirements of the bracing oriented perpendicular to the girder lines, when bracing is oriented parallel to the skew angle, skew angle has a significant impact on the stiffness

and strength requirements of the bracing (Wang and Helwig 2008). Brace elements should be designed for the basic stability requirements, considering the effects of cross-frame layout, stiffness, and strength requirements.

Stiffness of the brace system is dependent on both the brace elements and the type of connection made (Yura et al. 1992; Yura 2001). Moreover, effectiveness of the cross-frame/diaphragm is also dependent upon the stiffness of the girder web. Even if skewed brace elements have sufficient strength and stiffness to transfer lateral flange bending stresses, the connecting elements tying the brace elements to the girder may act as a "fuse" in the system if the connecting elements possess insufficient stiffness. Based on previous studies that the researchers have performed (Hassel et al. 2012), this can be the case when bent-plate connection types are utilized in a skewed bridge system.

The objective of this study was to provide guidance concerning the design of cross-frame/diaphragm elements oriented parallel to the skew angle as well as the connecting elements. Stability of the bridge girders is especially of concern during the construction stages, before the concrete deck is acting compositely with the steel girders, and in a non-composite bridge. Additionally, stability of bridge girders must be accounted for in design of girders in negative bending regions, even after composite action has been achieved between the girder and deck. If cross-frames/diaphragms are carried parallel to the skew angle for skews up to 40° in a non-composite bridge or in a negative bending moment region of a composite bridge, those brace elements must be carefully designed such that they have sufficient strength and stiffness to brace the girders against lateral torsional buckling. Detailed three-dimensional solid finite element models were used to investigate these parameters. The suite of models included the following parameter variations:

- skew angle (0°, 20°, and 40°);
- cross-frame spacing (4.6 m [15 ft], 9.1 m [30 ft], and 13.7 m [45 ft]);
- cross-frame orientation (skewed-staggered and skewed-parallel); and
- and cross-frame connection type (9.5 mm [3/8 in.] thick bent plate connection, 12.7 mm [1/2 in.] thick bent plate connection, 25.4 mm [1 in.] thick bent plate connection, and a half-pipe connection detail)

2. Bridge Geometry

The bridge geometry used within this study was adapted from American Iron and Steel Institute (AISI) Design Example 2 (AISI 1997). This geometry can be considered reasonably typical for a multi-girder highway overpass and its design is well-understood and widely available. The bridge consists two 27.4 m [90 ft] spans, composed of four continuous girders spaced at 3.1 m [10 ft] as presented in Figure 1. The girders were studied here in the non-composite condition, representative of bridge characteristics during construction. The girders were topped with a 203 mm [8.0 in.] thick wet concrete deck with a 1.1 m [3.5 ft] roadway overhang and a 0.7 m [2.3 ft] construction walkway. The total deck width was 12.7 m [41.7 ft]. Both the roadway overhang and construction walkway were considered to be supported by 1.8 m [70 in.] C-49-D overhang brackets, shown in Figure 2, spaced 1.0 m [40 in.] on center. Separate built-up cross-sections were used in regions of positive and negative bending, as shown in Figure 1(a) and 1(b). Each girder was supported by a pin at the central pier and roller supports at both ends.

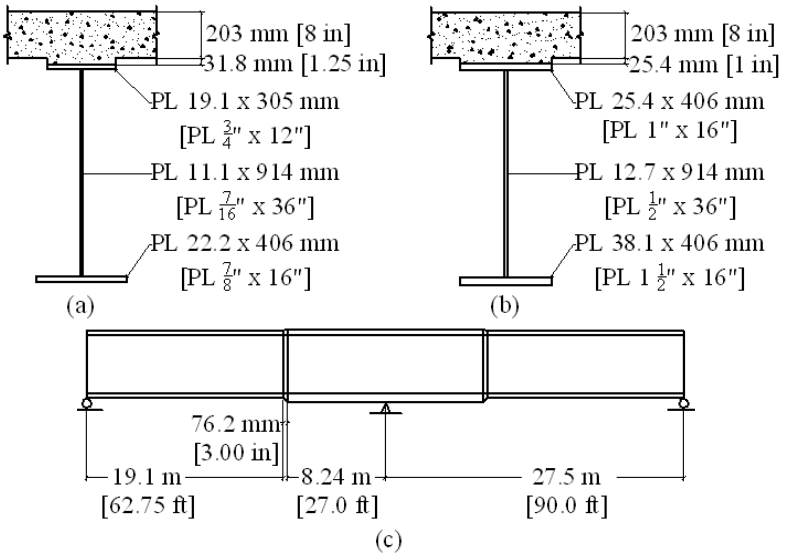

Figure 1 (a) Positive girder cross-section; (b) Negative girder cross-section; (c) Location of positive and negative cross-sections.

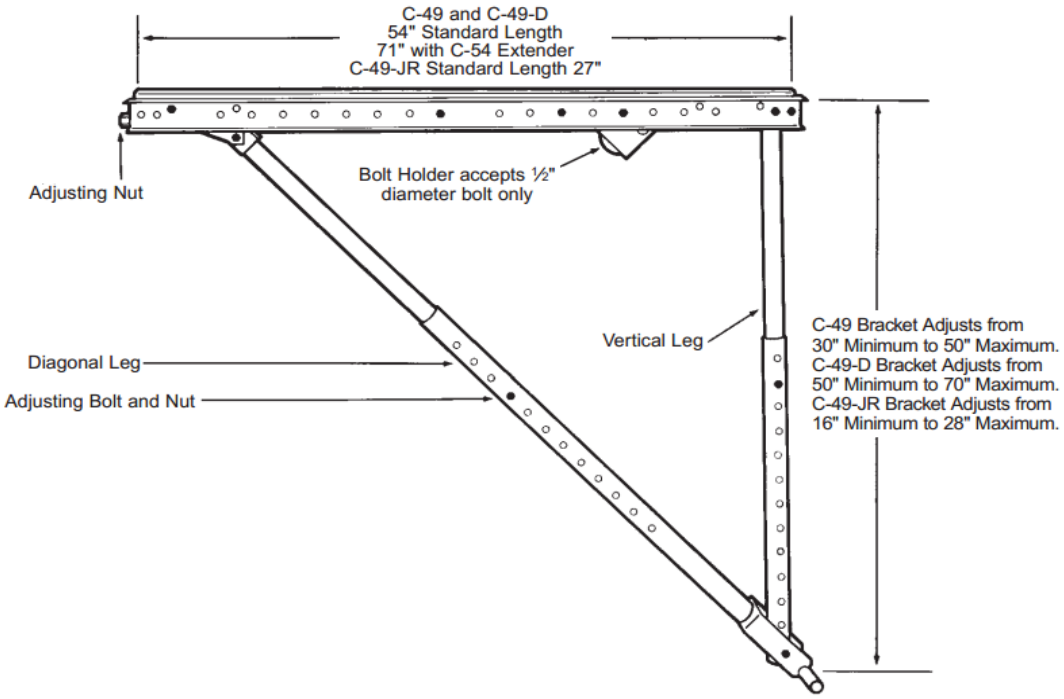

Figure 2 C-49 Overhang Bracket

Bridges with skewed supports are designed as such to accommodate highway alignment. Bracing may be placed parallel to the skew angle, or perpendicular to the girder line, usually in a staggered configuration. These configurations, shown in Figure 3 will be referred to as skewed-parallel and skewed-staggered, respectively.

AASHTO requires that bracing be placed perpendicular to the girder line whenever the skew angle is greater than 20°. However, KDOT design provisions allow the use of skewed-parallel configuration for angles up to 40° to reduce potential differential deflection and associated distortion-induced fatigue (KDOT 2010). For the analyses performed in this study, results for the skewed-parallel and skewed-staggered configurations with 0°, 20°, and 40° skews were considered. Cross-frame spacing of 4.6 m [15 ft], 9.1 m [30 ft], and 13.7 m [45 ft] were modeled to study effects on lateral flange bending and system stability, although usually brace spacing is kept to less than 7.62 m [25 ft].

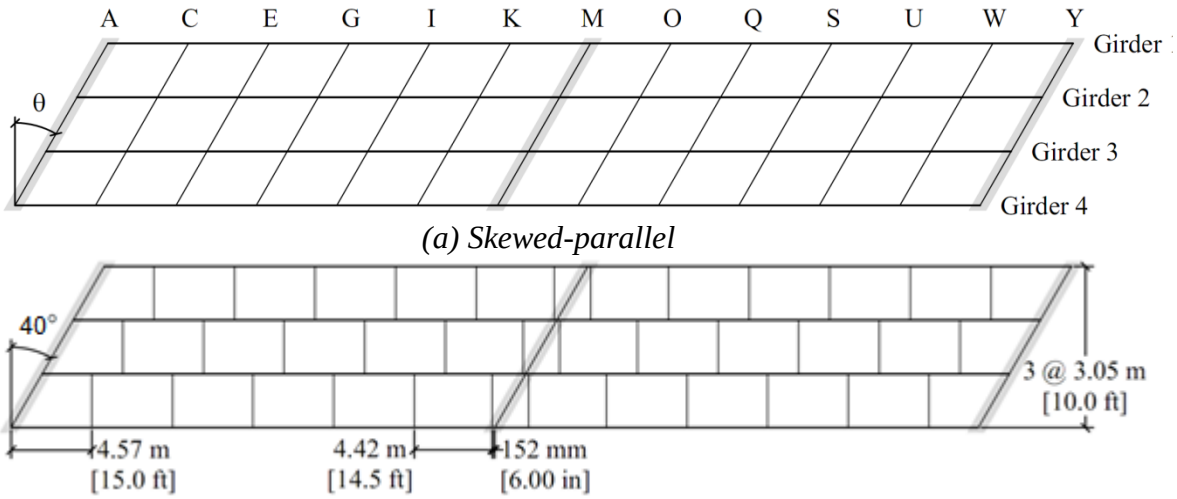

Figure 3 Bridge configurations (40° skew with 4.6 m [15.0 ft] cross-frame spacing)

Cross-frames, referring to truss-type lateral braces placed at discrete locations along a bridge layout, were used in all bridge configurations studied and consisted of three equal-leg angles spanning between connection stiffeners. A square plate was used to connect the diagonal legs at mid-length, as shown in Figure 4. Both connection stiffeners were modeled as being tied directly to the web and top and bottom flanges; attaching the connection stiffeners to the adjacent flanges is representative of current practice (post-1980s detailing). In bridges with skewed-parallel configurations, cross-frame length increased with skew angle and bent plate stiffeners were used to capture realistic construction considerations. The slenderness ratio for the single angles was computed using provisions in American Institute of Steel Construction's Steel Construction Manual (AISC Manual, 2010) Section E5, and cross-frame stiffness was compared based on the approximate relative stiffness, $A\cos^3\theta$,where A is the cross-sectional area of one angle and θ is the skew angle (Yura 2001; Wang & Helwig 2008). This was done to ensure that cross-frames selected in the different models had similar stiffnesses. A slenderness ratio of approximately 140 was used for all angles, which is a commonly-used slenderness limit in design. An L108 x 108 x 12.7 mm [L4-1/4 x 4-1/4 x 1/2 in.] angle was selected for the skewed-staggered bridge. An L114 x 114 x 15.9 mm [4-1/2 x 4-1/2 x 5/8 in.] angle was selected for the 20° skewed-parallel bridge. An L140 x 140 x 15.9 mm [5-1/2 x 5-1/2 x 5/8 in.] angle was selected for the 40° skewed-parallel bridge. More details regarding the brace sizing and rationale are provided in Hassel (2011).

Connection stiffener dimensions are shown in Figure 4. A thickness of 9.5 mm [3/8 in.] was selected for all connection stiffeners in skewed bridges with 4.6 m [15 ft] and 9.1 m [30 ft] cross-frame spacing. Stiffener thicknesses of 9.5 mm [3/8 in.], 12.7 mm [1/2 in.], and 25.4 mm [1 in.] were selected for a cross-frame spacing of 13.7 m [45 ft].

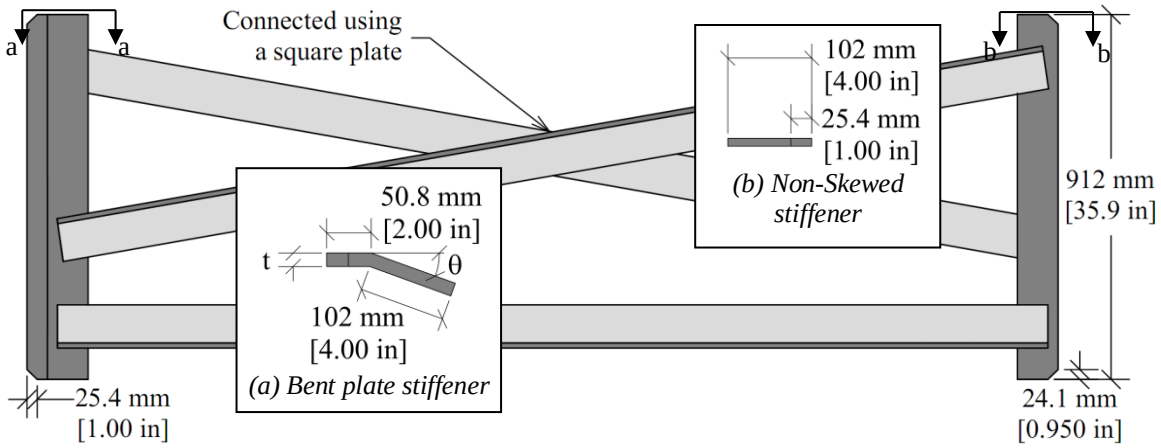

Figure 4 Connection stiffener geometry

Abutment diaphragms were modeled as having three equal-leg angle cross-sections spanning between connections plates in a K-brace, shown in Figure 5. A gusset plate was used to connect the diagonal legs to the bottom horizontal angle. The diagonal legs were tied directly to a MC12x50, which spans between connection stiffeners. L114 x 114 x 12.7 mm [4-1/2 x 4-1/2 x 1/2 in.] angles were selected for all abutment diaphragms, following the design of the skewed-staggered bridge. The abutment connection stiffeners were tied to the web and top and bottom flanges. Abutment connection stiffener dimensions are shown in Figure 5. An abutment connection stiffener thickness of 25.4 mm [1 in.] was selected for all bridges.

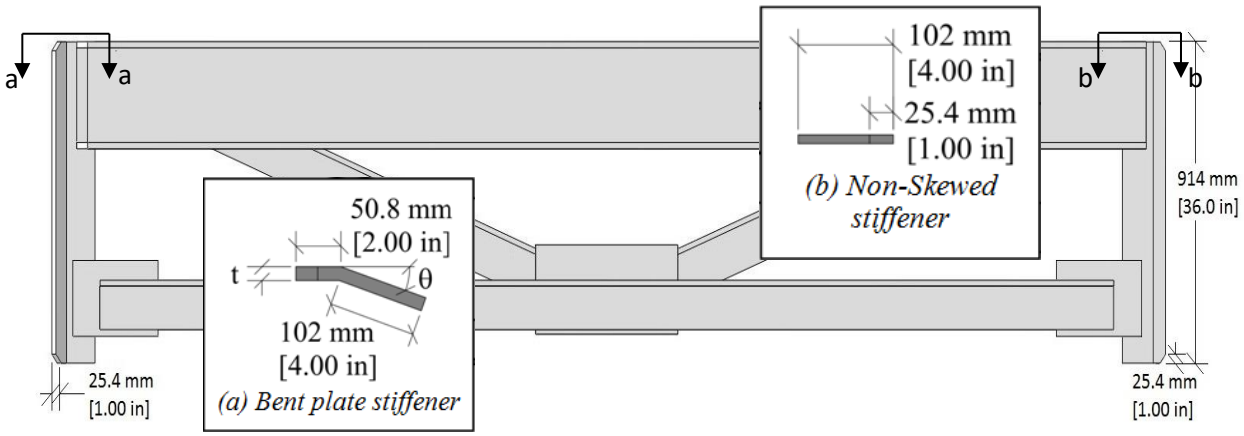

Figure 5 Abutment diaphragm and connection stiffener geometry

A round half-pipe connection stiffener developed at the University of Texas-Austin has been shown to increase buckling capacity by as much as 80% due to a significant increase in the warping stiffness of the cross section (Quadrato et al. 2010). An additional benefit of using a round stiffener is that perpendicular connections to the cross-frame tab can be made regardless of the skew angle. Cross-frames modeled with half-pipe connections consisted of three equal-leg angle cross-sections spanning between connection stiffeners. A square plate was used to connect the diagonal legs at mid-length, shown in Figure 6. The round half-pipe stiffener was connected to the web and top and bottom flanges. The same angles were used in the cross-frames with half-pipe connections as in the cross-frames with bent plate stiffeners. An L108 x 108 x 12.7 mm [L4-1/4 x 4-1/4 x 1/2 in.] angle was selected for the skewed-staggered bridge. An L114 x 114 x 15.9 mm [4-1/2 x 4-1/2 x 5/8 in.] angle was selected for the 20° skewed-parallel bridge. An L140 x 140 x 15.9 mm [5-1/2 x 5-1/2 x 5/8 in.] angle was selected for the 40° skewed-parallel bridge.

Quadrato et al. (2010) found that girder buckling capacity increased with pipe diameter significantly more than pipe thickness. Therefore, the half-pipe adopted in the models in this study were that of an HSS10-3/4 x 1/2, which is the largest diameter pipe that can be accommodated by the flange widths in the girder geometry studied. The half-pipe studied had an outer diameter of 273 mm [10-3/4 in.] and a thickness of 12.7 mm [1/2 in.], shown in Figure 6. The cross-frame tab connecting the angles to the half-pipe was 102 mm [4 in.] wide and 9.5 mm [3/8 in.] thick for all half-pipe connections.

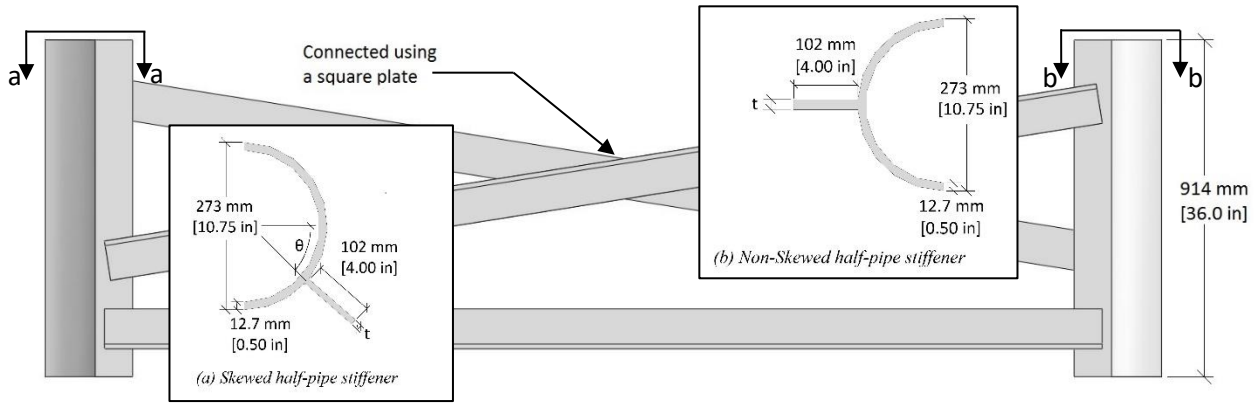

Figure 6 Cross-frame and half-pipe connection geometry

Abutment diaphragms with half-pipe connections were modeled with the same angle members as used with abutment diaphragms with the bent plate connection, in a K-brace configuration as shown in Figure 7. A gusset plate was used to connect the diagonal legs to the bottom horizontal angle as well, tied directly to a MC12x50 spanning between the connection stiffeners. An HSS10.75x1/2 was used for the half-pipe connection, with an outer diameter of 273 mm [10.75 in.] and a thickness of 12.7 mm [1/2 in.]. The half-pipe stiffeners were tied directly to the web and both top and bottom flanges. Abutment connection half-pipe and stiffener dimensions are shown in Figure 6. An abutment connection stiffener thickness of 25.4 mm [1 in.] was used for all bridges modeled.

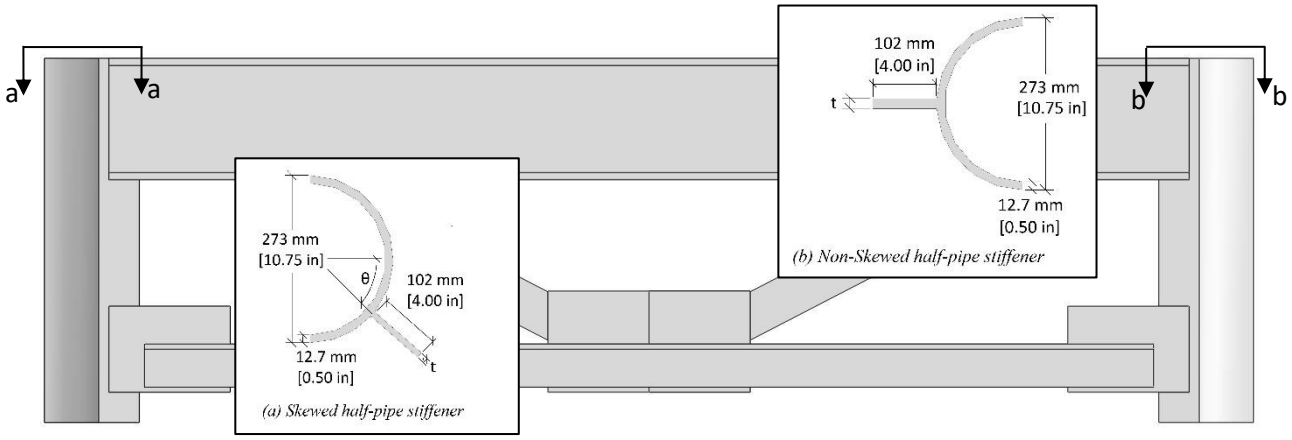

Figure 7 Abutment diaphragm and half-pipe connection geometry

Intermediate transverse stiffeners with a thickness of 9.5 mm [1/2 in.] were modeled every 4.6 m [15 ft] in bridges with 9.14 m [30 ft] and 13.7 m [45 ft] cross-frame spacing. Figure 8 shows the transverse stiffener placement in a finite element model of the bridge with 9.14m [30 ft] cross-

frame spacing. No intermediate transverse stiffeners were modeled in bridges with 4.6 m [15 ft] cross-frame spacing. 12.7 mm [1/2 in.] thick transverse stiffeners were also used to stiffen the girder web at the abutments and pier supports. Two stiffeners spaced at 406 cm [16 in.] were placed at each abutment girder support on each side of the web, except for the exterior girders where two additional stiffeners were placed 203 mm [8 in.] apart on the exterior side of the web. Three 12.7 mm [1/2 in.] thick transverse stiffeners spaced 203 mm [8 in.] apart were placed on the exterior side of the web of the exterior girders at the center piers. Transverse stiffeners were tied directly to the web and to the top and bottom flanges.

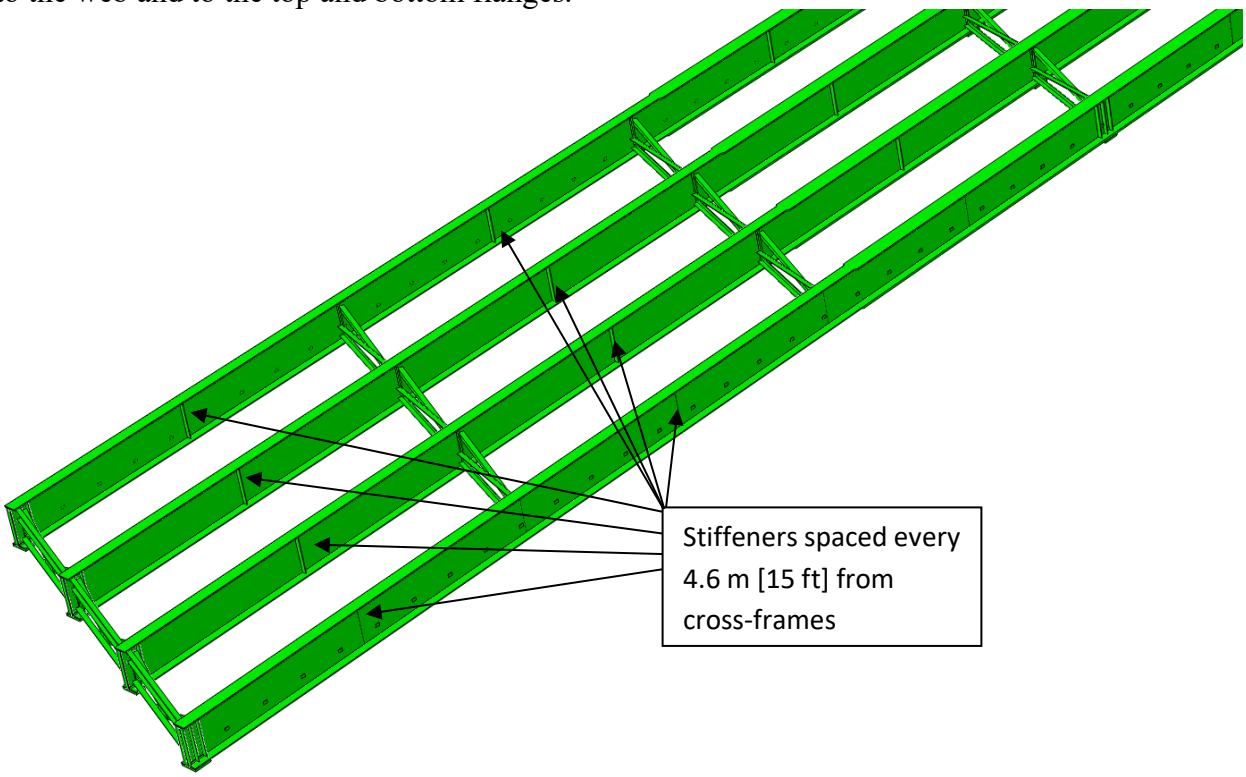

Figure 8 Stiffener placement in bridges with 9.14 m [30 ft] cross-frame spacing

3. MODELING METHODOLOGY

Three-dimensional, solid-element finite element (FE) models of the entire bridge were constructed using Abaqus v.6.10-2 for parametric analysis (Simulia, 2010). An example of one the bridge models is represented in Figure 9. C3D8R brick elements were used in the majority of the model, but C3D4 tetrahedral and C3D6 wedge elements were used to transition between mesh sizes where needed. Geometric nonlinearity was considered within the analyses.

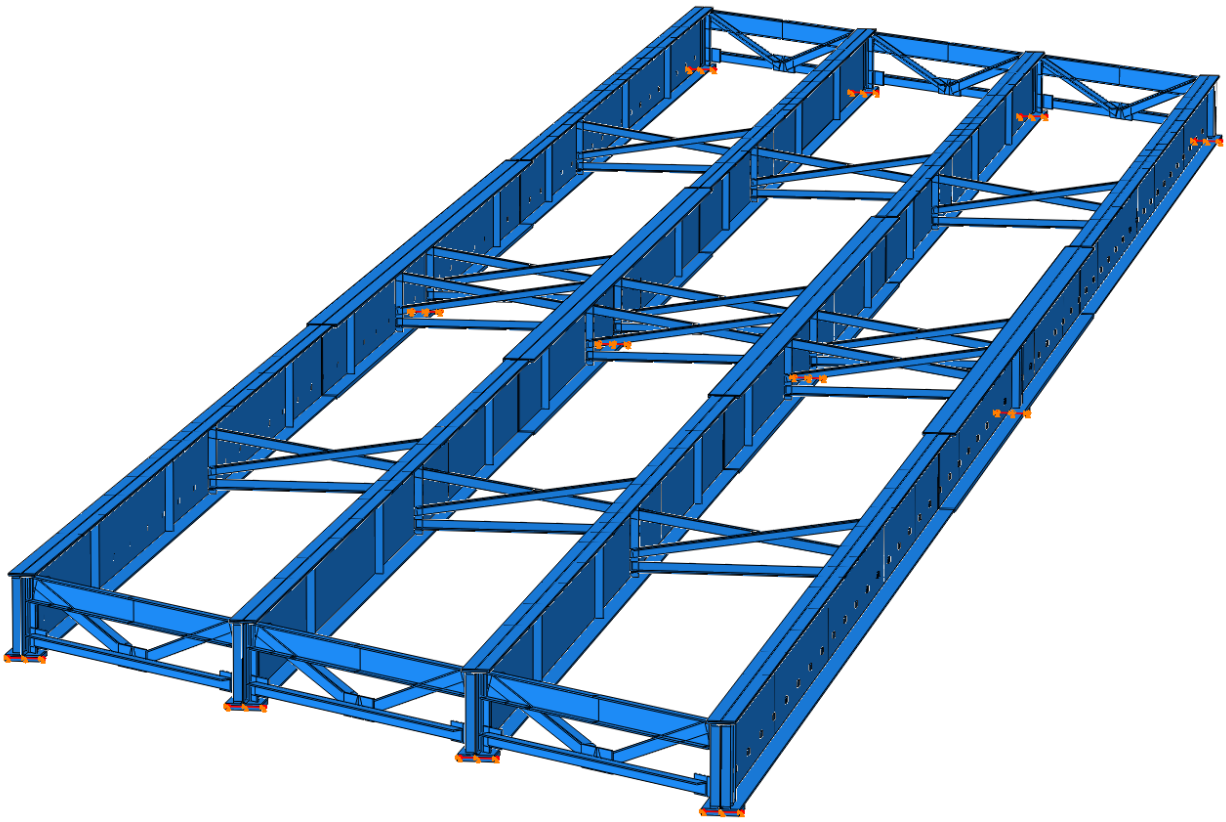

Figure 9 3D FEM model geometry of skewed-staggered bridge configuration (9.1 m [30 ft] cross-frame spacing)

Girder flanges and webs were modeled to have a modulus of elasticity of 200,000 MPa [29,000 ksi] and Poisson's ratio of 0.3. A mesh size of 25.4 mm [1 in.] was used for web and flange elements. The cross-frame angles were partitioned such that each leg was divided into two equal lengths and each angle into four equal parts, as shown in Figure 10. The cross-frame angles and stiffeners were then merged in Abaqus retaining intersecting boundaries. This procedure allowed the mesh to have a consistent size throughout each of the cross-frame members. A mesh size of 127 mm [5 in.] was used for abutment diaphragm and cross-frames. A finer mesh size for the cross-

frames resulted in convergence errors in some models. A mesh size of 965 mm [38 in.] was used for the top flange covers, the purpose of which is described later. For all other parts, including transverse stiffeners, plates, and bearing pads, the mesh size was equal to the thickness of the part.

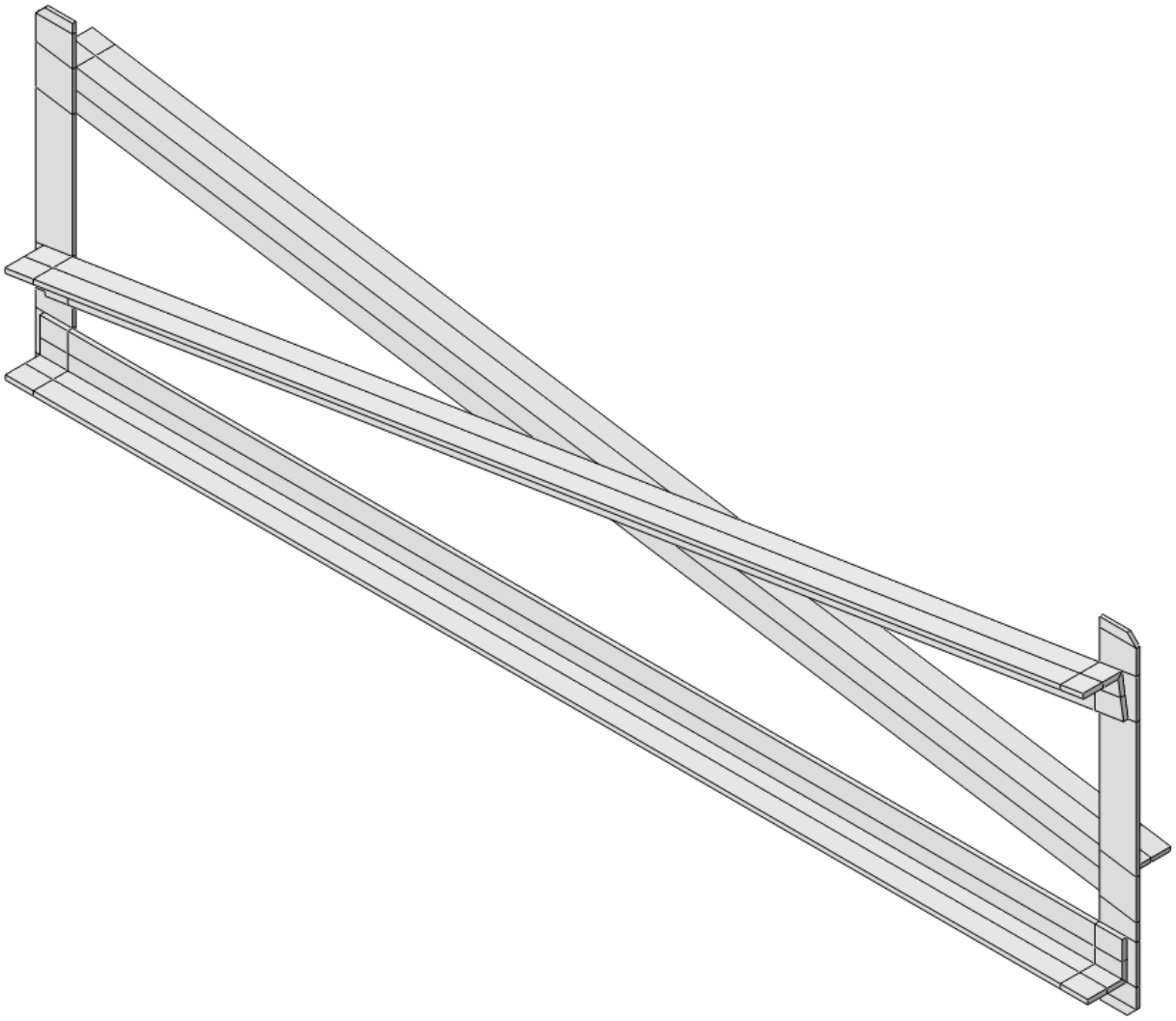

Figure 10 Cross-frame Angle Partitions

Steel overhang brackets typically support the construction walkway and screed rail during the construction phase of a bridge structure. The overhang brackets were not modeled directly within the parametric analysis, but the loads that they induced on the exterior girders were included in the parametric analysis. Reaction forces from the brackets on the web were calculated using a preliminary structural analysis model in Mastan (Figure 11) and applied to 63.5x102 mm [2-1/2 x 4 in.] bracket plates that were connected to the web using tie constraints. A total of 53 brackets spaced at 1 m [40 in.] on center were used and each overhang bracket was modeled to be 1.8 m

[70 in.] long. Overhang brackets modeled in the preliminary Mastan analysis were considered to hold three 51x51 mm [2x2 in.] wall stud joists (timber) supporting the 711 mm [28 in.] wide construction walkway and a 102x102 mm [4x4 in.] stud (timber) supporting the screed rail on each side of the bridge. Walkway loads were distributed over timber studs spaced 305 mm [12 in.] on center.

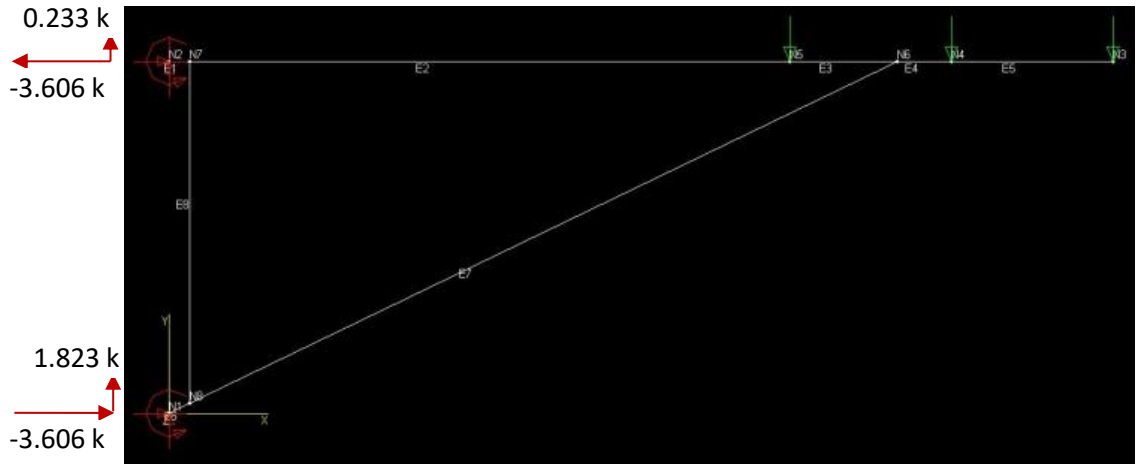

Figure 11 Bracket forces calculated from preliminary beam analysis performed in Mastan

Plywood formwork supporting the wet concrete deck, typically used during construction, was not included in the parametric models because the slight stiffness contribution from the attached plywood was found to affect lateral bending stresses significantly within the models. Since real connections between plywood formwork and steel girders are generally not considered to develop sufficient lateral support, designers rightfully neglect the contributions of such formwork. Therefore, it was determined that the models would better reflect design practices by neglecting the plywood formwork from the models.

Given the geometric nonlinear characteristics of the models, it was not surprising that challenges with convergence were initially encountered and high-order buckling modes occurred as modeling artifacts. To eliminate high-order buckling modes that tended to occur in girder flanges in trial model executions, a very thin and flexible top flange "cover", with the same width as the top flange, was used to damp localized responses in the top flange. This compliant layer was assigned a thickness of 25 mm [1.0 in.] in the positive moment region and 13 mm [1/2 in.] in the negative moment region to accommodate the difference in thickness of the top flange in these two regions. The compliant layer was assigned a modulus of elasticity of 6895 MPa [1000 ksi]. Due to

its low stiffness, use of this model control technique did not significantly affect the bending moment results, and this was verified through a comparison of models that included / did not include the compliant layer on the flange. To help mitigate localized instabilities, a dissipated energy fraction of 0.0002 with a maximum ratio of stabilization to strain energy of 0.05 was specified for automatic stabilization.

Surface-to-surface tie constraints were used to attach parts within models. Welds were not explicitly modeled, but rather, webs were tied directly to the flanges and all stiffeners were tied directly to the web and flanges. A 25.4 mm [1 in.] triangular "weld" 406 mm [16 in.] long was tied to the web and flanges at the girder ends to reduce high, localized stresses at abutment ends. Girder boundary conditions were modeled by applying a translational constraint over a narrow, 12.7 mm [1/2 in.] strip of the bearing plate at support locations. The square 406 mm [16 in.] bearing plate was 51 mm [2 in.] thick and was tied to the bottom flange at the mid-span and ends of the girders. Pinned support conditions were used to represent the center pier while roller support conditions were used to represent abutment piers.

4. APPLIED LOADS

The following dead and live loads applied in the models during the construction stage were based on The Kansas Department of Transportation Design Manual: Volume III Section 5.3 (KDOT 2010).

- A 203 mm [8 in.] thick wet concrete deck with a density of 2563 kg/m^3 [160 lb/ft^3] was applied as a uniform pressure over the vertical projection of the web on the top flange cover and roadway overhang. The density included the weight of reinforcing steel and forms.
- A 27.2 mm [1.1 in.] effective height of the concrete deck haunches was applied as a uniform pressure using a 2563 kg/m^3 [160 lb/ft^3] density over the vertical projection of the web on the top flange cover. This density included the weight of reinforcing steel and forms.
- Steel weight was applied to all steel parts (i.e. girders, stiffeners, and cross-frames) as a gravity load using a density of 7849 kg/m^3 [490 lb/ft^3].
- A 366 kg/m^2 [75 lb/ft^2] construction live load was applied as a uniform pressure over the vertical projection of the web on the top flange cover.
- A 744 kg/m [500 lb/ft] screed load was applied as a uniform pressure over a width of 102 mm [4 in.] on the plywood screed rail. The reaction force from the bracket overhang was applied to the bracket plate on the girder web.
- A 801 kg/m^3 [50.0 lb/ft^3] walkway load was applied as a uniform pressure over the construction 711 mm [28 in.] walkway surface. The reaction force from the bracket overhang was applied to the bracket plate on the girder web.

Dead and live loads from the tributary area on the deck were applied as a 13 mm [1/2 in.] wide uniform pressure over the vertical projection of the web on the top flange cover, as shown in Figure 12. These loads were applied over the vertical web projection on the top flange cover rather than over the entire flange cover to prevent further artifacts of high-order buckling from occuring in the top flange. Screed and walkway loads were carried by overhang brackets. Reaction forces from the screed and walkway loads on the

brackets were calculated using finite element analysis, as discussed. The horizontal component of the reaction force was applied over a 64 mm [2.5 in.] by 102 mm [4.0 in.] bracket plate tied to the web, as described previously.

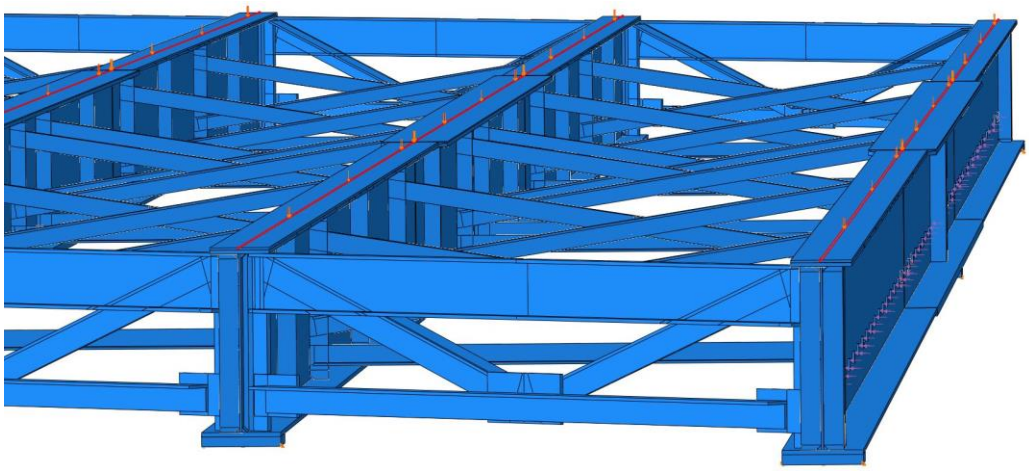

Figure 12 Deck dead load and construction live load applied to a bridge system model

Load combinations and load factors are presented in AASHTO Section 3.4 (AASHTO 2010). The Strength load combinations and load factors from AASHTO Table 3.4.1-1 were found to produce the controlling load combination during the construction stage (Zhou et al. 2015). Of the Strength load combinations and load factors, Strength 1 was found to produce the highest stresses for all bridge configurations. Therefore, the Strength 1 load combination and load factor were used in the analyses.

Strength 1 (S1): 1.25 DC + 1.25 DW + 1.75 LL

Strength 3 (S2): 1.25 DC + 1.25 DW + 1.4 WS (including uplift)

Strength 4 (S4): 1.50 DC + 1.50 DW

Strength 5 (S5): 1.25 DC + 1.25 DW + 1.35 LL + 0.4 WS (no uplift)

where

DC = dead load of structural components

DW = dead load of wearing surface

LL = construction live load

WS = wind load on structure

5. STRESS CALCULATIONS

Flexural stresses, σ, were calculated from these moments using the bending stress equation:

$$\sigma = Mc/I$$

where:

M = flange or section bending moment

c = distance from the extreme fiber to the neutral axis

I = moment of inertia of the flange or section

Major and minor axis bending moments about the girder cross-section were obtained using section cuts along Girder 3 and Girder 4. Girder 3 is an interior girder, and Girder 4 is an exterior girder; thus, different behavior was expected to occur between those girders. Due to symmetry within the models, Girder 3 produced similar results compared to Girder 2 (the other interior girder) and Girder 4 produced similar results compared to Girder 1 (the other exterior girder). Therefore, only Girder 3 and Girder 4 stresses are presented.

A free body cross-section in Abaqus is an area across which resultant forces and moments can be computed. Once such a cross-section is defined is defined within a model, Abaqus can be used to output vectors that include the magnitude and direction of the resultant moments across the specified area. Figure 13 shows the resultant moments occurring over the entire girder section (Figure 13a) and over just a flange (Figure 13b).

In all cases, moment values were extracted from locations where cross-frames connected to the web (where lateral flange bending stresses were expected to be at a maximum) and at the mid-point between two cross-frame locations along the girder (where localized effects were expected to be least influential).

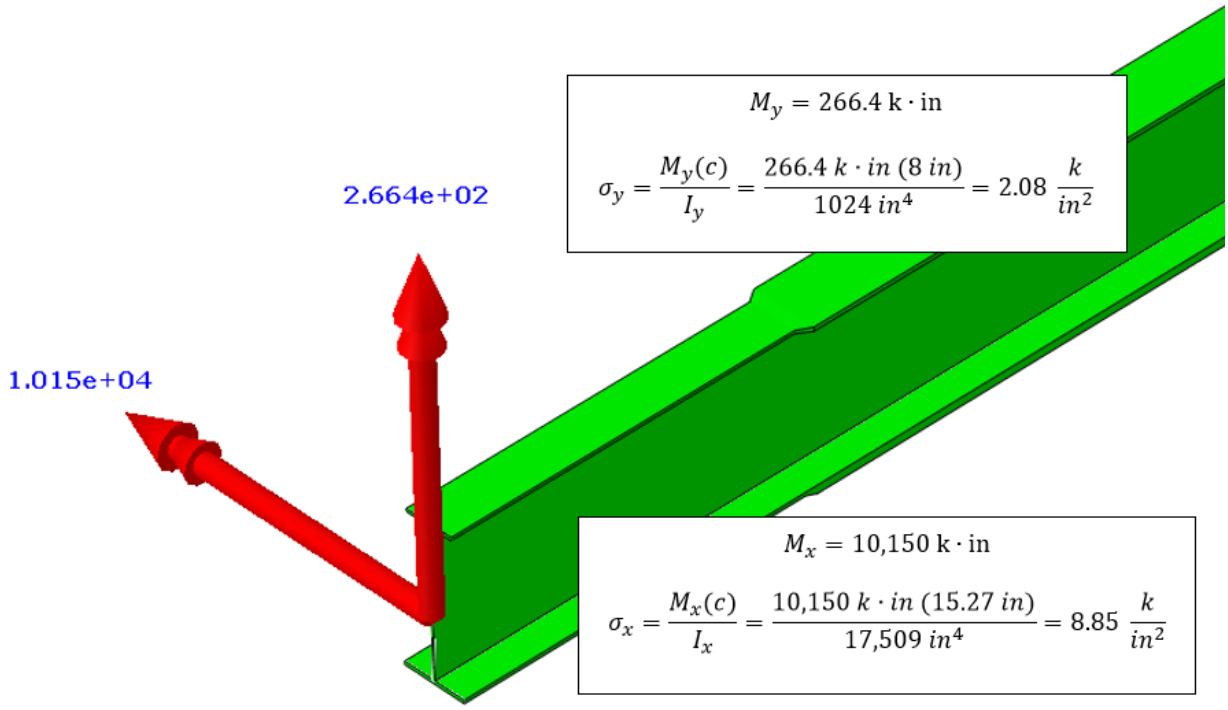

(a) Girder Section

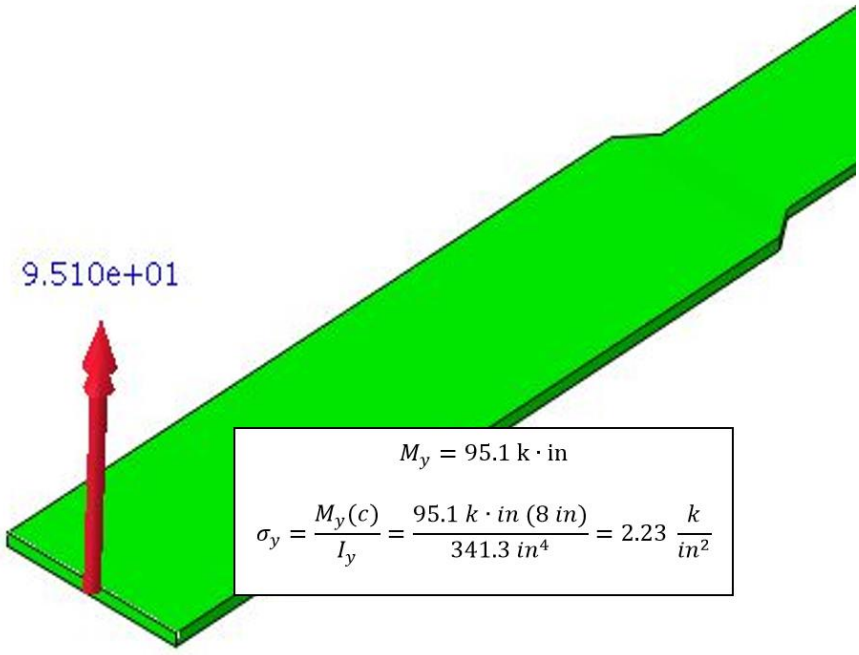

(b) Top Flange Section

Figure 13 Resultant moments displayed on the free body section and sample stress computation for (a) Girder Section and (b) Top Flange Section

5.1. Strong-Axis Bending Stress Computations

For the girder section in strong-axis bending in the positive flexure region, *c* was -538 mm [-21.2 in.] from the top (compression) flange to the neutral axis. Stresses were also calculated for a *c* value of 419 mm [16.48 in.] taken from the bottom (tension) flange to the neutral axis. The girder section had an I_x value of 3.86×10^{-4} m^4 [9278 in^4] in strong-axis bending for the positive flexure region. For the girder section in strong-axis bending in the negative flexure region, the *c* value was 603 mm [23.7 in.] taken from the top (tension) flange to the neutral axis. Stresses were also calculated from a c value of 389 mm [15.3 in.] taken from the bottom (compression) flange to the neutral axis. The girder section had an I_x value of 7.28×10^{-4} m^4 [17500 in^4] in strong-axis bending for the negative flexure region.

Figure 14 shows the strong-axis bending stress distributions computed for the top flange and the bottom flange in the 40° skewed-parallel bridge with 13.7 m [45 ft] cross-frame spacing and half-pipe connections.

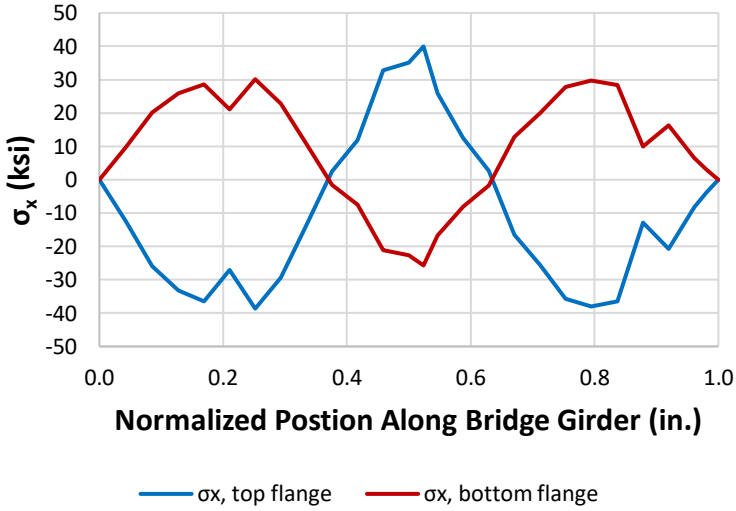

Figure 14 Girder 4 strong-axis sectional stresses (computed from M_x) in the 40° skewed-parallel bridge with 13.7 m [45 ft] cross-frame spacing and half-pipe connections.

5.2. Weak-Axis Bending Stress Computations

Two methods for computing lateral flange bending stresses were used:

(1) Weak-axis stresses in the flanges were computed using the weak-axis moment, M_y, extracted over the full-depth of the cross-section. This moment was used in conjunction with the weak-axis bending moment of inertia for the entire cross-section. In this case,

the c value for the girder section was computed as 152 mm [6 in.] for the top flange and 203 mm [8 in.] for the bottom flange in weak-axis bending in the positive flexure region. The c value was taken as 203 mm [8 in.] for the bottom flange in the both the positive and negative regions. The girder section had an I_y value of 1.69×10^{-4} m^4 [407 in^4] in weak-axis bending for the positive flexure region and an I_y value of 4.26×10^{-4} m^4 [1024 in^4] in weak-axis bending for the negative flexure region.

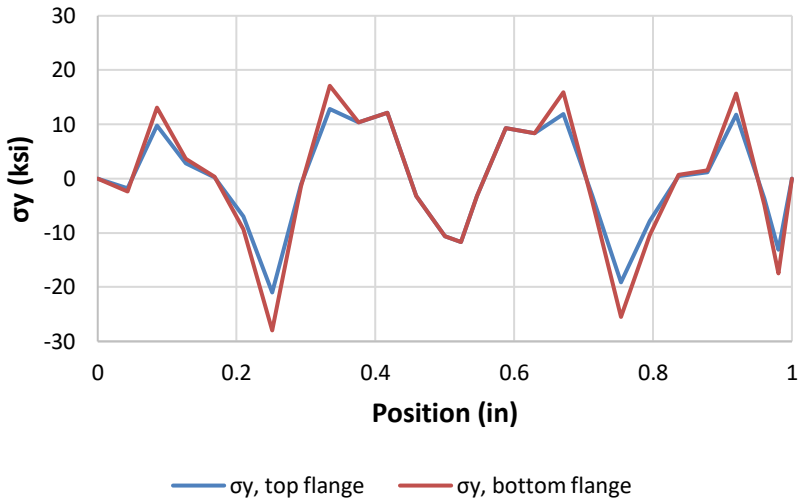

Figure 15 Girder 4 weak-axis sectional stress (computed from M_y) in the 40° skewed-parallel bridge with 13.7 m [45 ft] cross-frame spacing and half-pipe connections.

(2) Weak-axis stresses in the flanges were also computed using moments that were extracted from the top and bottom flanges, individually. When using this method, the moments were used in conjunction with the weak-axis bending moment of inertia for just the appropriate flange section. The top flange section cut is shown in Figure 13(b) along with the resultant lateral flange bending moment.

The top flange had a c value of 152 mm [6 in.] in out-of-plane bending and an $I_{y,fl}$ value of 4.50×10^{-5} m^4 [108 in^4] in the positive flexure region and a c value of 203 mm [8 in.] and an $I_{y,fl}$ value of 1.42×10^{-4} m^4 [341 in^4] in the negative flexure region. The bottom flange had a c value of 203 mm [8 in] in out-of-plane bending and an $I_{y,fl}$ value of 1.24×10^{-4} m^4 [298 in^4] in the positive flexure region and a c value of 203 mm [8 in] and an $I_{y,fl}$ value of 2.13×10^{-4} m^4 [683 in^4] in the negative flexure region.

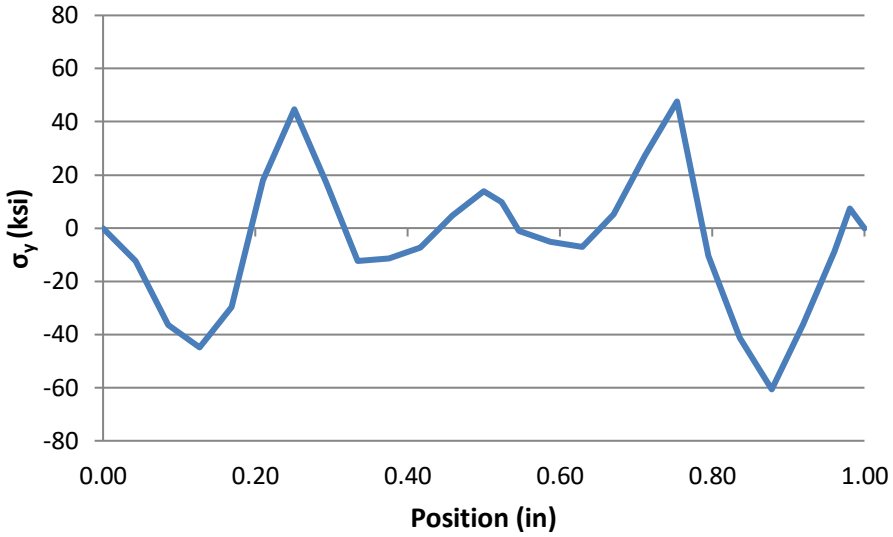

Figure 16 Girder 4 top flange out-of-plane stress (computed from $M_{y,fl}$) in the 40° skewed-parallel bridge with 13.7 m [45 ft] cross-frame spacing and half-pipe connections.

5.3. Comparison of Stresses Computed from Moments and Model-Extracted Stresses

Stresses were extracted directly from the top flange of Girder 4 in the FE models to compare against flexural stresses calculated from bending moment. This comparison was performed because the stresses extracted directly from the models can be expected to include contributions from all directions of loading, and the comparison allowed for an assessment of the reasonableness of the assumption of pure strong-axis and pure weak-axis bending stress computations described in 5.1 and 5.2. The results between stresses directly extracted from the model and calculating stresses from bending moments were found to be congruent. Stresses were extracted from paths along the extreme edges and centerline of the exterior girder's top flange, as shown in Figure 17. *S11* is indicative of stresses in the out-of-plane direction relative to the bridge girder line. *S22* are stresses in the vertical direction, and *S33* are stresses in the longitudinal direction. *S33* captures bending stresses about both strong and weak axes. Stresses – both computed and directly extracted – for the 40° skewed-parallel bridge with 13.7 m [45 ft] cross-frame spacing and half-pipe connections are shown in Figure 18 through Figure 21. *S33* stresses along the center Path B, shown in Figure 18, were similar to strong-axis sectional stresses calculated from *c* taken to the top flange. Strong-axis bending stress was found to dominate stresses

at the center of the flange. The average of the two edge stresses in Figure 18 also produced values similar to the strong-axis bending stress. The average of the difference between S33 Path A and S33 Path C also produced similar results compared to the top flange out-of-plane bending stress, shown in Figure 19 and Figure 20; the values are inverted for Path A stresses compared to Path C stresses due to sign convention.

Axial stress values, shown in Figure 21, were also examined. They were found to be small compared to strong and weak-axis sectional stresses at non-cross-frame locations and are not presented for the other bridge models.

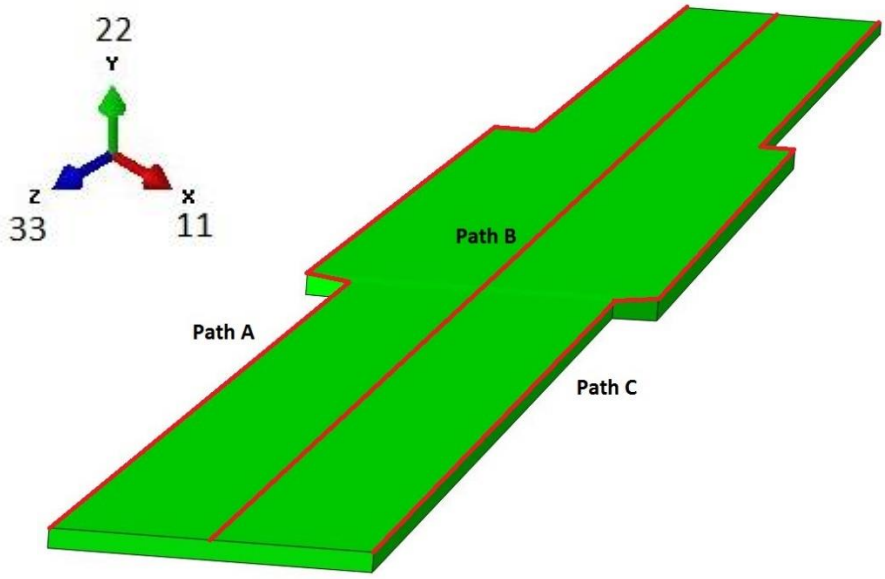

Figure 17 Stress paths along top flange used for direct extraction of stresses from the models

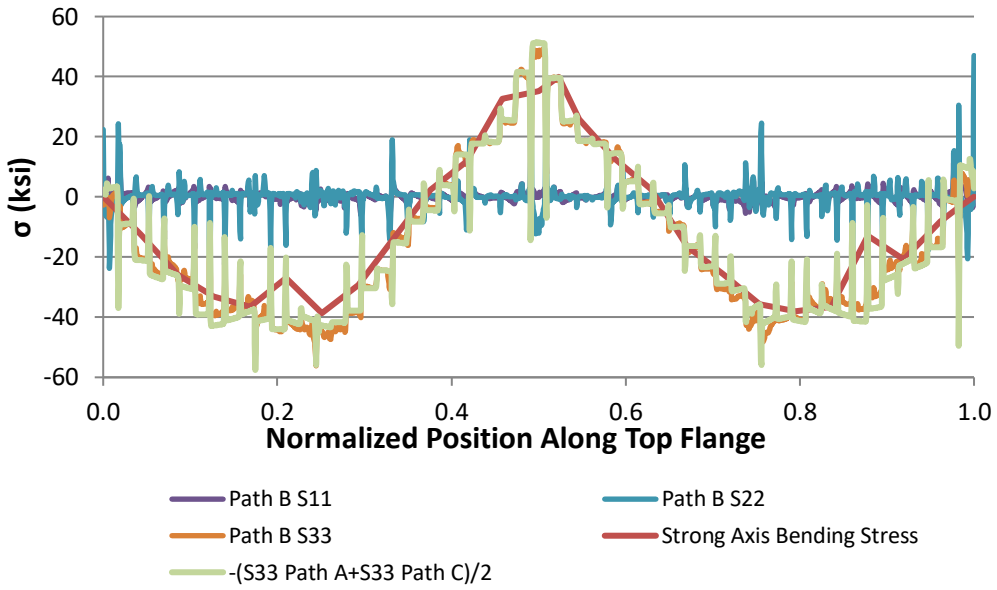

Figure 18 Stresses extracted directly from Path B in Girder 4, compared against strong-axis bending stresses computed using Mc/I

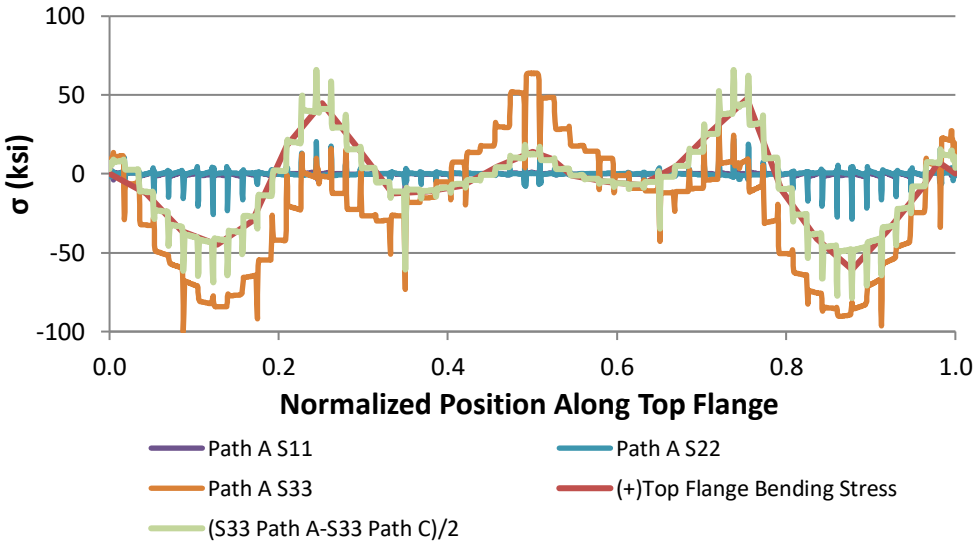

Figure 19 Stresses along Path A in Girder 4, compared against weak-axis tensile bending stresses in top flange computed using Mc/I

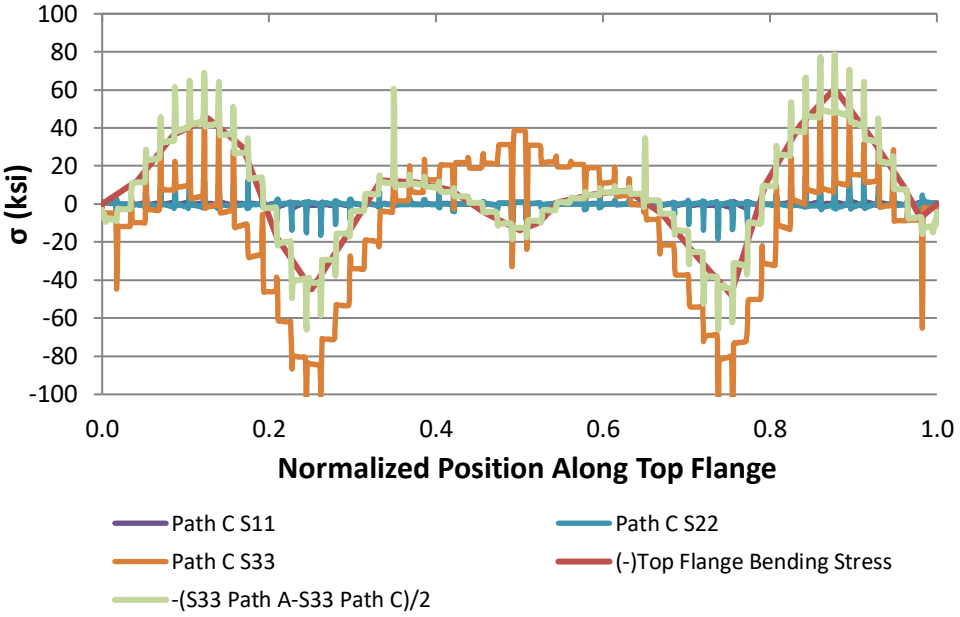

Figure 20 Stresses along Path C in Girder 4, compared against compressive weak-axis bending stresses in the top flange computed using Mc/I

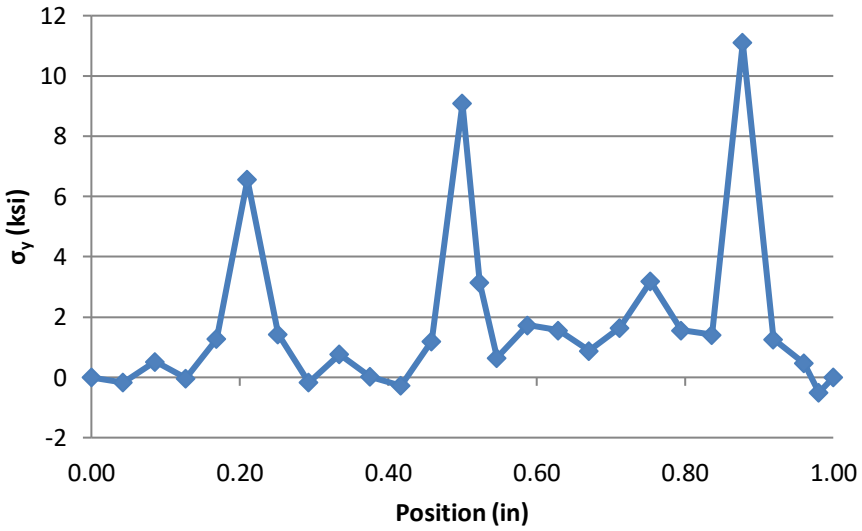

Figure 21 Girder 4 axial sectional stress

Given the general agreement, especially in trend, between extracted and computed stresses, the results for stresses are presented in terms of computed stresses. However, since some notable differences in magnitude between lateral flange bending stresses were found for the two computation methods, results for both techniques are presented.

6. RESULTS

The results of this study are described in the following sections. First, a case is made for how material non-linearity was considered in the modeling efforts, and why it was not included in the full parametric analysis. Then, the influence of the bracket overhangs is examined through a comparison of models that included and did not include the bracket overturning forces. Finally, the full parametric study is discussed in terms of load-deflection relationships, girder stresses, cross-frame stresses, and deformation modes. Throughout these discussions, reference will made to Span 1 or Span 2 of the bridge; the two bridge spans are labeled in Figure 22 for reference.

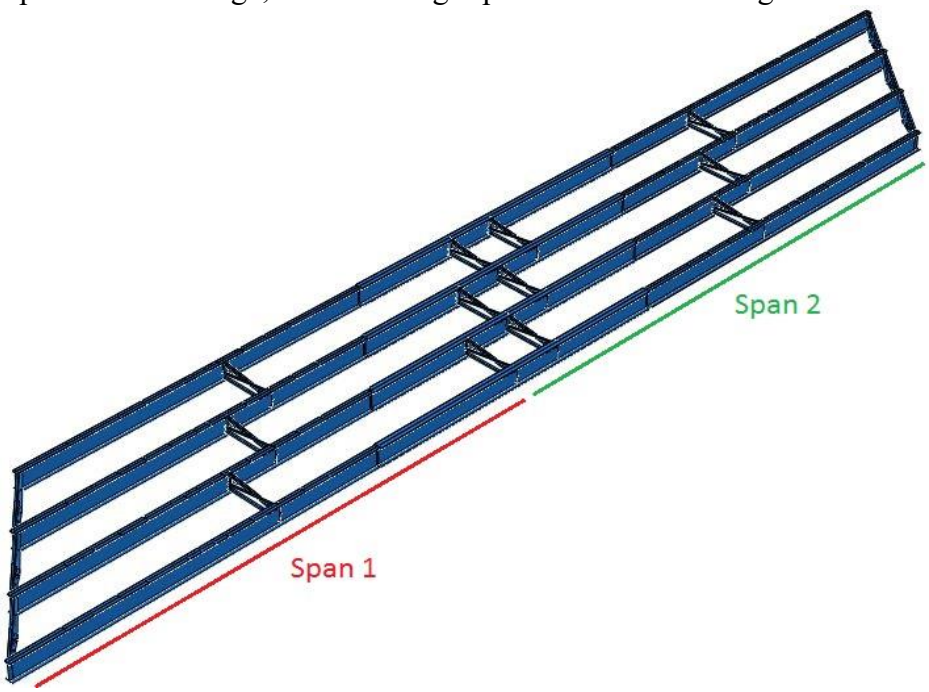

Figure 22 Spans labels

6.1. Effect of Material Non-Linearity

The 40° skewed-staggered bridge model with 4.6 m [15.0 ft] cross-frame spacing was examined both with and without material nonlinearity to determine the influence of material nonlinearity in the analysis. Both models with linear elastic material definition and non-linear material definition include geometric nonlinearity (i.e., captured second-order effects due to deformed geometry). The adopted nonlinear material properties are presented in Table 1 and Figure 23.

Table 1 Isotropic plastic hardening definition

Yield Stress (ksi)	Plastic Strain (in/in)
0	0
54.66	0
55.33	0.0367
58.20	0.0444
64.68	0.097
65.54	0.110
67.01	0.178
67.10	1.000

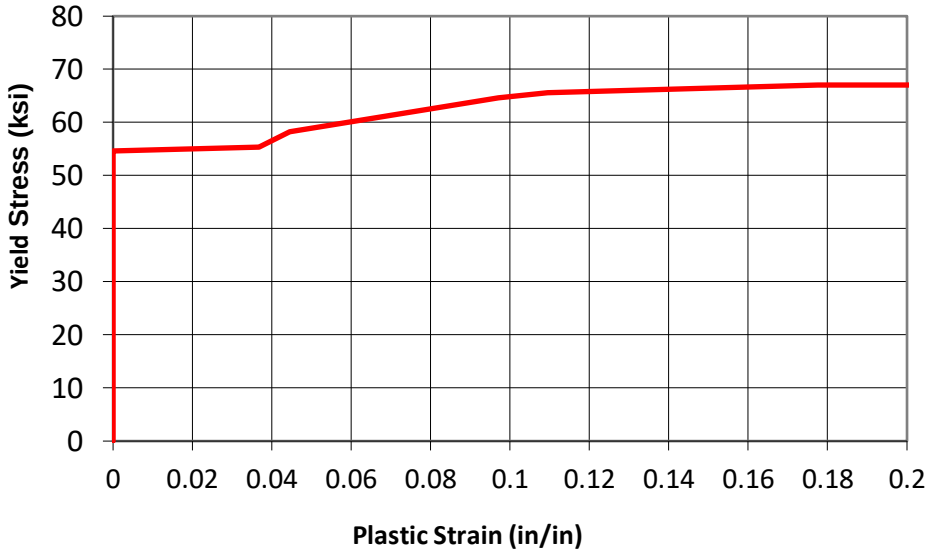

Figure 23 Steel material stress-strain curve used in the FE model with non-linear material behavior

The plots that follow are labeled by skew angle, configuration, and cross-frame spacing, and present a comparison of girder behavior between models that include linear-elastic and non-linear material properties. Configurations are designated by *SS* for skewed-staggered and *SP* for skewed-parallel.

Figure 24 shows lateral deflection in Girder 4 along Path B in the top flange. Figure 25 shows the applied load versus peak lateral deflection in Girder 4 along Path B in the top flange. Figure 26 through Figure 33 shows bending stresses for Girder 3 and Girder 4. Strong-axis bending stresses from a simple beam analysis is also shown in comparison with the 3D FEA results for the respective strong-axis bending stress in each girder, Figure 26 and Figure 27. It was found that

including a non-linear material model in the produced negligible differences in both lateral deflection and bending stresses. Therefore, material non-linearity was not included in subsequent analyses, since it is a computationally expensive modeling technique.

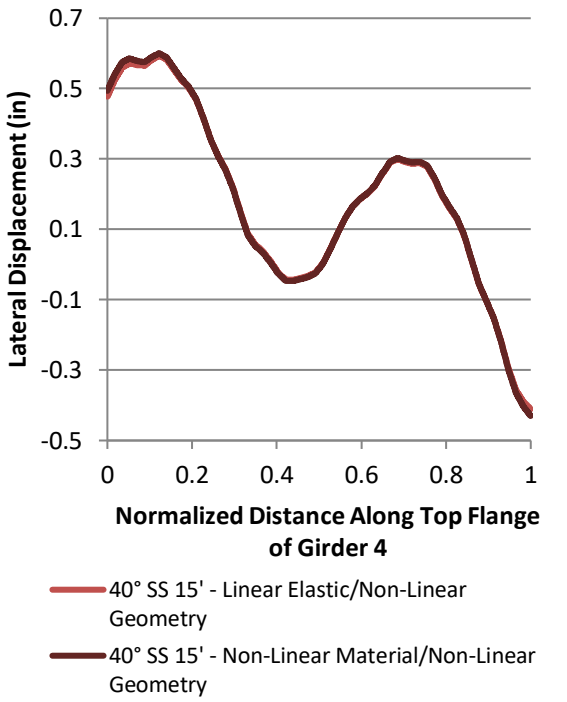

Figure 24 Girder 4 lateral displacement along the top flange for model with linear elastic vs. non-linear material

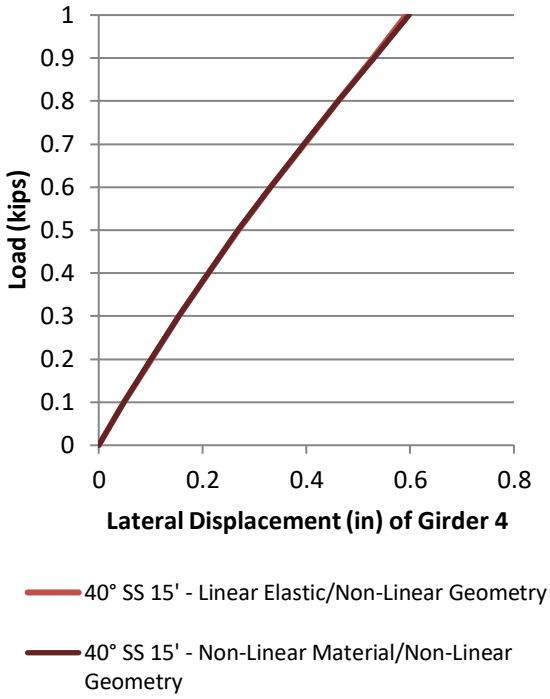

Figure 25 Girder 4 load vs. peak lateral displacement for model with linear elastic vs. non-linear material

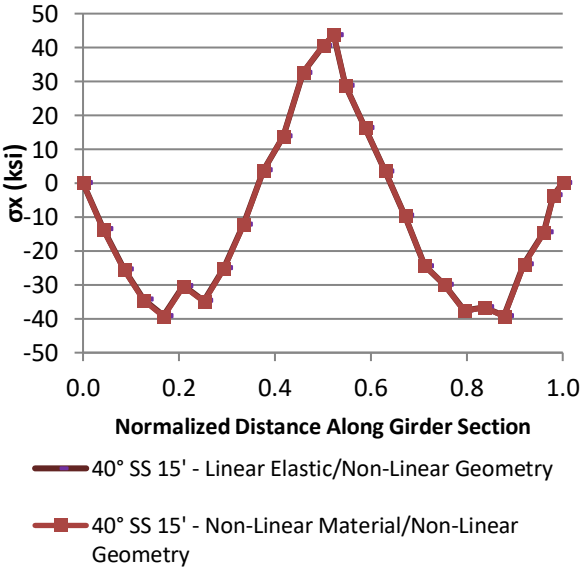

Figure 26 Girder 4 strong-axis sectional

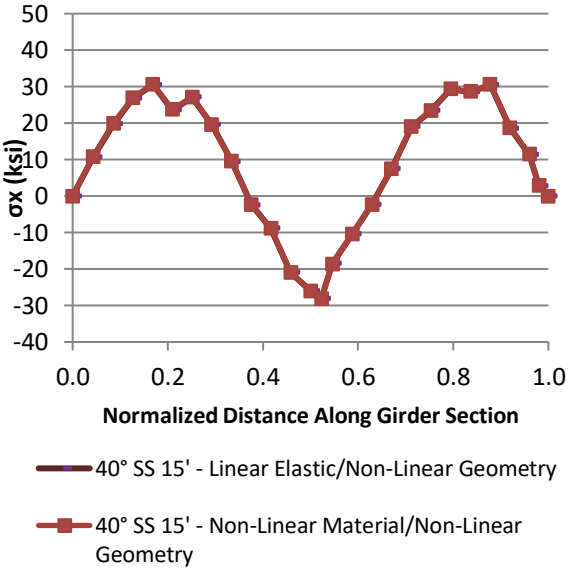

Figure 27 Girder 4 strong-axis sectional stress

stress from top flange for model with linear elastic vs. non-linear material

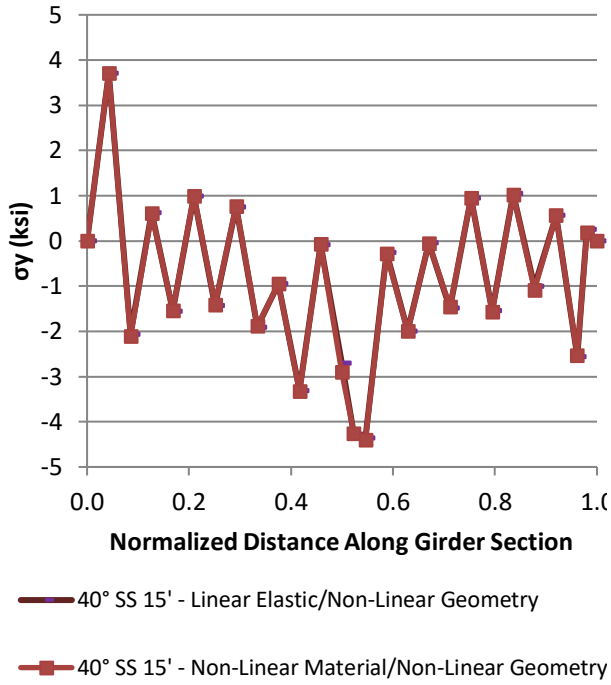

Figure 28 Girder 4 weak-axis sectional stress from top flange for model with linear elastic vs. non-linear material

from bottom flange for model with linear elastic vs. non-linear material

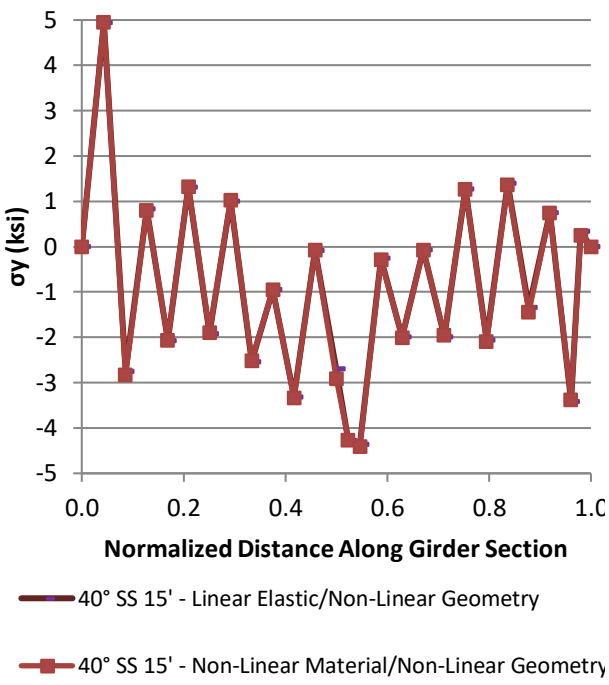

Figure 29 Girder 4 weak-axis sectional stress from bottom flange for model with linear elastic vs. non-linear material

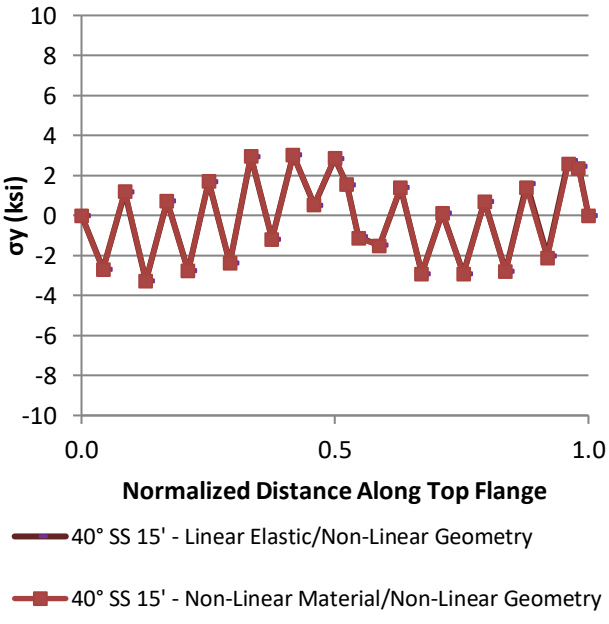

Figure 30 Girder 4 top flange out-of-plane stress for model with linear elastic vs. non-linear material

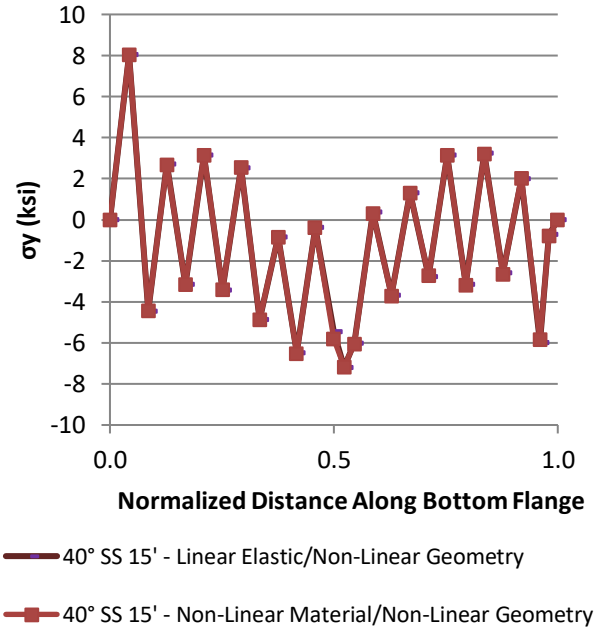

Figure 31 Girder 4 bottom flange out-of-plane stress for model with linear elastic vs. non-linear material

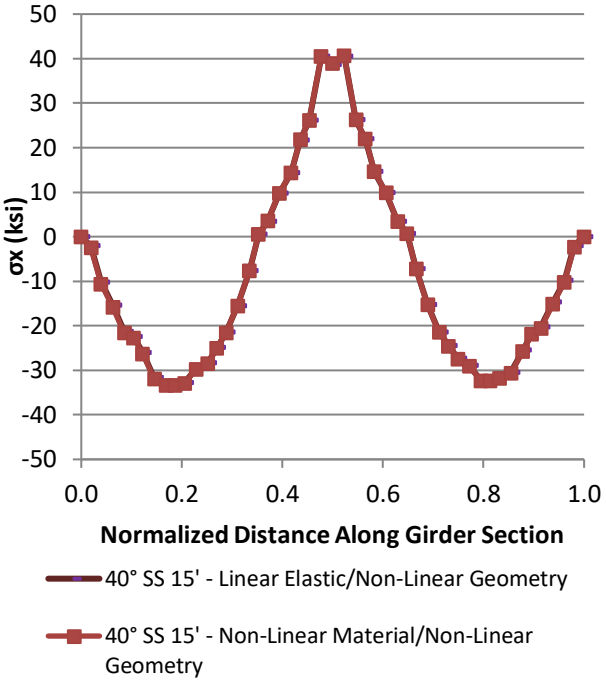

Figure 32 Girder 3 strong-axis sectional stress from top flange for model with linear elastic vs. non-linear material

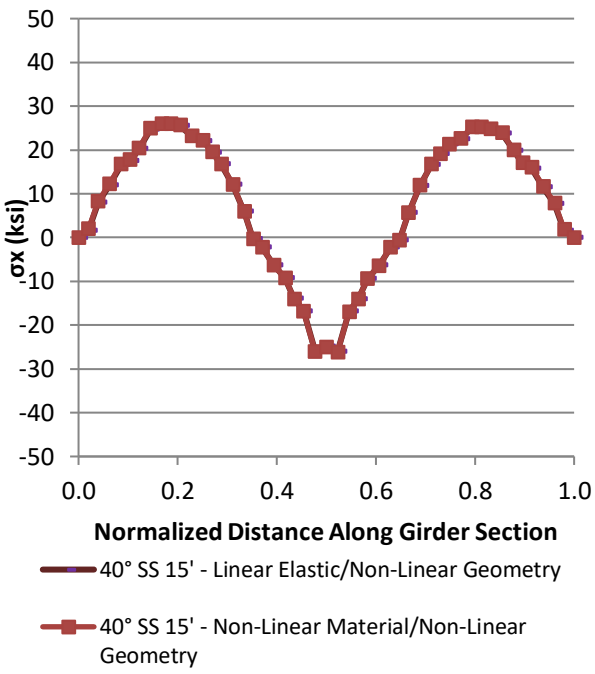

Figure 33 Girder 3 strong-axis sectional stress from bottom flange for model with linear elastic vs. non-linear material

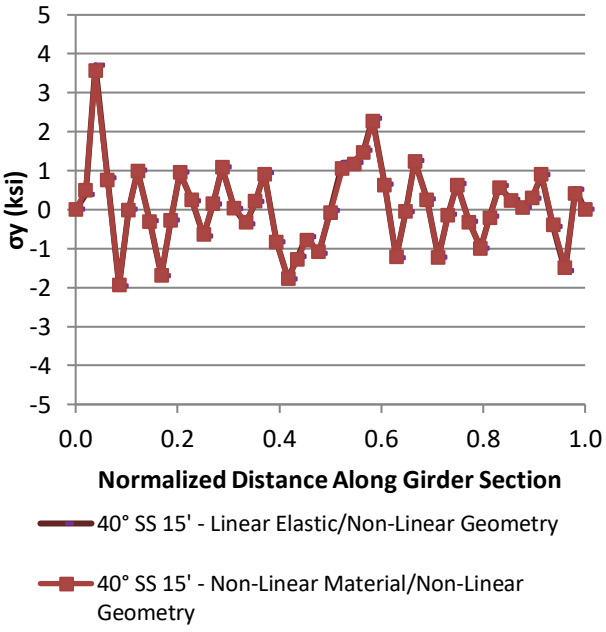

Figure 34 Girder 3 weak-axis sectional stress from the top flange for model with linear elastic vs. non-linear material

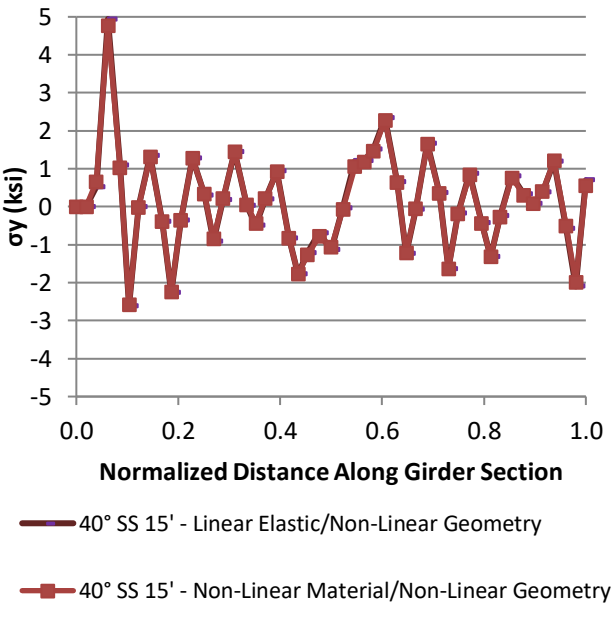

Figure 35 Girder 3 weak-axis sectional stress from the bottom flange for model with linear elastic vs. non-linear material

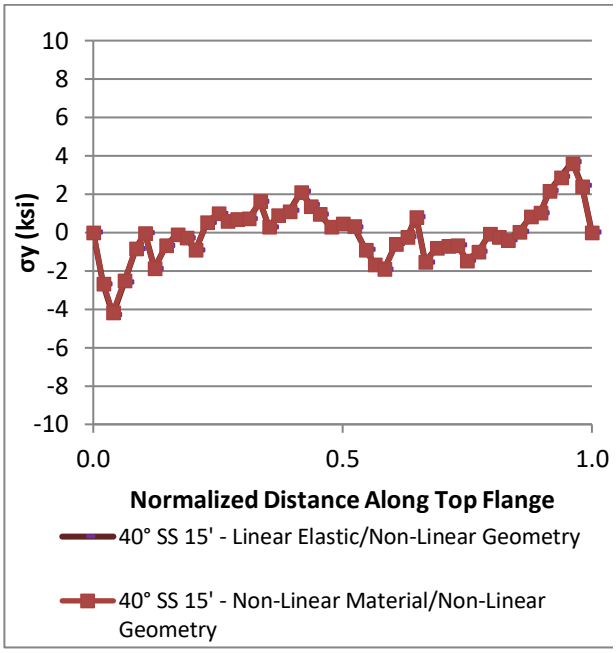

Figure 36 Girder 3 top flange out-of-plane stress for model with linear elastic vs. non-linear material

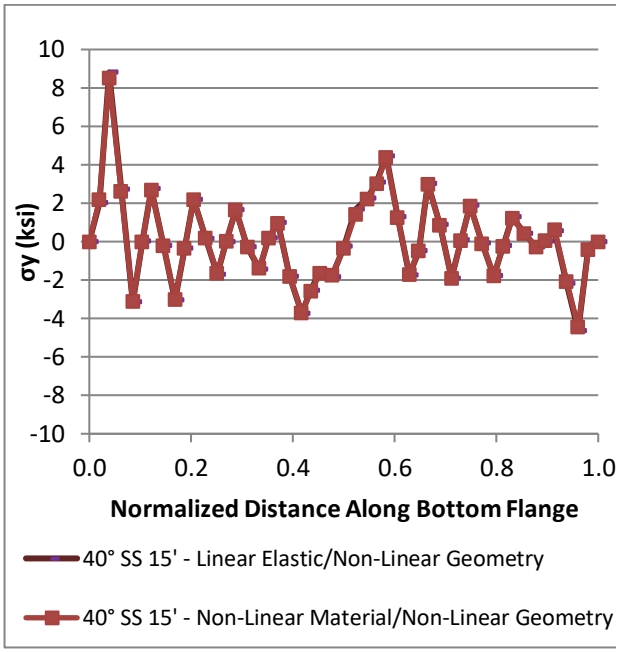

Figure 37 Girder 3 bottom flange out-of-plane stress for model with linear elastic vs. non-linear material

6.2. Effects of Overhang Bracket on System Behavior and Stability

Significant flange lateral bending may be caused by torsion from eccentric concrete deck and walkway overhang loads acting on cantilever forming brackets placed along the exterior girders, shown in Figure 38, in conjunction with skew angles exceeding 20° (AASHTO 2010). In these cases, the flange lateral bending may be considered at the discretion of the Engineer.

Data from a model of the 40° skewed-staggered bridge that included overhang bracket forces was compared with data from a model that accounted for the gravity load collected on the overhang but that was applied to the top flange of the exterior girders over the Girder 4 web, along the thick red line as shown in Figure 39.

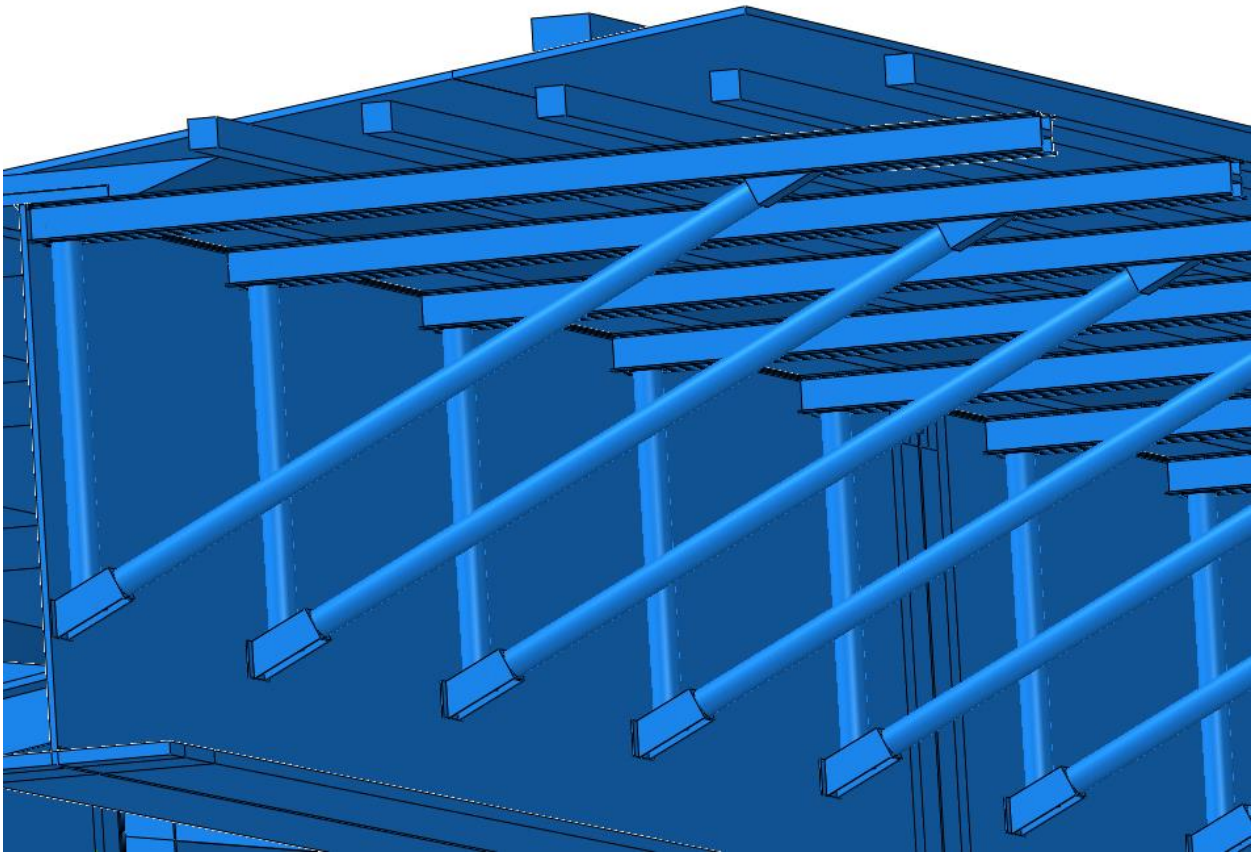

Figure 38 Overhang bracket geometry on exterior girder (not used in data collection)

The results show significant contribution of overhang loads to both lateral deflection in the exterior girder at all loading stages (Figure 40 and Figure 41) and out-of-plane flexural stresses in the exterior girder (Figure 44 through Figure 47). In-plane flexural stress for Girder 4, shown in Figure 42 and Figure 43, and stresses in Girder 3, shown in Figure 48 and Figure 49, remained consistent between the model with overhang loads and the model without overhang loads. Therefore, it can be concluded that overhang brackets loads contribute greatly to out-of-plane deflection and stresses in the exterior girders and had little effect on in-plane bending stresses. This comparison is an interesting one, because it highlights the difference in lateral flange bending stress that occurs in girders with and without the overturning effect of the overhangs, and shows that the overhang brackets induce significant levels of lateral deformation and lateral stress in the exterior girders.

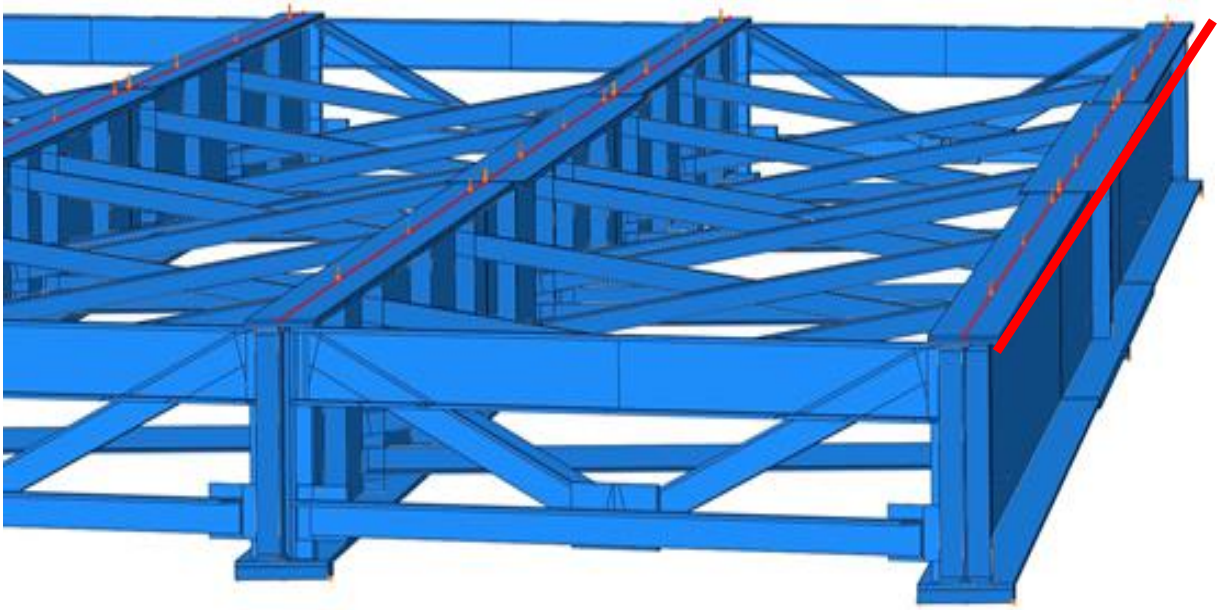

Figure 39 Model with no overhang bracket plates and overhang loads applied to the top of the exterior girder

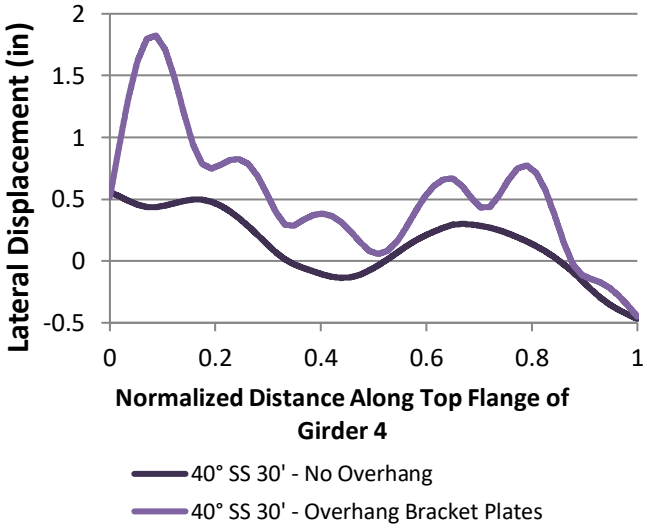

Figure 40 Girder 4 lateral displacement along the top flange for model with overhang bracket plates vs. no overhang brackets

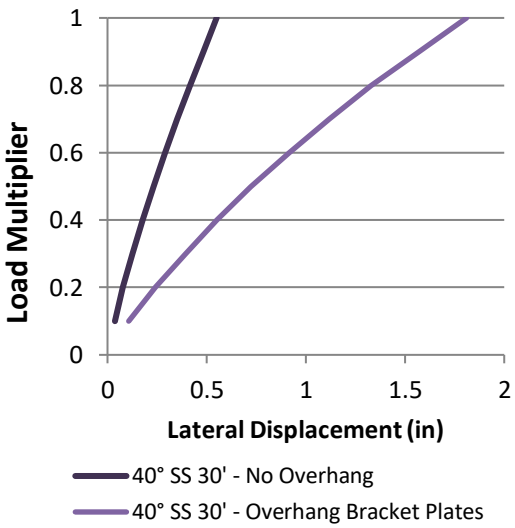

Figure 41 Girder 4 load vs. peak lateral displacement for model with overhang bracket plates vs. no overhang brackets

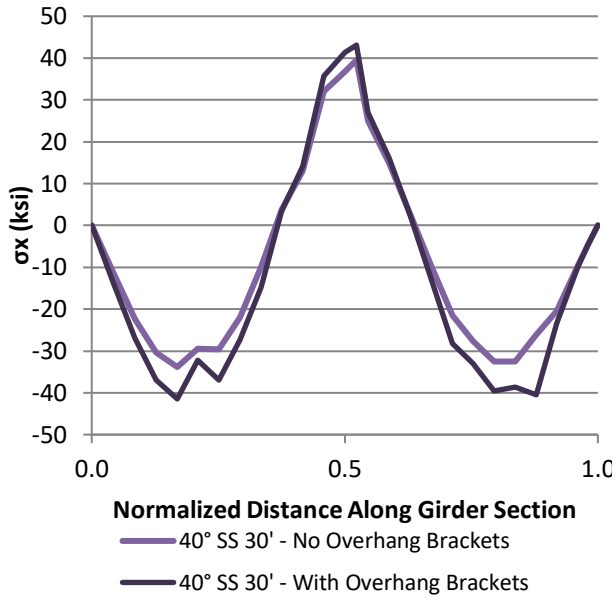

Figure 42 Girder 4 (Exterior Girder) strong-axis sectional stress from top flange for model with overhang bracket plates vs. no overhang brackets

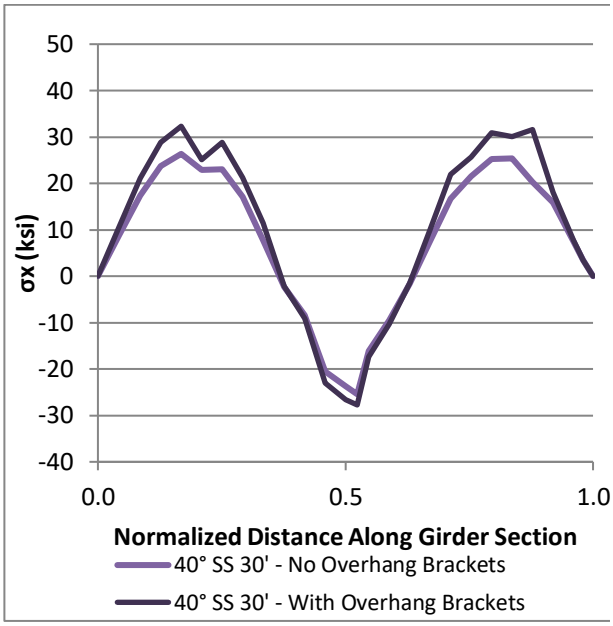

Figure 43 Girder 4 (Exterior Girder) strong-axis sectional stress from bottom flange for model with overhang bracket plates vs. no overhang brackets

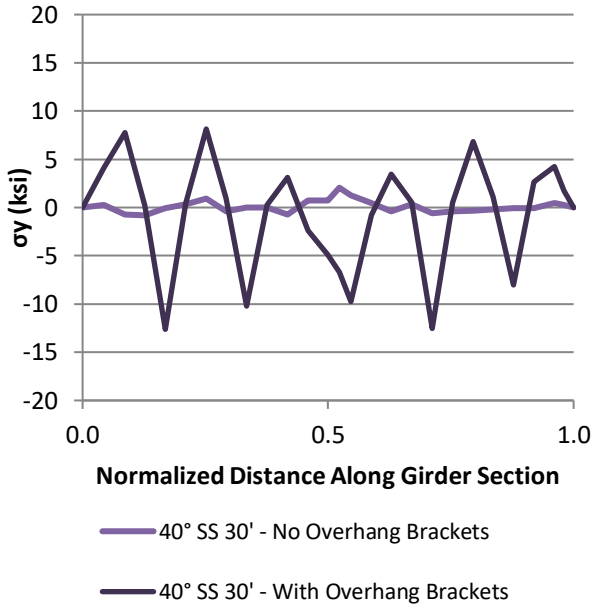

Figure 44 Girder 4 weak-axis sectional stress from the top flange for model with overhang bracket plates vs. no overhang brackets

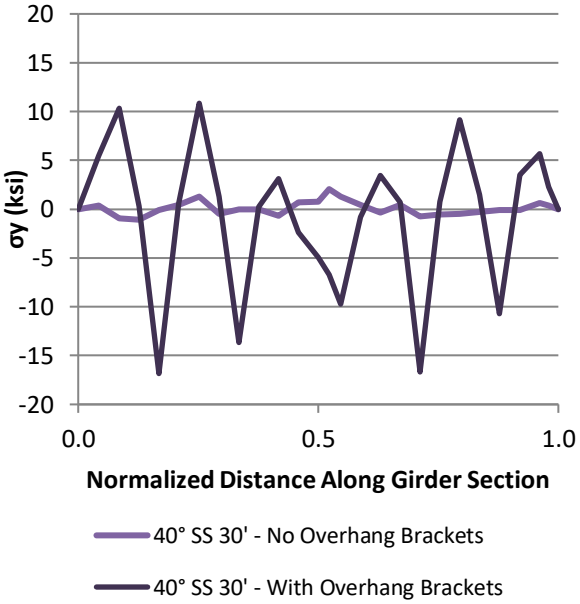

Figure 45 Girder 4 weak-axis sectional stress from the bottom flange for model with overhang bracket plates vs. no overhang brackets

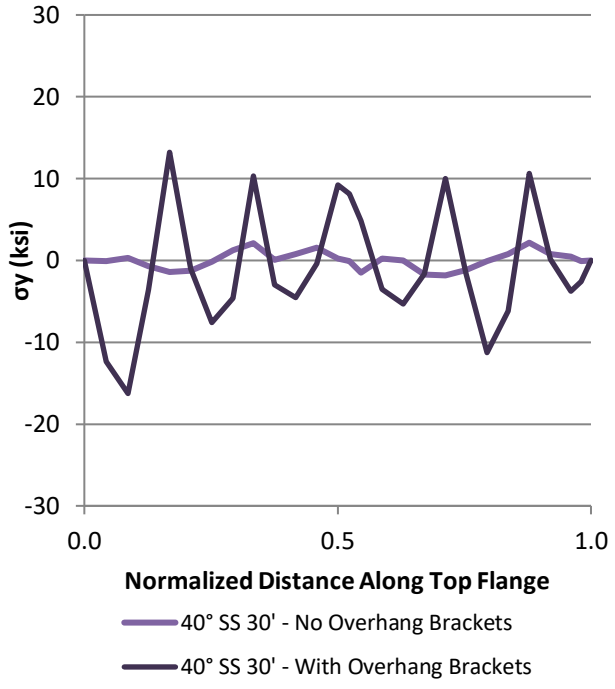

Figure 46 Girder 4 top flange out-of-plane stress for model with overhang bracket plates vs. no overhang brackets

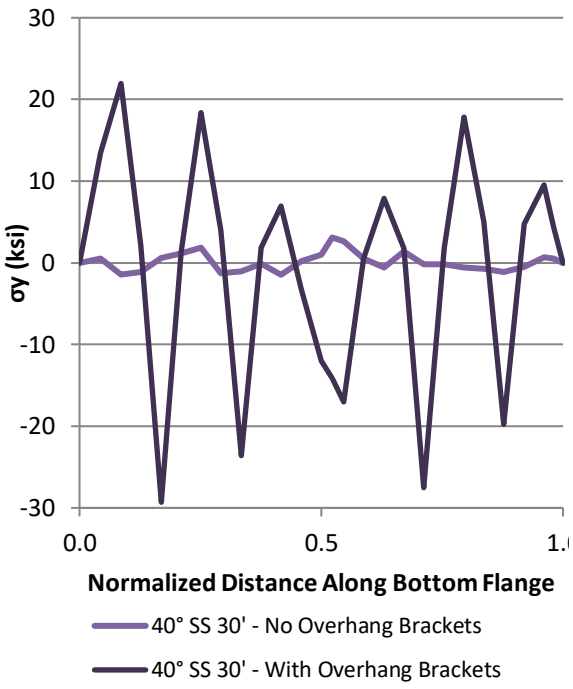

Figure 47 Girder 4 bottom flange out-of-plane stress for model with overhang bracket plates vs. no overhang brackets

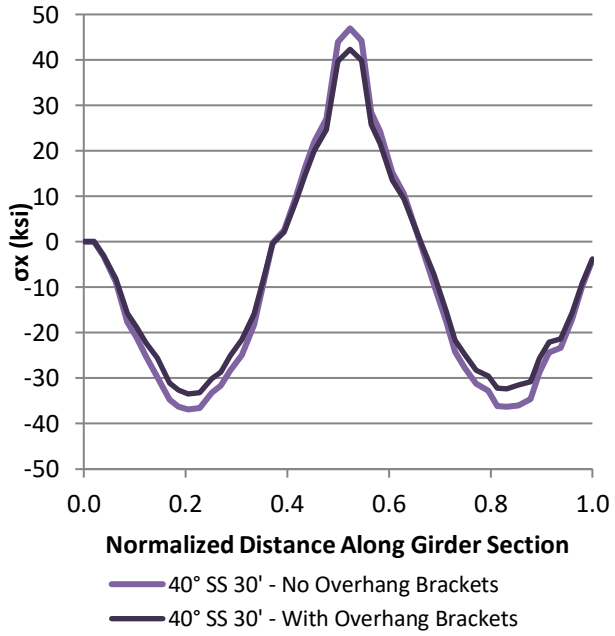

Figure 48 Girder 3 (Interior Girder) strong-axis sectional stress from top flange for model with overhang bracket plates vs. no overhang brackets

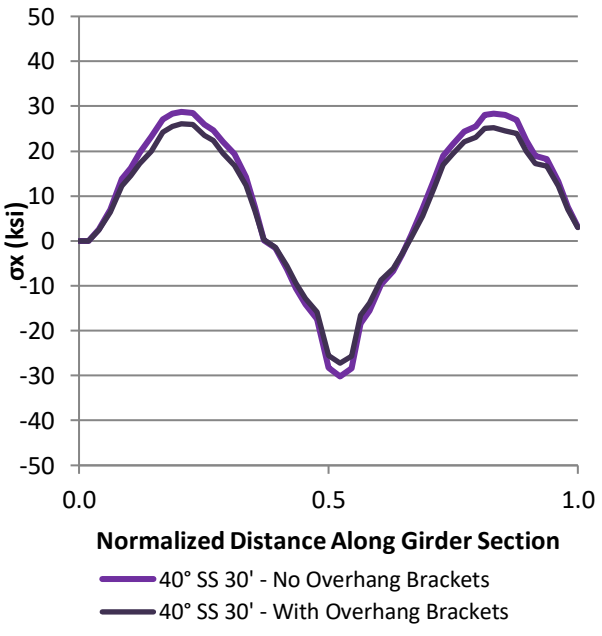

Figure 49 Girder 3 (Interior Girder) strong-axis sectional stress from bottom flange for model with overhang bracket plates vs. no overhang brackets

6.3. Examination of Skewed System Stability through Parametric Analysis

As described, the parametric study included variations of:

- Skew angle (0°, 20°, and 40°);
- Cross-frame spacing (4.6 m [15 ft.], 9.1 m [30 ft.], and 13.7 m [45 ft.]);
- Cross-frame orientation (skewed-staggered and skewed-parallel); and
- Cross-frame connection type (9.5 mm [3/8 in.] thick bent plate connection, 12.7 mm [1/2 in.] thick bent plate connection, 25.4 mm [1 in.] thick bent plate connection, and a half-pipe connection detail)

Results from the parametric study were analyzed in terms of load-deflection behavior, lateral flange stresses, cross-frame forces, and structural deformations. **Throughout the discussion that follows, results for the bridge system with 13.7 m [45 ft] cross-frame spacing is often focused on. This is not because such a system is necessarily believed to be practical or advisable, but because it highlights and amplifies the stability characteristics of the bridge systems as the parameters studied were varied, allowing differences in behavior to be examined.**

6.3.1. Lateral Deflections

Peak deflections were extracted from Span 1 because unbraced length was consistent between skewed-staggered and skewed-parallel configurations in that span.

Figure 50 shows the peak lateral deflection at varying loads in Span 1 of the exterior Girder 4, grouped by connection type for the 13.7 m [45 ft] spacing models and by configuration for models with 4.6 m [15 ft] and 9.14 m [30 ft] cross-frame spacing. Almost all the load-deflection curves were smooth and slowly flattened as load was increased, showing that rapid loss of load-carrying resistance in the girder did not occur for most models. Many of these exterior girders appeared to be exhibiting roll-over behavior, as a small increment of load resulted in a significant increase in deflection towards 100 percent of the load applied. This behavior is believed to be largely driven by the overturning force from the overhang brackets, which produces significant geometric nonlinearity (P-delta effects) in the exterior girders. The roll-over response became more exaggerated with increased cross-frame spacing, as might be expected.

The 0° non-skewed bridge with 4.6 m [15 ft] cross-frame spacing and the 20° skewed-parallel bridge with 4.6 m [15 ft] cross-frame spacing exhibited a sudden increase in lateral displacement near full loading, which may indicate a more conventional lateral-torsional buckling response. Correspondingly, shorter spans and cross-frames placed parallel to the skew angle may correspond more with traditional buckling behavior in the girder as load increases; these configurations are more effective at preventing buckling at lower loads until a critical load is reached and large lateral deflections occur. Nevertheless, the exterior girder flange in bridges that had 9.1 m [30 ft] cross-frame spacing did not displace laterally more than 46 mm [1.8 in.] and bridges with 4.6 m [15 ft] cross-frame spacing did not displace laterally more than 22 mm [0.87 in.].

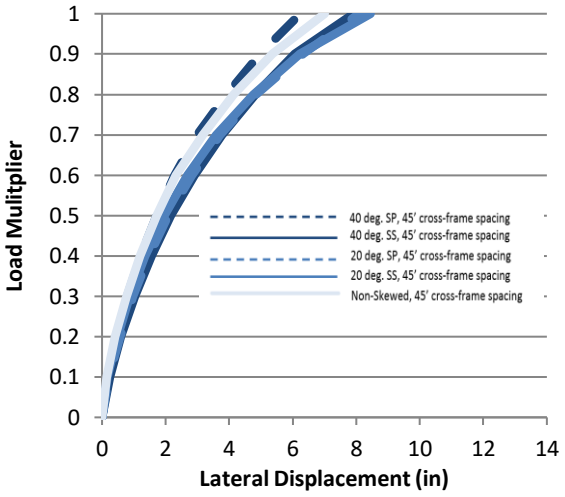

a) Half-pipe connection; 45 ft. cross-frame spacing

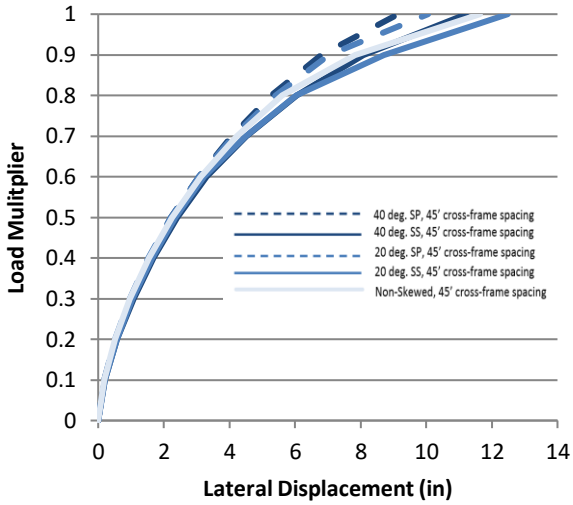

b) 25.4mm [1 in.] stiffener connection; 45 ft. cross-frame spacing

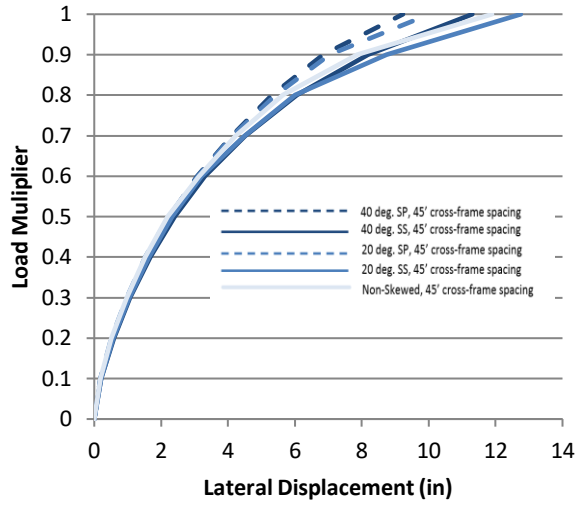

c) **12.7mm [1/2 in.] stiffener connection; 45 ft. cross-frame spacing**

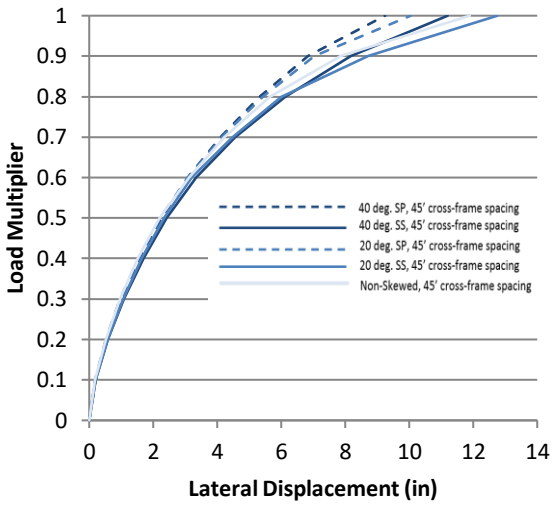

d) **9.53mm [3/8 in.] stiffener connection; 45 ft. cross-frame spacing**

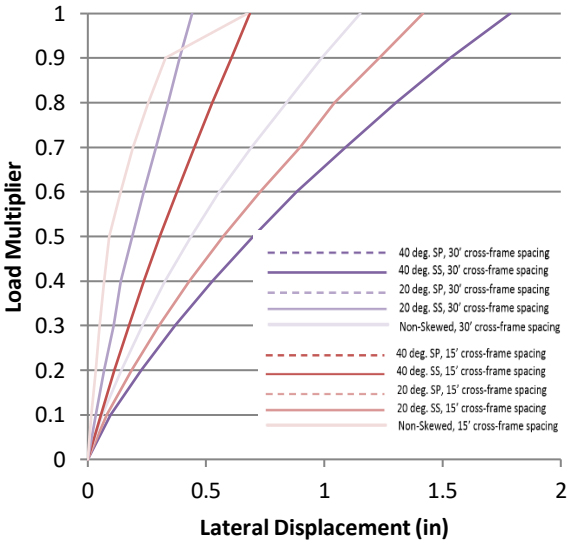

e) **Skewed-staggered, 30 and 15 ft. cross-frame spacing**

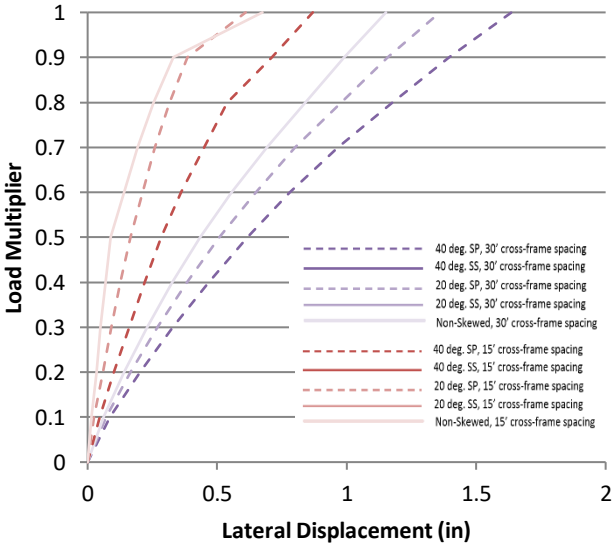

f) **Skewed-parallel, 30 and 15 ft. cross-frame spacing**

Figure 50 Load vs. peak lateral displacement

Figure 51 shows the peak lateral displacement in the top (compression) flange of Girder 4 in the positive bending region of the bridge, *grouped by connection type* for the 13.7 m [45 ft] cross-frame spacing models. The 40° skewed-parallel bridge was most resistant to lateral displacement while the 20° skewed-staggered bridge with stiffener connections was most susceptible to lateral deformations for any given connection type. The 20° skewed-staggered

bridges with 9.5 mm [3/8 in.] and 13 mm [1/2 in.] thick stiffeners produced the maximum lateral displacements of 325 mm [12.8 in.] while the 40° skewed-parallel bridge with half-pipe connection produced the lowest lateral displacement value of 158 mm [6.2 in.]. For the same skew angle, the skewed-parallel configuration performed better than the skewed-staggered configuration in the 13.7 m [45 ft] spacing models (i.e., corresponded with lower lateral displacements of the compression flange). Lateral displacements also increased with decreasing skew angle for all models except the 0° non-skewed bridge with half-pipe connection, where the lateral displacements were between that of the 40 and 20° skewed bridges.

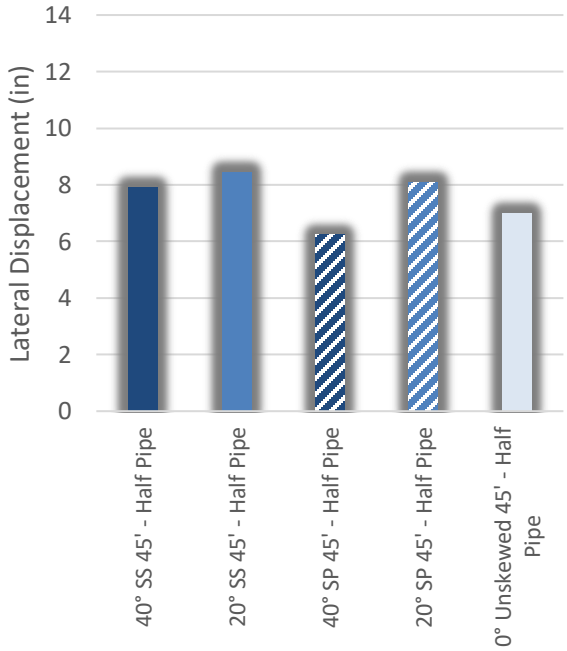

a) Half-pipe connection

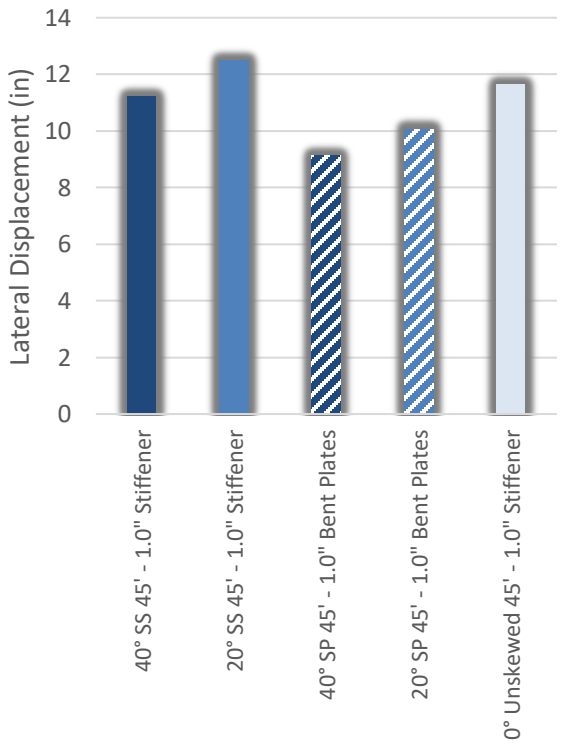

b) 25.4 mm [1 in.] stiffener connection

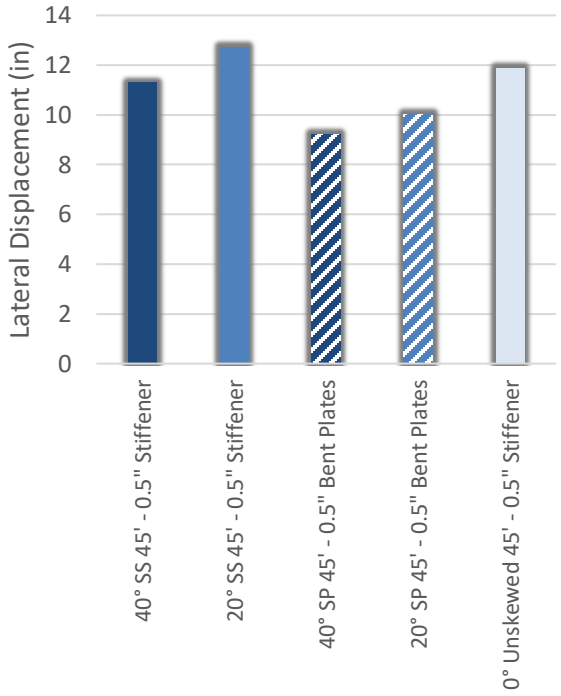

c) 12.7 mm [1/2 in.] stiffener connection

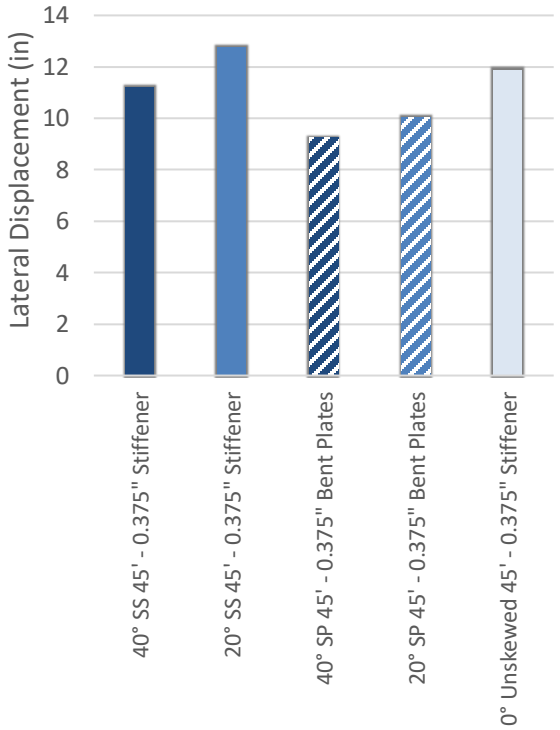

d) 9.5 mm [3/8 in.] stiffener connection

Figure 51 Girder 4 peak lateral displacement at 100% load, grouped by connection type

Figure 52 (a) through (e) shows the peak lateral displacements in the top (compression) flange of Girder 4 in the positive bending region, *grouped by skew angle and configuration*. The results show that the half-pipe connection performed best for any given skew angle and configuration (i.e., this connection was found to best limit girder compression flange lateral displacements). Lateral displacements in the exterior girder were minimally affected by varying cross-frame stiffener thicknesses.

Figure 52 (f) and (g) show peak lateral displacements for the 4.6 m [15 ft] and 9.1 m [30 ft] spacing models. Lateral displacements decreased with decreasing angle of skew, with the exception of the non-skewed bridge with 4.6 m [15 ft] cross-frame spacing. The non-skewed bridge with 4.6 m [15 ft] spacing produced lateral displacements between that of the 40 and 20° skewed bridges with the same cross-frame spacing. The overall magnitude of the displacements for the 4.6 m [15 ft] and 9.1 m [30 ft] cross-frame spacing models were relatively low. The 40° skewed-staggered bridge with 9.1 m [30 ft] cross-frame spacing produced a maximum deflection of 4.5 mm [1.8 in.] and the 40° skewed-parallel bridge with 4.6 m [15 ft] cross-frame spacing produced

a maximum deflection of 22 mm [0.87 in.]. The differences in deflection values between the skewed-staggered and skewed-parallel configurations for the same skew angle were small as well for these shorter cross-frame spacing.

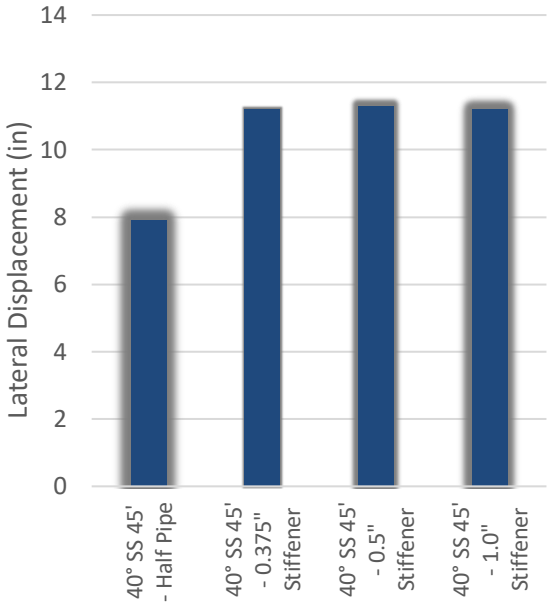

a) 40° skewed-staggered

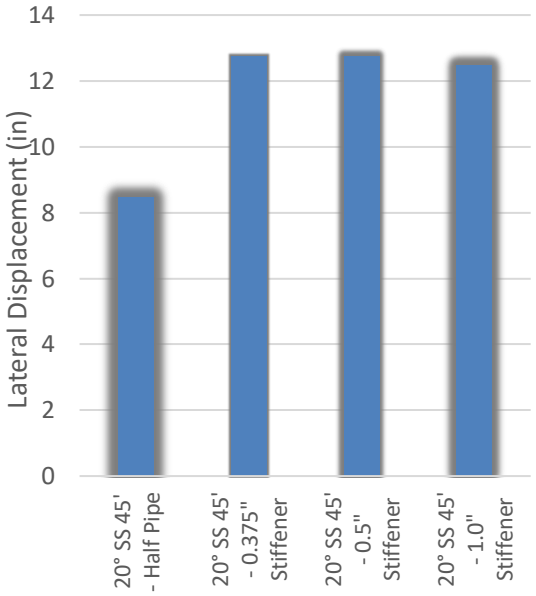

b) 20° skewed-staggered

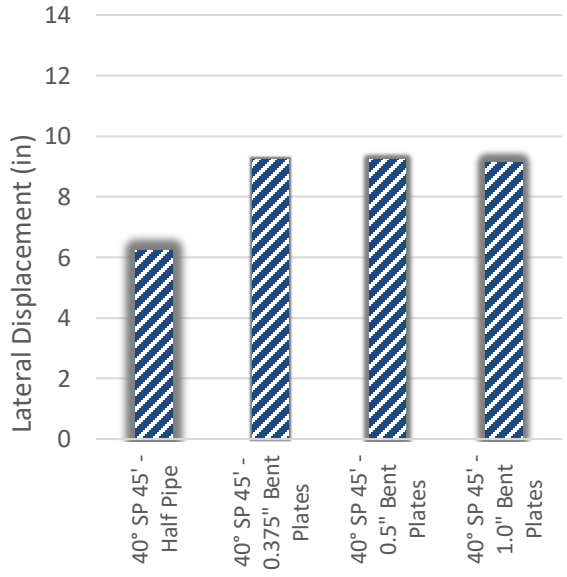

c) 40° skewed-parallel

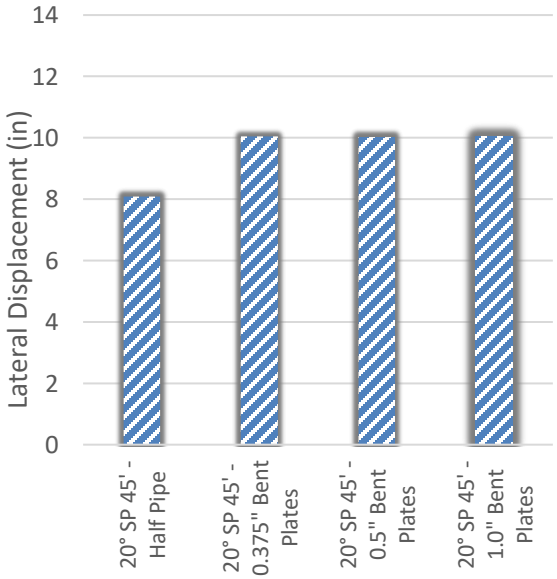

d) 20° skewed-parallel

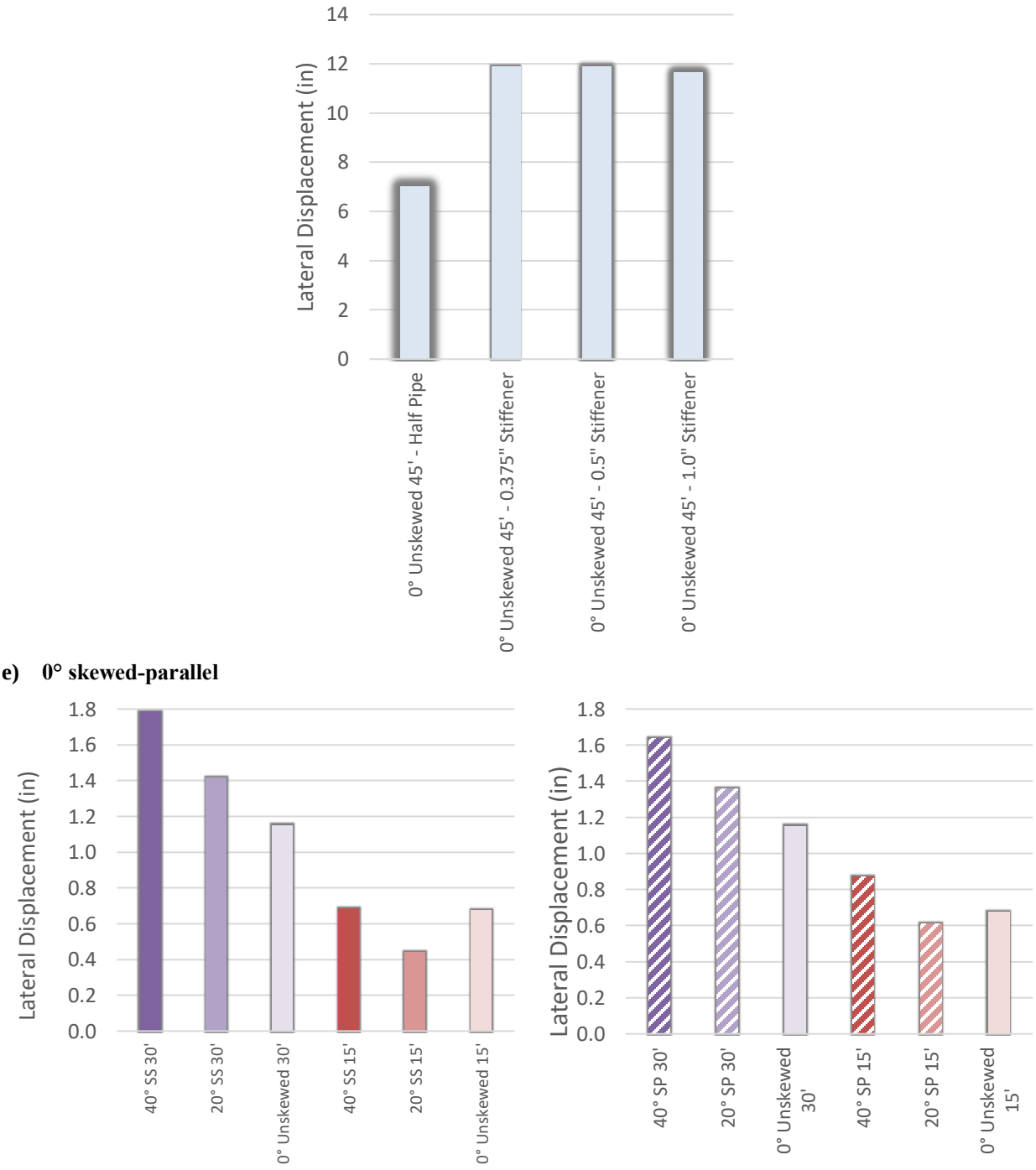

e) 0° skewed-parallel

f) Skewed-staggered, 30 and 15 ft. cross-frame spacing

g) Skewed-parallel, 30 and 15 ft. cross-frame spacing

Figure 52 Girder 4 peak lateral displacement at 100% load, grouped by skew angle and configuration

6.3.2. Cross-Frame Stresses and Behavior

The FE results were examined in terms of cross-frame stresses and behavior to gain a fuller picture of the bridge system behavior from the parametric analyses. A schematic of the cross-frame geometry included in the models is shown in Figure 53 with labeled cross-frame members.

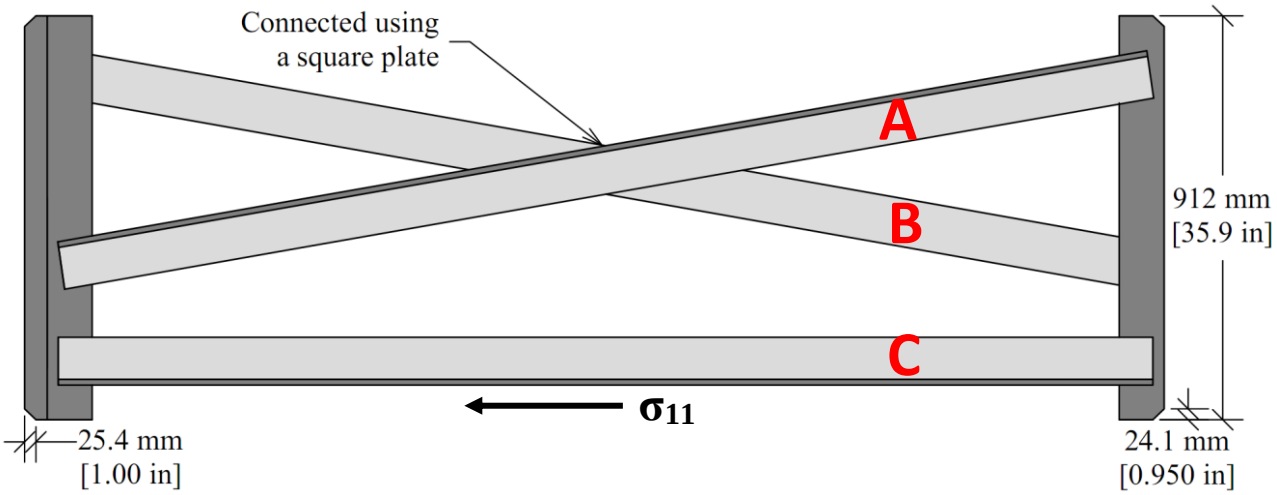

Figure 53 Cross-frame angle member labels and stress direction

Results for cross-frame Member C are presented because Member C is a compression member and has the longest unbraced length of Members A, B, and C, and therefore it controlled buckling capacity amongst the cross-frame angle members. (Members A and B were connected at the midpoint and thus have a shorter unbraced length.)

For the 13.7 m [45 ft] and 9.14 m [30 ft] cross-frame spacing models, the first interior cross-frame in Span 1, shown in Figure 54, was selected because the peak lateral deflection occurred near that location and maximum stresses were found in that cross-frame. For the 4.16 m [15 ft] cross-frame spacing models, the cross-frame at mid-span of Span 1 was selected because it produced the maximum stresses and it matches the location of the cross-frame selected for the 13.7 m [45 ft] spacing models.

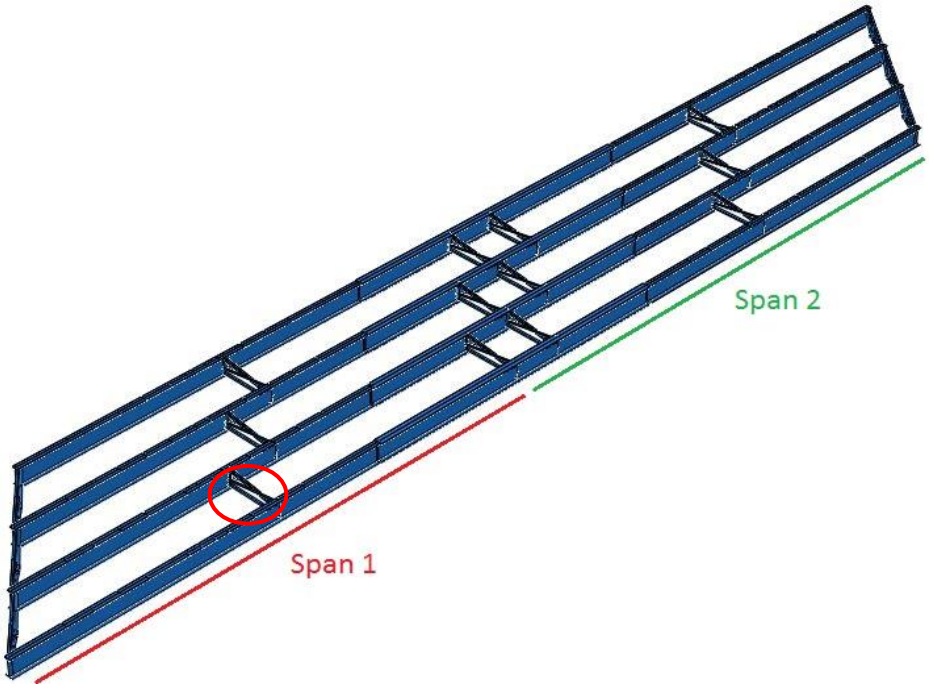

Figure 54 Cross-frame location corresponding to presented results for cross-frame stresses

Figure 55 and Figure 56 show the cross-frame member stresses in the local longitudinal direction of Member C, as labeled in Figure 53. The longitudinal stress direction of the cross-frame angle members, denoted as σ_{11}, captures all stresses in the *11*-direction, and includes both axial and bending stresses. Stresses were calculated as the average of the element stresses obtained by creating a cross-sectional cut through Member C.

Figure 55 presents the cross-frame angle member stresses, *grouped by connection type* for the 13.7 m [45 ft] cross-frame spacing models. The 40° skewed-parallel model always produced the lowest stress magnitudes for varying skew angles and configurations, followed by the 20° skewed-parallel model. It should be noted that although the cross-frame member length increases with increasing skew angle for a skewed-parallel configuration, the component of the force perpendicular to the girder line, that is the direct path for transferring lateral forces between girders, decreases with increasing skew angle. It can be seen that the skewed-parallel configuration always produced lower axial stresses than the skewed-staggered configuration for the same skew angle. Varying skew angles with the same skewed-staggered configuration also produced similar stress values, as the cross-frame member length and orientation are the same for the skewed-staggered configuration regardless of skew angle.

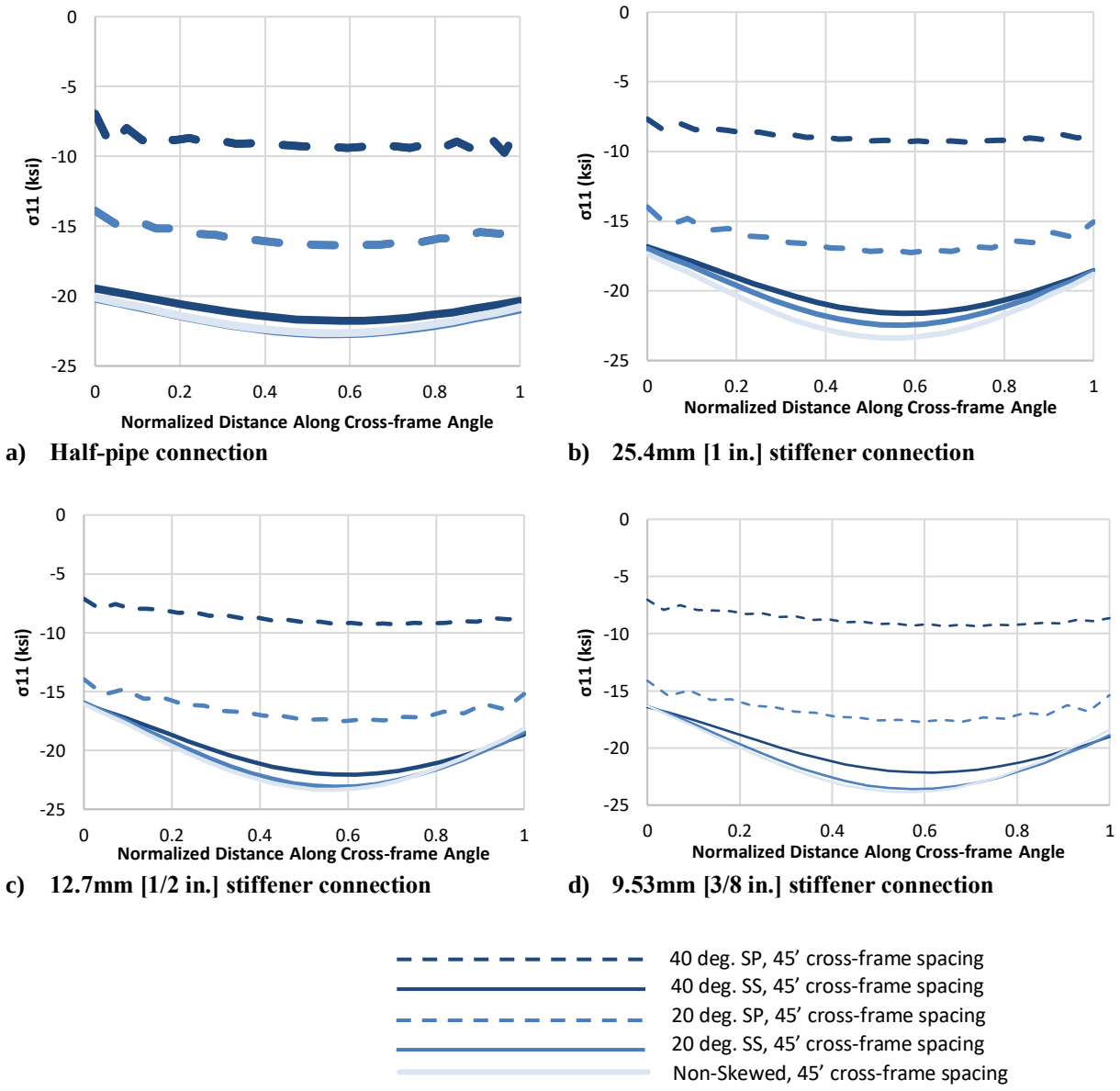

Figure 55 Cross-frame angle σ_{11} in member C, grouped by connection type

Figure 56 (a) through (e) shows the cross-frame angle member stresses in the local longitudinal direction of Member C, *grouped by skew angle and configuration* for the 13.7 m [45 ft] cross-frame spacing models. For any given skew angle and configuration, the 4.6 m [15 ft] cross-frame spacing models always produced the lowest cross-frame stresses while the 13.7 m [45 ft] cross-frame spacing always produced the highest stresses. While the models that included the half-pipe connection sometimes produced higher stresses near the connection ends, the connection

type did not produce significant differences in stress magnitudes at a location removed from the connection. Figure 56 (f) and (g) groups cross-frame angle member stresses by configuration for the 4.6 m [15 ft] and 9.14 m [30 ft] cross-frame spacing models. The 4.6 m [15 ft] cross-frame spacing models produced lower stresses than the 9.14 m [30 ft] cross-frame spacing models, which can be expected as there are twice as many braces when the cross-frame spacing is halved.

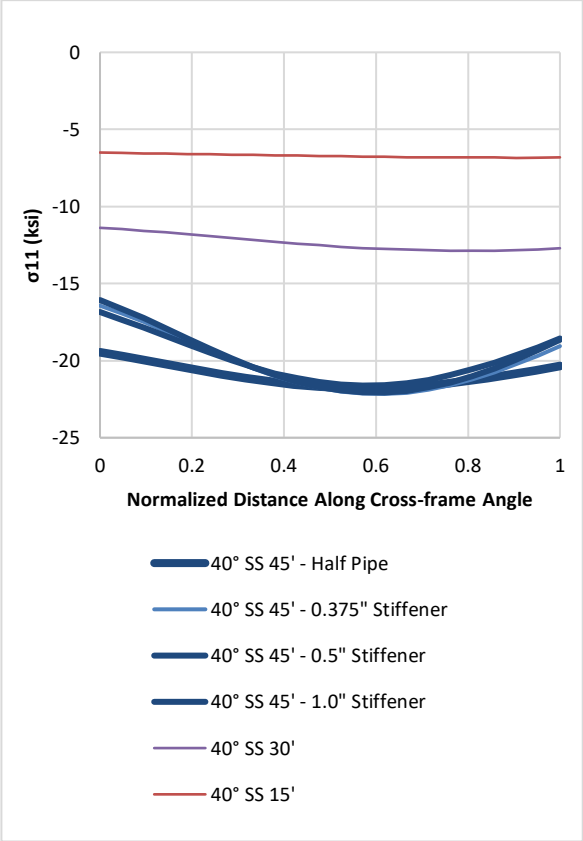

a) 40° skewed-staggered

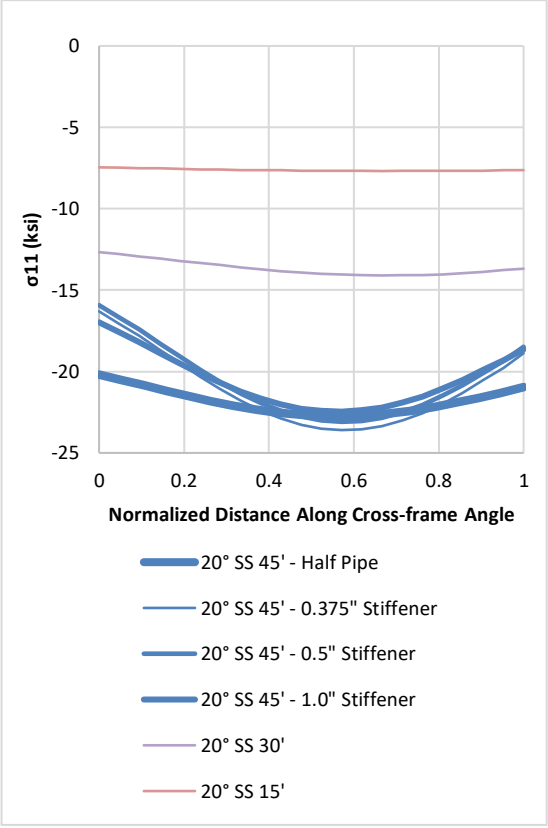

b) 20° skewed-staggered

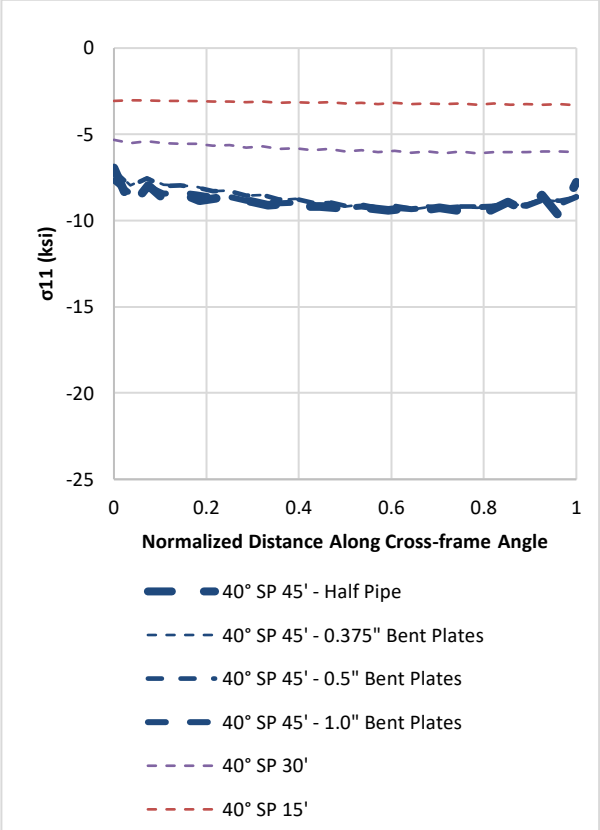

c) 40° skewed-parallel

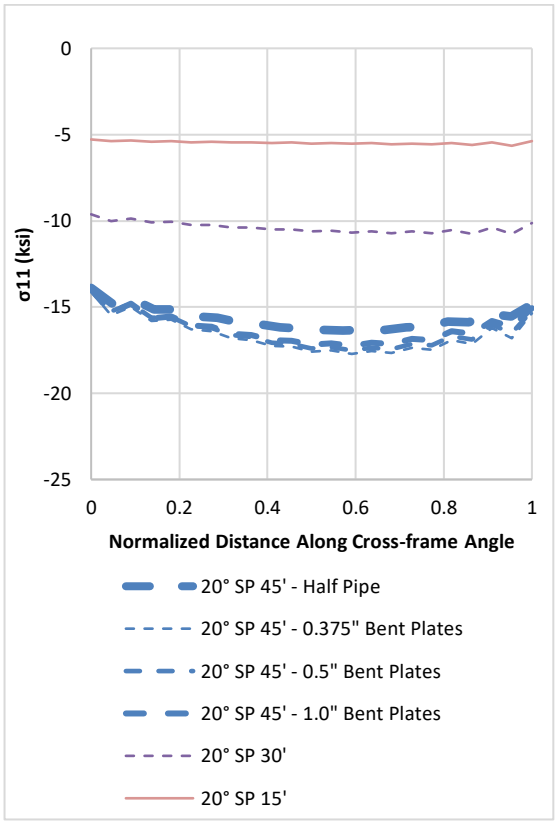

d) 20° skewed-parallel

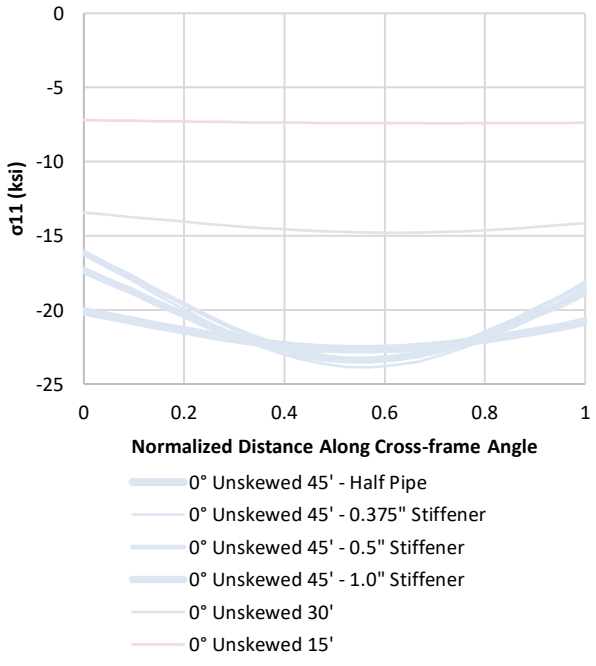

e) Non-skewed

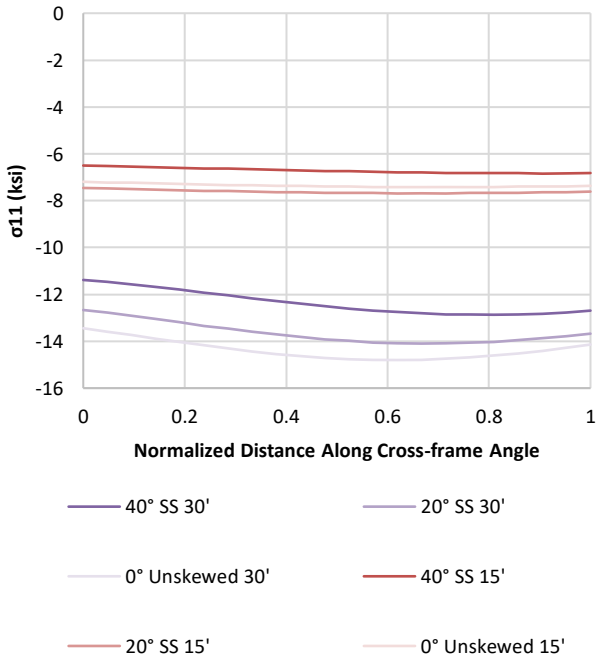

f) Skewed-staggered, 30 and 15 ft. spacing

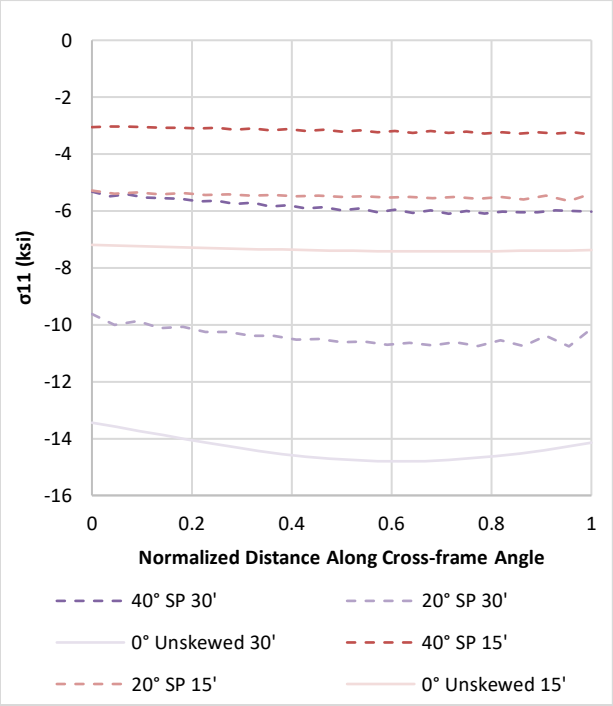

g) Skewed-parallel, 30 and 15 ft. spacing

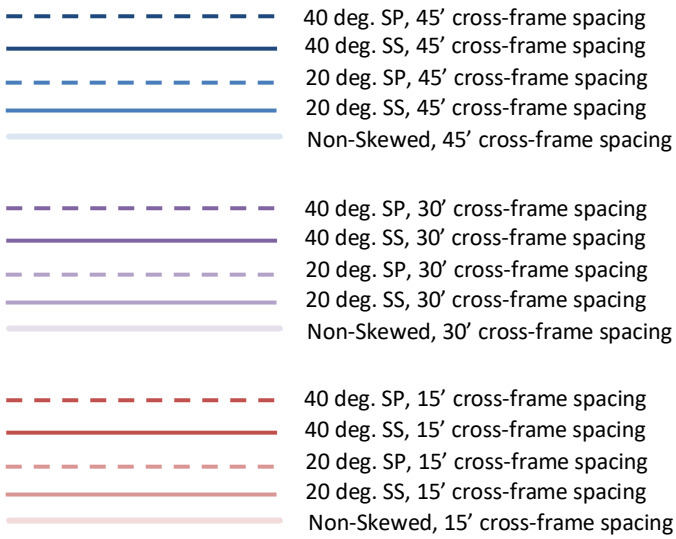

Note: heavier line weights indicate stiffer connection elements

Figure 56 Cross-frame angle σ_{11} in member C, grouped by skew angle and configuration

In Figure 57 and Figure 58, the peak cross-frame angle member stresses, σ_{11}, in Member C are shown normalized by their critical buckling stress. Normalizing the angle member stresses by their respective critical buckling values allowed for a comparison between angle members of

different lengths. Member C angle lengths, L, and critical buckling stresses, σ_{cr}, are shown in Table 2. The critical buckling stress, σ_{cr}, was equated as Euler's critical load, P_{cr}, applied per cross-sectional area, A, of the cross-frame angle member:

$$\sigma_{cr} = P_{cr}/A$$

where

P_{cr} = Euler's critical buckling load

A = cross-sectional area

Euler's critical load, P_{cr}, is given by the expression:

$$P_{cr} = \frac{\pi^2 E * I_z}{(K*L)^2}$$

where

E = modulus of elasticity of the member material

I_z = moment of inertia about the weak principal axis

K = effective length factor, conservatively taken as 1.0 for pinned-pinned

L = unsupported length of the member

Table 2 Member C angle section properties and critical buckling values

Skew Angle	Configuration	Connection Type	I_z (mm^4) [in^4]	L (mm) [in.]	P_{cr} (kN) [kips]	A (mm^2) [in^2]	σ_{cr} (MPa) [ksi]
0, 20, 40	Skewed-Staggered	Stiffener	1.153E+06 [2.769]	2985 [117.5]	255.6 [57.45]	2581 [4.000]	99.03 [14.36]
0, 20, 40	Skewed-Staggered	Half-pipe	1.153E+06 [2.769]	2713 [106.8]	309.3 [69.53]	2581 [4.000]	119.8 [17.38]
20	Skewed-Parallel	Stiffener	1.679E+06 [4.035]	3086 [121.5]	348.2 [78.27]	3377 [5.234]	103.1 [14.95]
20	Skewed-Parallel	Half-pipe	1.679E+06 [4.035]	2924 [115.1]	388.0 [87.22]	3377 [5.234]	114.9 [16.66]
40	Skewed-Parallel	Stiffener	3.136E+06 [7.535]	3840 [151.2]	419.6 [94.32]	4183 [6.484]	100.3 [14-1/25]
40	Skewed-Parallel	Half-pipe	3.136E+06 [7.535]	3706 [145.9]	450.6 [101.3]	4183 [6.484]	107.7 [15.62]

Figure 57 shows the peak cross-frame angle member σ_{11} in Member C normalized by the critical buckling stress, *grouped by connection type* for the 13.7 m [45 ft] cross-frame spacing models. All skewed-staggered and non-skewed models were beyond the critical buckling stress, with the 20 and 0° skew angle models producing the highest cross-frame angle member stress

ratios. Smaller skew angles produced higher stresses for the same configuration and connection type. The skewed-parallel configuration produced much lower stress ratios compared to the skewed-staggered configuration, with the 40° skewed-parallel bridge with 13.7 m [45 ft] cross-frame spacing having the lowest stress ratio at around 60 percent for all connection types.

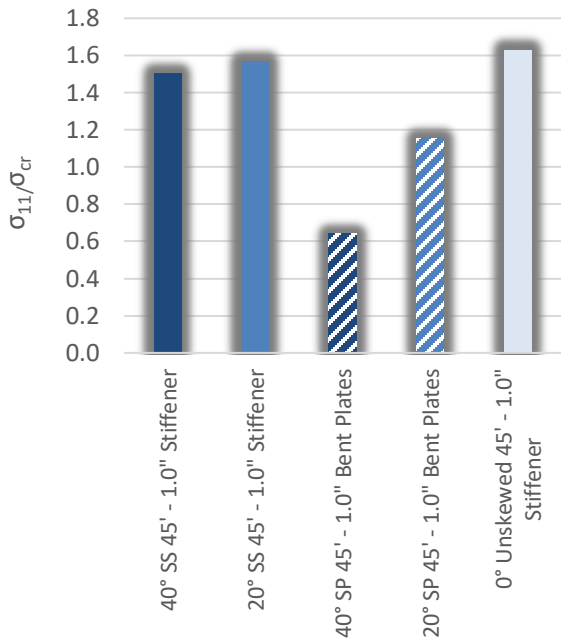

a) Half-pipe connection

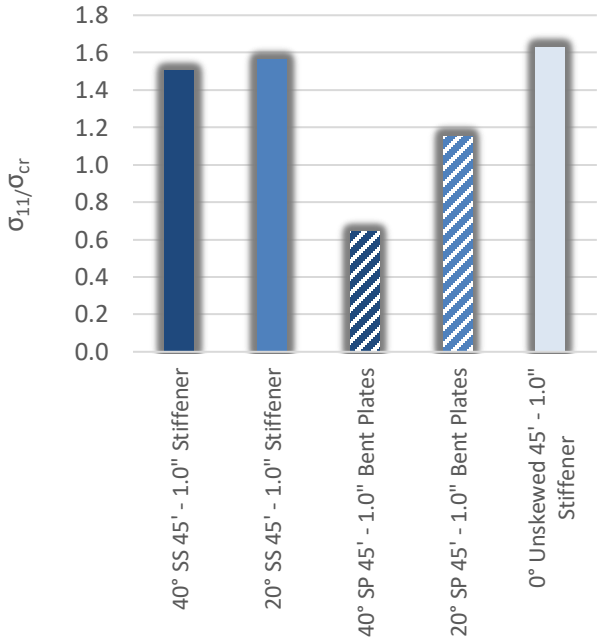

b) 25.4mm [1 in.] stiffener connection

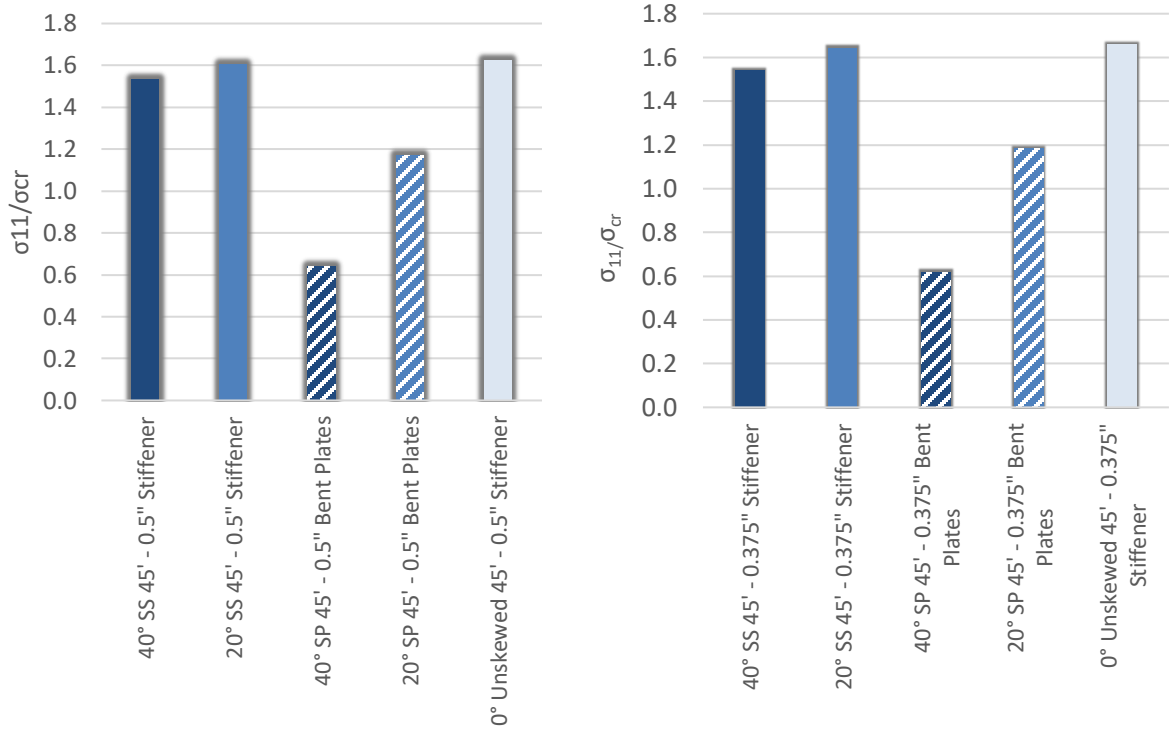

c) 12.7mm [1/2 in.] stiffener connection **d) 9.53mm [3/8 in.] stiffener connection**

Figure 57 Cross-frame angle σ_{11} normalized by critical buckling stress in member C, grouped by connection type

Figure 58 (a) through (e) shows the peak cross-frame angle Member C σ_{11} normalized by the critical buckling stress, *grouped by skew angle and configuration* for the 13.7 m [45 ft] cross-frame spacing models. The half-pipe connection produced lower stress ratios compared to stiffener connections of any thickness. While stress ratios typically decreased with increasing stiffener thickness, the differences in stress ratios between varying stiffener thicknesses were not significant. The 40° skewed-parallel bridge with 13.7 m [45 ft] cross-frame spacing produced the lowest stress ratio and stress variations in the cross-frame member for different connection types were minimal.

Figure 58 (f) and (g) groups peak cross-frame angle member stress ratios by configuration for the 4.6 m [15 ft] and 9.14 m [30 ft] cross-frame spacing models. Stress ratios increased with decreasing skew angle for these shorter cross-frame spacing models. The exception was the non-skewed bridge with 4.6 m [15 ft] cross-frame spacing, which had almost the same stress ratio as the 20° skewed-staggered model with the same cross-frame spacing. This stress increase for

decreasing skew angle was more pronounced for the skewed-parallel configuration than for the skewed-staggered configuration even though the magnitude of the stress ratios were lower for the skewed-parallel configuration.

While finite element analysis can generally reproduce trends in the variation of stress values, the magnitudes may not be reliably predicted. A course meshing for the cross-frame members was chosen to efficiently run these bridge models using large displacement theory. A more detailed modeling of cross-frame members and connections is recommended in future simulations to more accurately model the stress gradients within the members and restraints provided by the physical cross-frames.

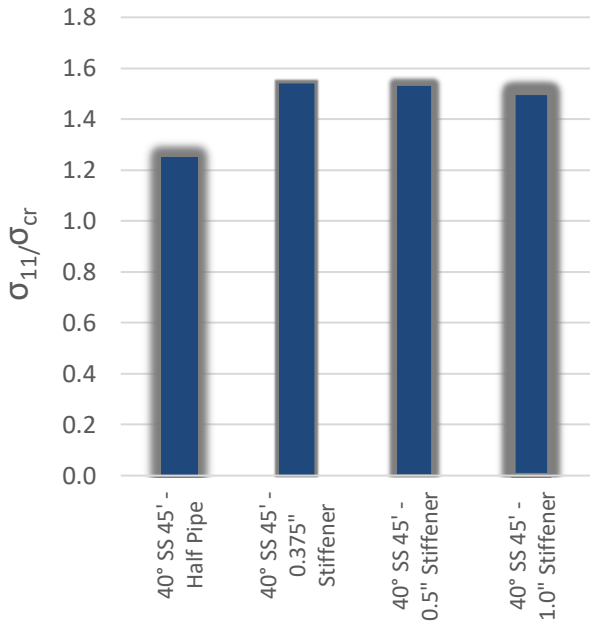

a) 40° skewed-staggered

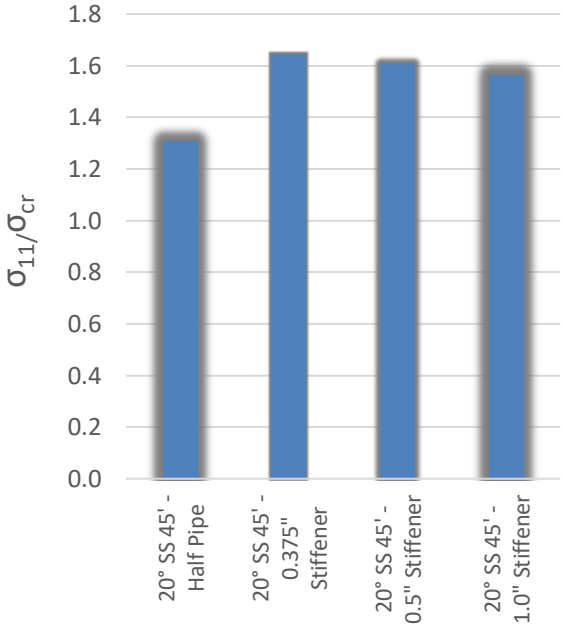

b) 20° skewed-staggered

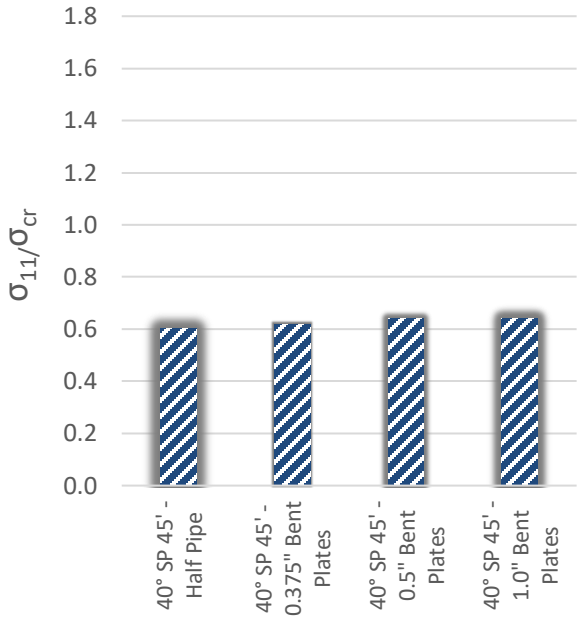

c) 40° skewed-parallel

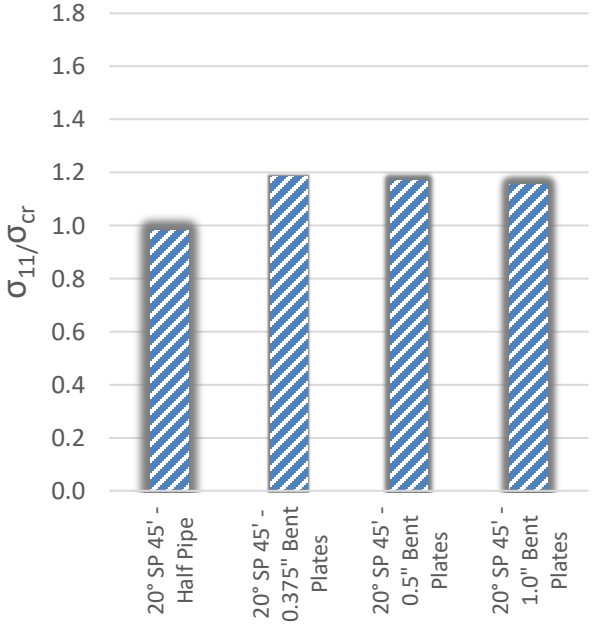

d) 20° skewed-parallel

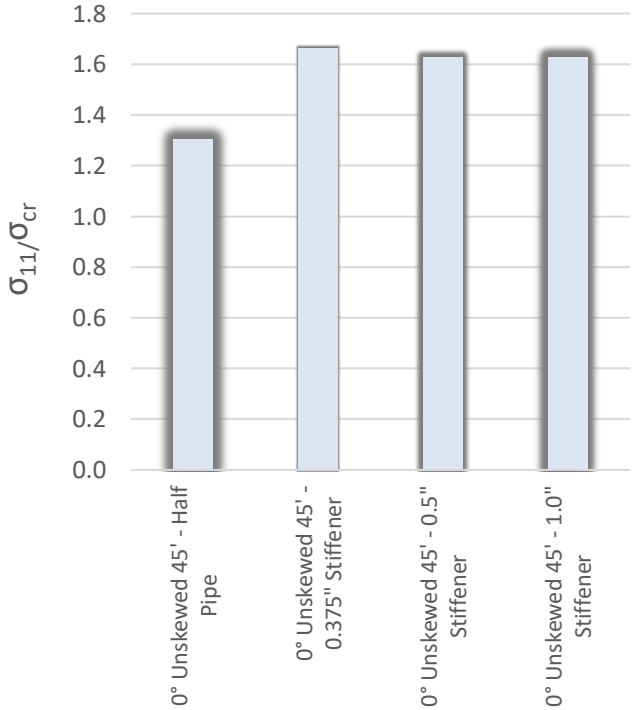

e) Non-skewed bridge

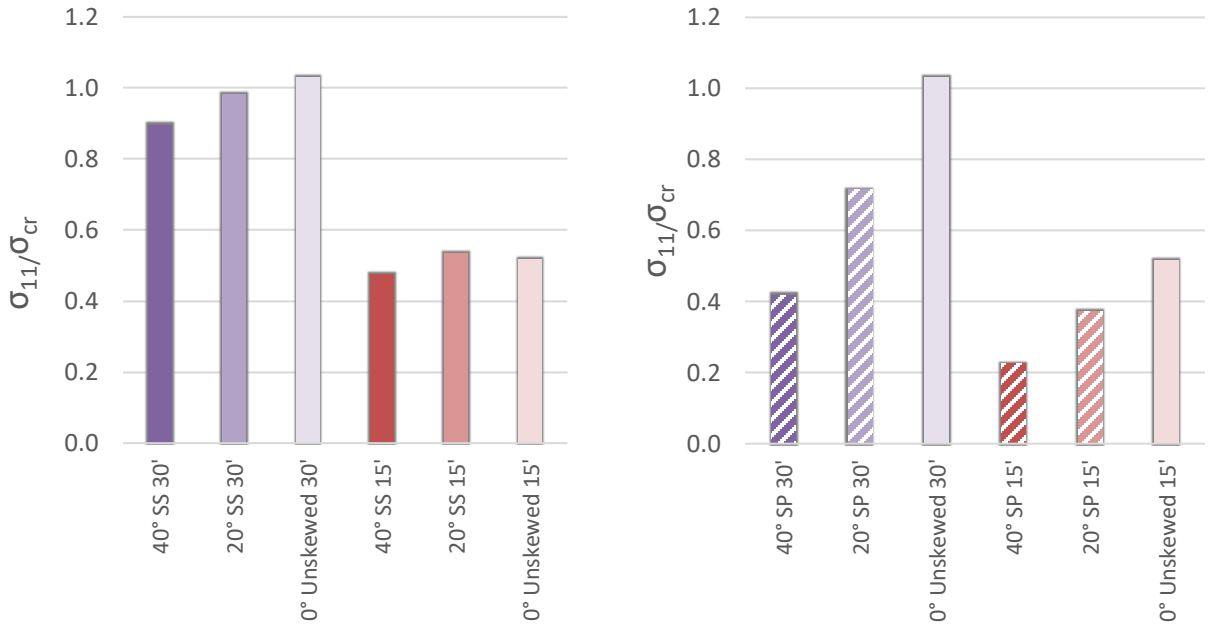

f) Skewed-staggered, 30 and 15 ft. spacing **g) Skewed-parallel, 30 and 15 ft. spacing**

Figure 58 Cross-frame angle σ_{11} normalized by critical buckling stress in member C, grouped by skew angle and configuration

6.3.3. Deformed Shapes of the Bridge FE Models, and Cross-Frame Effectiveness

Figure 59, Figure 60, Figure 61, and Figure 62 present views of the deformed configurations for a 40° and 20° bridge system in both the skewed-parallel and skewed-staggered configuration. Overall, it can be seen that the cross-frames are effective brace members for all connections, configurations, and spacing. This is apparent in that there is no apparent girder deflection at the brace points, showing that the braces are effective in producing the expected mode of girder buckling. Appendix A of this report also presents deformed shapes for every model in the parametric analyses.

Figure 59 shows the 40° skewed-parallel bridge with 13.7 m [45 ft] cross-frame spacing and stiffener connections in plan view. Only the cross-frames, webs, and bottom flanges are shown. The image is scaled to twice the actual deformation, with the color map showing Mises stresses from 0 MPa [0 ksi] in dark blue to 345 MPa [50 ksi] in red. Both the first and second unbraced lengths of the exterior girder in Span 1, better shown in Figure 60, are buckled and exhibiting roll-

over behavior. Even with high stresses in the cross-frame members and stiffeners, these images show that the cross-frames are effectively bracing the girder and producing an inflection point between the two unbraced lengths.

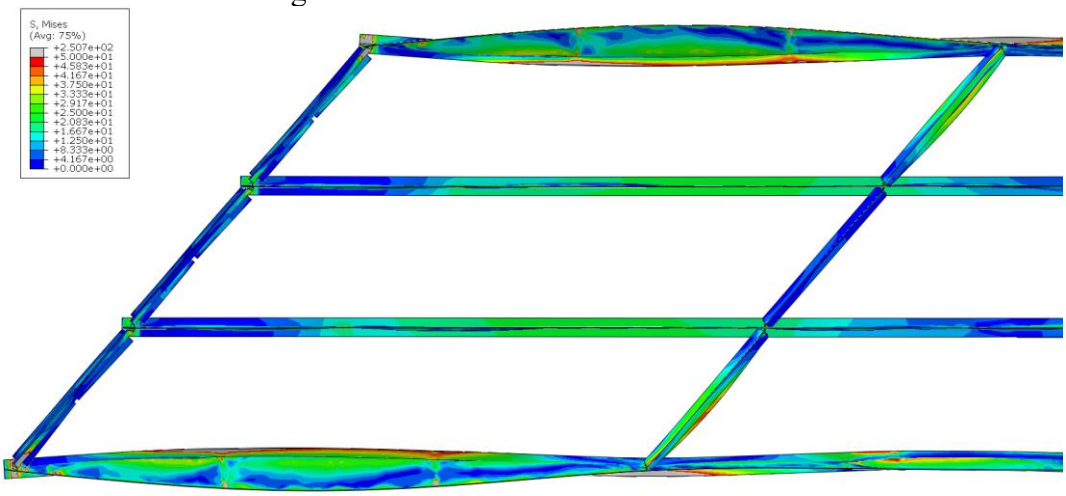

Figure 59 Deformed shape of the 40° skewed-parallel bridge with 13.7 m [45 ft] cross-frame spacing (plan view)

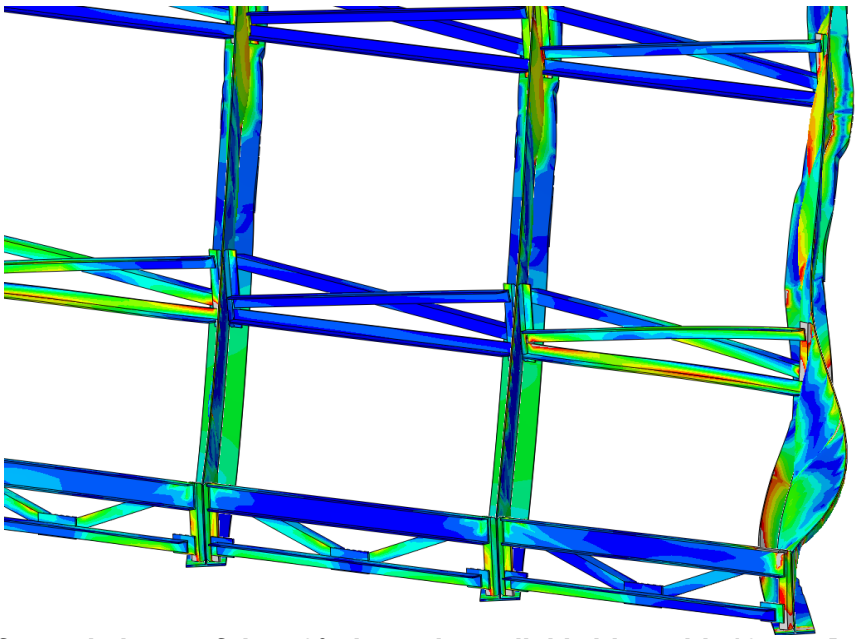

Figure 60 Deformed shape of the 40° skewed-parallel bridge with 13.7 m [45 ft] cross-frame spacing in Span 1 (plan view)

Figure 61 show the 20° skewed-staggered bridge with 13.7 m [45 ft] cross-frame spacing and half-pipe connections in plan view. Again, only the cross-frames, webs, and bottom flanges are shown. The image is scaled to twice the actual deformation, with the color map showing Mises stresses from 0 MPa [0 ksi] in dark blue to 345 MPa [50 ksi] in red. Not only does the half-pipe

connection brace the girders better than the stiffener connections, but there are lower stresses in the half-pipe connection itself, as shown in Figure 62.

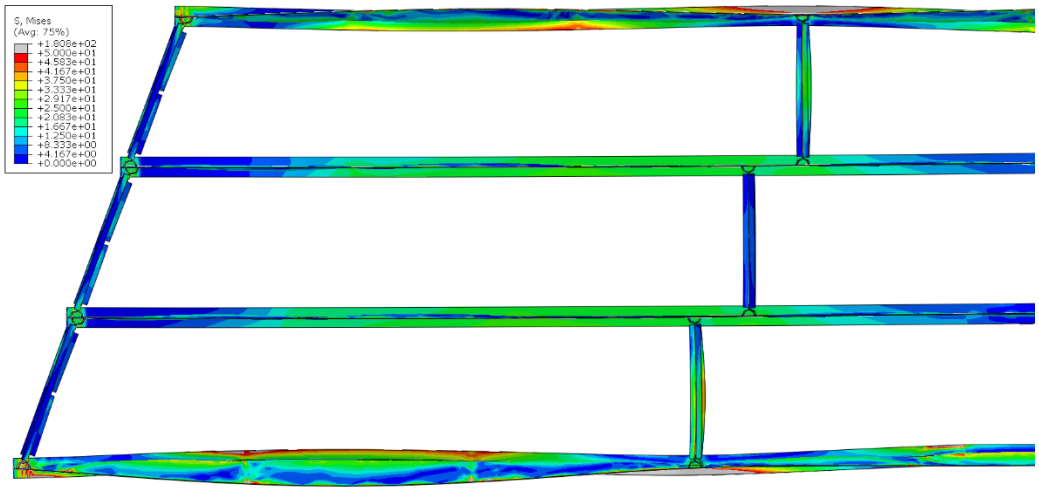

Figure 61 Deformed shape of the 20° skewed-staggered bridge with 13.7 m [45 ft] cross-frame spacing in plan view

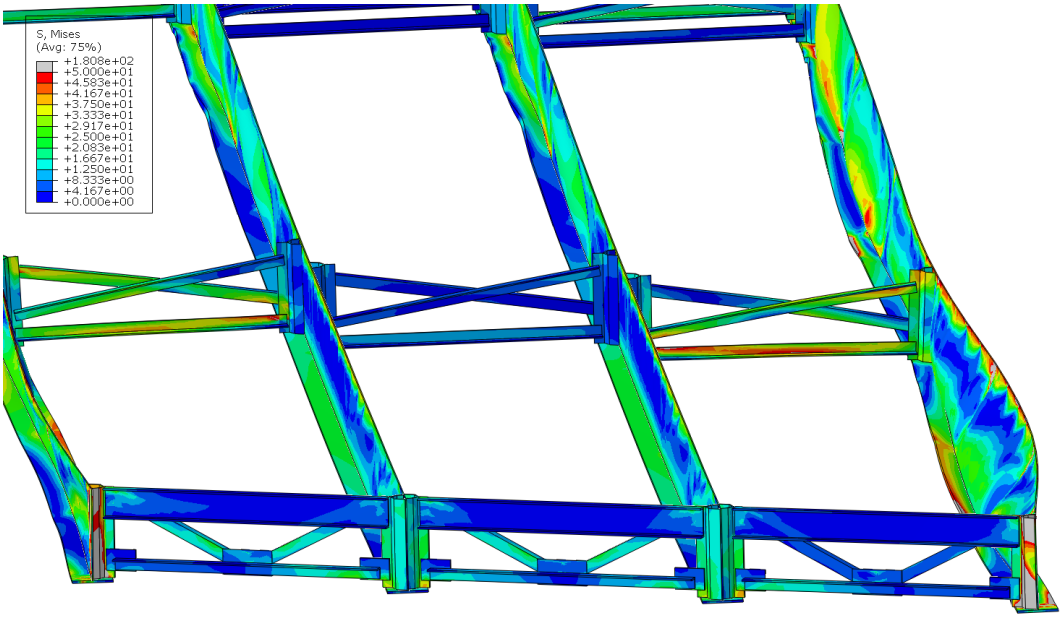

Figure 62 Deformed shape of the 20° skewed-staggered bridge with 13.7 m [45 ft] cross-frame spacing in Span 1

6.3.4. Interior Girder Strong-axis and Weak-axis Stresses

Figure 63, Figure 64, Figure 65, and Figure 66 present strong-axis bending stress, weak-axis bending stress, top flange out-of-plane bending stress, and bottom flange out-of-plane bending

stress respectively for interior Girder 3, grouped by connection type, for the 13.7 m [45 ft] cross-frame spacing models. It was found that the skewed-staggered configuration produced significantly higher out-of-plane stresses in the interior girder near mid-span compared to the skewed-parallel configuration. This is due to unbalanced, lateral cross-frame forces from the exterior girder being transferred as bending in the interior girder. Not only is there a higher component of the lateral load transferred through the cross-frames between girders for the skewed-staggered configuration, that load must also be transferred through weak-axis bending of the interior girder to reach the brace on the opposite side of the girder.

Results from a simple beam-line analysis of the respective girders are again presented with strong-axis sectional stresses. The data shows that all out-of-plane stresses for Girder 3 were significantly lower than out-of-plane exterior girder stresses due to the bracket overhang loading on the exterior girder. The maximum out-of-plane weak-axis sectional stress was less than 68.9 MPa [10 ksi]. Strong-axis girder stresses for the interior girder were also lower compared to the exterior girder. As a result, lateral torsional buckling will likely occur in the exterior girders prior to it occurring in the interior girders due to the significant eccentricity coming from the overhang brackets.

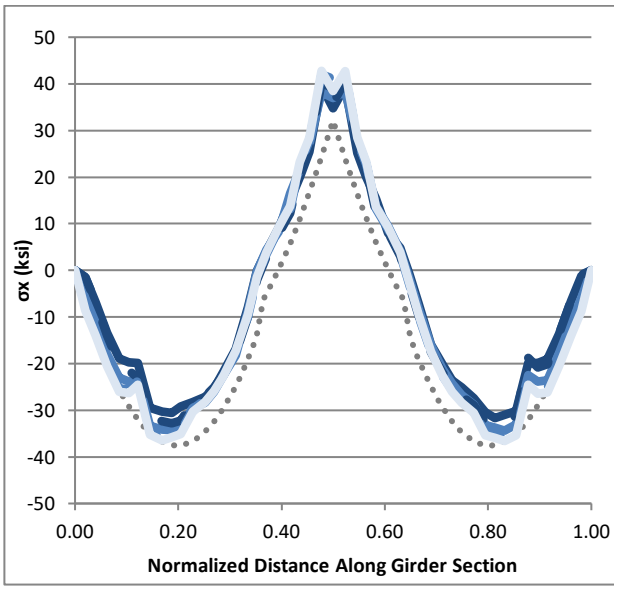

a) Half-pipe connection – Top Flange

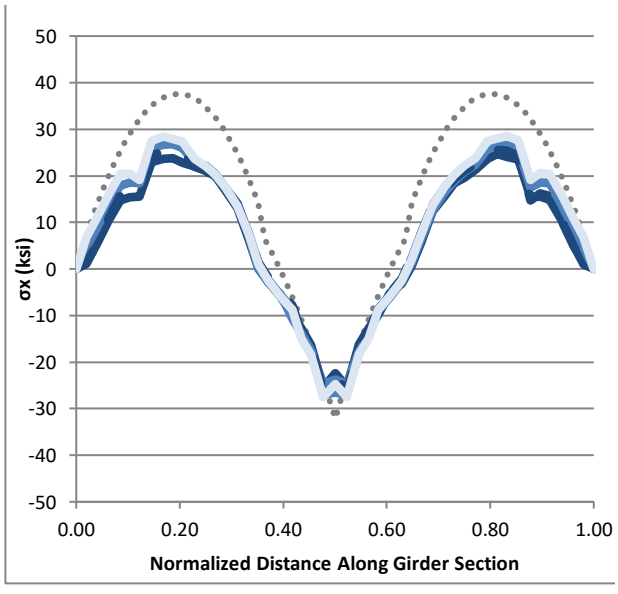

b) Half-pipe connection – Bottom Flange

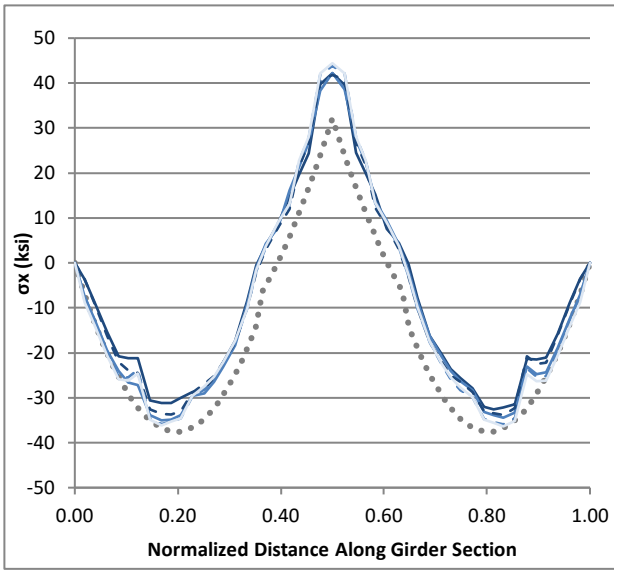

c) .53mm [3/8 in.] stiffener connection – Top Flange

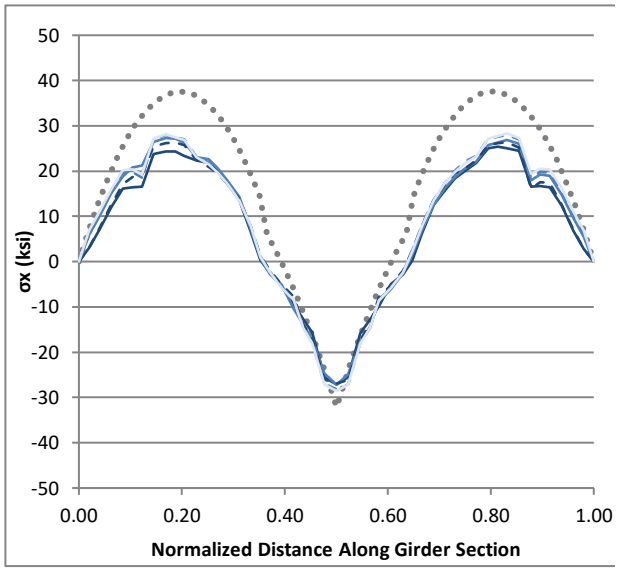

d) 9.53mm [3/8 in.] stiffener connection – Bottom Flange

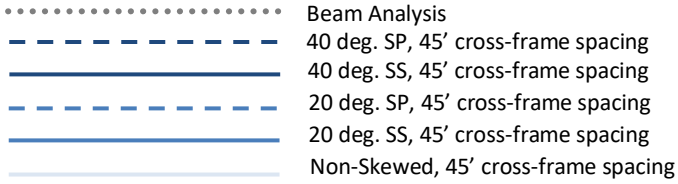

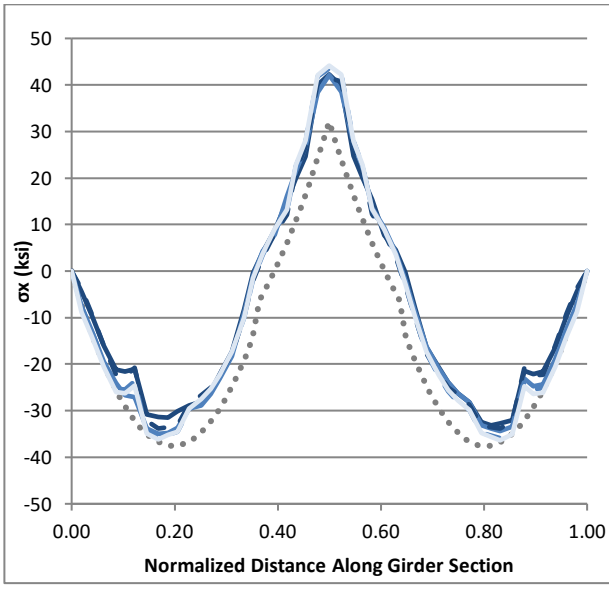

e) 12.7mm [1/2 in.] stiffener connection – Top Flange

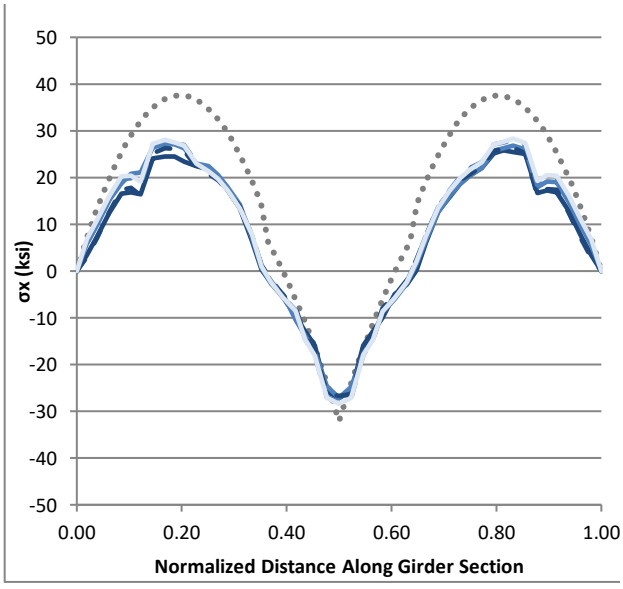

f) 12.7mm [1/2 in.] stiffener connection – Bottom Flange

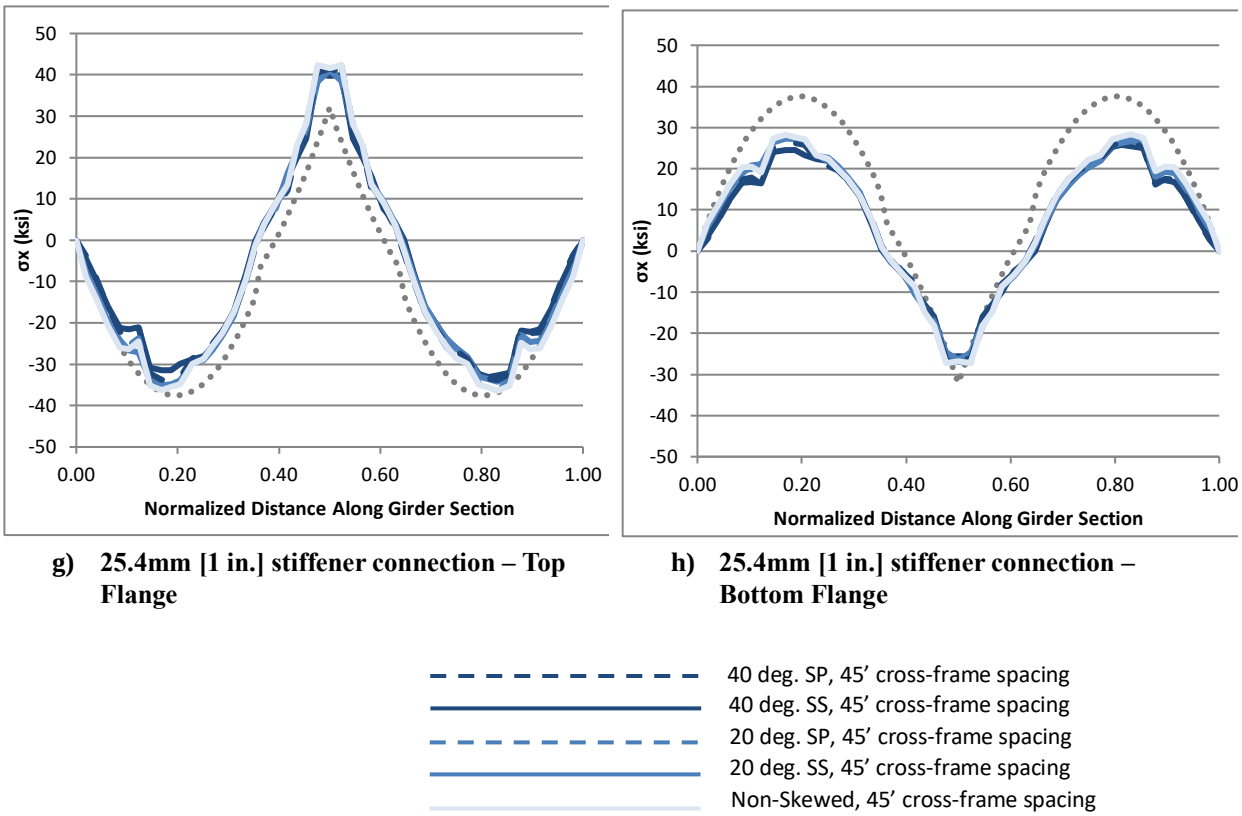

g) 25.4mm [1 in.] stiffener connection – Top Flange

h) 25.4mm [1 in.] stiffener connection – Bottom Flange

Figure 63 Girder 3 strong-axis sectional stresses, grouped by connection type

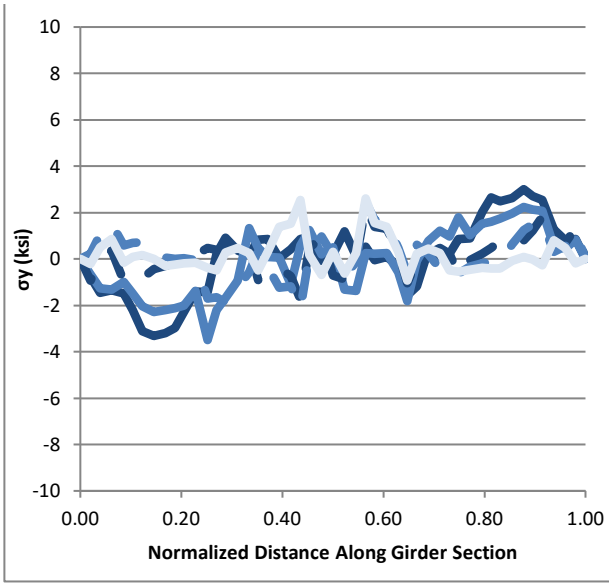

a) **Half-pipe connection – Top Flange**

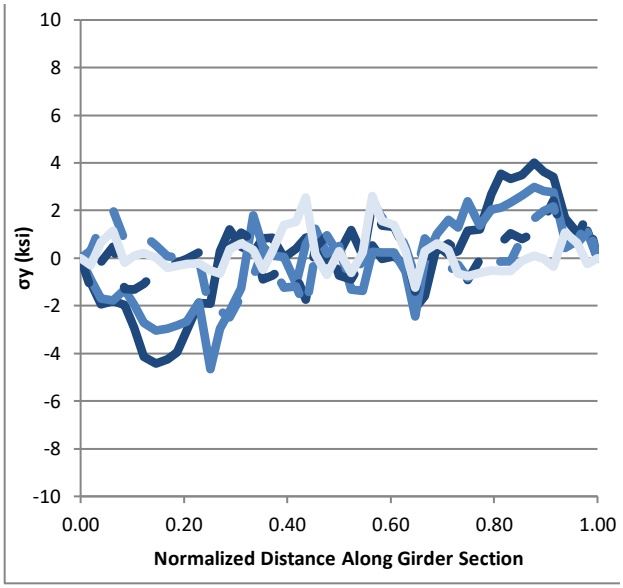

b) **Half-pipe connection - Bottom Flange**

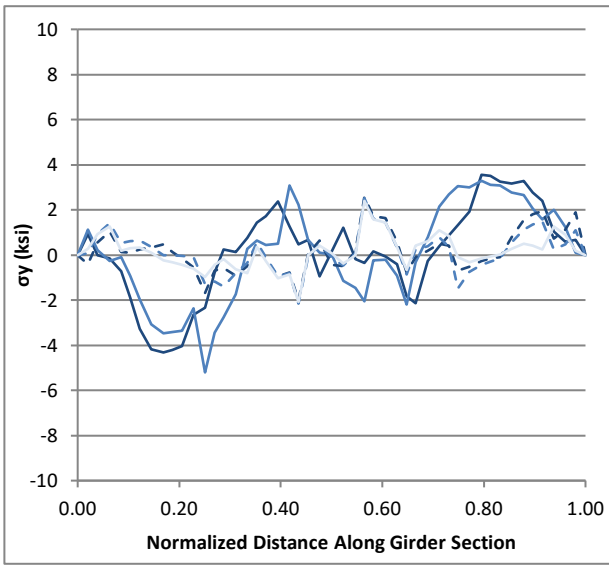

c) **9.53mm [3/8 in.] stiffener connection - Top Flange**

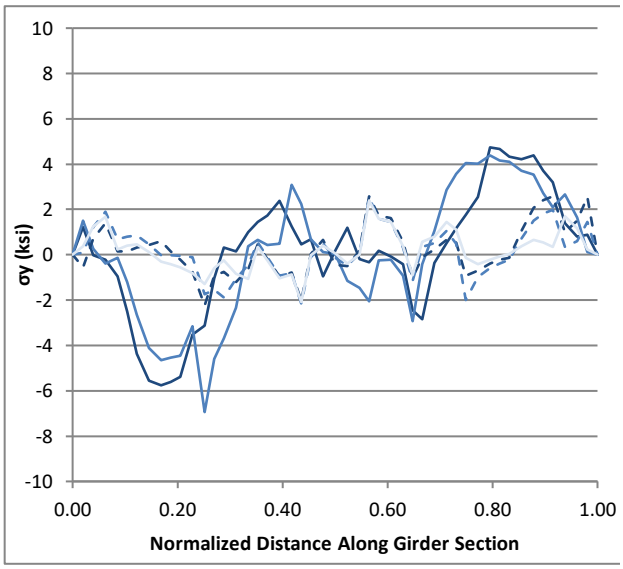

d) **9.53mm [3/8 in.] stiffener connection - Bottom Flange**

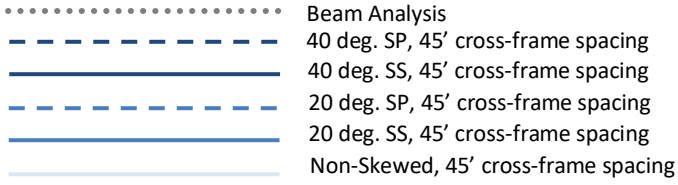

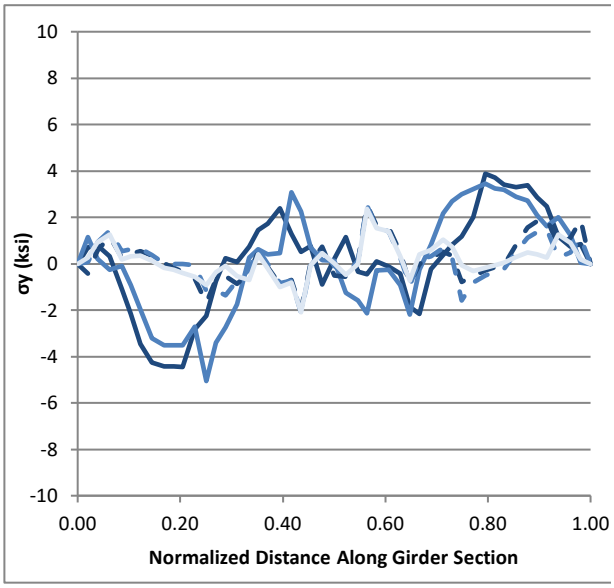

e) 12.7mm [1/2 in.] stiffener connection - Top Flange

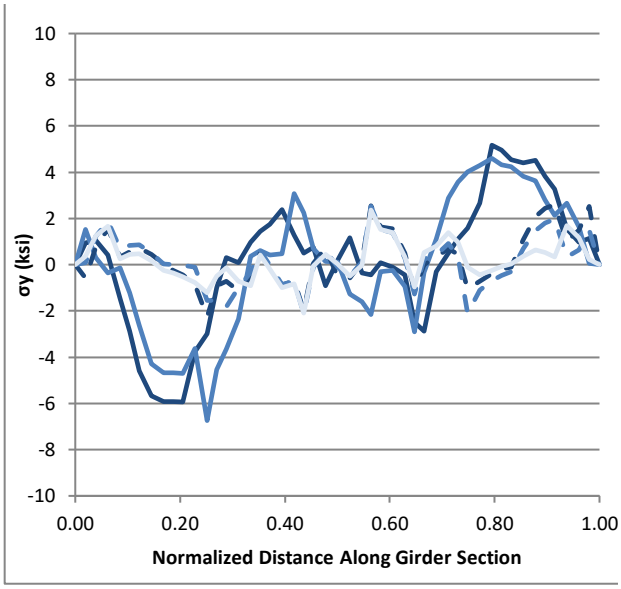

f) 12.7mm [1/2 in.] stiffener connection - Bottom Flange

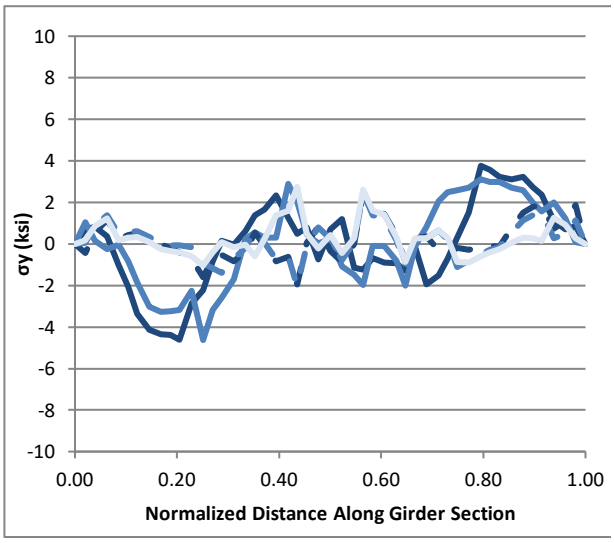

g) 25.4mm [1 in.] stiffener connection - Top Flange

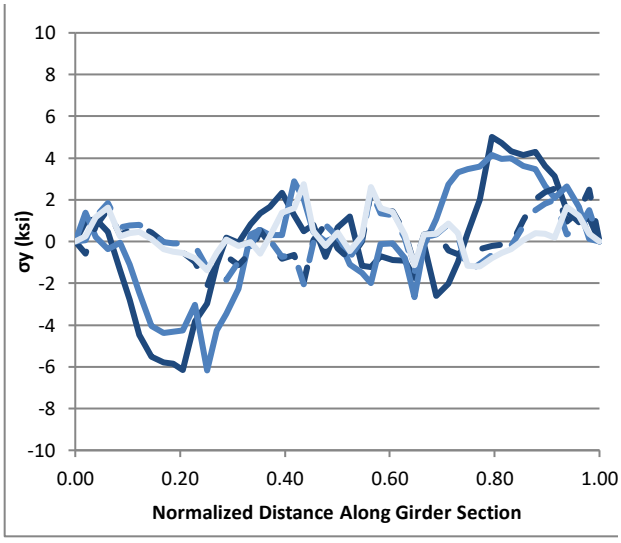

h) 25.4mm [1 in.] stiffener connection - Bottom Flange

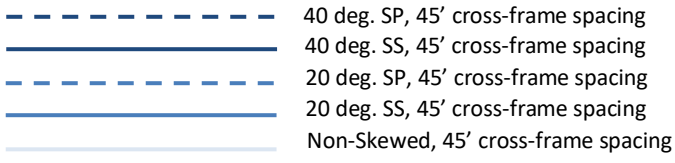

Figure 64 Girder 3 weak-axis sectional stresses, grouped by connection type

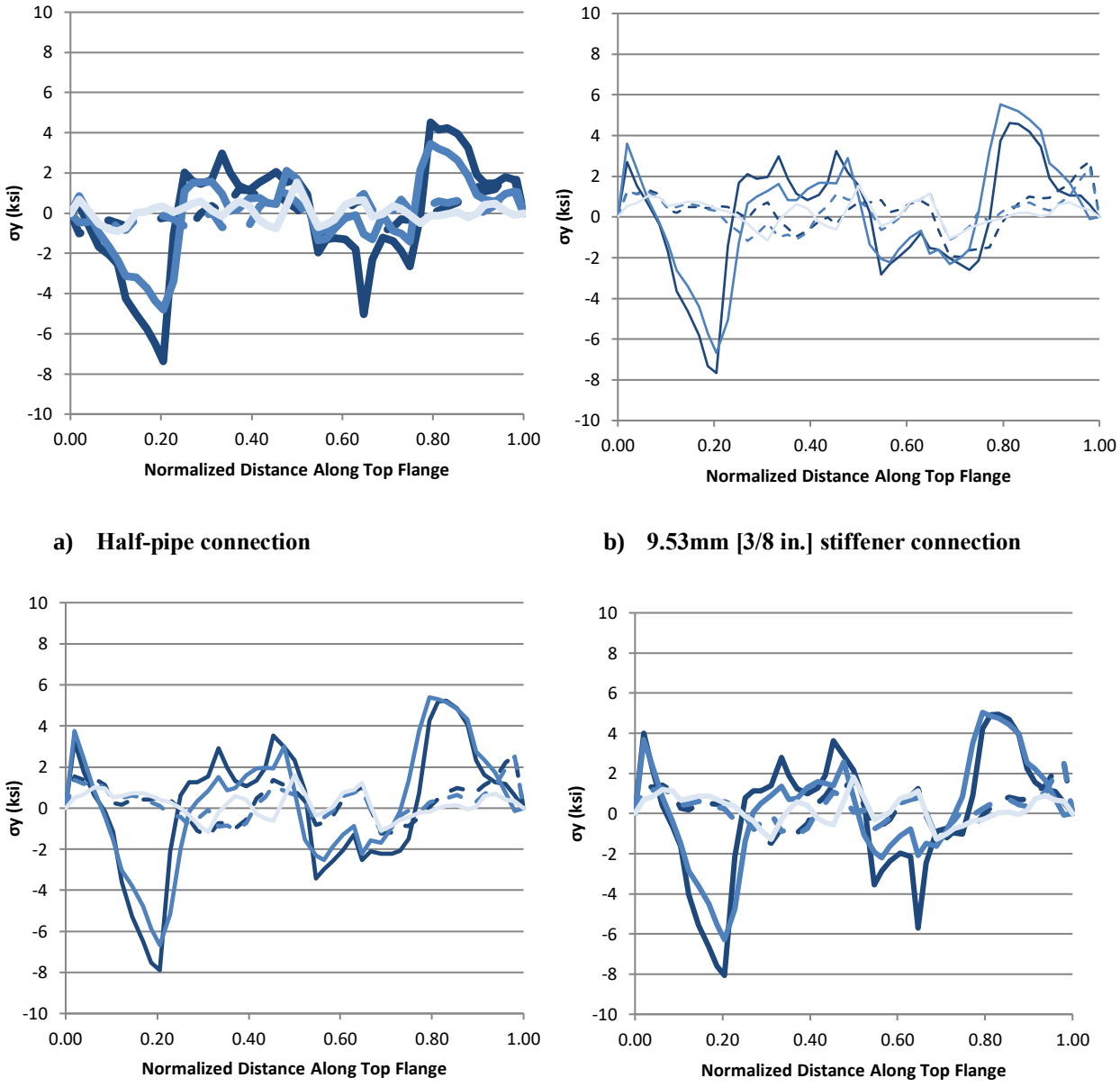

Figure 65 Girder 3 top flange out-of-plane stresses, grouped by connection type

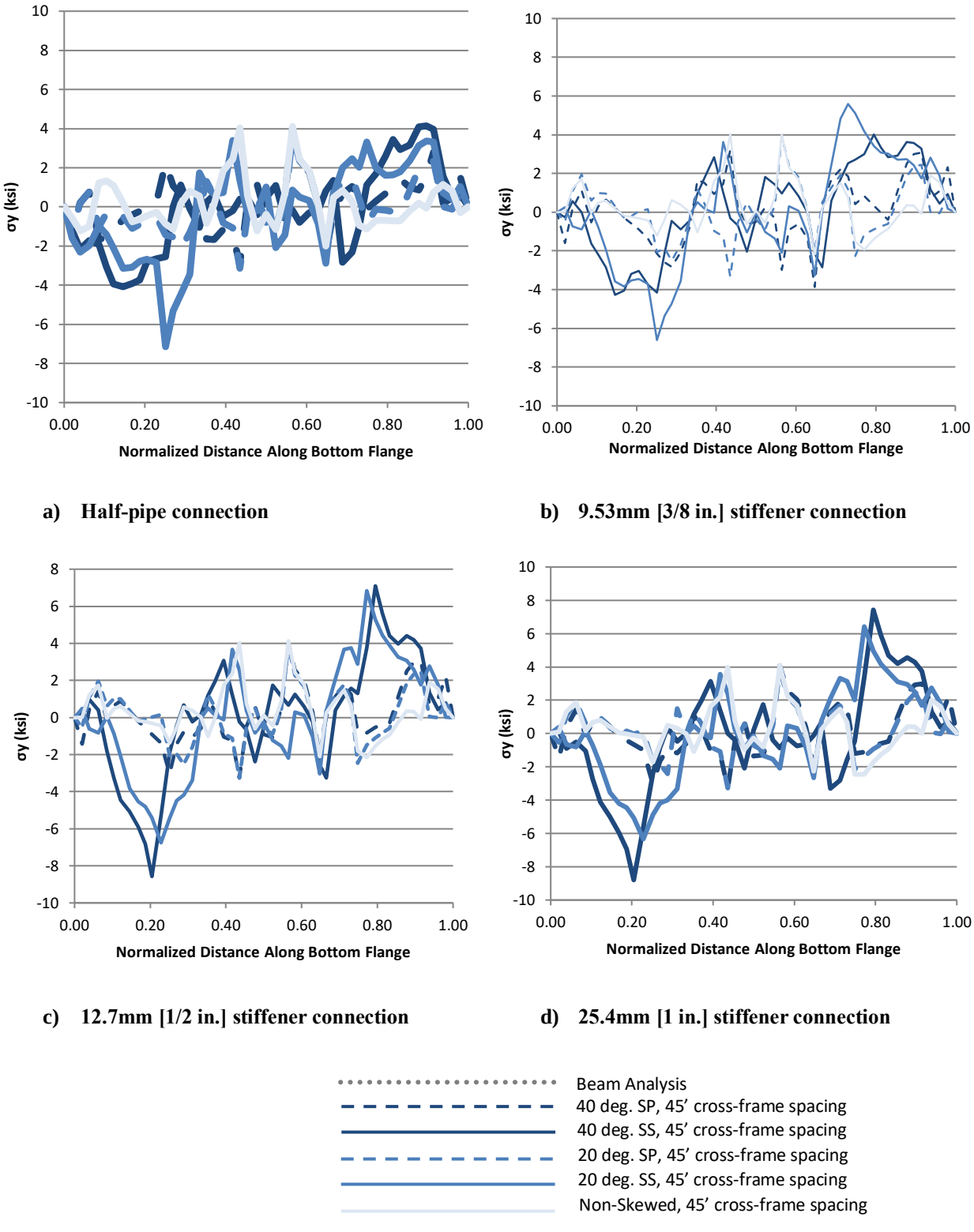

Figure 66 Girder 3 bottom flange out-of-plane stresses, grouped by connection type

6.3.5. Exterior Girder Strong-axis and Weak-axis Stresses

Figure 67 shows strong-axis Girder 4 bending stress calculated for the top and bottom flanges for bridges with 13.7 m [45 ft] cross-frame spacing, grouped by connection type. Results from a simple beam-line analysis of the respective girders are also presented with strong-axis bending stresses. The non-skewed configuration yielded the lowest strong-axis sectional stress followed by the 40° skewed-parallel configuration for any given connection type. The 20° skewed-parallel configuration produced the highest strong-axis sectional stress of the three skewed-parallel configurations. Both the 20° and 40° skewed-staggered configurations had similar magnitudes and resulted in the highest in-plane sectional stresses, with a maximum value of 290 MPa [42 ksi].

Figure 68, Figure 69, and Figure 70 show the weak-axis bending stress, top flange out-of-plane bending stress, and bottom flange out-of-plane bending stress respectively for Girder 4 of the 13.7 m [45 ft] cross-frame spacing models, also grouped by connection type. Weak-axis bending stresses were plotted based on *c* values for the top flange and bottom flange. Strong-axis bending stresses were calculated for *c* values from the top flange and bottom flange. Results for the out-of-plane stresses were similar to the variation in lateral deflections for any given connection type. That is, larger skew angles produced lower weak-axis sectional and out-of-plane flange stresses. The skewed-staggered configuration also exhibited larger out-of-plane stresses compared to the skewed-parallel configuration for any given skew angle and connection type. Peak bottom flange out-of-plane bending stresses were almost the same across all skew angles and configurations for any given connection type. Weak-axis sectional stresses in the exterior girder had a maximum value of 250 MPa [36 ksi], top flange out-of-plane bending stresses had a maximum value of 560 MPa [81 ksi], and bottom flange out-of-plane bending stresses had a maximum value of 500 MPa [73 ksi] in Girder 4.

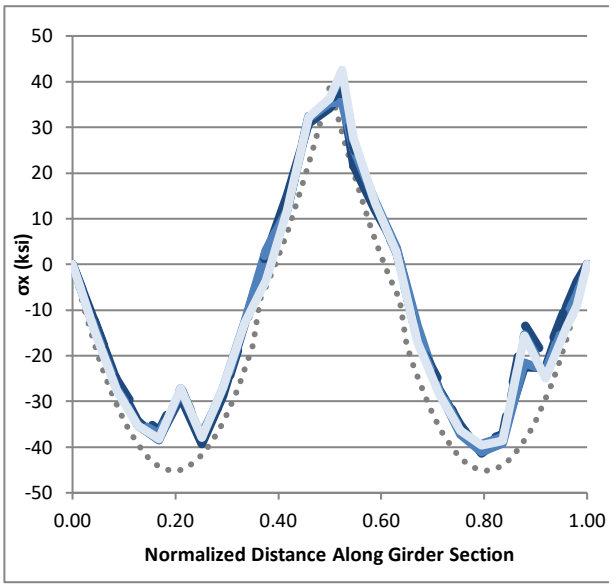

a) Half-pipe connection – Top Flange

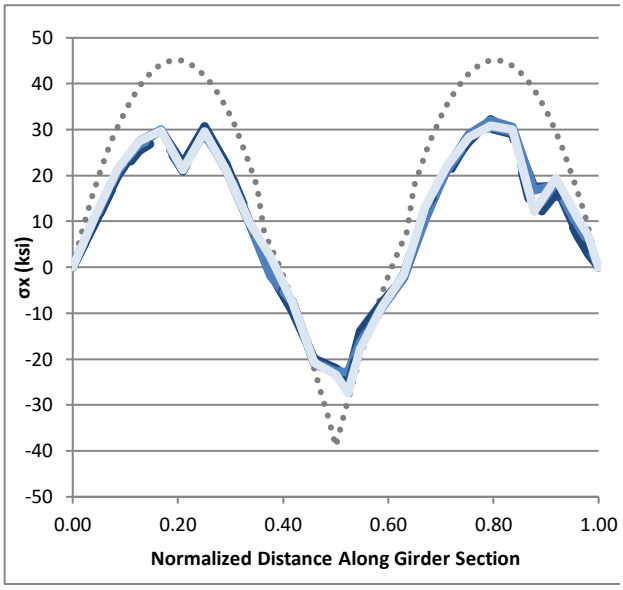

b) Half-pipe connection – Bottom Flange

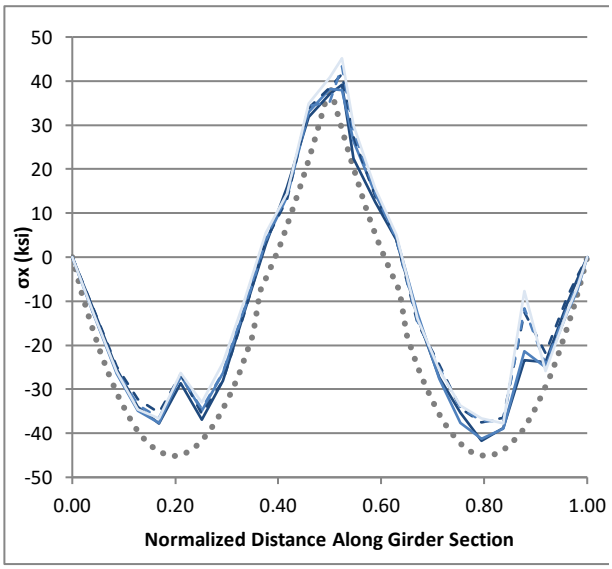

c) 9.53mm [3/8 in.] stiffener connection – Top Flange

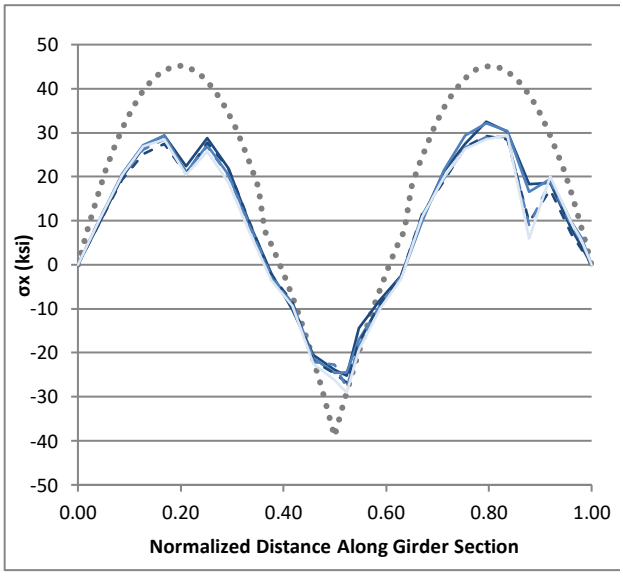

d) 9.53mm [3/8 in.] stiffener connection – Bottom Flange

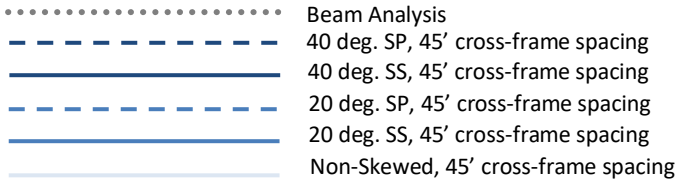

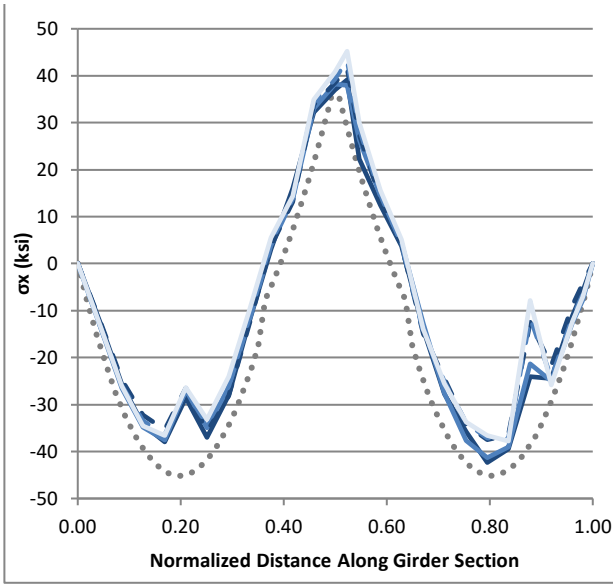

e) 12.7mm [1/2 in.] stiffener connection – Top Flange

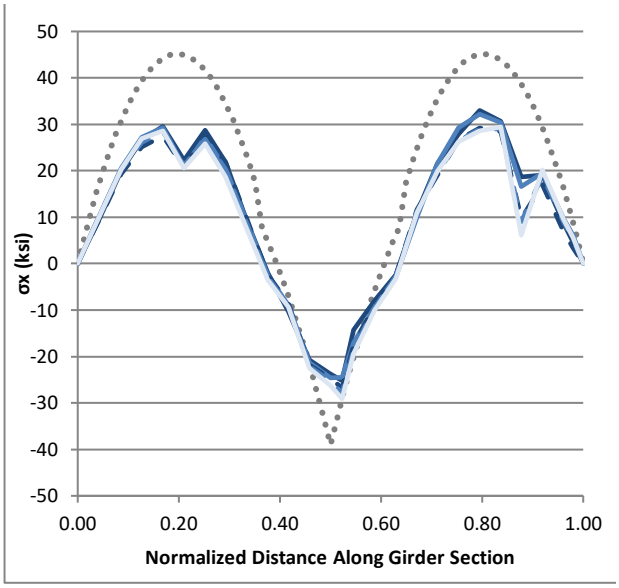

f) 12.7mm [1/2 in.] stiffener connection – Bottom Flange

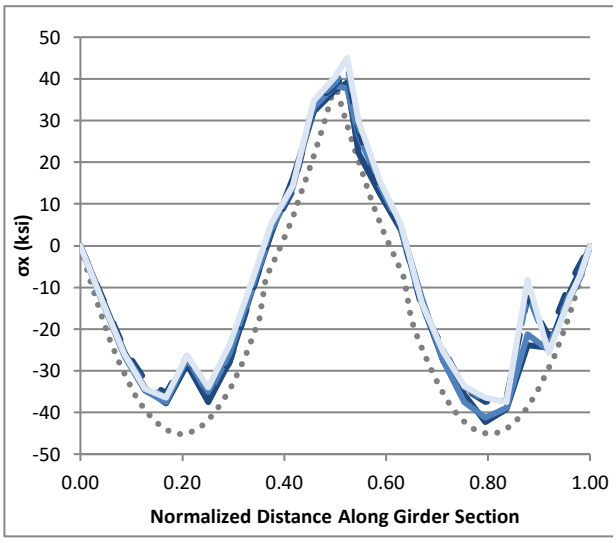

g) 25.4mm [1 in.] stiffener connection – Top Flange

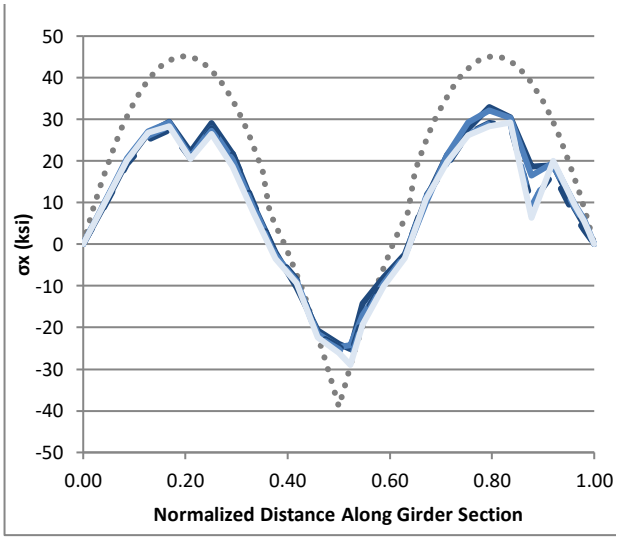

h) 25.4mm [1 in.] stiffener connection – Bottom Flange

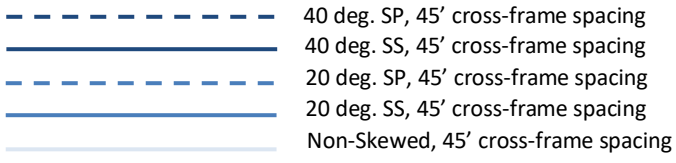

Figure 67 Girder 4 strong-axis sectional stresses, grouped by connection type

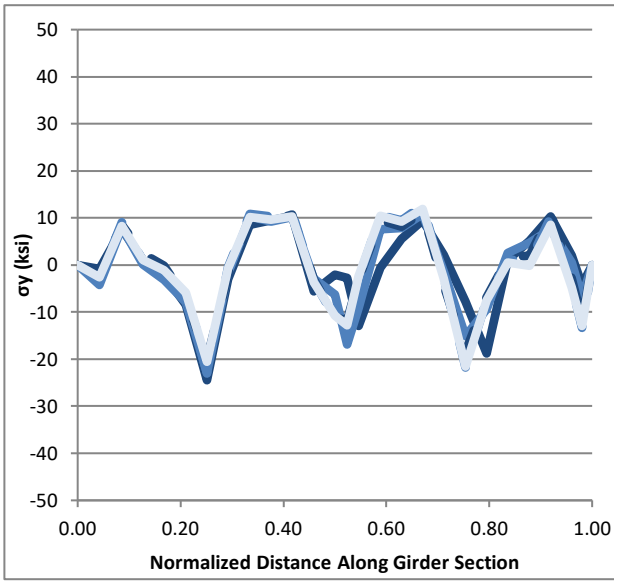

a) Half-pipe connection – Top Flange

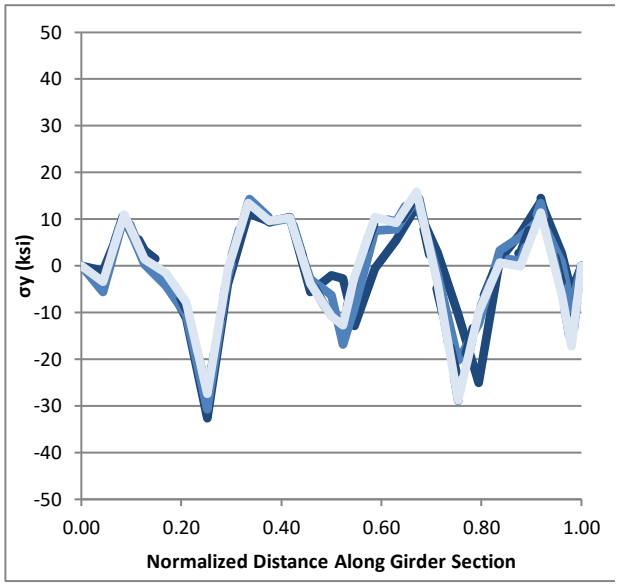

b) Half-pipe connection - Bottom Flange

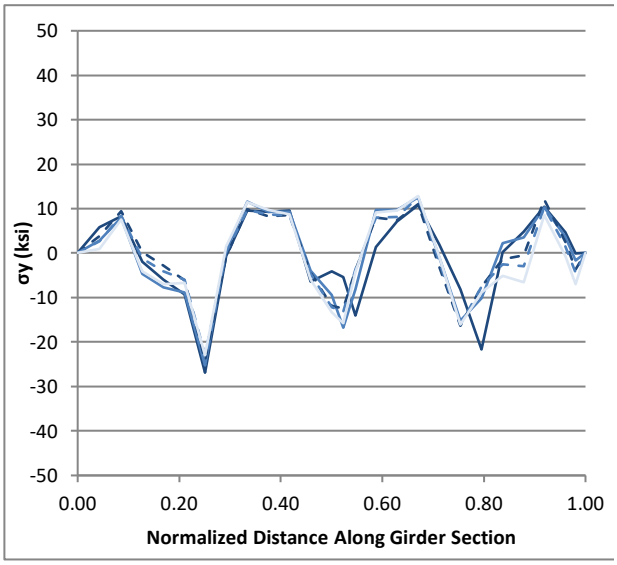

c) 9.53mm [3/8 in.] stiffener connection - Top Flange

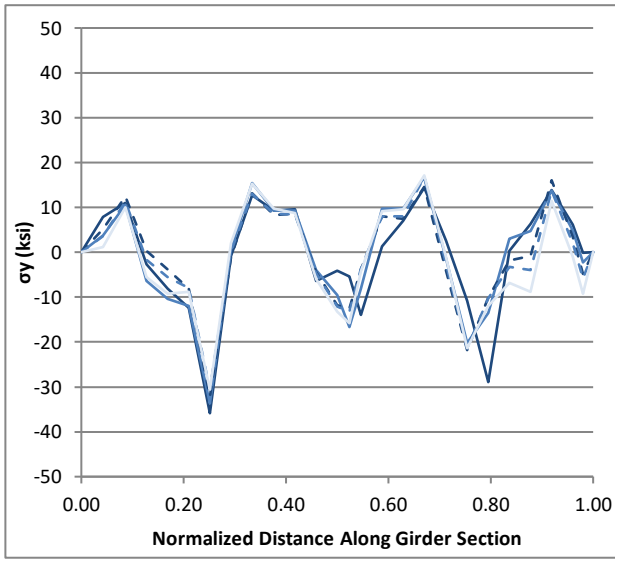

d) 9.53mm [3/8 in.] stiffener connection - Bottom Flange

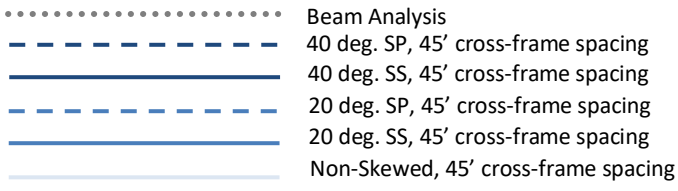

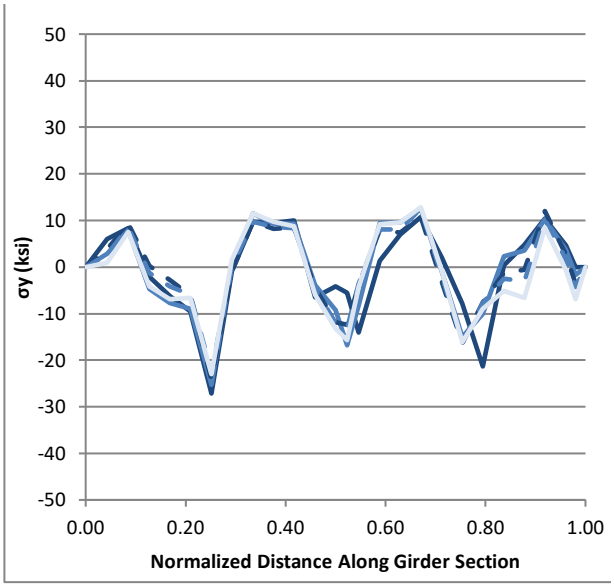

e) 12.7mm [1/2 in.] stiffener connection - Top Flange

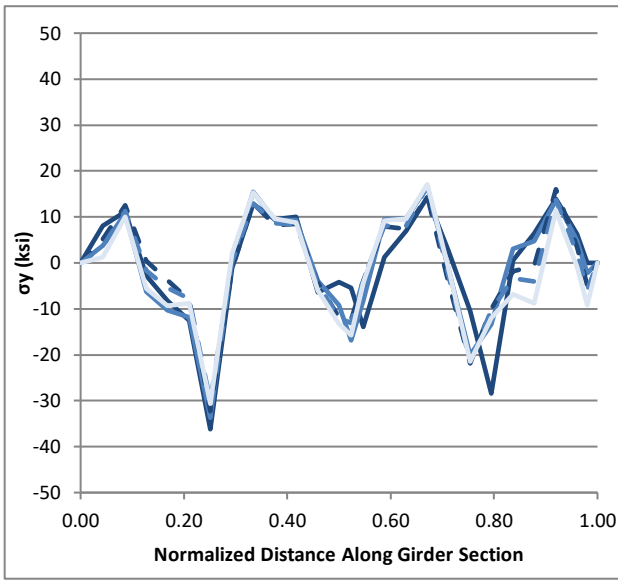

f) 12.7mm [1/2 in.] stiffener connection - Bottom Flange

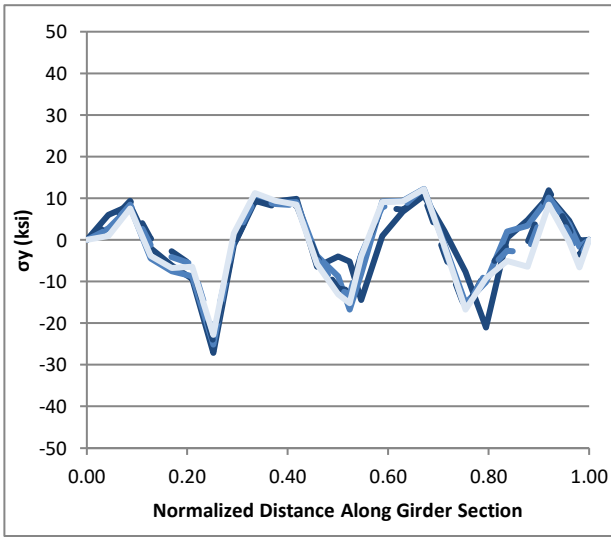

g) 25.4mm [1 in.] stiffener connection - Top Flange

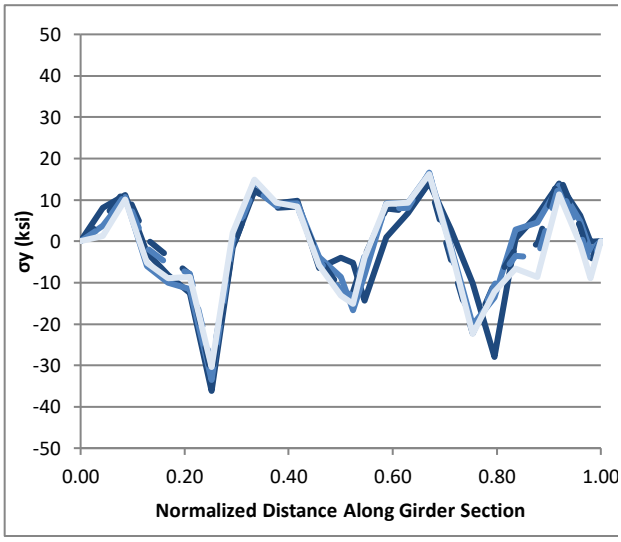

h) 25.4mm [1 in.] stiffener connection - Bottom Flange

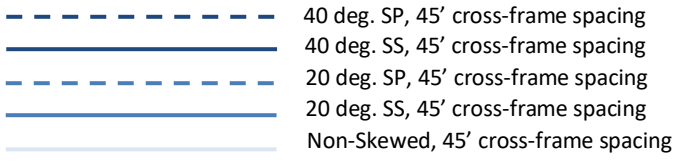

Figure 68 Girder 4 weak-axis sectional stresses, grouped by connection type

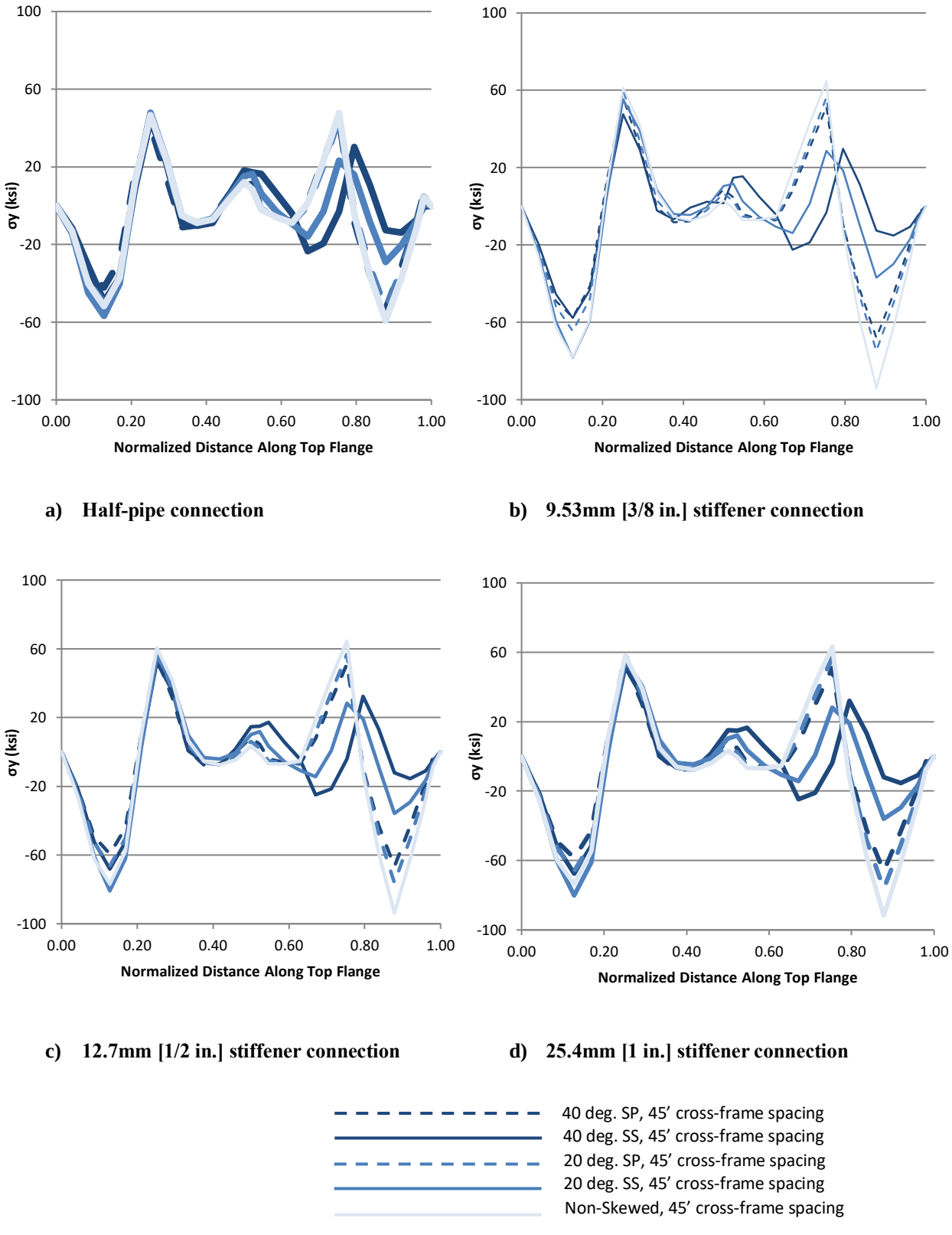

a) Half-pipe connection

b) 9.53mm [3/8 in.] stiffener connection

c) 12.7mm [1/2 in.] stiffener connection

d) 25.4mm [1 in.] stiffener connection

Figure 69 Girder 4 top flange out-of-plane stresses, grouped by connection type

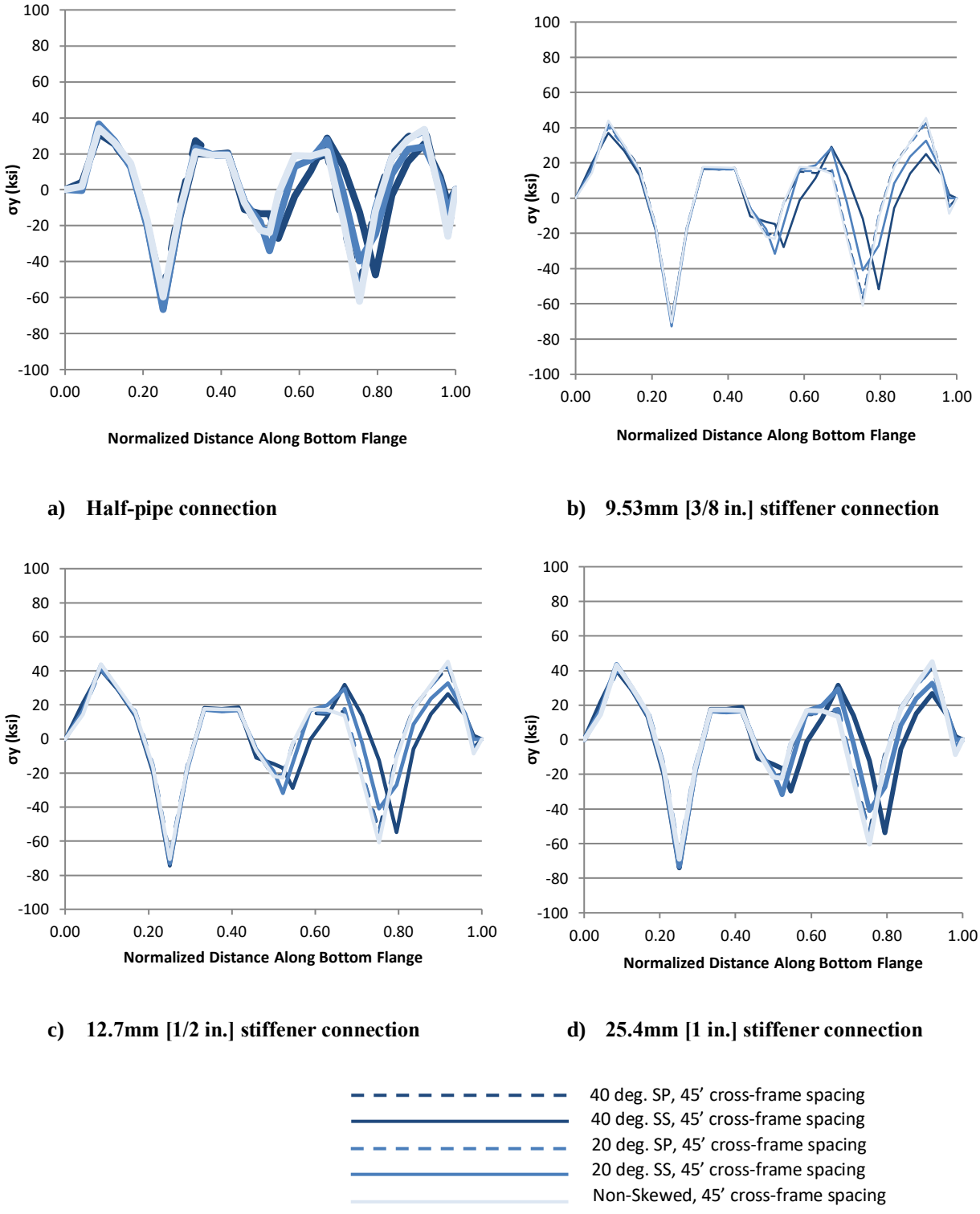

Figure 70 Girder 4 bottom flange out-of-plane stresses, grouped by connection type

7. CONCLUSIONS

This report has presented a study of a bridge system where bridge configuration, skew angle, cross-frame spacing, and cross-frame connection stiffness were varied to examine the implications on stability and lateral flange bending stresses.

The results were examined in terms of lateral displacement of the top (compression) flange in the positive flexure region, which produced the highest lateral deflections; girder stresses extracted from the interior and exterior girders; and stresses in the cross-frame angles to determine the lateral force transfer in the members and its susceptibility to buckling. Bridge configuration, cross-frame spacing skew angle, and connection type all affected the susceptibility of the bridge to lateral torsional buckling.

From these data, the following conclusions can be drawn:

- The skewed-staggered configuration produced higher exterior top flange lateral displacements and higher out-of-plane girder stresses than the skewed-parallel configuration for the 13.7 m [45 ft] cross-frame spacing models.
- The exterior top flange lateral displacements for the 4.6 m [15 ft] and 9.14 m [30 ft] cross-frame spacing models had a maximum deflection of 45.2 mm [1.78 in.] found in the 40° skewed-staggered bridge with 9.14 m [30 ft] cross-frame spacing. As would be expected, the lateral deflections in systems with larger cross-frame spacing (13.7 m [45 ft]) became extremely large. Therefore, even *if* the braces in such a system were found to be effective from a strength and stiffness standpoint, and *if* the girder was able to remain stable for such a long unbraced length, the lateral displacements in the girders would be untenable. This observation was not unexpected, as the goal of examining a system with such long unbraced lengths was to amplify differences between the various connection stiffness parameters examined, and it is reiterated here for clarity.
- Larger skew angles produced smaller exterior top flange lateral displacements and smaller lateral flange bending stresses than smaller skew angles for the 13.7 m [45 ft] cross-frame spacing models.
- Smaller skew angles produced smaller exterior top flange lateral displacements than larger skew angles for 4.6 m [15 ft] and 9.14 m [30 ft] cross-frame spacing models, with the exception of the 0° non-skewed bridge with 4.6 m [15 ft] cross-frame spacing, which

resulted in slightly higher displacements than the 20° bridge with the same configuration and cross-frame spacing.

- The skewed-staggered configuration resulted in higher cross-frame stresses in the bottom horizontal angle member, Member C, than the skewed-parallel configuration for any given skew angle, connection type, and cross-frame spacing.
- Smaller skew angles corresponded with higher cross-frame stresses in Member C.
- Variations in stiffener thicknesses produced very small or insignificant differences in lateral displacements of the compression flange or cross-frame stresses.
- The half-pipe connection produced the lowest lateral displacements, out-of-plane girder stresses, and cross-frame stresses, in all systems examined.
- Cross-frame spacing had a great effect on girder lateral displacements than skew angle, cross-frame configuration (SS vs SP), or connection stiffness.

For the cross-frames / diaphragms carried parallel to skew, the data showed that as the cross-frame forces are balanced on the opposite side of the girder cross-section, generally lower lateral deflections and smaller cross-frame stresses were produced. The results showed that stiffener thickness had little effect on cross-frame stresses, but did result in noticeable differences in terms of peak lateral displacements. Even with an unusually long cross-frame spacing of 13.7 m [45 ft], cross-frames in all skew angles and configurations effectively braced the girders (although the girders themselves did exhibit extremely large lateral displacements when too few cross-frames were present). For cross-frames spaced within KDOT's maximum requirement of 7.62 m [25 ft], lateral torsional buckling was not a significant problem for any skew angle or configuration tested.

Finally, the data showed that cross-frame placed parallel to skew up to an angle of 40° performed similar or better than cross-frames oriented perpendicular to skew for every given skew angle and connection type. However, it is stressed that in all cases studied the longer (more flexible) cross-frames used in the skewed-parallel systems remained sufficient to restrain the girder; this must be ensured by designing the cross-frames to have sufficient strength and stiffness to restrain girder buckling, otherwise the results of this study may not translate to practice.

8. REFERENCES

- AASHTO (2010). “LRFD Bridge Design Specifications.” *American Association of State Highway and Transportation Officials,* Washington, D.C.
- AISC (2010). “Steel Construction Manual, 14th Ed.” *American Institute of Steel Construction*, Chicago, IL.
- AISI Example 2: Two-Span Continuous Composite I Girder (1997). *American Iron and Steel Institute*.
- Bishara, A. and Elmir, W. (1990). "*Interaction between Cross Frames and Girders*." J. Struct. Eng., 10.1061/(ASCE)0733-9445(1990)116:5(1319), 1319-1333.
- Gupta, Y.P., Kumar, A. (1983). “Structural Behaviour of Interconnected Skew Slab-Girder Bridges,” Journal of the Institution of Engineers (India), Civil Engineering Division, 64, 119-124.
- Hassel, H. (2011). “An Analytical Evaluation of Distortion-Induced Fatigue in Steel Bridges,” thesis, presented to University of Kansas, at Lawrence, KS in partial fulfillment of the requirements for the° of Master of Civil Engineering.
- Hassel, H., Bennett, C., Matamoros, A., and Rolfe, S. (2012). “Parametric analysis of cross-frame layout on distortion-induced fatigue in skewed steel bridges.” J. Bridge Eng., 10.1061/(ASCE)BE.19435592.0000388, 601–611.
- KDOT. (2010). “Design Manual: Volume III – Bridge Selection.” *Kansas Department of Transportation*.
- Krupicka, G., and Poellot, B. (1993). “Nuisance Stiffness,” HDR Engineering, Inc., Bridgeline, 4(1), 3.
- McConnell, J., Ambrose, K., and Radovic, M. (2013). “Cross-Frame Forces in Skewed Steel I-Girder Bridges: Field Testing and Applications to System-Capacity”, Presented at 2013 ASCE / SEI Structures Congress, Pittsburgh, PA, May 2-4, 2013.
- McConnell, J., Radovic, M. (2014). “Evaluation of Cross-frame Designs for Highly Skewed Steel I-Girder Bridges.” Presented at 31st Annual International

Bridge Conference, Engineers Society of Western Pennsylvania, Pittsburg, PA, IBC 14-47.

- McConnell, J., Radovic, M., and Ambrose, K. (2014). "Cross-Frame Forces in Skewed Steel I-Girder Bridges: Field Measurements and Finite Element Analysis", University of Delaware Center for Bridge Engineering, Final Report to Delaware Department of Transportation.
- Ozgur, C. (2011). "Influence Of Cross-Frame Detailing On Curved And Skewed Steel I-Girder Bridges", Doctoral Dissertation, Georgia Institute of Technology.
- Quadrato, C., Battistini, A., Frank, K., Helwig, T., & Engelhardt, M. (2010). Improved cross-frame connection details for steel bridges with skewed supports. Transportation Research Record: Journal of the Transportation Research Board, (2200), 29-35.
- Wang, L. and Helwig, T.A. (2008). "Stability Bracing Requirements for Steel Bridge Girders with Skewed Supports." *Journal of Bridge Engineering*, 13(2), 149-157.
- Yura, J. (2001). "Fundamentals of Beam Bracing." *Engineering Journal*, AISC, First Quarter, 11-26.
- Winter, G. (1958). "Lateral Bracing of Columns and Beams." J. Struct. Div., Vol. 84(ST2), 1-22.
- Zhou, J., Bennett, C., Matamoros, A., Li, J., and Rolfe, S. "Skewed Steel Bridges, Part I: Effect of CrossFrame Layout on Lateral Flange Bending Stresses," Final Report to the Kansas Department of Transportation, Project KTRAN KU-13-3, September, 2015.

APPENDIX A:

Deformed Shapes of all Finite Element Models Included in the Parametric Study

40° SKEWED-PARALLEL BRIDGE

45 FT CROSS-FRAME SPACING;

3/8" THICK STIFFENERS

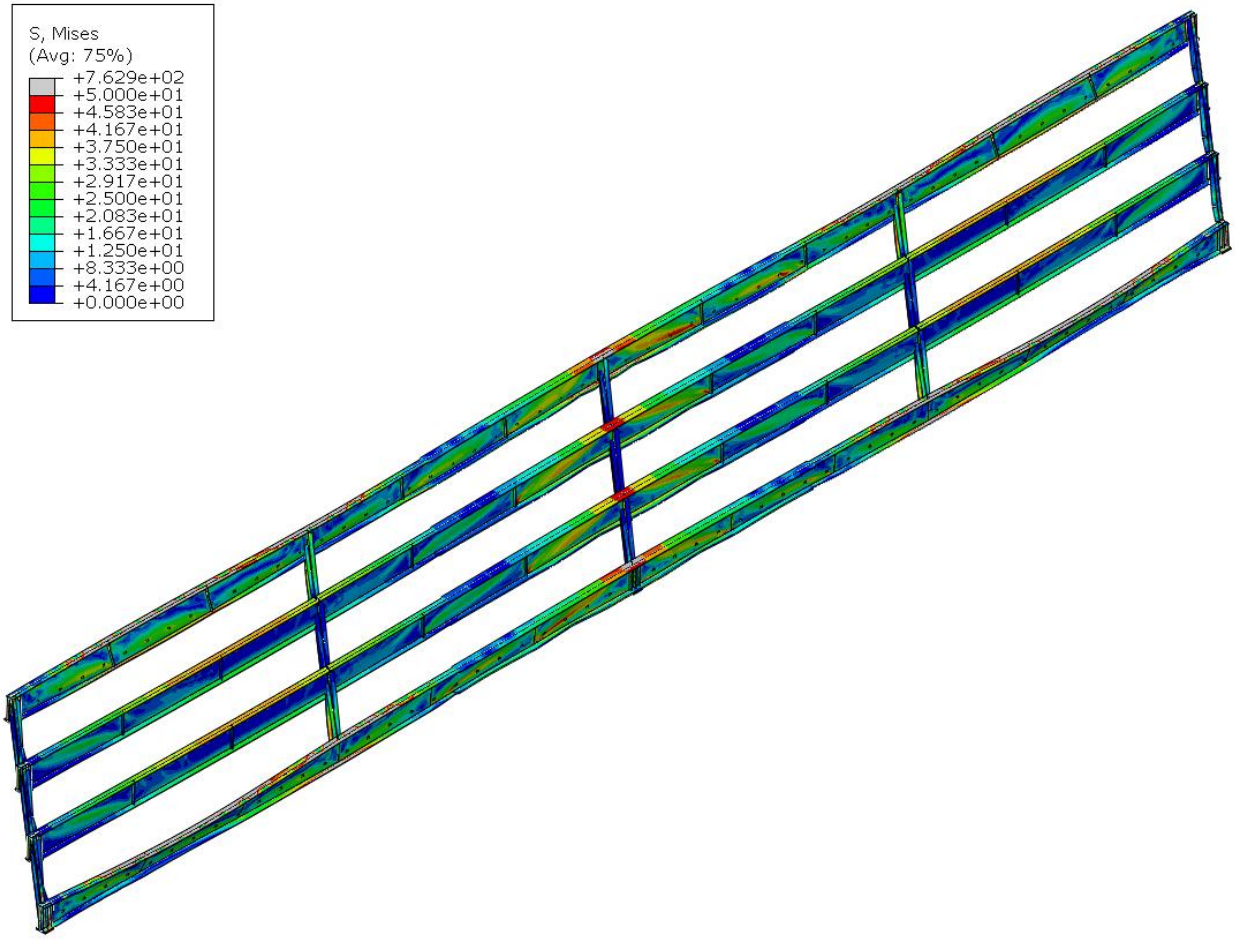

Figure 71 Deformed shaped of the 40° skewed-parallel bridge with 13.7 m [45 ft] cross-frame spacing and 9.53 mm [3/8 in.] thick stiffeners in isotropic view

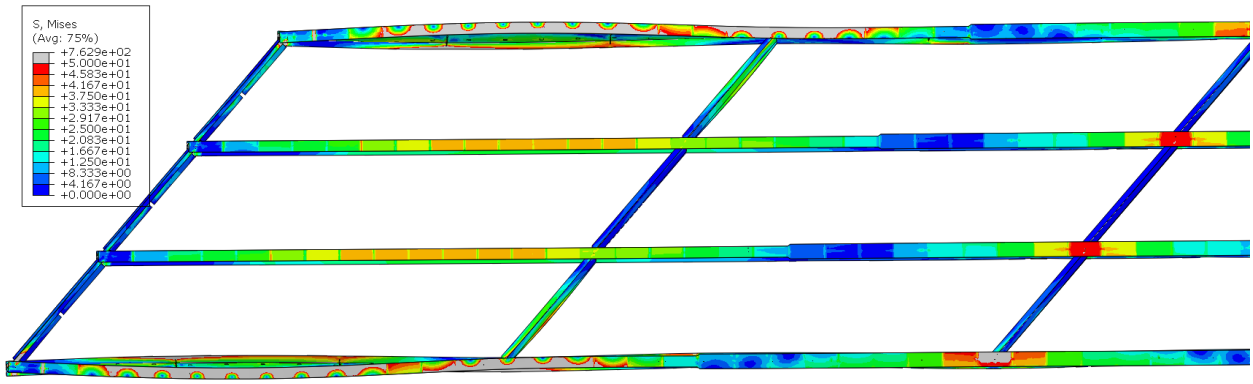

Figure 72 Deformed shape of the 40° skewed-parallel bridge in Span 1 with 13.7 m [45 ft] cross-frame spacing and 9.53 mm [3/8 in.] thick stiffeners in plan view

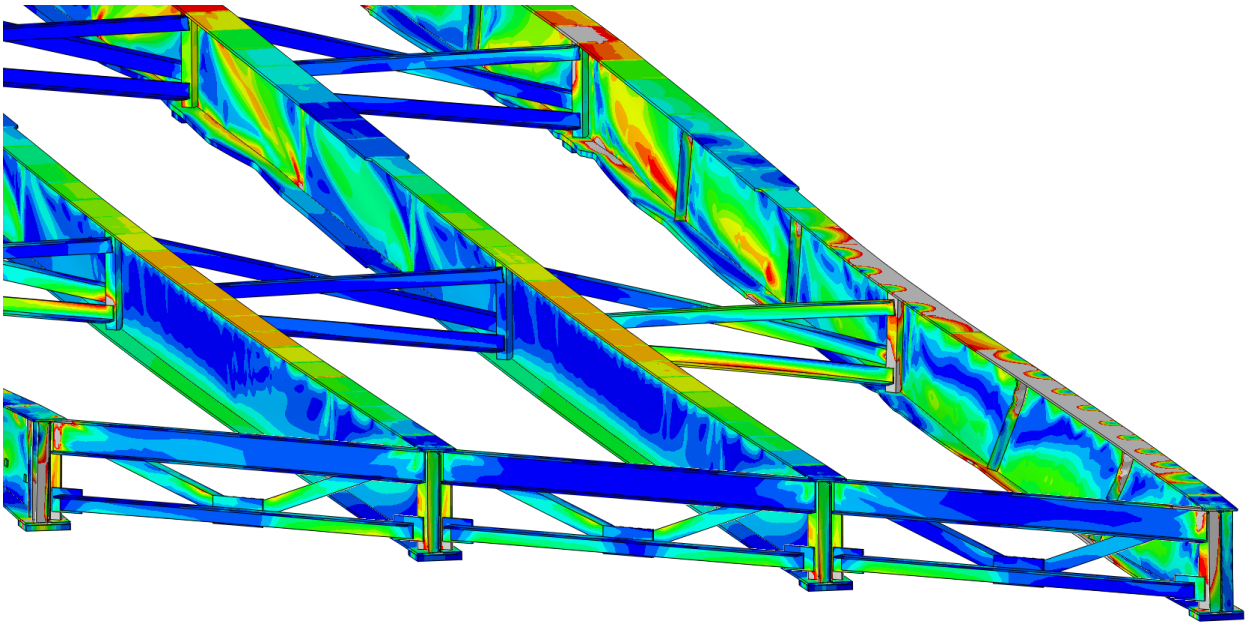

Figure 73 Girder deformation of the 40° skewed-parallel bridge with 13.7 m [45 ft] cross-frame spacing and 9.53 mm [3/8 in.] thick stiffeners

40° SKEWED-STAGGERED BRIDGE

45 FT CROSS-FRAME SPACING;

3/8" THICK STIFFENERS

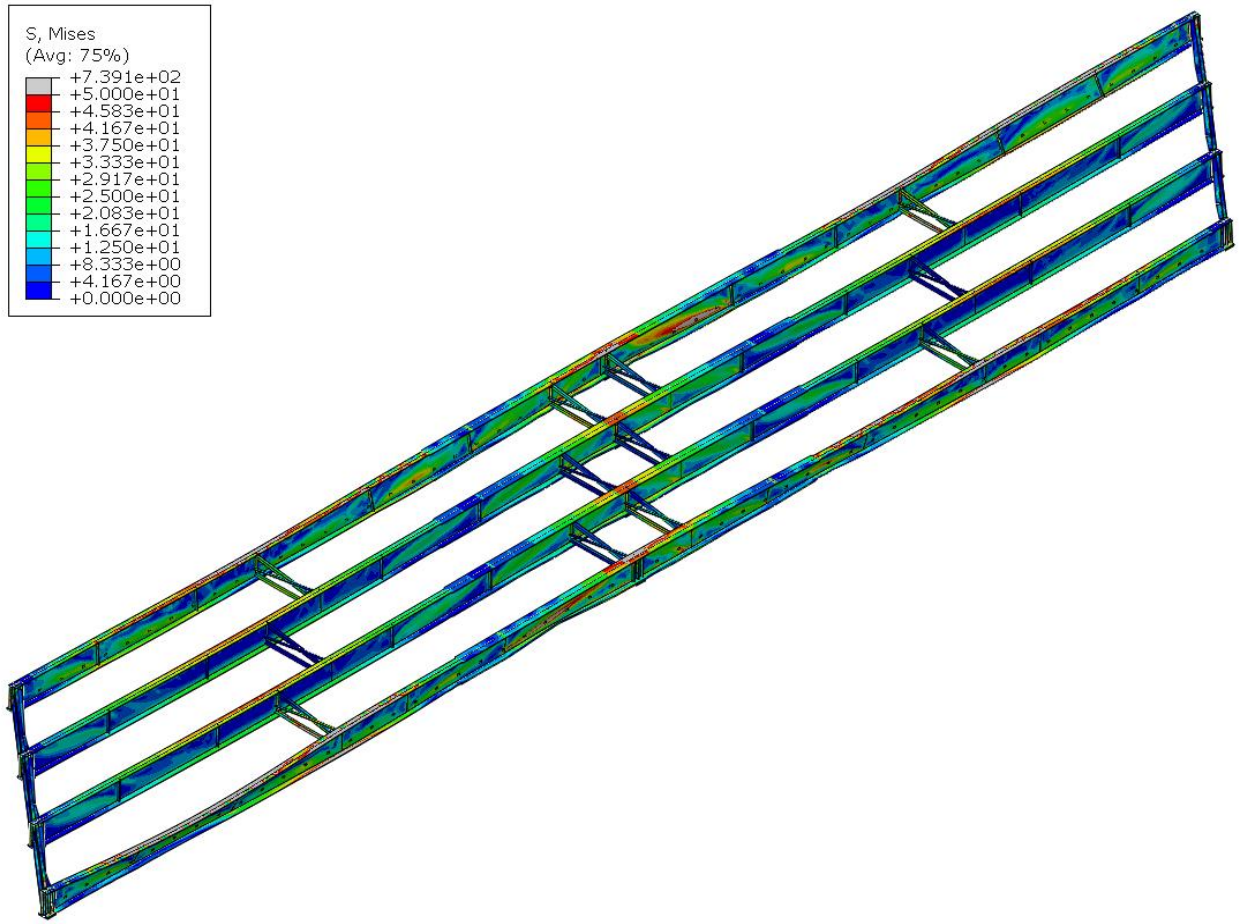

Figure 74 Deformed shaped of the 40° skewed-staggered bridge with 13.7 m [45 ft] cross-frame spacing and 9.53 mm [3/8 in.] thick stiffeners in isotropic view

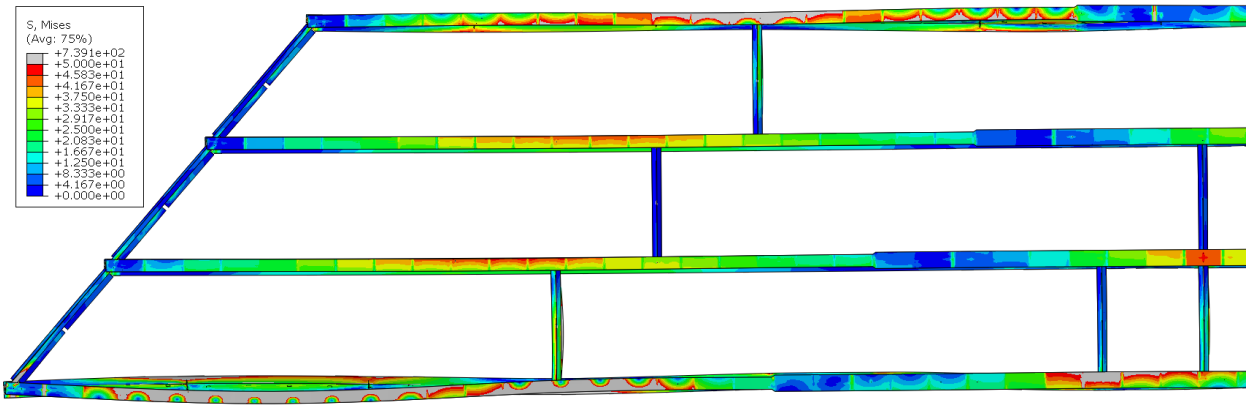

Figure 75 Deformed shape of the 40° skewed-staggered bridge in Span 1 with 13.7 m [45 ft] cross-frame spacing and 9.53 mm [3/8 in.] thick stiffeners in plan view

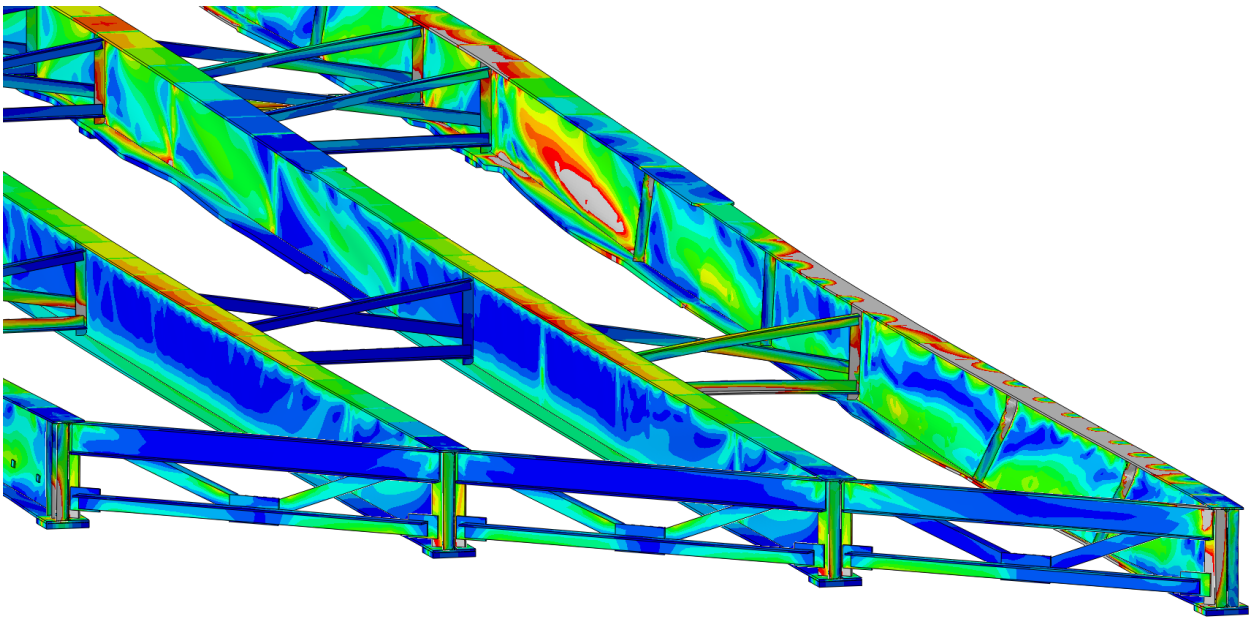

Figure 76 Girder deformation of the 40° skewed-staggered bridge with 13.7 m [45 ft] cross-frame spacing and 9.53 mm [3/8 in.] thick stiffeners

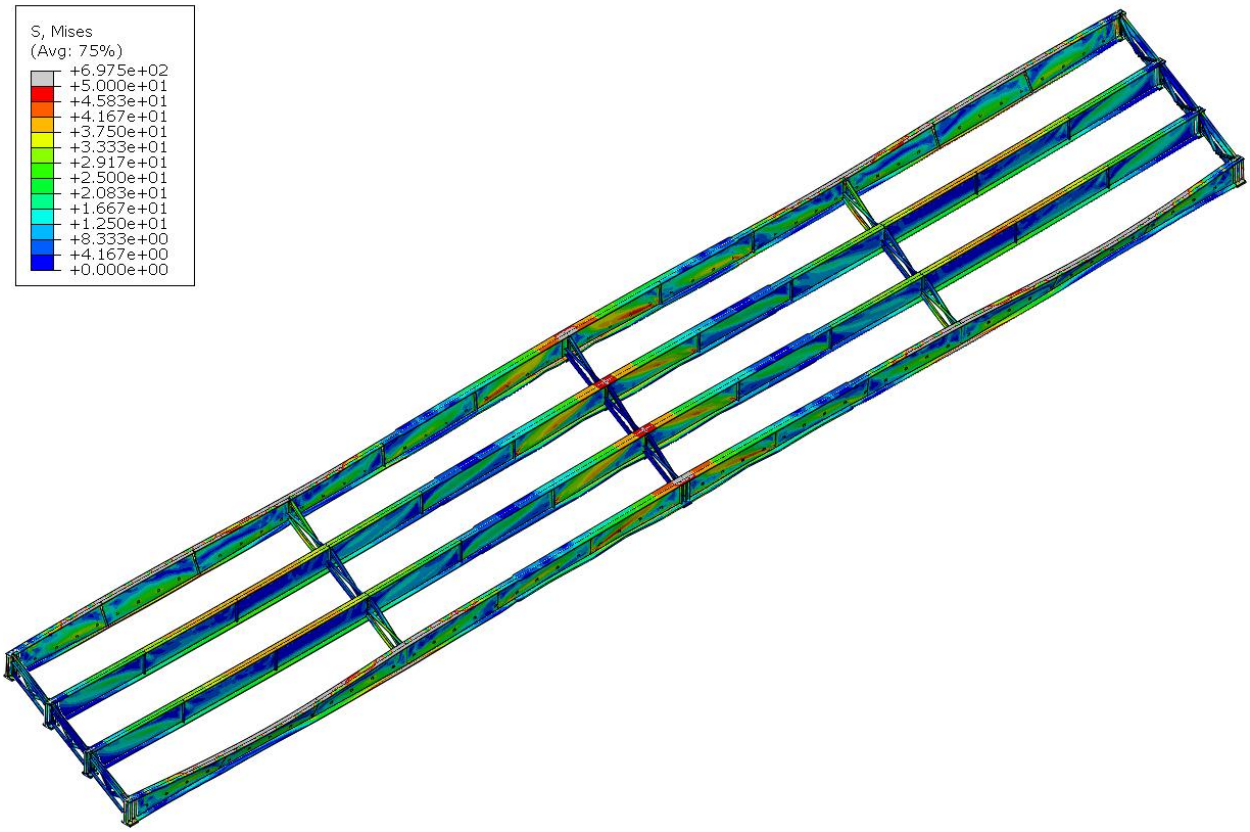

Figure 77 Deformed shaped of the 20° skewed-parallel bridge with 13.7 m [45 ft] cross-frame spacing and 9.53 mm [3/8 in.] thick stiffeners in isotropic view

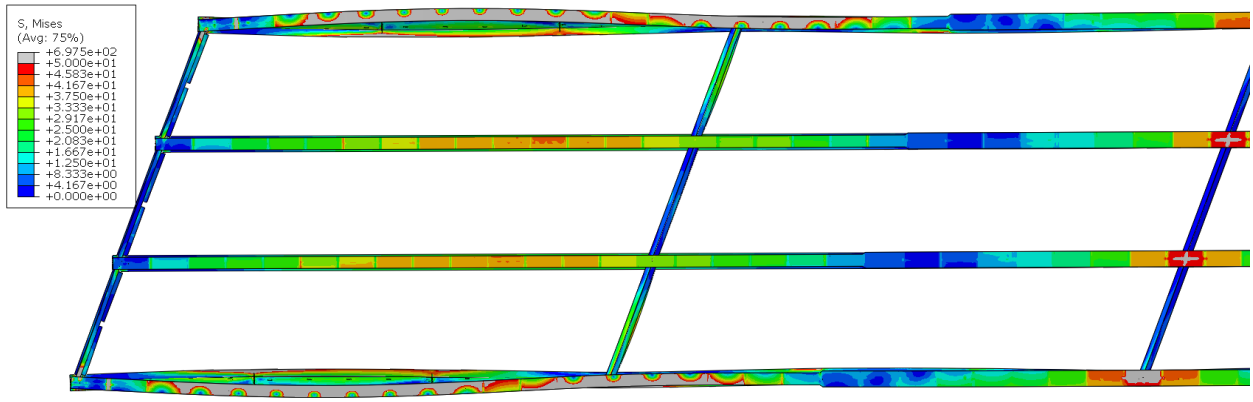

Figure 78 Deformed shape of the 20° skewed-parallel bridge in Span 1 with 13.7 m [45 ft] cross-frame spacing and 9.53 mm [3/8 in.] thick stiffeners in plan view

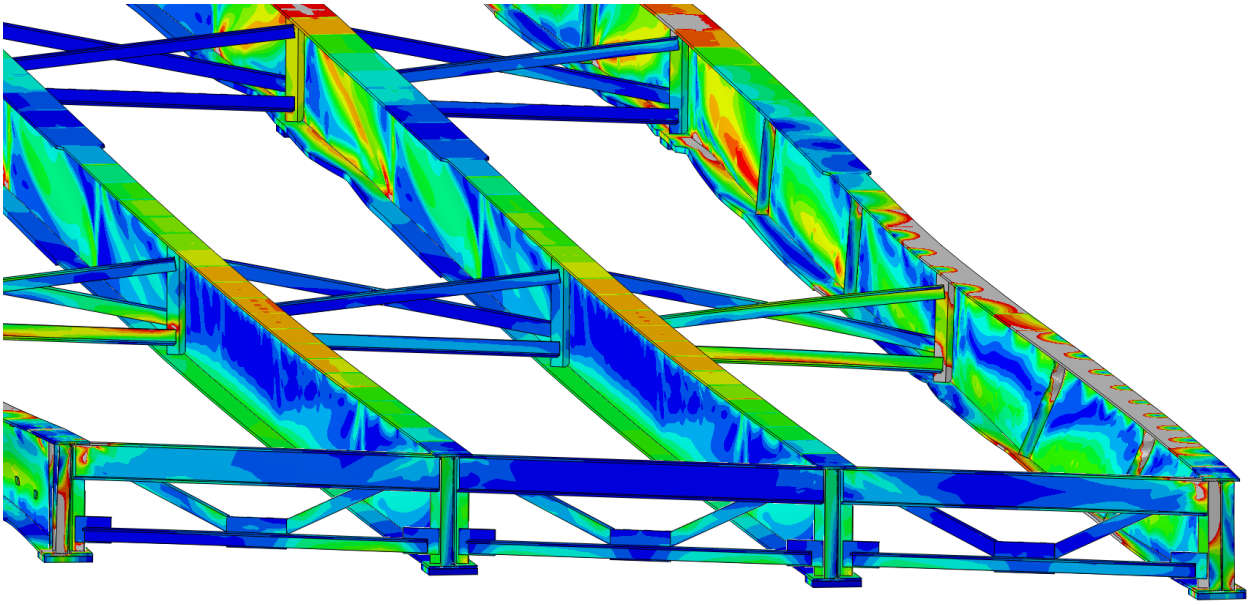

Figure 79 Girder deformation of the 20° skewed-parallel bridge with 13.7 m [45 ft] cross-frame spacing and 9.53 mm [3/8 in.] thick stiffeners

20° SKEWED-STAGGERED BRIDGE

45 FT CROSS-FRAME SPACING;

3/8" THICK STIFFENERS

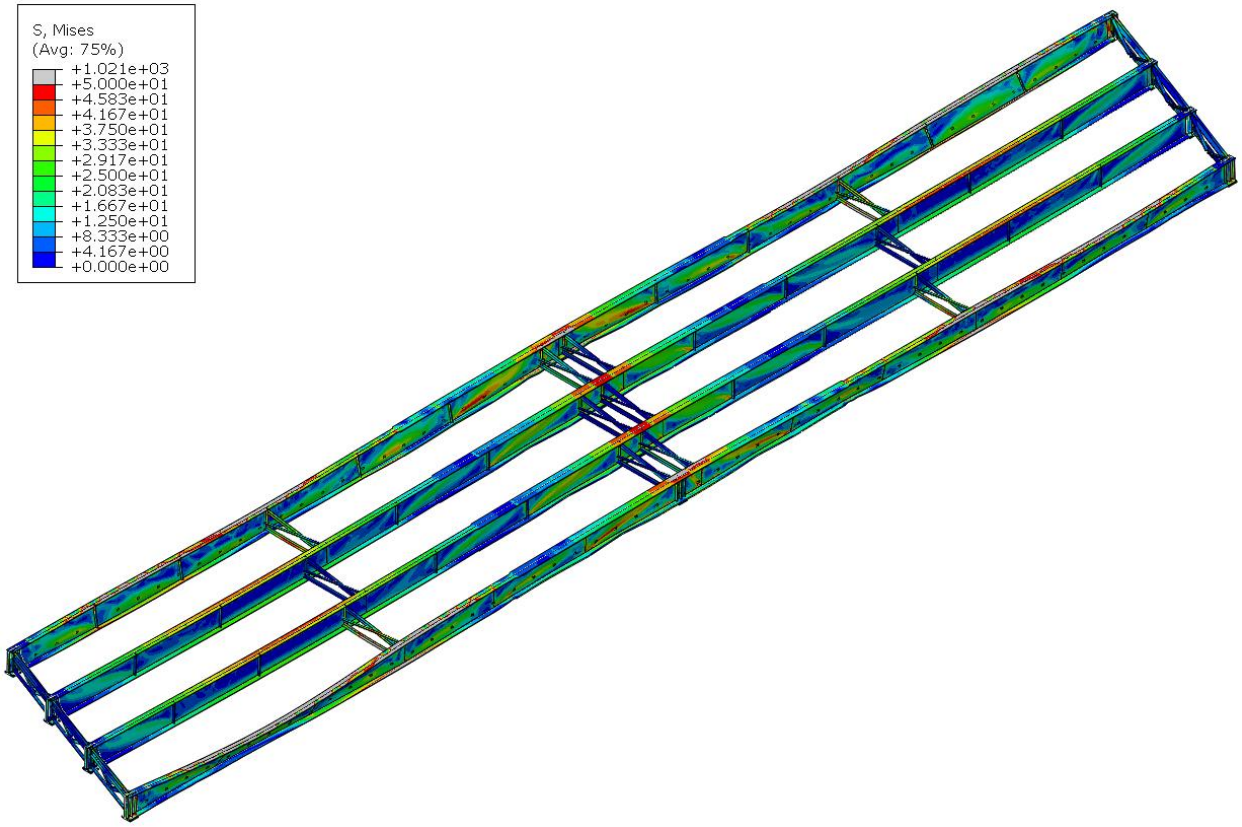

Figure 80 Deformed shaped of the 20° skewed-staggered bridge with 13.7 m [45 ft] cross-frame spacing and 9.53 mm [3/8 in.] thick stiffeners in isotropic view

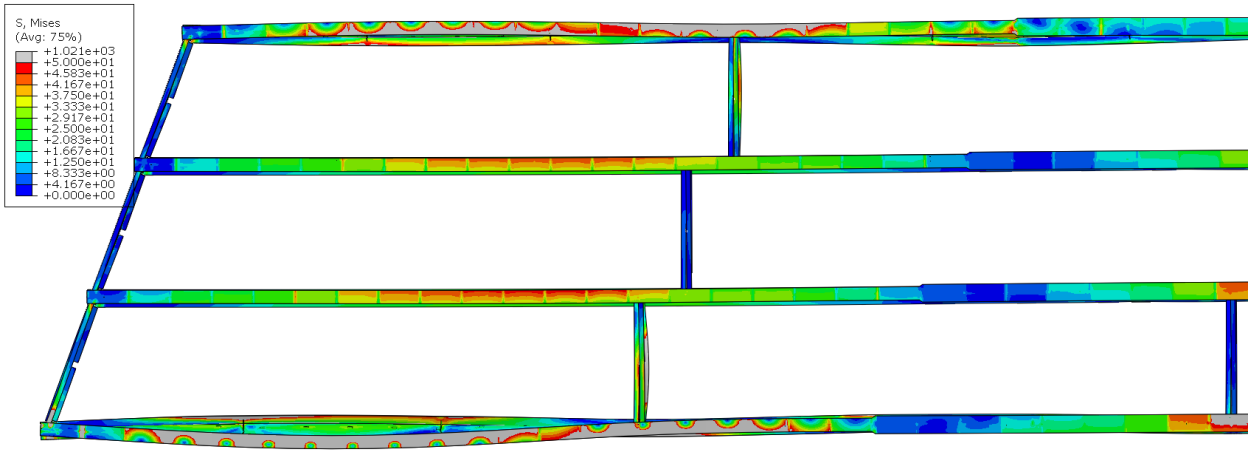

Figure 81 Deformed shape of the 20° skewed-staggered bridge in Span 1 with 13.7 m [45 ft] cross-frame spacing and 9.53 mm [3/8 in.] thick stiffeners in plan view

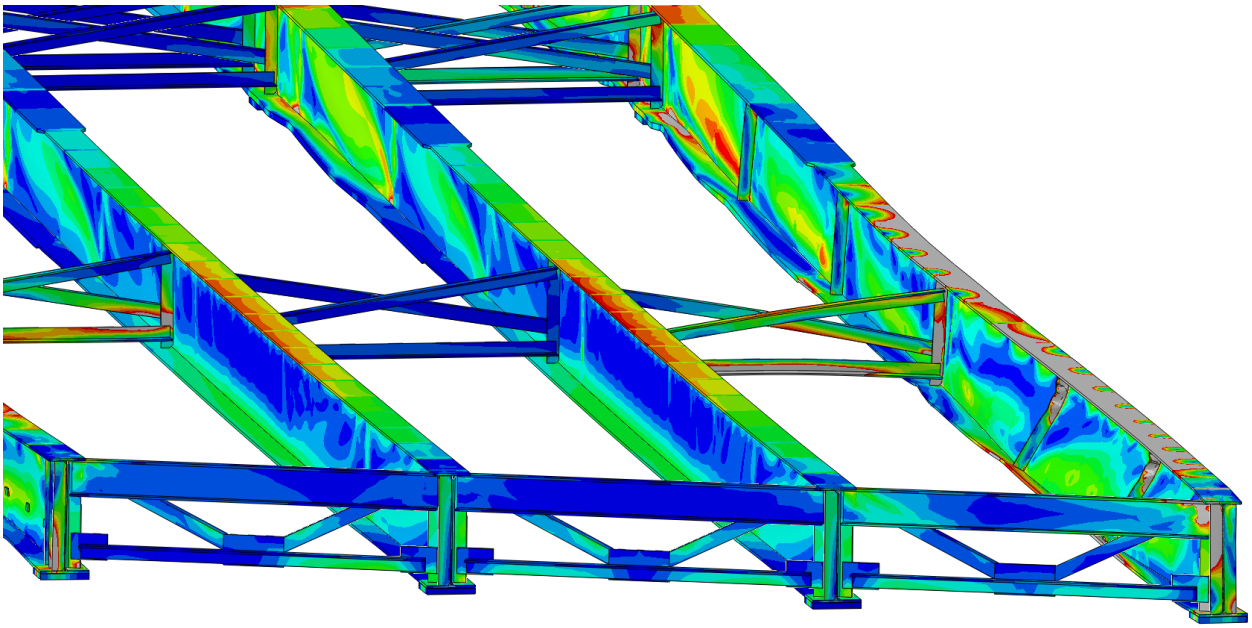

Figure 82 Girder deformation of the 20° skewed-staggered bridge with 13.7 m [45 ft] cross-frame spacing and 9.53 mm [3/8 in.] thick stiffeners

NON-SKEWED BRIDGE

45 FT CROSS-FRAME SPACING;

3/8" THICK STIFFENERS

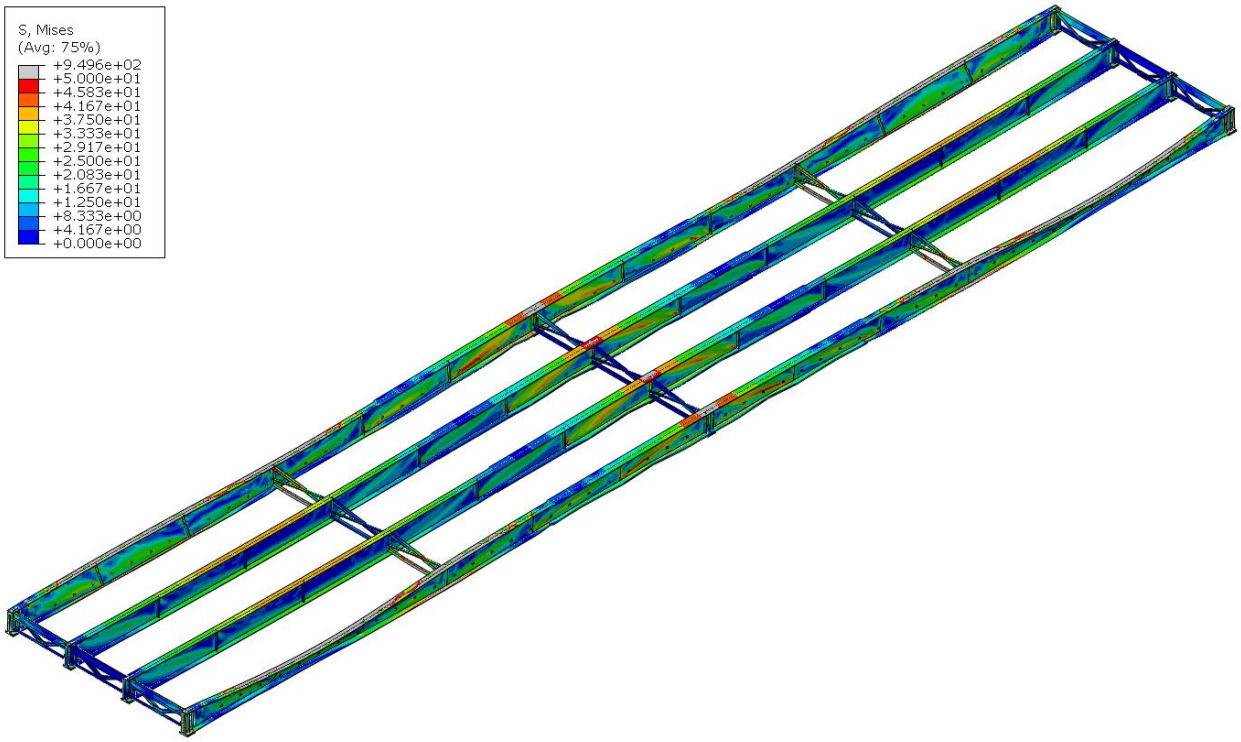

Figure 83 Deformed shaped of the non-skewed bridge with 13.7 m [45 ft] cross-frame spacing and 9.53 mm [3/8 in.] thick stiffeners in isotropic view

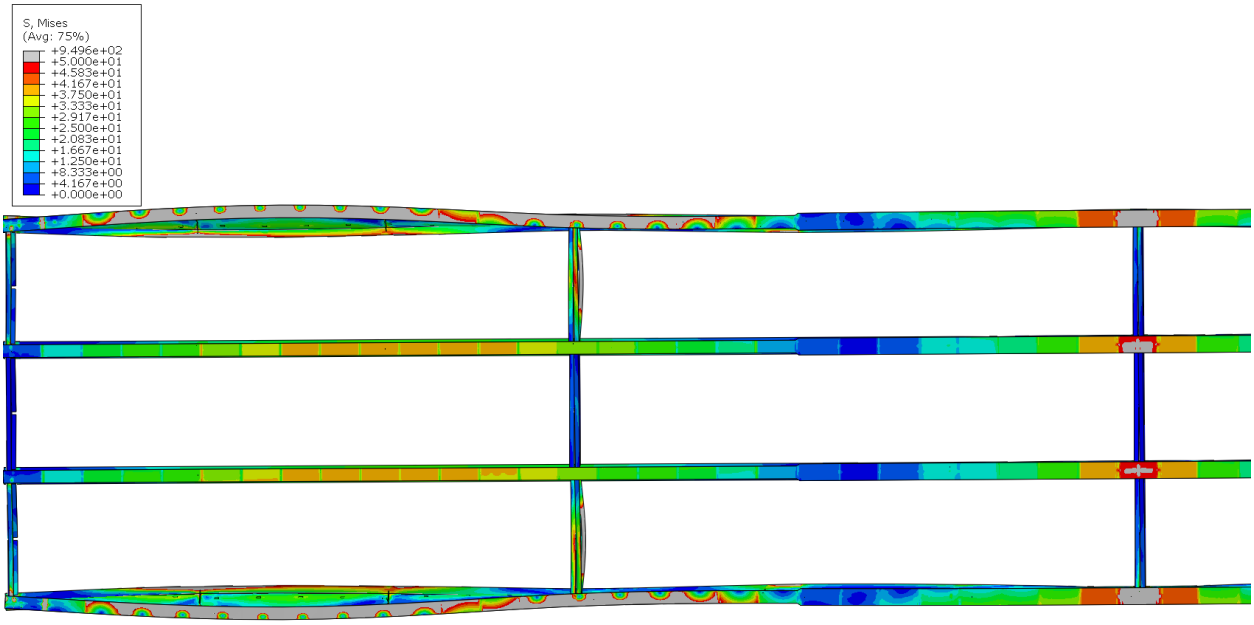

Figure 84 Deformed shape of the non-skewed bridge in Span 1 with 13.7 m [45 ft] cross-frame spacing and 9.53 mm [3/8 in.] thick stiffeners in plan view

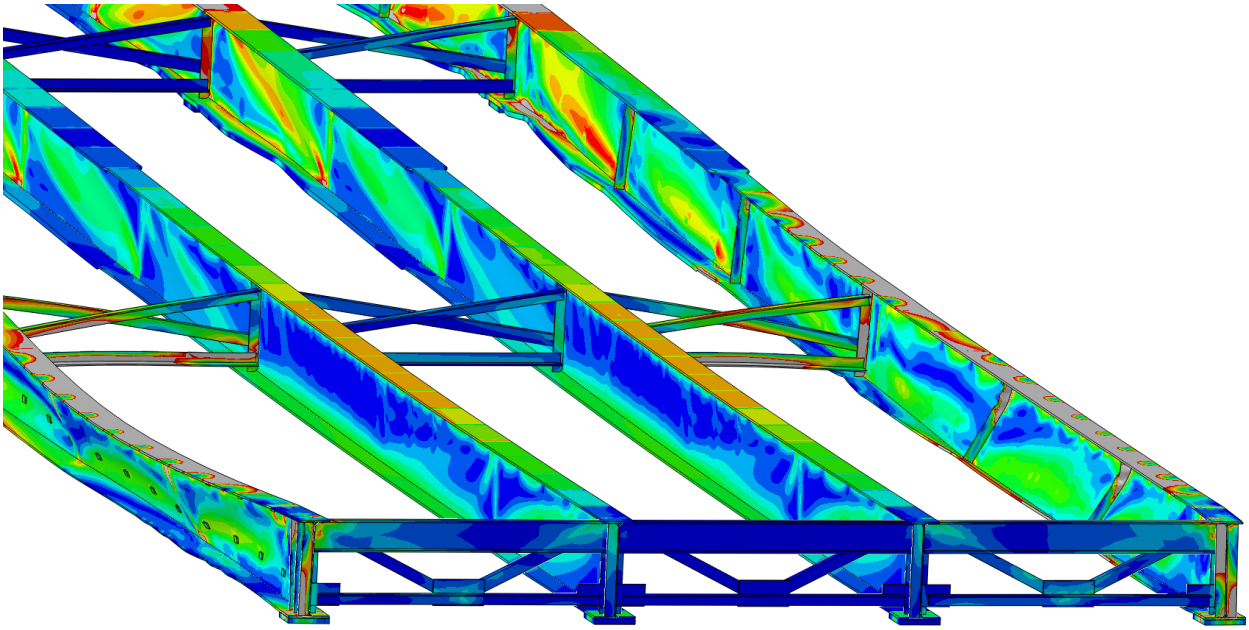

Figure 85 Girder deformation of the non-skewed bridge with 13.7 m [45 ft] cross-frame spacing and 9.53 mm [3/8 in.] thick stiffeners

40° SKEWED-PARALEL BRIDGE

45 FT CROSS-FRAME SPACING;

½" THICK STIFFENERS

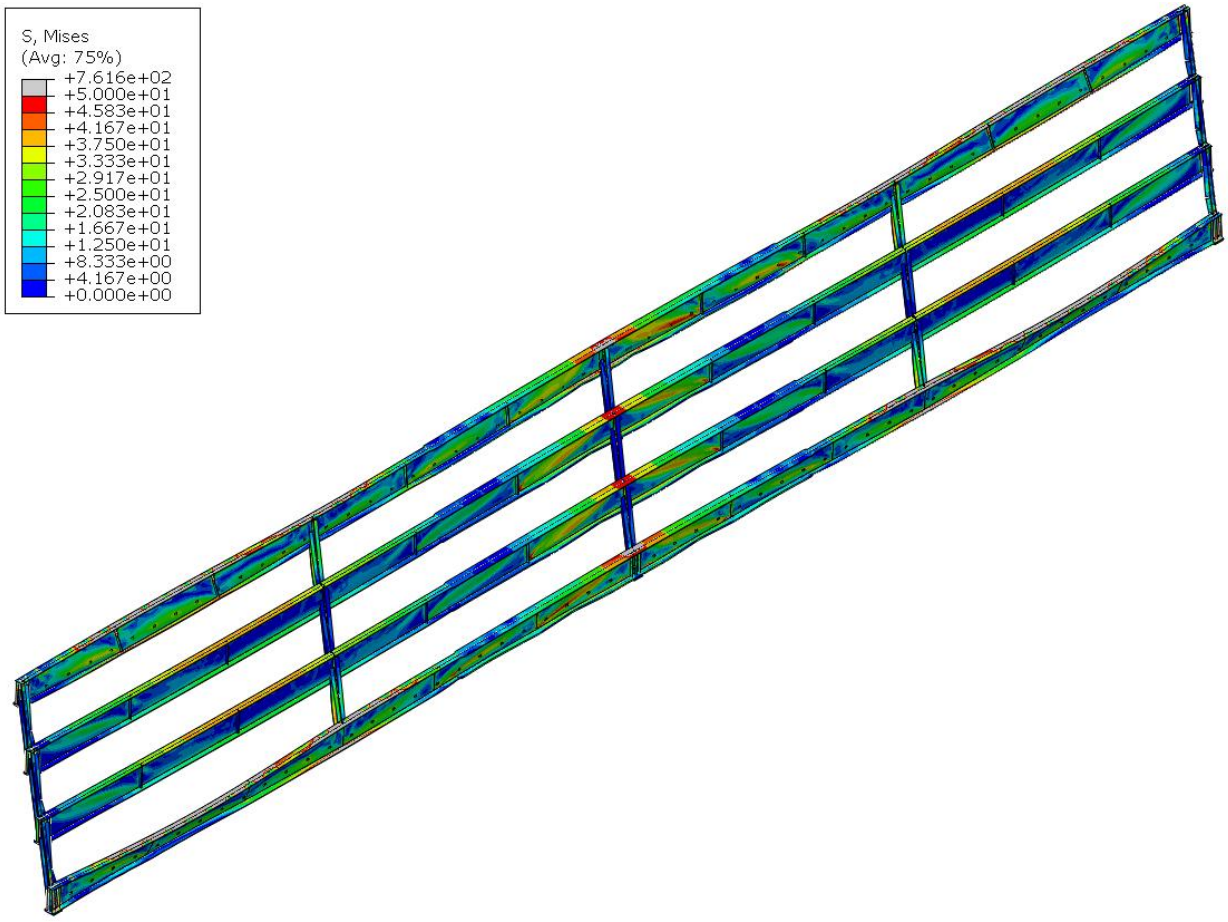

Figure 86 Deformed shaped of the 40° skewed-parallel bridge with 13.7 m [45 ft] cross-frame spacing and 12.7 mm [1/2 in.] thick stiffeners in isotropic view

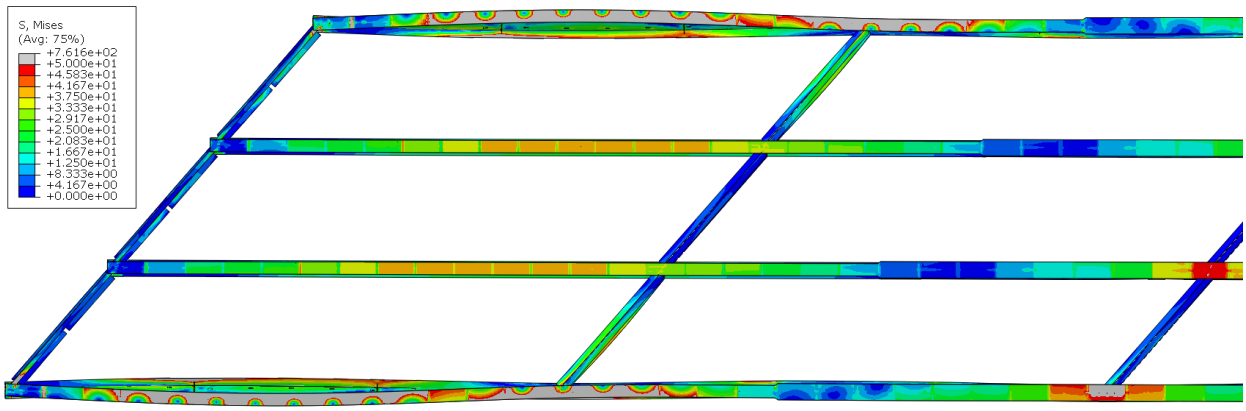

Figure 87 Deformed shape of the 40° skewed-parallel bridge in Span 1 with 13.7 m [45 ft] cross-frame spacing and 12.7 mm [1/2 in.] thick stiffeners in plan view

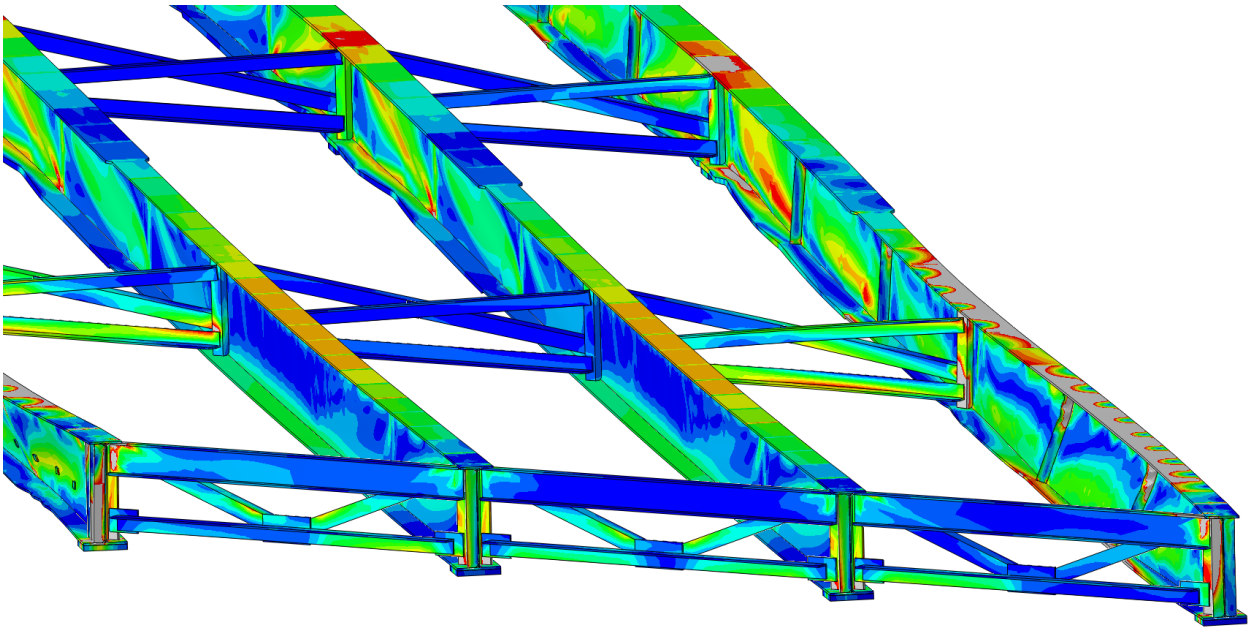

Figure 88 Girder deformation of the 40° skewed-parallel bridge with 13.7 m [45 ft] cross-frame spacing and 12.7 mm [1/2 in.] thick stiffeners

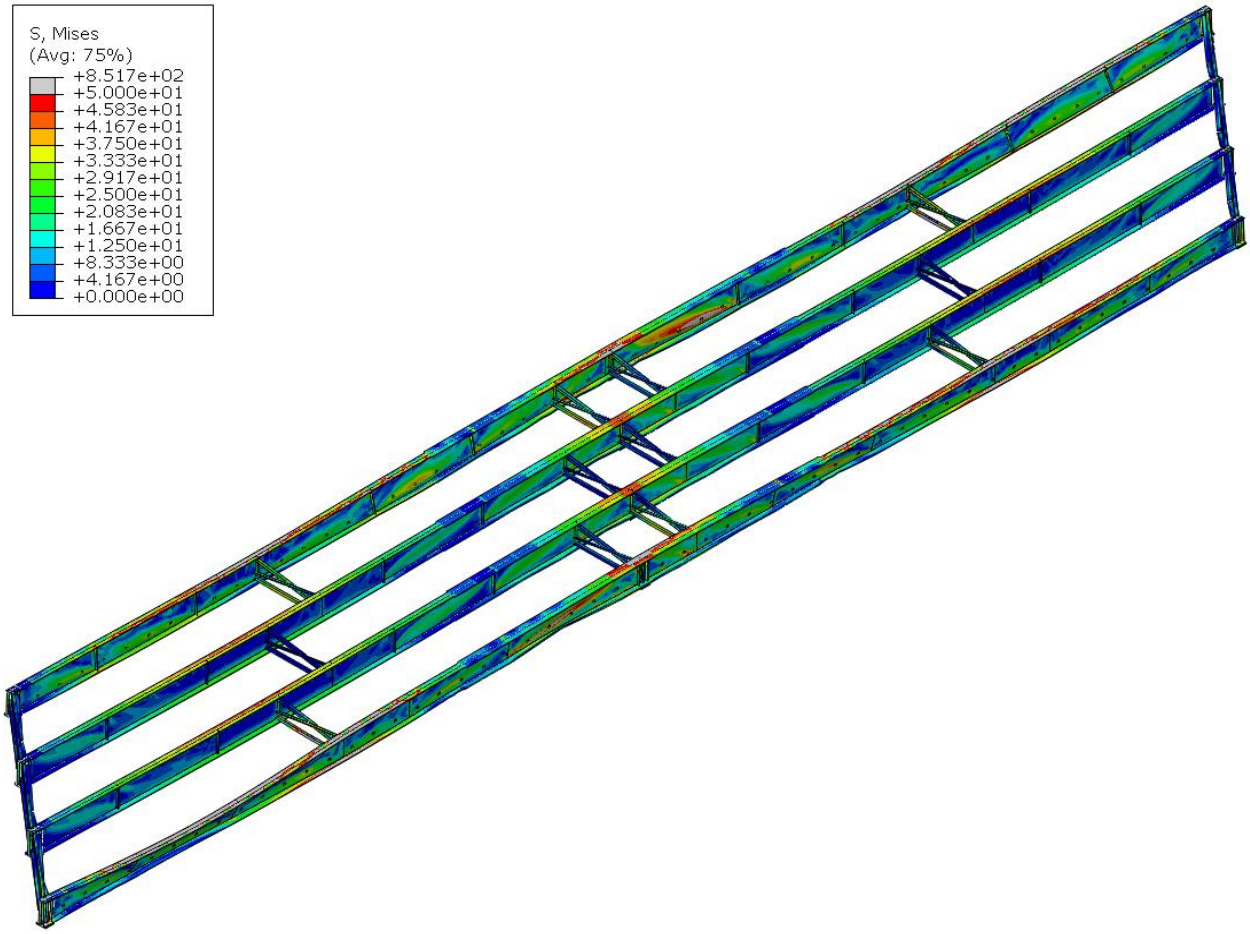

Figure 89 Deformed shaped of the 40° skewed-staggered bridge with 13.7 m [45 ft] cross-frame spacing and 12.7 mm [1/2 in.] thick stiffeners in isotropic view

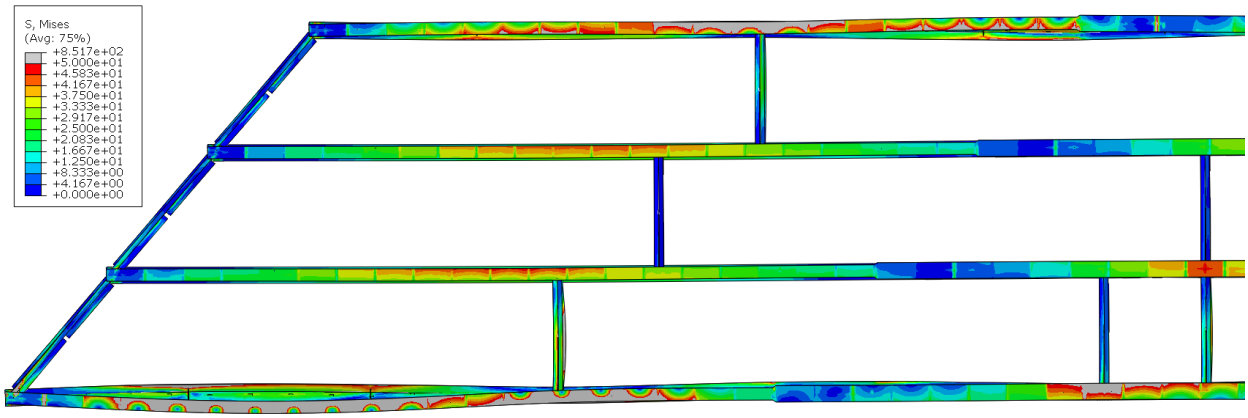

Figure 90 Deformed shape of the 40° skewed-staggered bridge in Span 1 with 13.7 m [45 ft] cross-frame spacing and 12.7 mm [1/2 in.] thick stiffeners in plan view

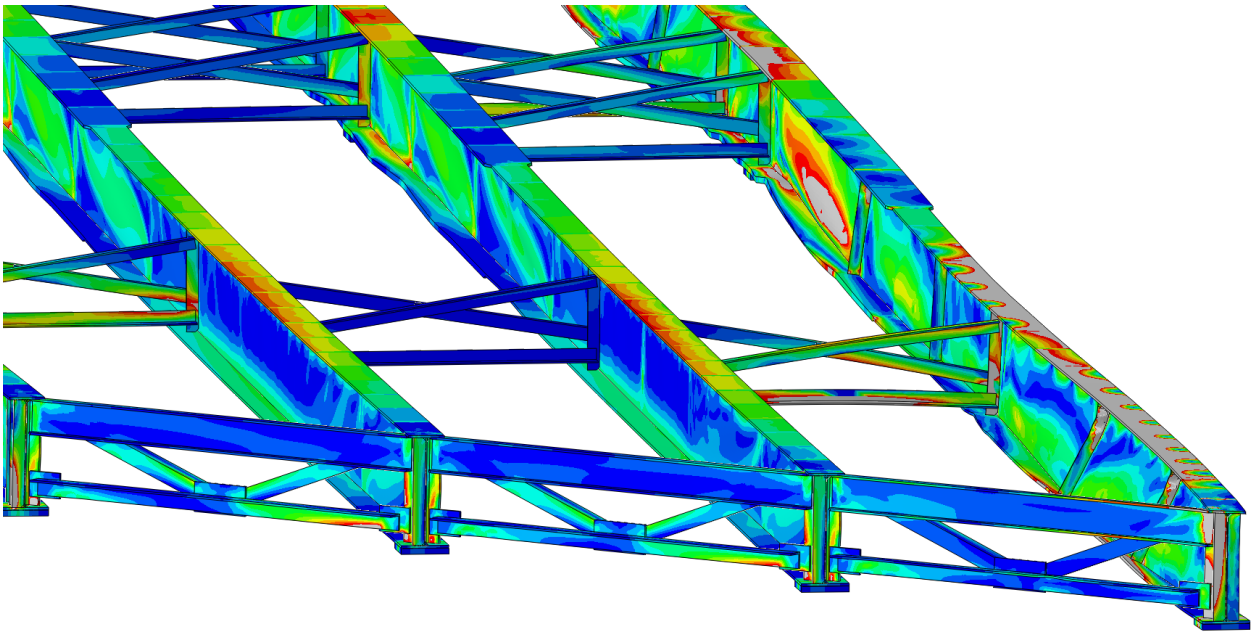

Figure 91 Girder deformation of the 40° skewed-staggered bridge with 13.7 m [45 ft] cross-frame spacing and 12.7 mm [1/2 in.] thick stiffeners

20° SKEWED-PARALLEL BRIDGE

45 FT CROSS-FRAME SPACING;

1/2" THICK STIFFENERS

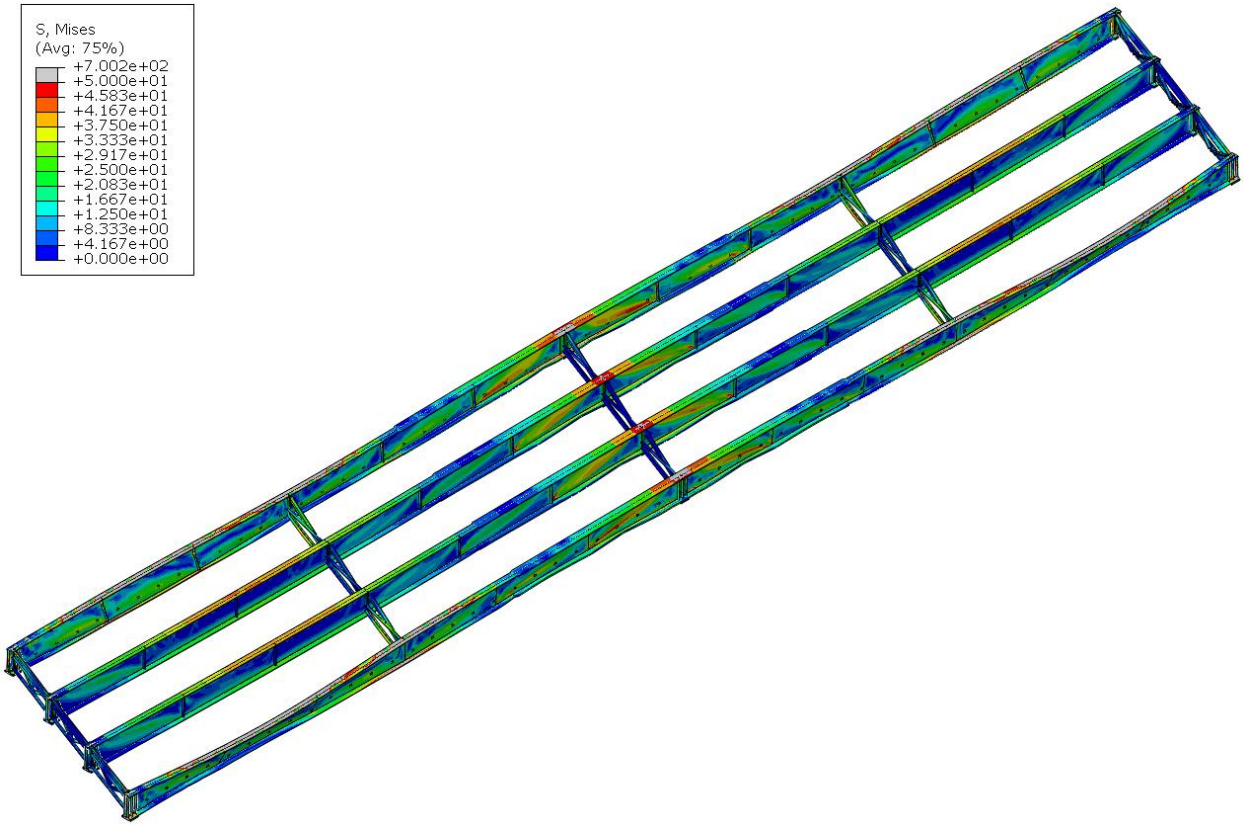

Figure 92 Deformed shaped of the 20° skewed-parallel bridge with 13.7 m [45 ft] cross-frame spacing and 12.7 mm [1/2 in.] thick stiffeners in isotropic view

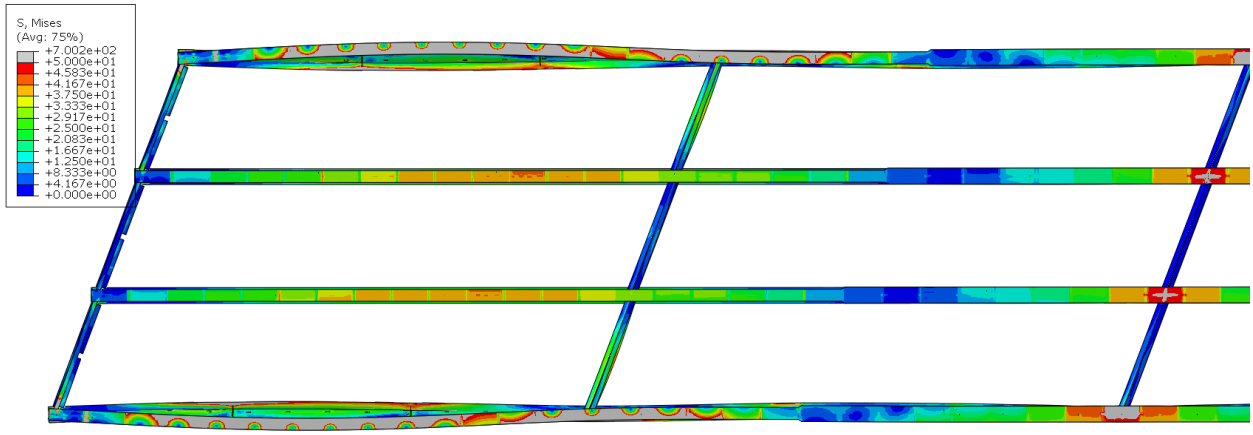

Figure 93 Deformed shape of the 20° skewed-parallel bridge in Span 1 with 13.7 m [45 ft] cross-frame spacing and 12.7 mm [1/2 in.] thick stiffeners in plan view

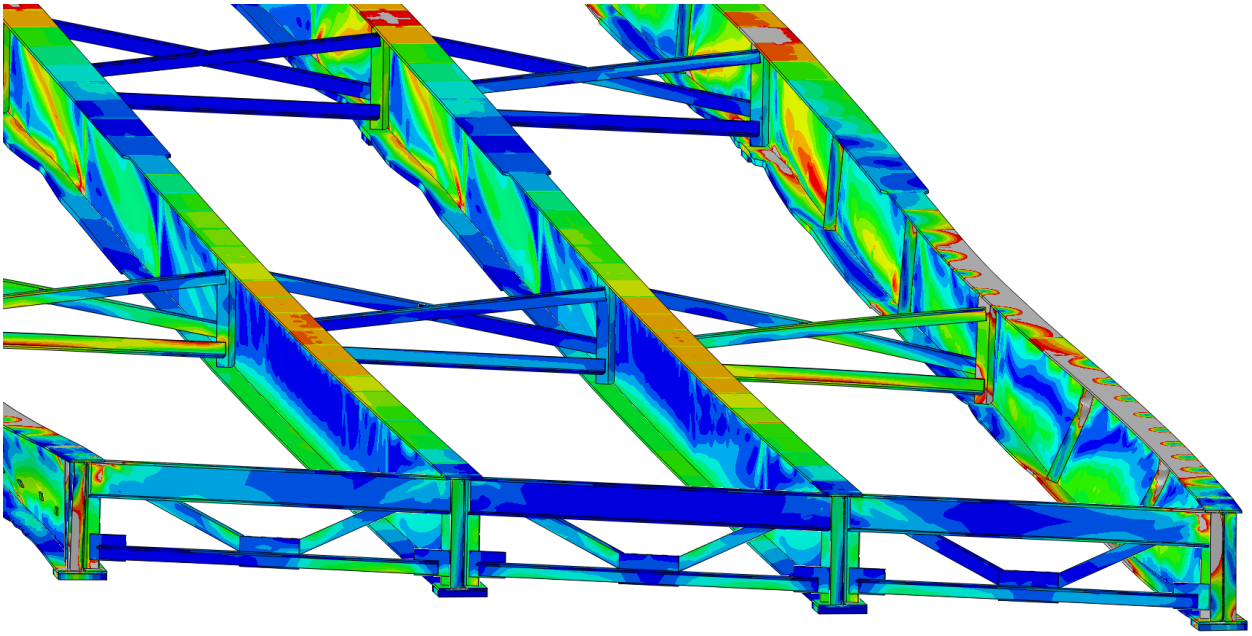

Figure 94 Girder deformation of the 20° skewed-parallel bridge with 13.7 m [45 ft] cross-frame spacing and 12.7 mm [1/2 in.] thick stiffeners

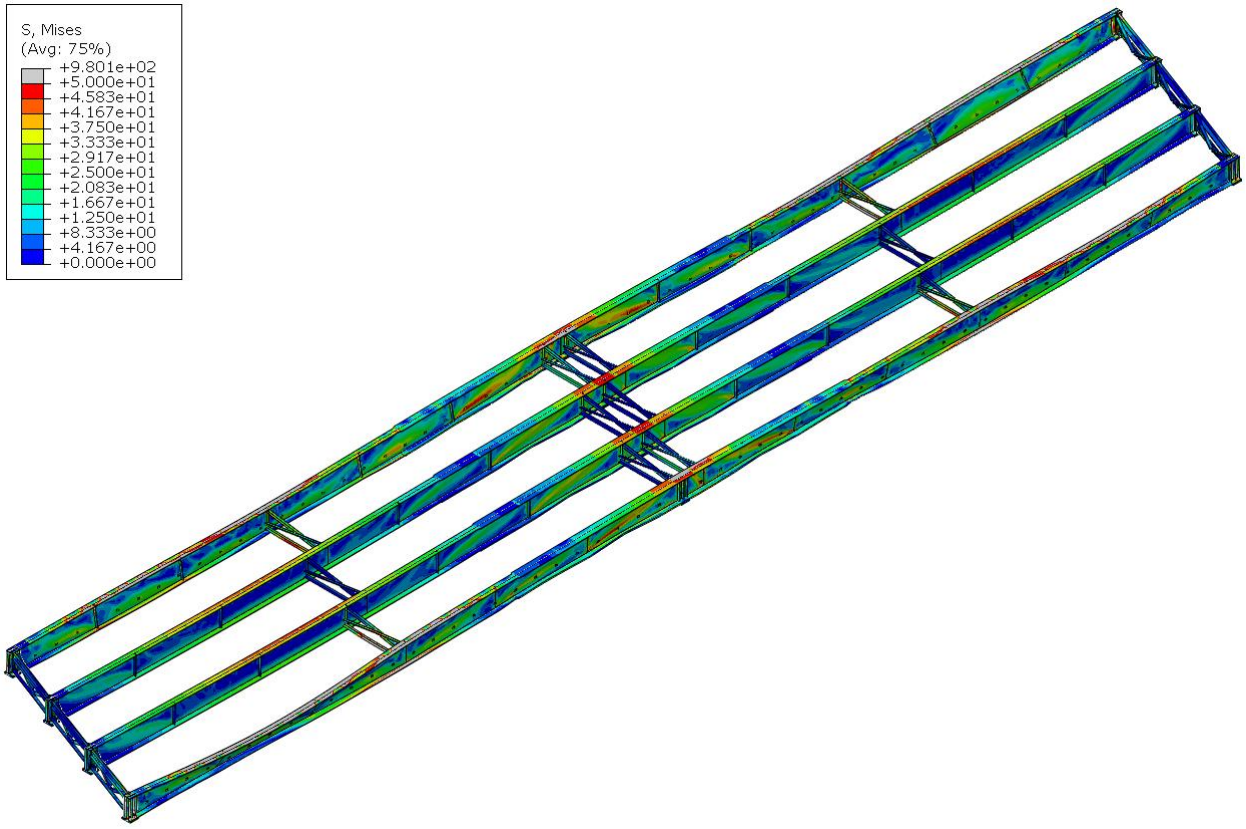

Figure 95 Deformed shaped of the 20° skewed-staggered bridge with 13.7 m [45 ft] cross-frame spacing and 12.7 mm [1/2 in.] thick stiffeners in isotropic view

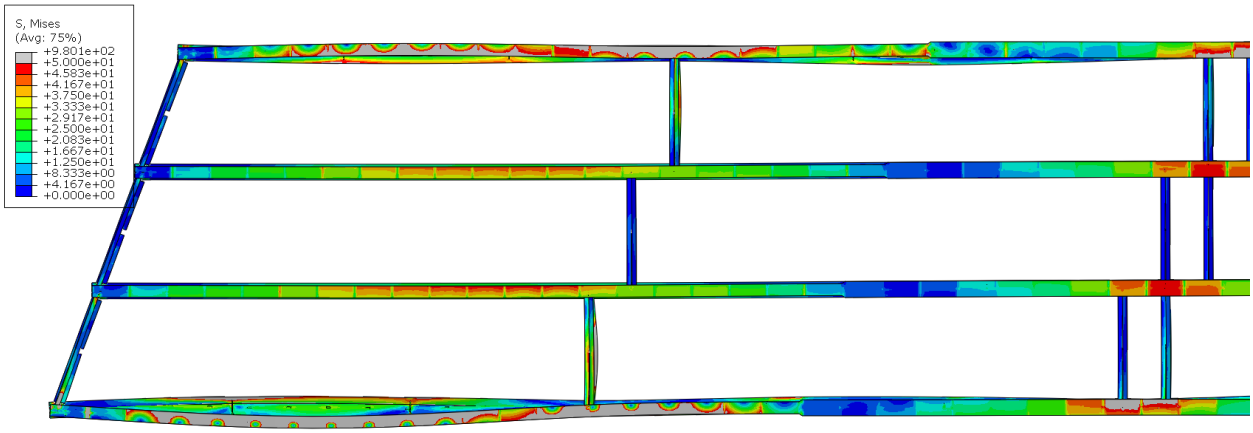

Figure 96 Deformed shape of the 20° skewed-staggered bridge in Span 1 with 13.7 m [45 ft] cross-frame spacing and 12.7 mm [1/2 in.] thick stiffeners in plan view

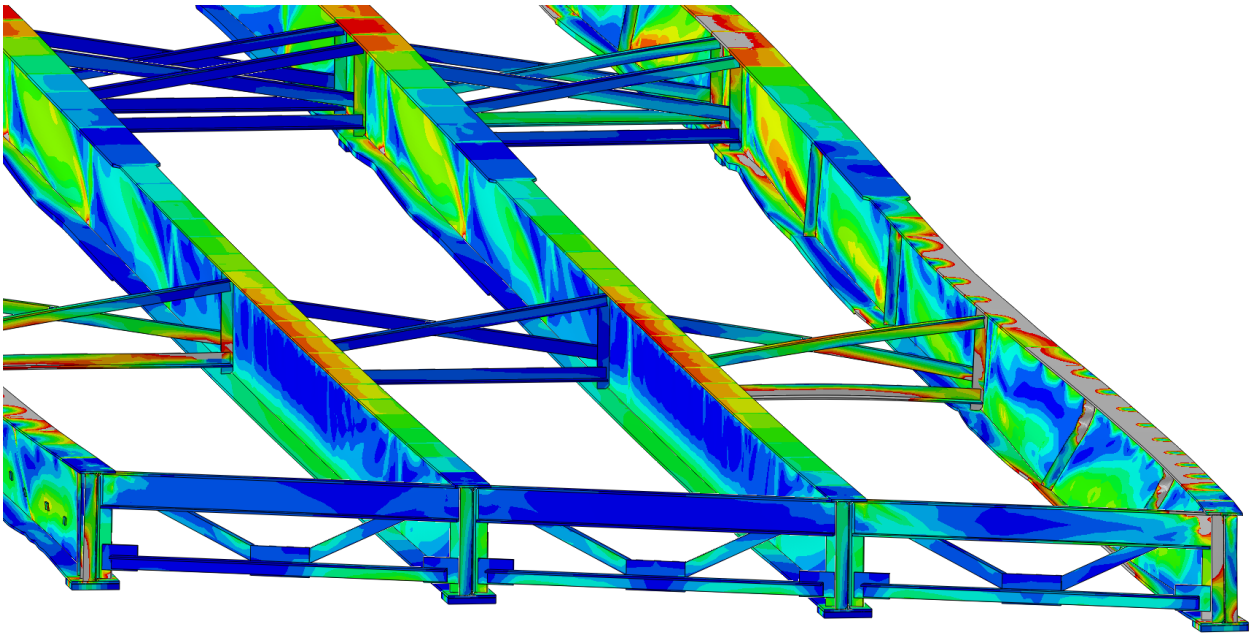

Figure 97 Girder deformation of the 20° skewed-staggered bridge with 13.7 m [45 ft] cross-frame spacing and 12.7 mm [1/2 in.] thick stiffeners

NON-SKEWED BRIDGE

45 FT CROSS-FRAME SPACING;

1/2" THICK STIFFENERS

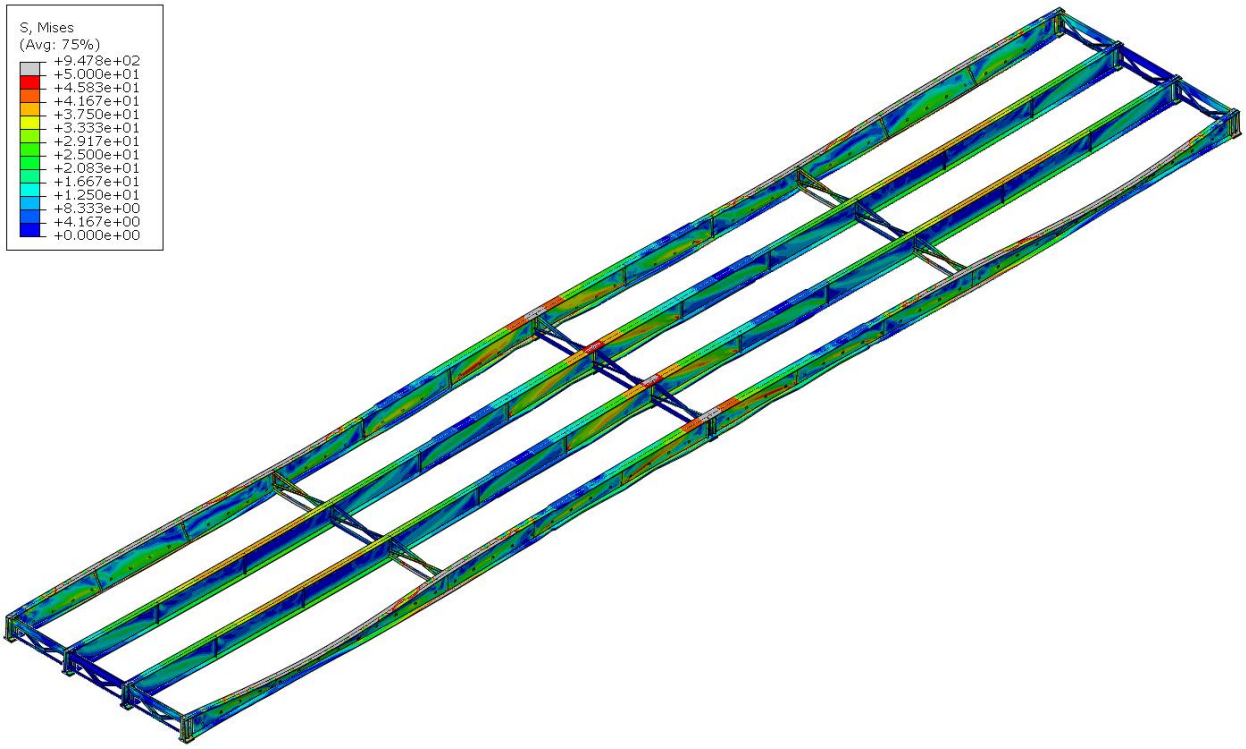

Figure 98 Deformed shaped of the non-skewed bridge with 13.7 m [45 ft] cross-frame spacing and 12.7 mm [1/2 in.] thick stiffeners in isotropic view

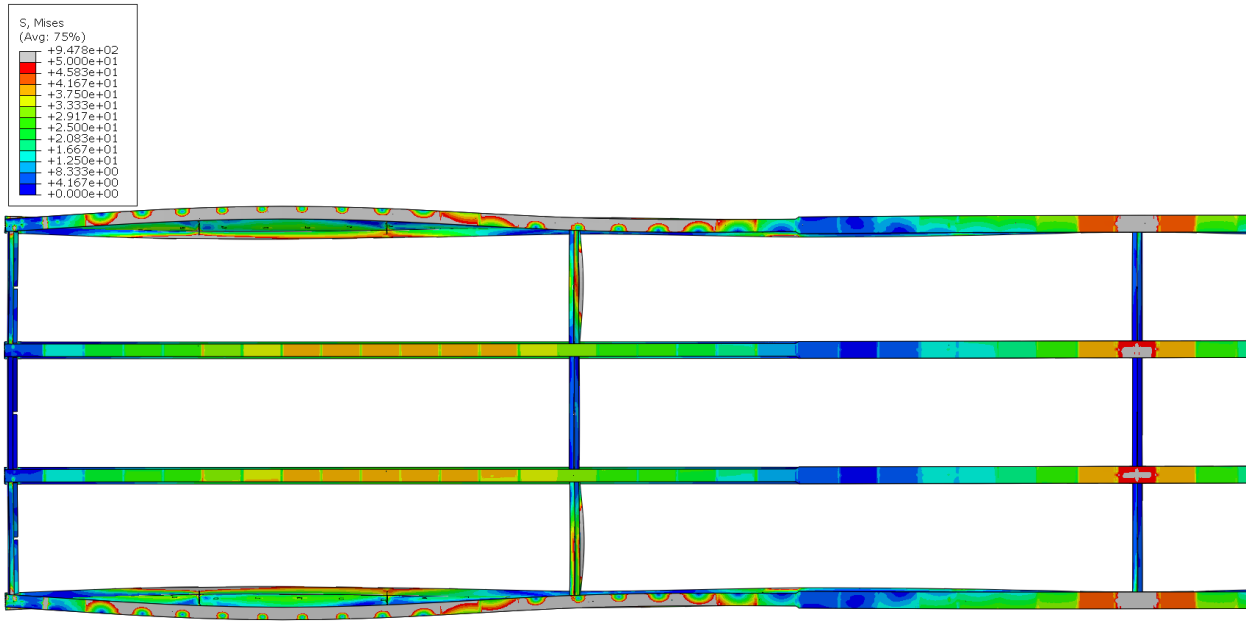

Figure 99 Deformed shape of the non-skewed bridge in Span 1 with 13.7 m [45 ft] cross-frame spacing and 12.7 mm [1/2 in.] thick stiffeners in plan view

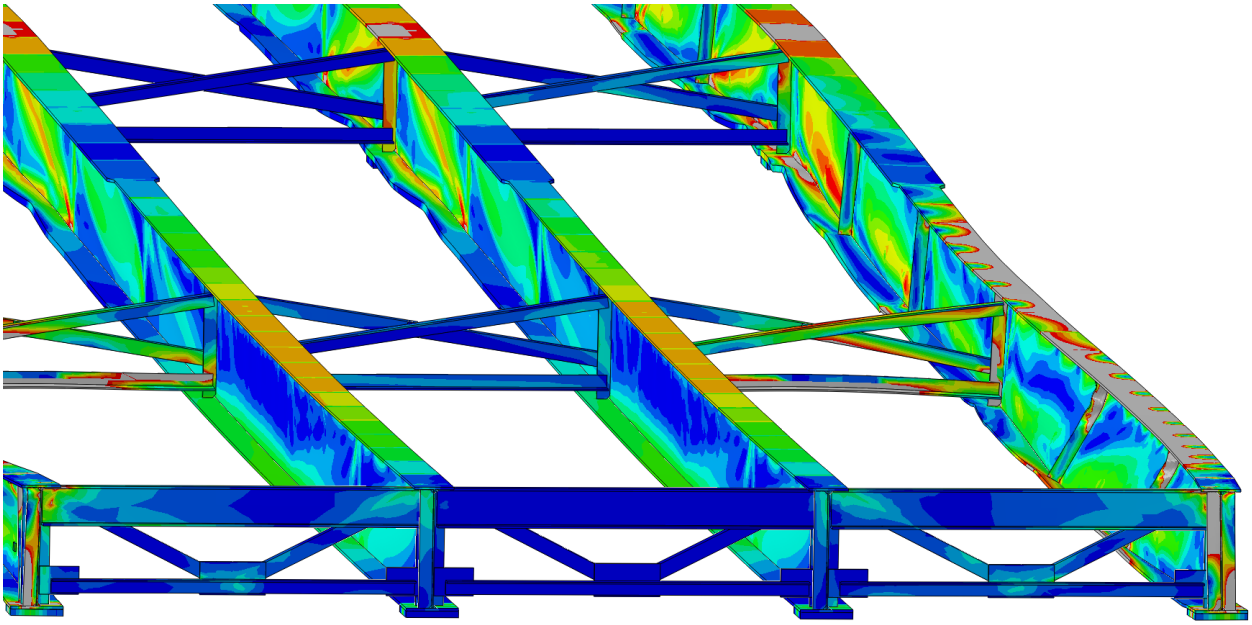

Figure 100 Girder deformation of the non-skewed bridge with 13.7 m [45 ft] cross-frame spacing and 12.7 mm [1/2 in.] thick stiffeners

40° SKEWED-PARALLEL BRIDGE

45 FT CROSS-FRAME SPACING;

1" THICK STIFFENERS

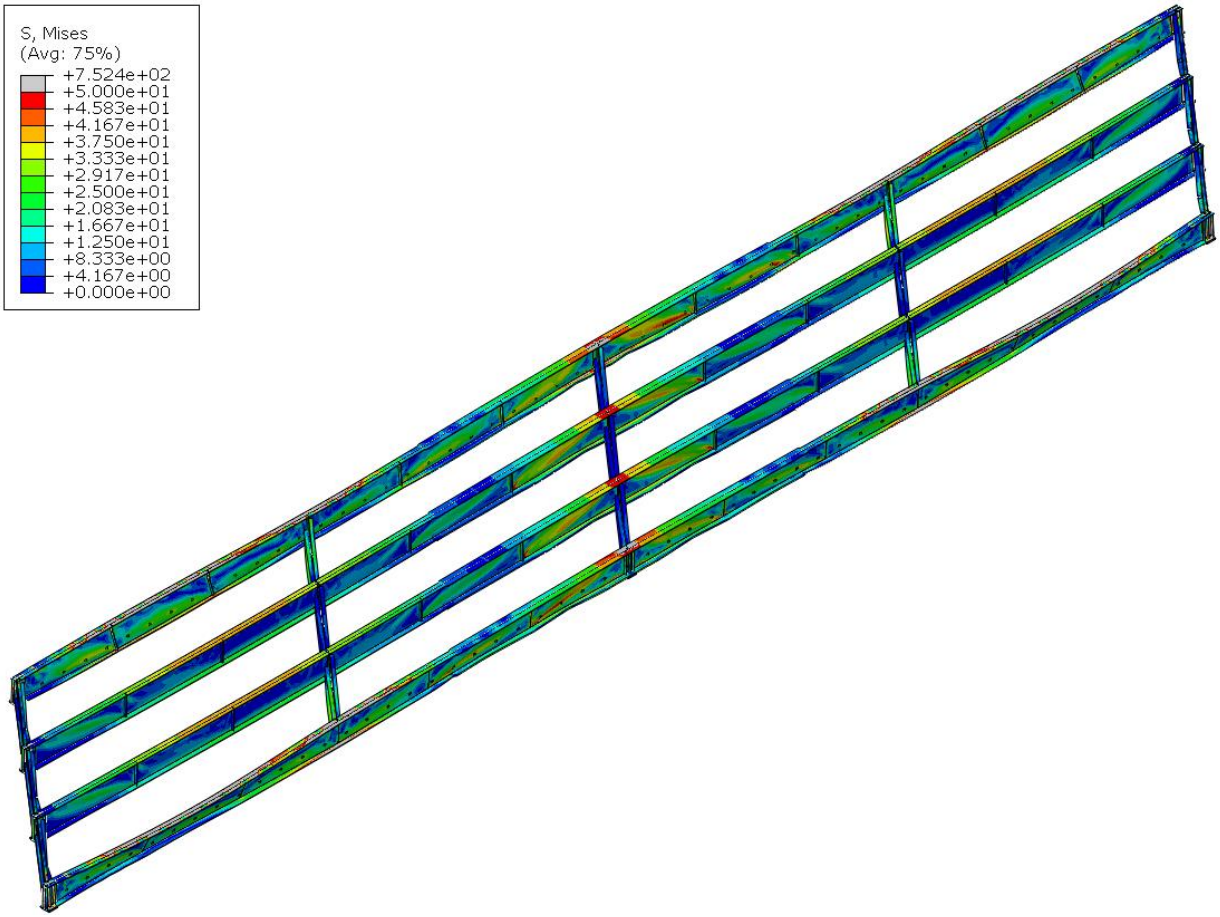

Figure 101 Deformed shaped of the 40° skewed-parallel bridge with 13.7 m [45 ft] cross-frame spacing and 25.4 mm [1.0 in.] thick stiffeners in isotropic view

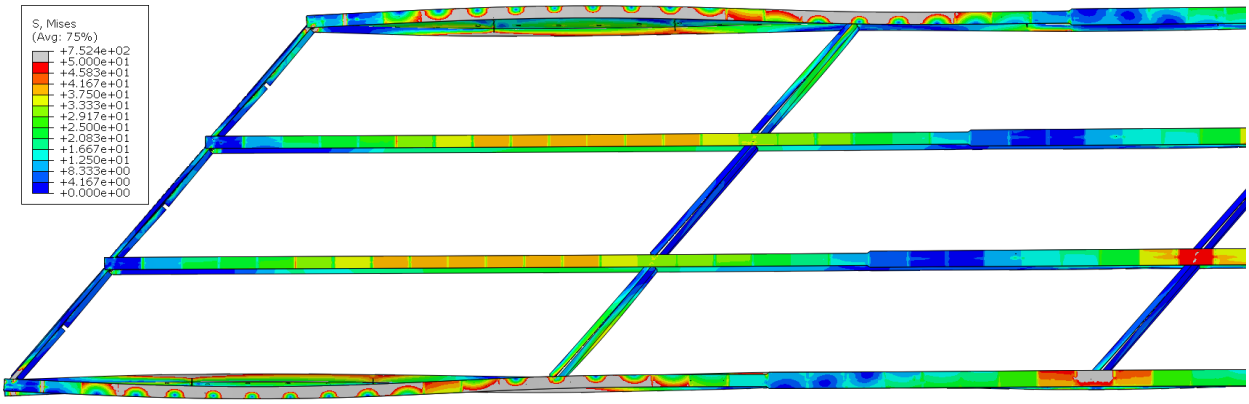

Figure 102 Deformed shape of the 40° skewed-parallel bridge in Span 1 with 13.7 m [45 ft] cross-frame spacing and 25.4 mm [1.0 in.] thick stiffeners in plan view

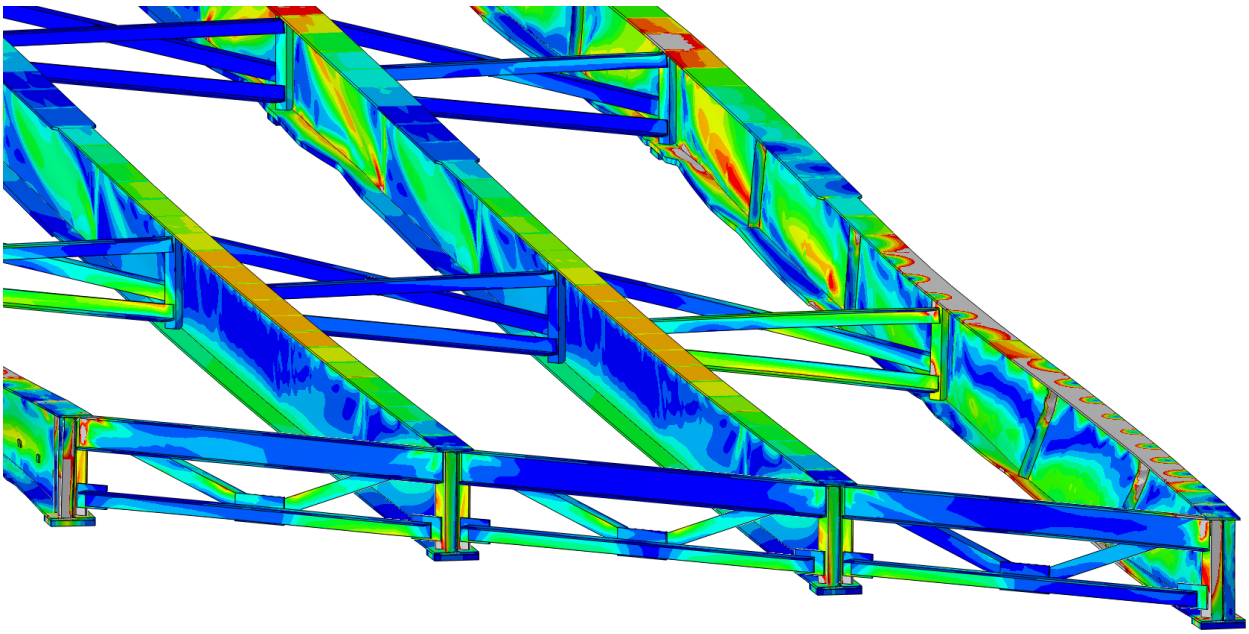

Figure 103 Girder deformation of the 40° skewed-parallel bridge with 13.7 m [45 ft] cross-frame spacing and 25.4 mm [1.0 in.] thick stiffeners

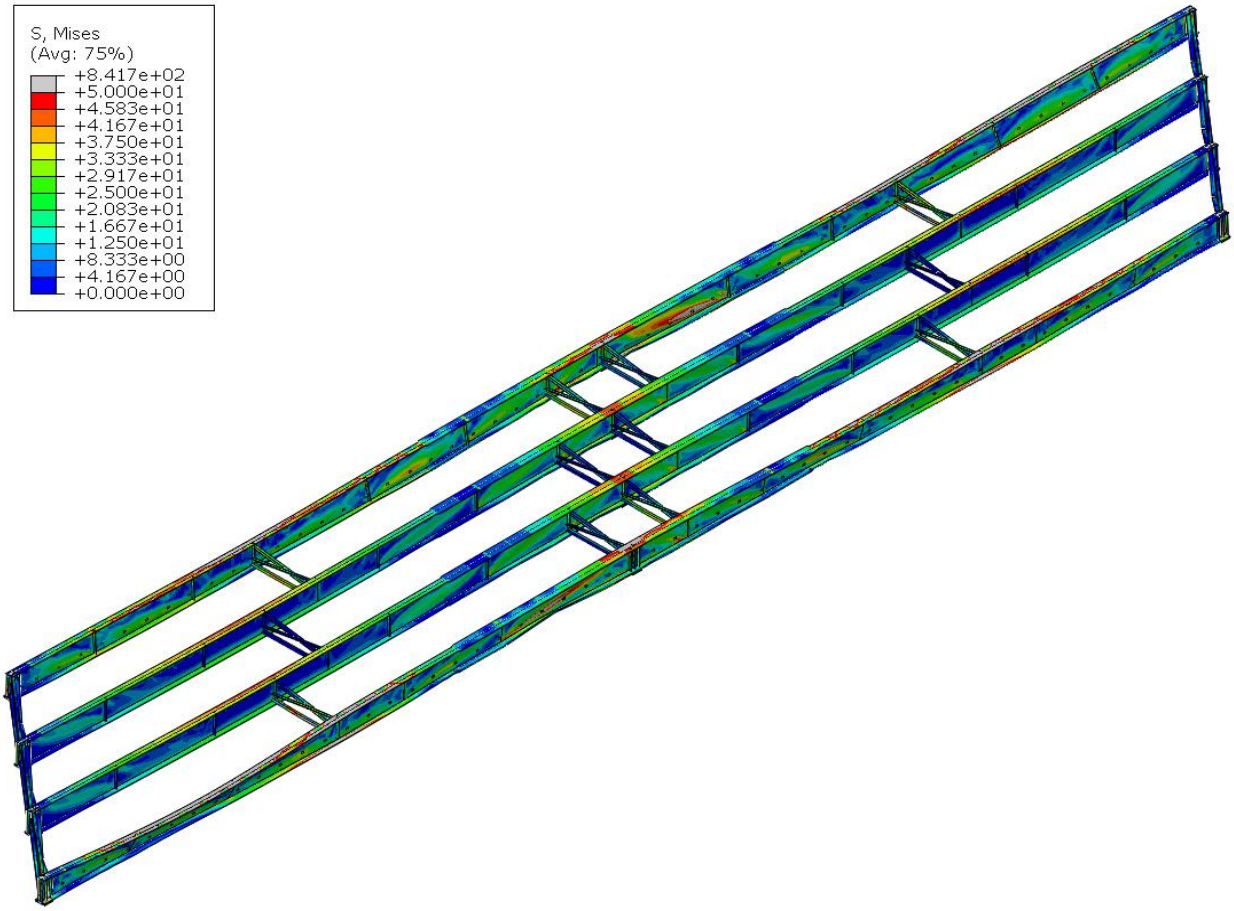

Figure 104 Deformed shaped of the 40° skewed-staggered bridge with 13.7 m [45 ft] cross-frame spacing and 25.4 mm [1.0 in.] thick stiffeners in isotropic view

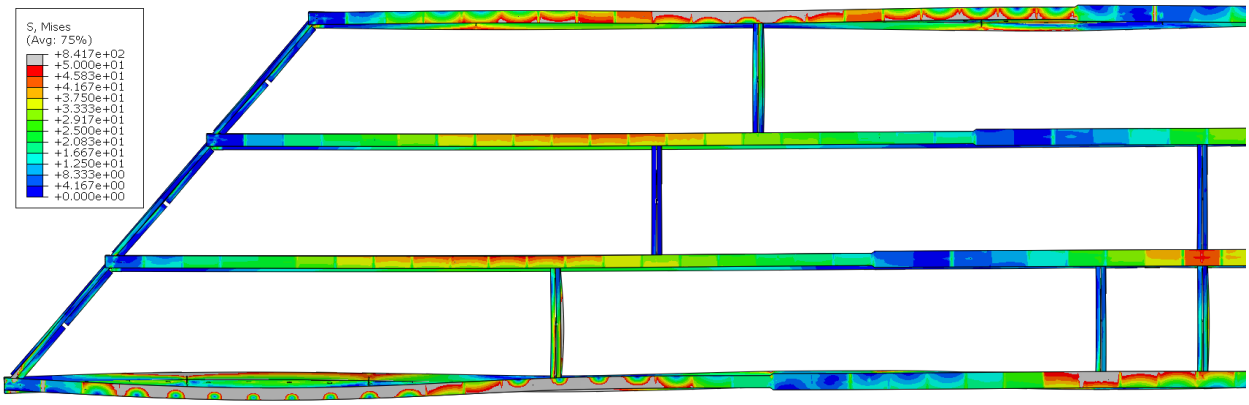

Figure 105 Deformed shape of the 40° skewed-staggered bridge in Span 1 with 13.7 m [45 ft] cross-frame spacing and 25.4 mm [1.0 in.] thick stiffeners in plan view

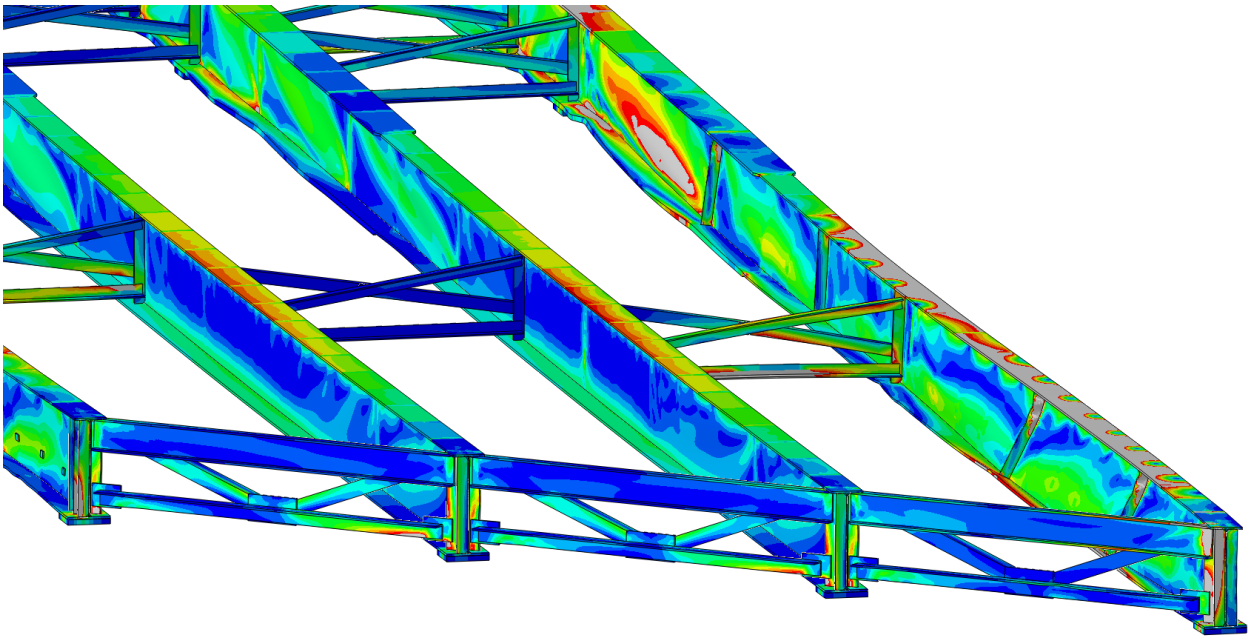

Figure 106 Girder deformation of the 40° skewed-staggered bridge with 13.7 m [45 ft] cross-frame spacing and 25.4 mm [1.0 in.] thick stiffeners

20° SKEWED-PARALLEL BRIDGE

45 FT CROSS-FRAME SPACING;

1" THICK STIFFENERS

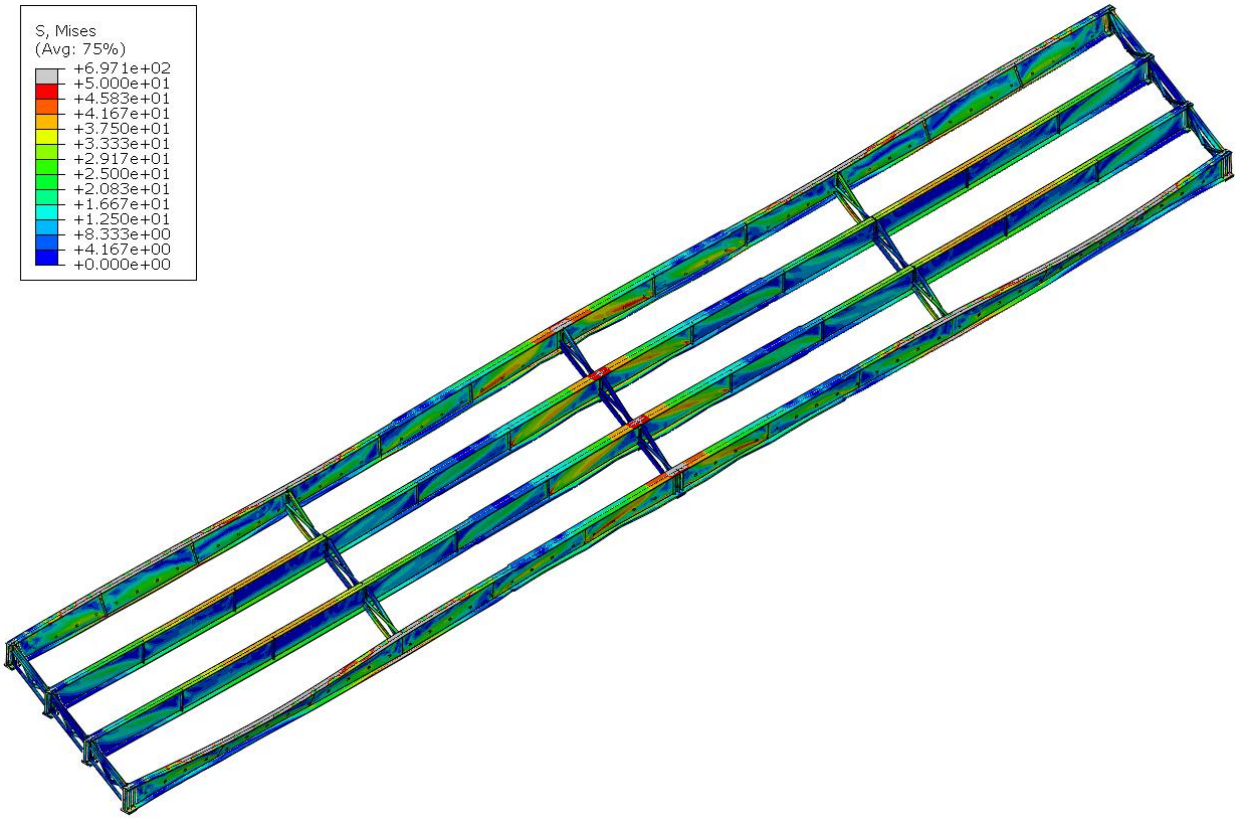

Figure 107 Deformed shaped of the 20° skewed-parallel bridge with 13.7 m [45 ft] cross-frame spacing and 25.4 mm [1.0 in.] thick stiffeners in isotropic view

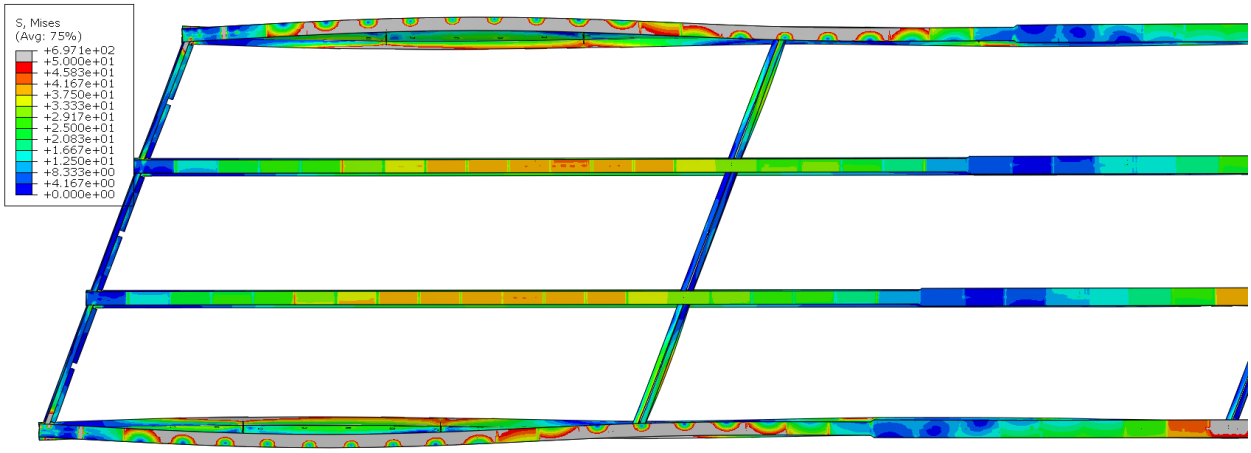

Figure 108 Deformed shape of the 20° skewed-parallel bridge in Span 1 with 13.7 m [45 ft] cross-frame spacing and 25.4 mm [1.0 in.] thick stiffeners in plan view

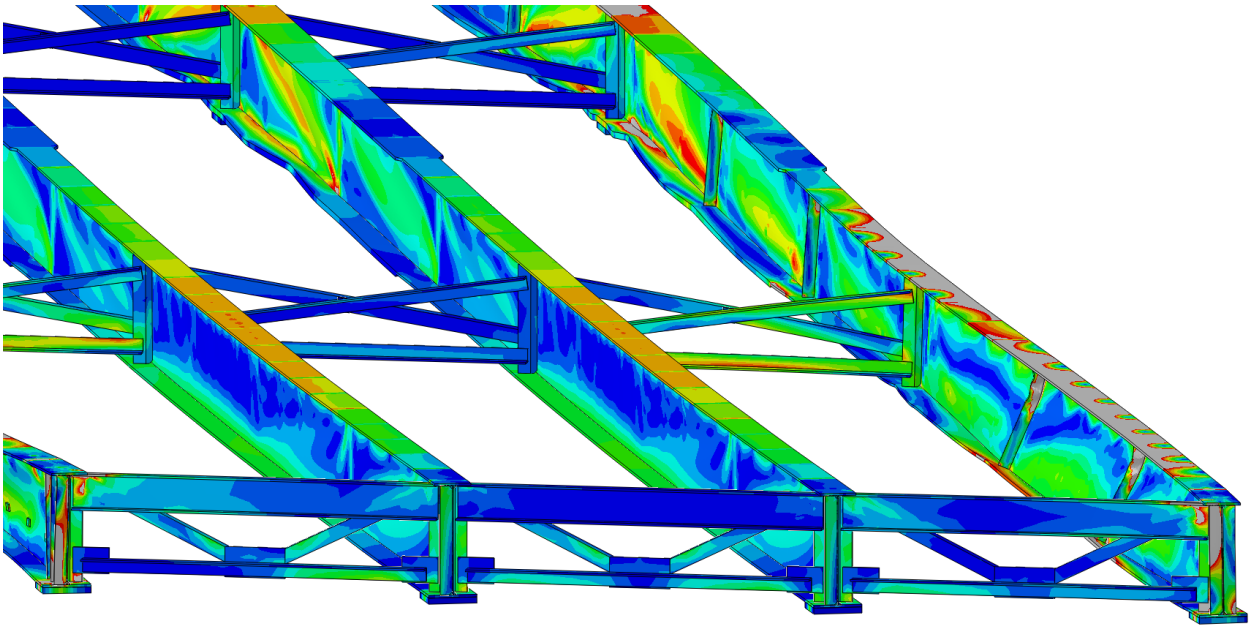

Figure 109 Girder deformation of the 20° skewed-parallel bridge with 13.7 m [45 ft] cross-frame spacing and 25.4 mm [1.0 in.] thick stiffeners

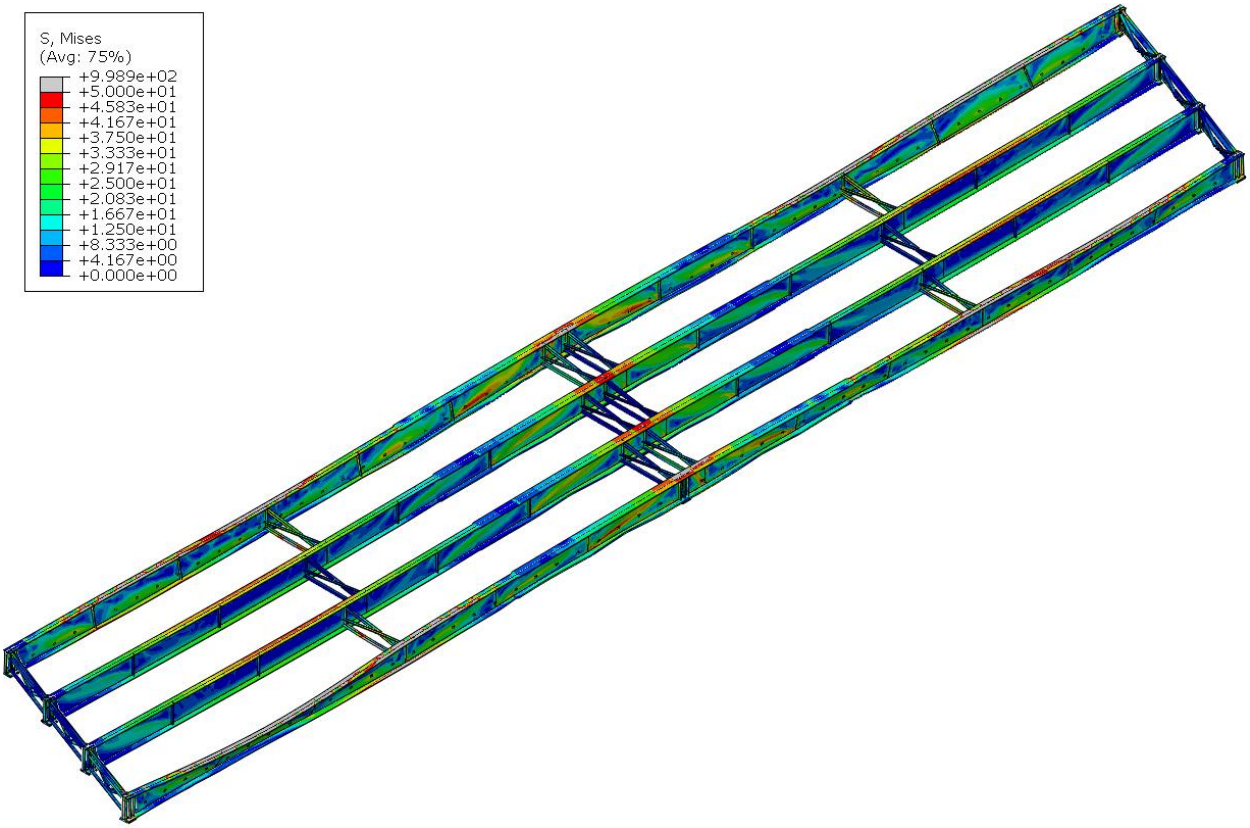

Figure 110 Deformed shaped of the 20° skewed-staggered bridge with 13.7 m [45 ft] cross-frame spacing and 25.4 mm [1.0 in.] thick stiffeners in isotropic view

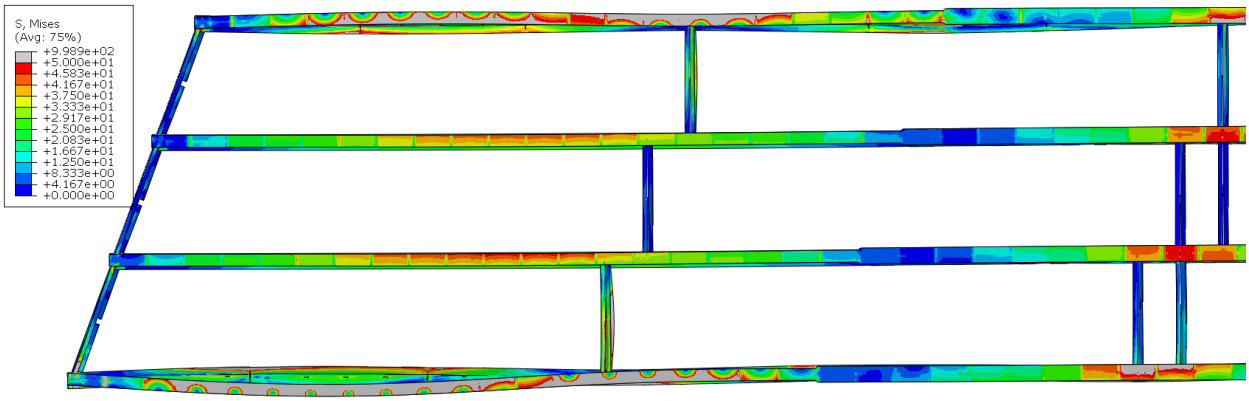

Figure 111 Deformed shape of the 20° skewed-staggered bridge in Span 1 with 13.7 m [45 ft] cross-frame spacing and 25.4 mm [1.0 in.] thick stiffeners in plan view

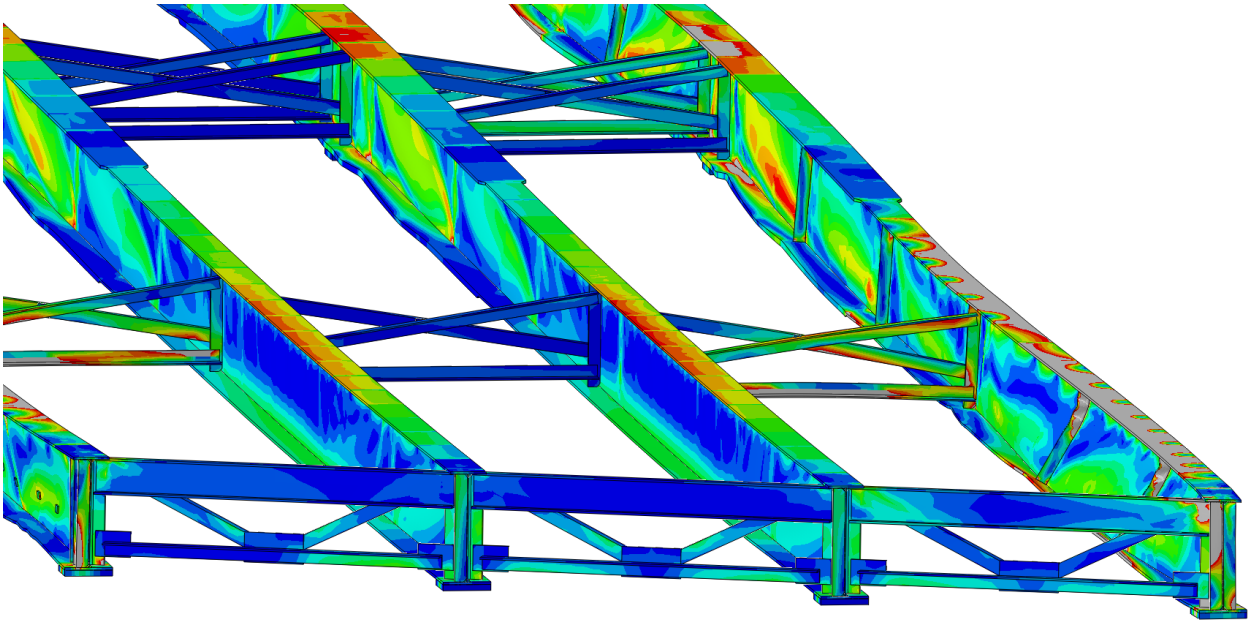

Figure 112 Girder deformation of the 20° skewed-staggered bridge with 13.7 m [45 ft] cross-frame spacing and 25.4 mm [1.0 in.] thick stiffeners

NON-SKEWED BRIDGE

45 FT CROSS-FRAME SPACING;

1" THICK STIFFENERS

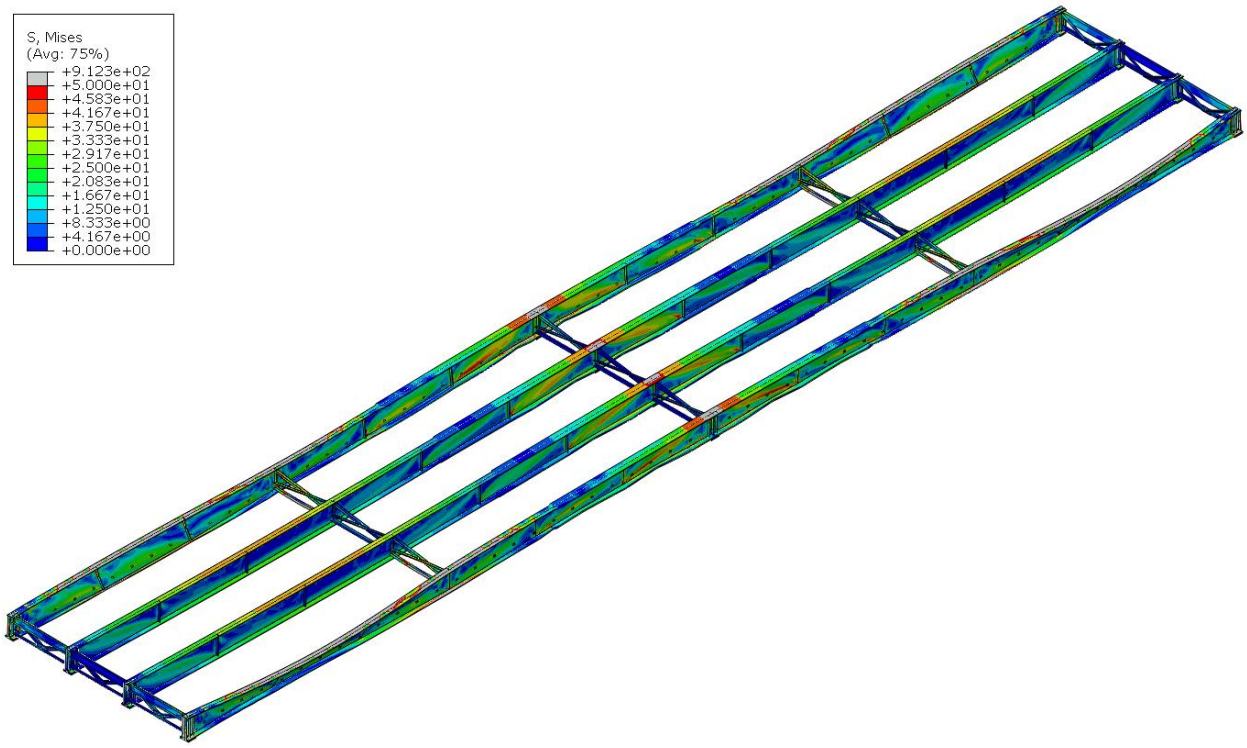

Figure 113 Deformed shaped of the non-skewed bridge with 13.7 m [45 ft] cross-frame spacing and 25.4 mm [1.0 in.] thick stiffeners in isotropic view

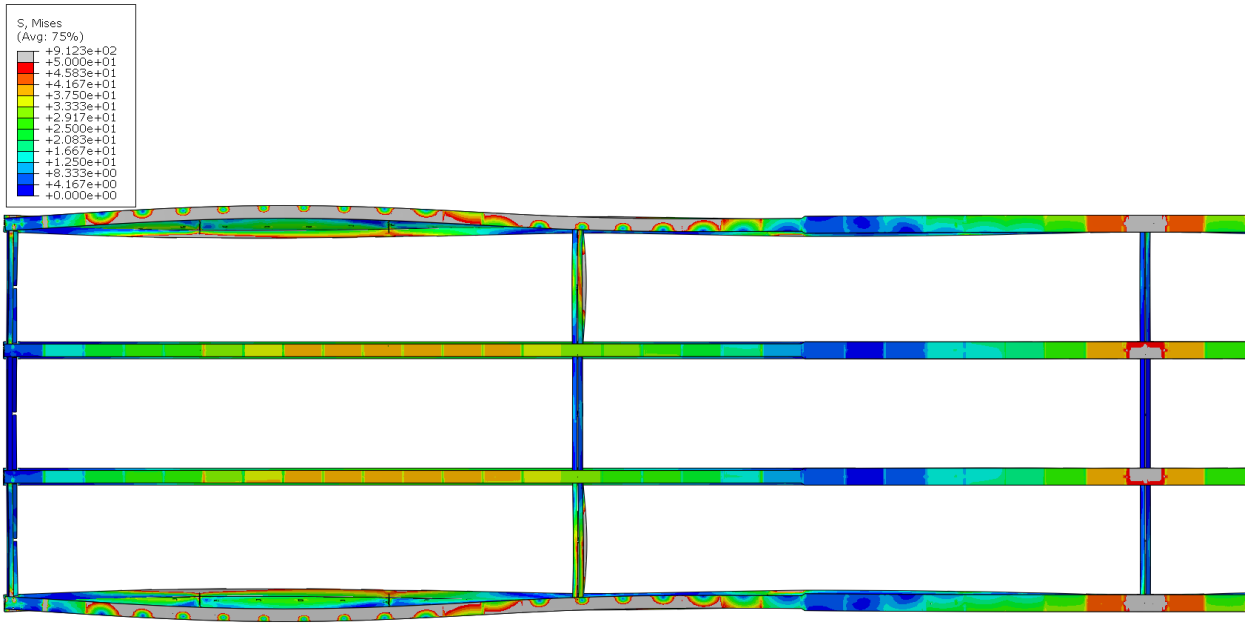

Figure 114 Deformed shape of the non-skewed bridge in Span 1 with 13.7 m [45 ft] cross-frame spacing and 25.4 mm [1.0 in.] thick stiffeners in plan view

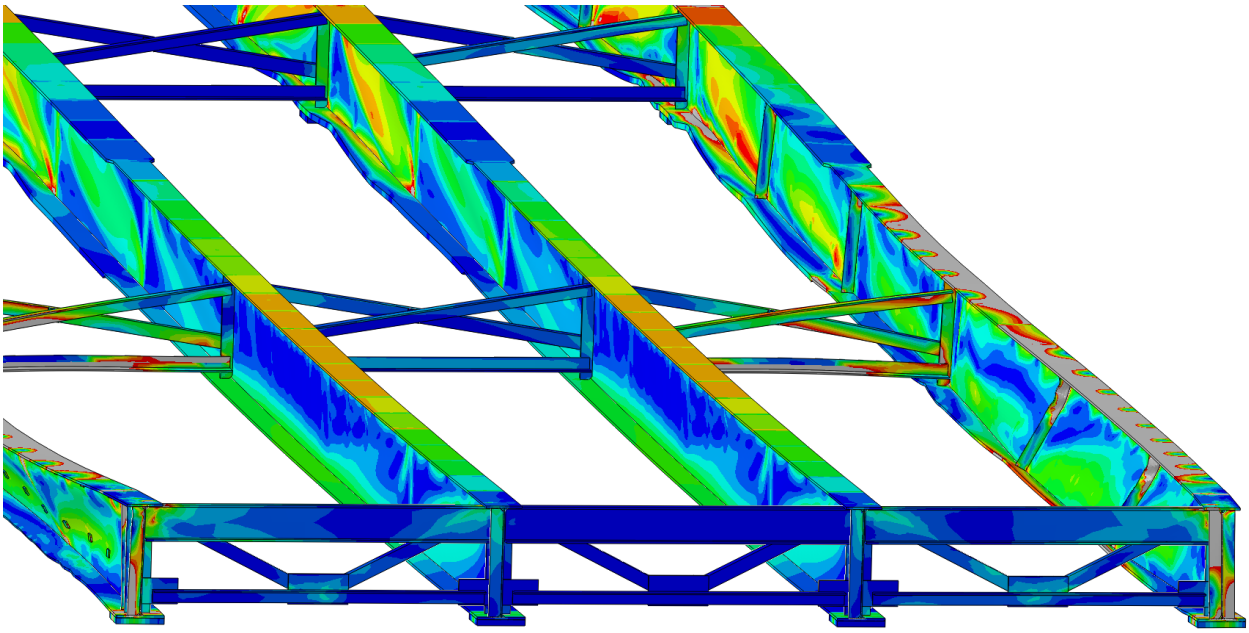

Figure 115 Girder deformation of the non-skewed bridge with 13.7 m [45 ft] cross-frame spacing and 25.4 mm [1.0 in.] thick stiffeners

40° SKEWED-PARALLEL BRIDGE

45 FT CROSS-FRAME SPACING;

HALF-PIPE STIFFENERS

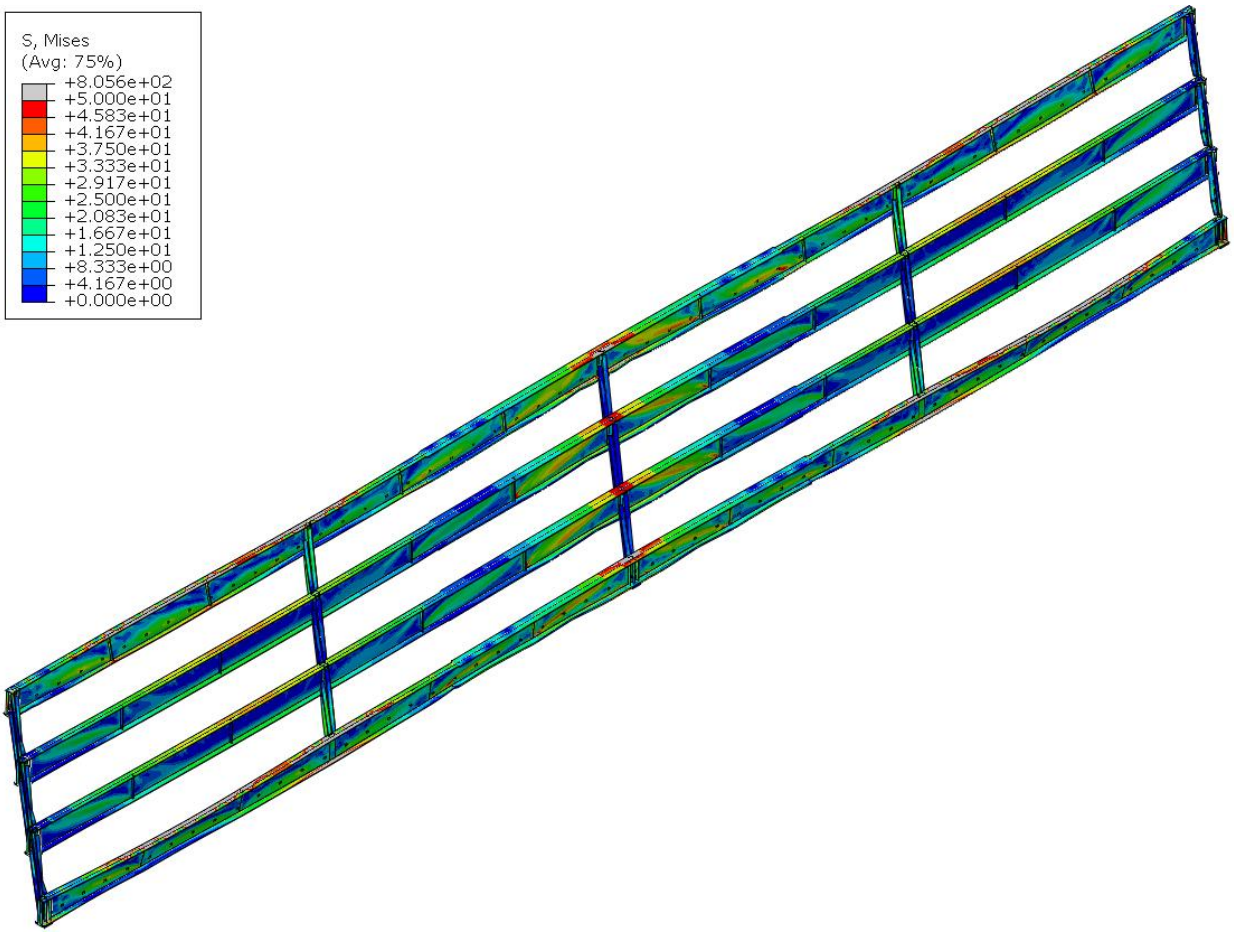

Figure 116 Deformed shaped of the 40° skewed-parallel bridge with 13.7 m [45 ft] cross-frame spacing and half-pipe connection in isotropic view

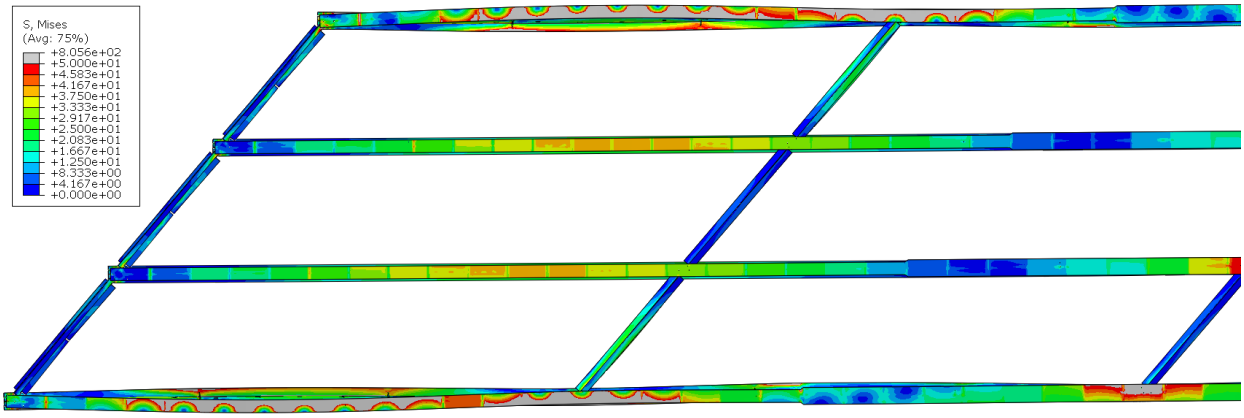

Figure 117 Deformed shape of the 40° skewed-parallel bridge in Span 1 with 13.7 m [45 ft] cross-frame spacing and half-pipe connection in plan view

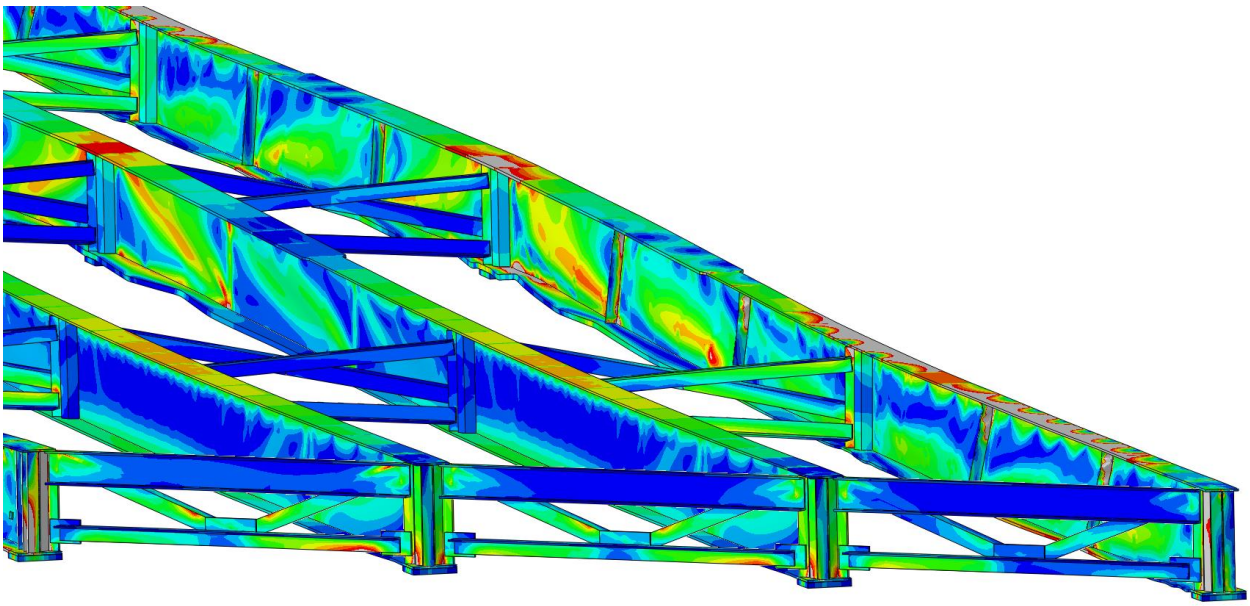

Figure 118 Girder deformation of the 40° skewed-parallel bridge with 13.7 m [45 ft] cross-frame spacing and half-pipe connection

40° SKEWED-STAGGERED BRIDGE

45 FT CROSS-FRAME SPACING;

HALF-PIPE STIFFENERS

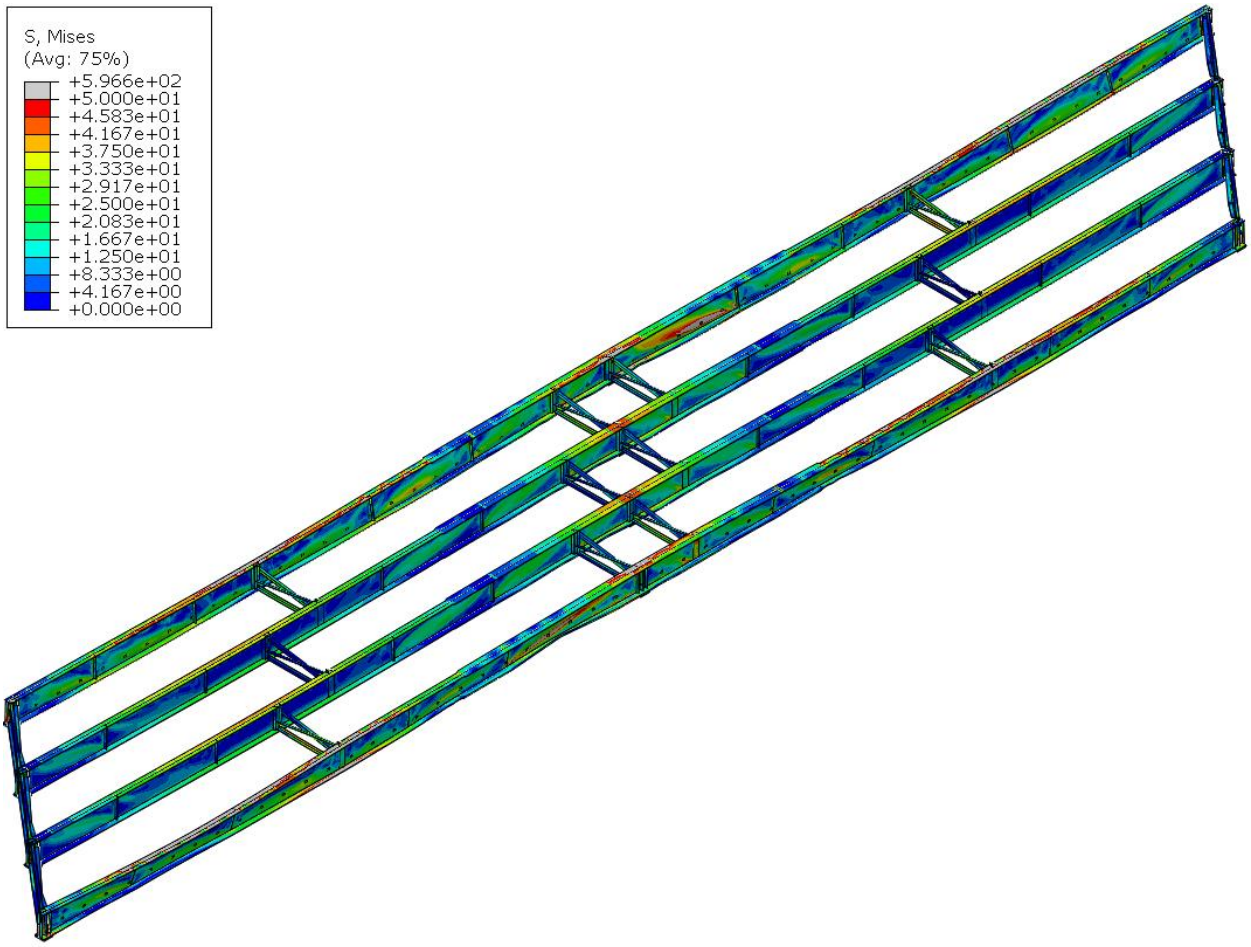

Figure 119 Deformed shaped of the 40° skewed-staggered bridge with 13.7 m [45 ft] cross-frame spacing and half-pipe connection in isotropic view

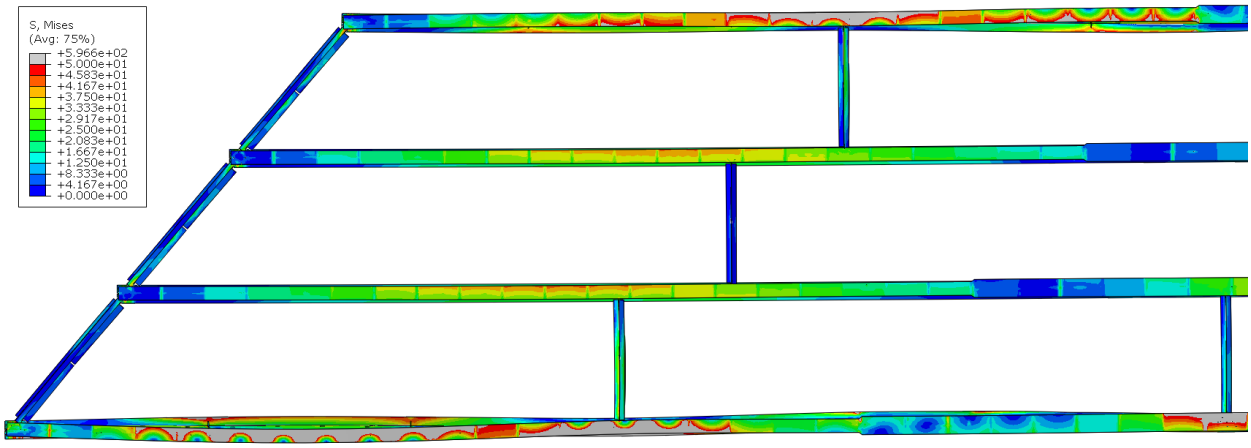

Figure 120 Deformed shape of the 40° skewed-staggered bridge in Span 1 with 13.7 m [45 ft] cross-frame spacing and half-pipe connection in plan view

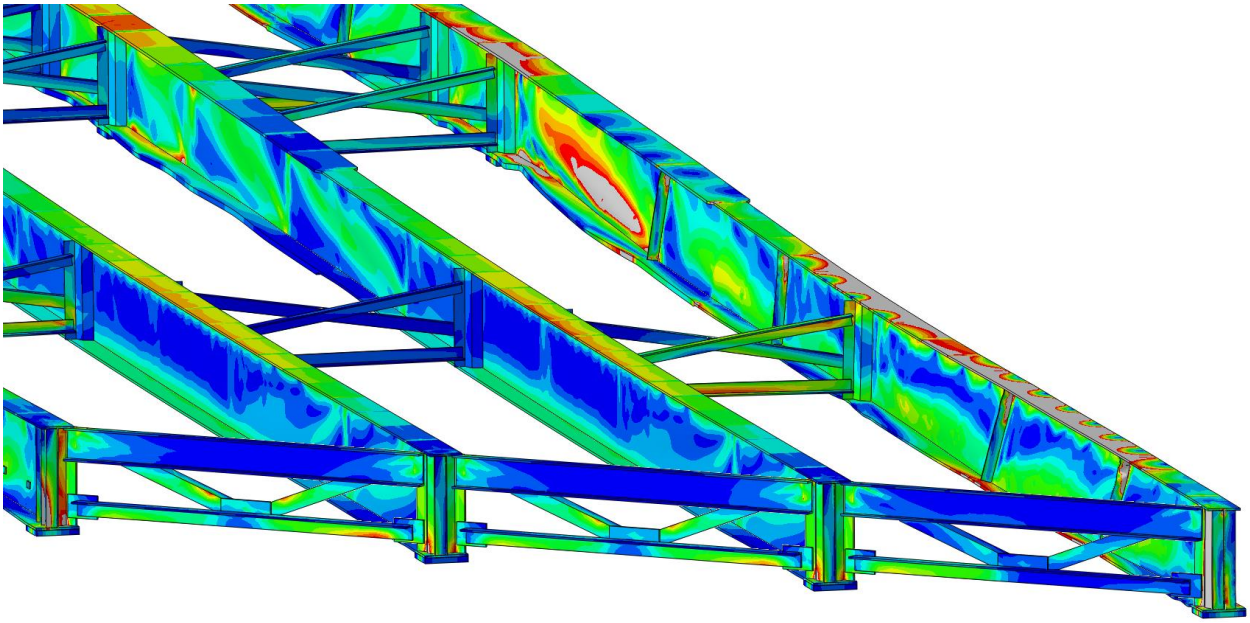

Figure 121 Girder deformation of the 40° skewed-staggered bridge with 13.7 m [45 ft] cross-frame spacing and half-pipe connection

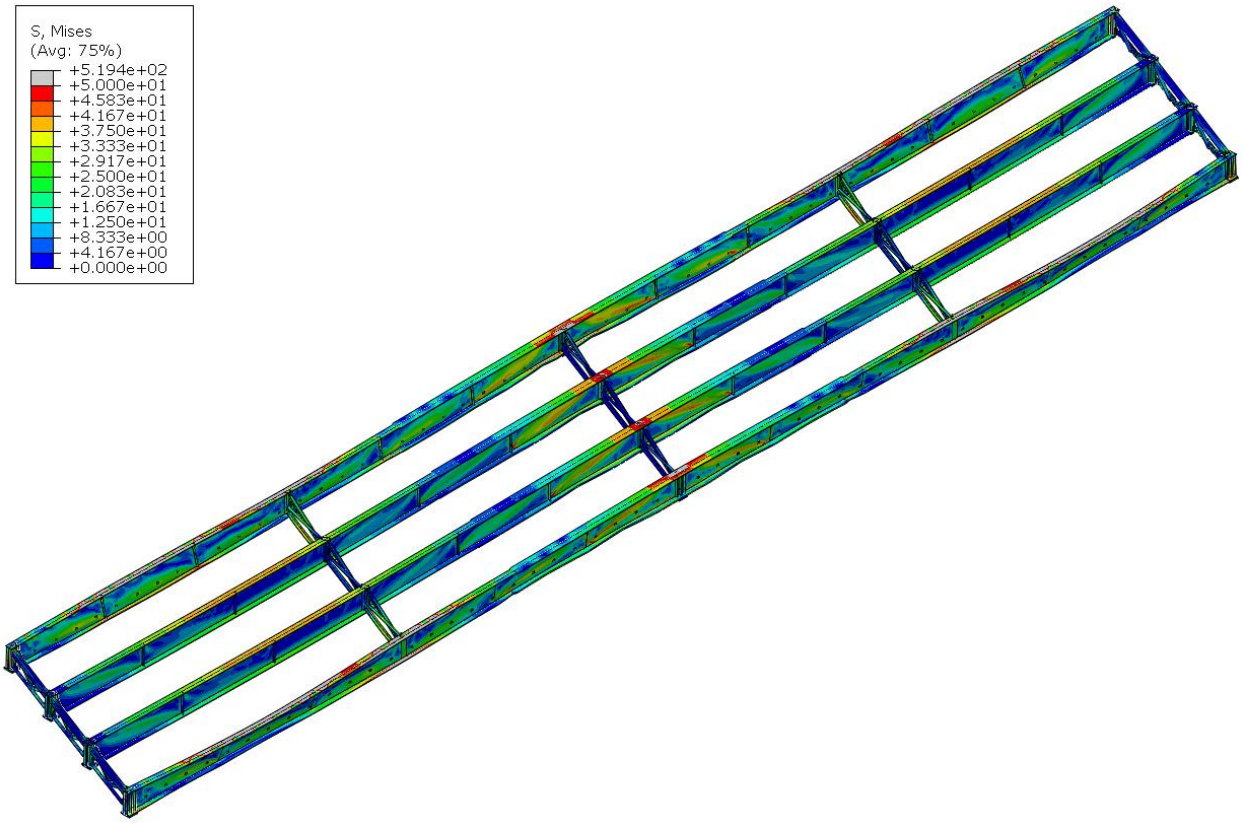

Figure 122 Deformed shaped of the 20° skewed-parallel bridge with 13.7 m [45 ft] cross-frame spacing and half-pipe connection in isotropic view

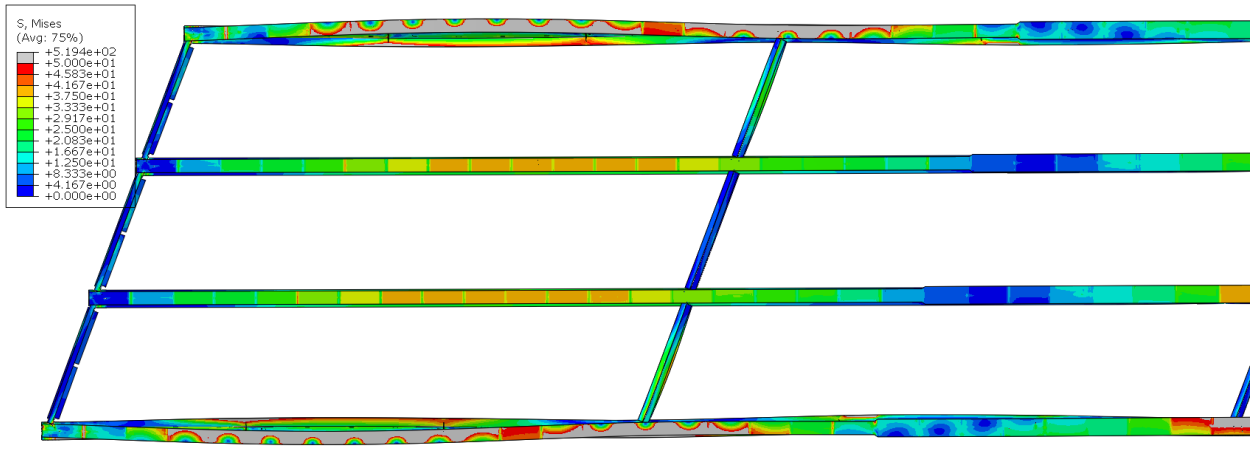

Figure 123 Deformed shape of the 20° skewed-parallel bridge in Span 1 with 13.7 m [45 ft] cross-frame spacing and half-pipe connection in plan view

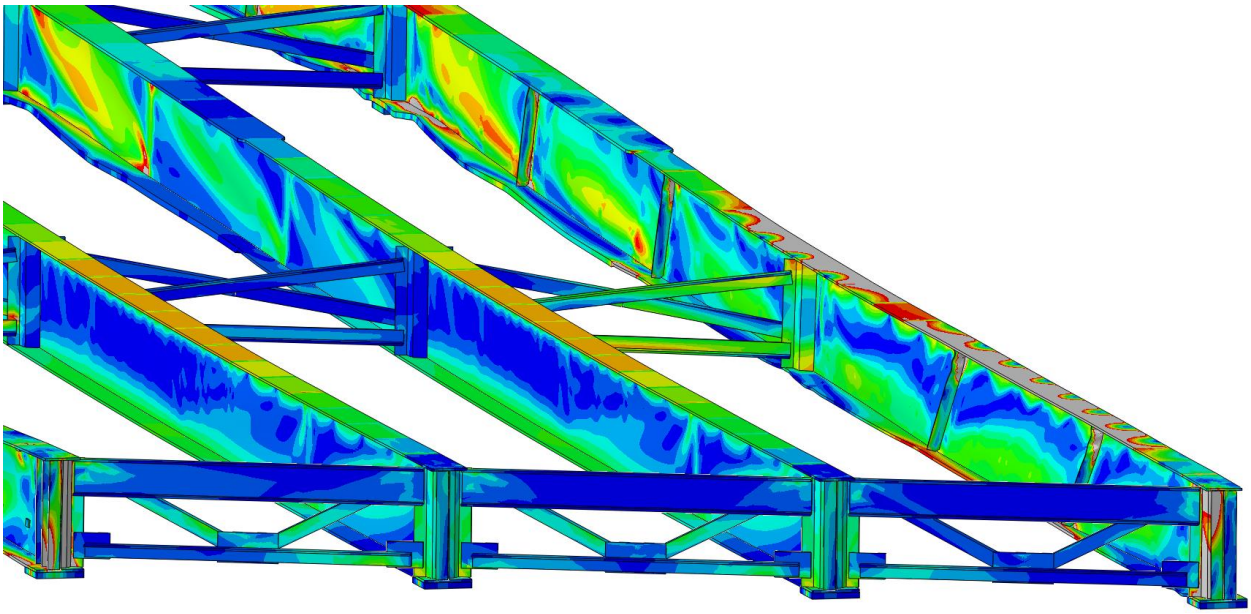

Figure 124 Girder deformation of the 20° skewed-parallel bridge with 13.7 m [45 ft] cross-frame spacing and half-pipe connection

20° SKEWED-STAGGERED BRIDGE

45 FT CROSS-FRAME SPACING;

HALF-PIPE STIFFENERS

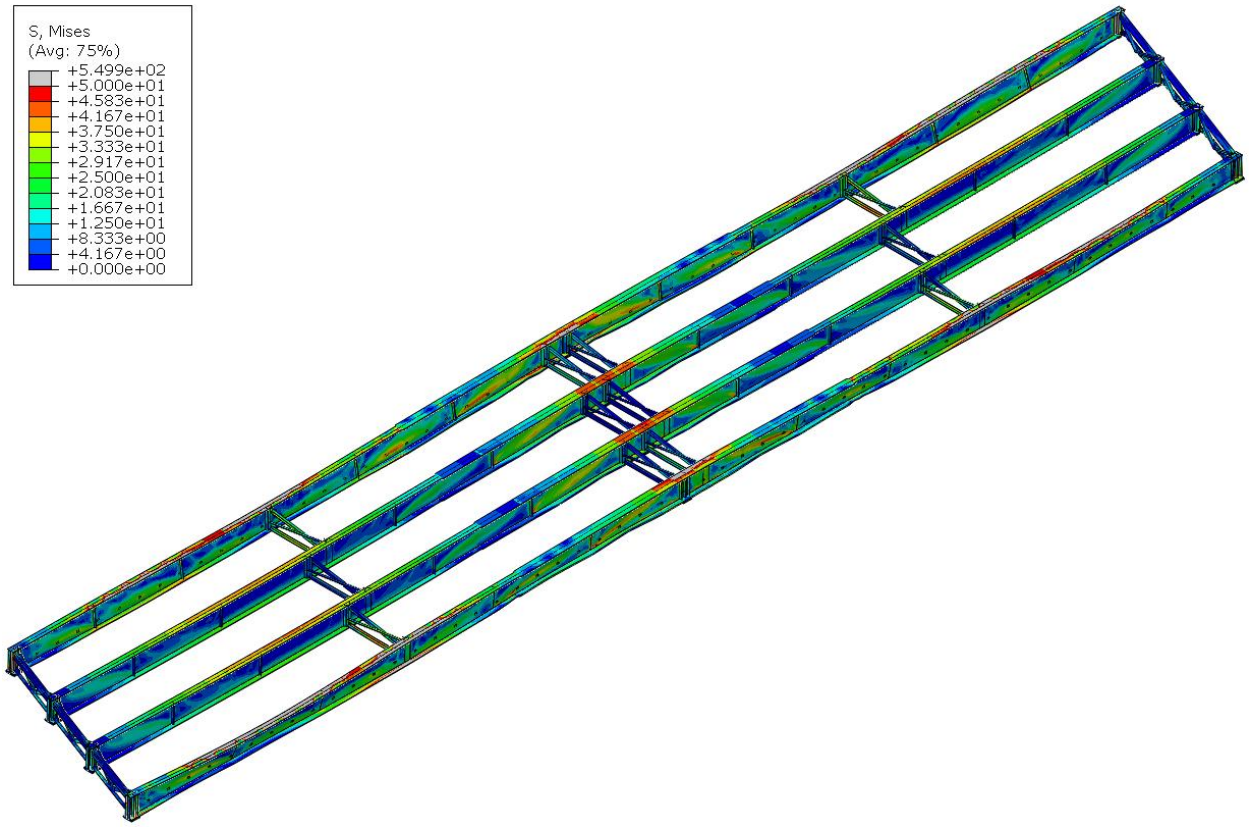

Figure 125 Deformed shaped of the 20° skewed-staggered bridge with 13.7 m [45 ft] cross-frame spacing and half-pipe connection in isotropic view

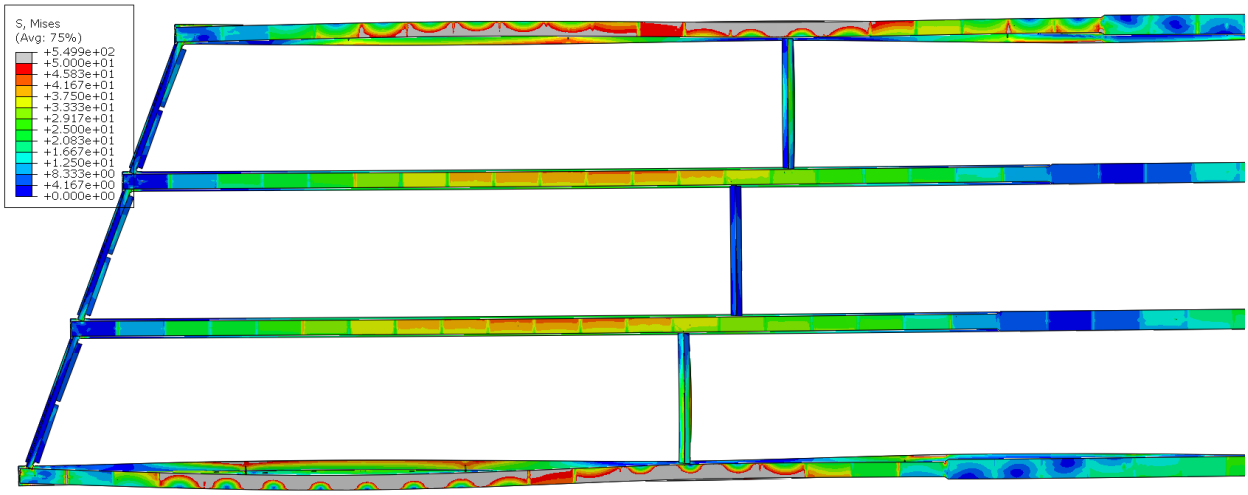

Figure 126 Deformed shape of the 20° skewed-staggered bridge in Span 1 with 13.7 m [45 ft] cross-frame spacing and half-pipe connection in plan view

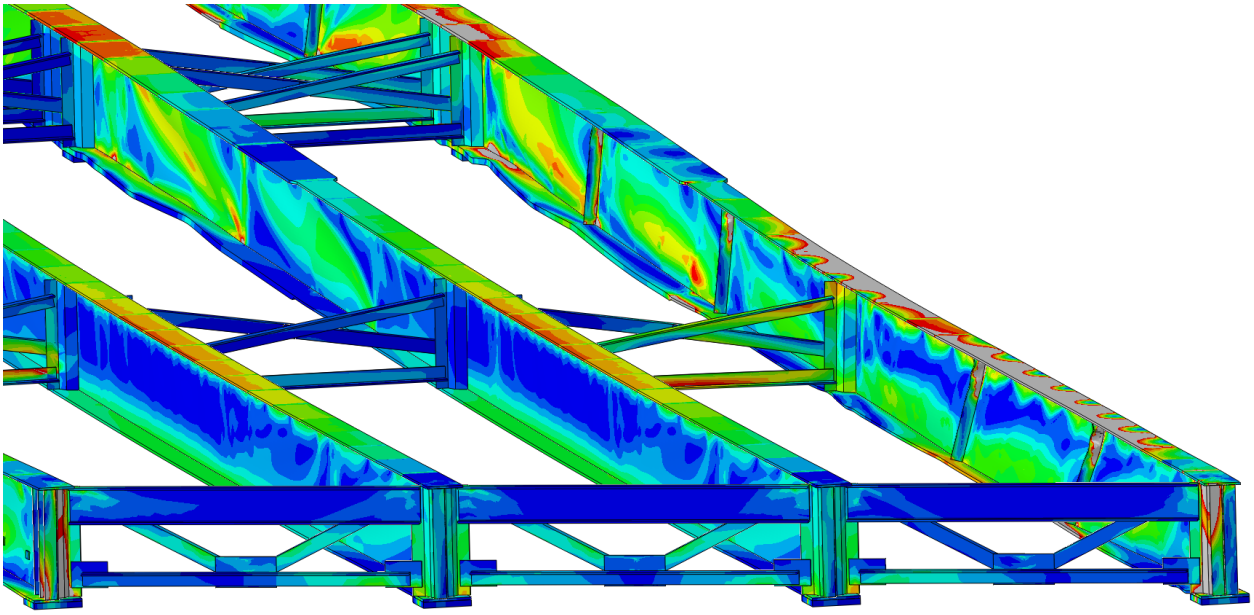

Figure 127 Girder deformation of the 20° skewed-staggered bridge with 13.7 m [45 ft] cross-frame spacing and half-pipe connection

NON-SKEWED BRIDGE

45 FT CROSS-FRAME SPACING;

HALF-PIPE STIFFENERS

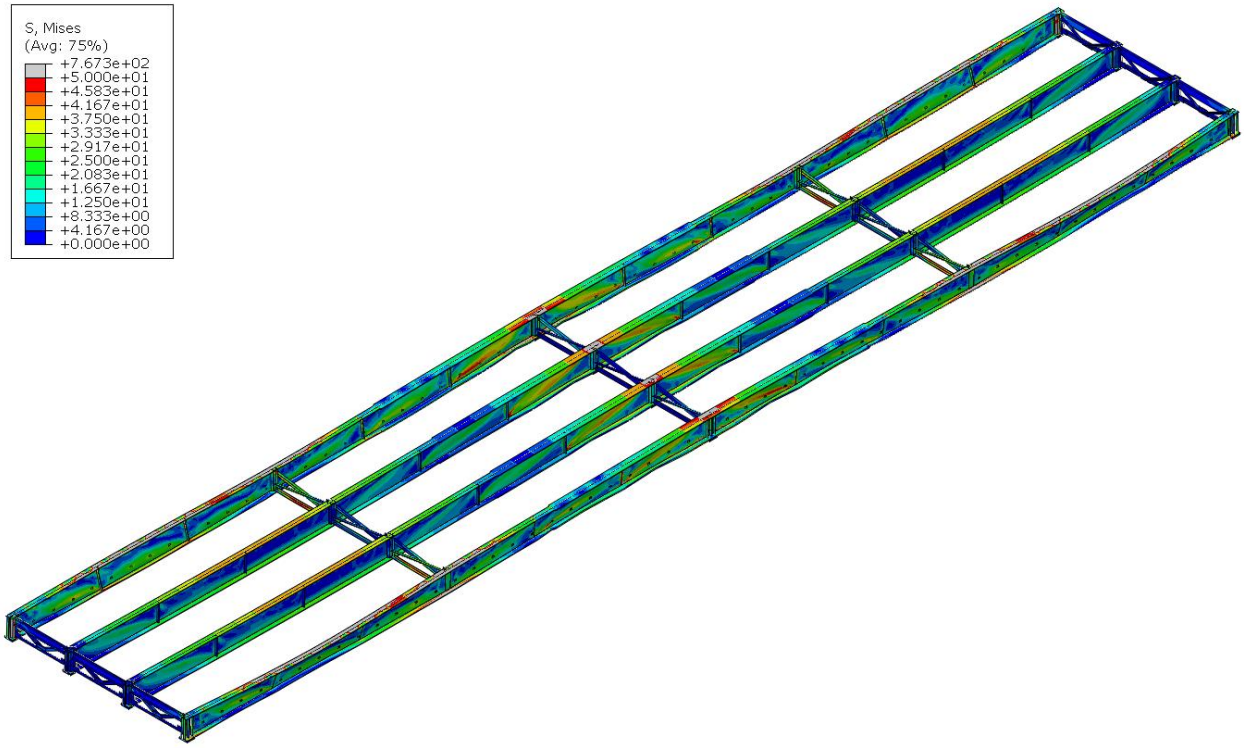

Figure 128 Deformed shaped of the non-skewed bridge with 13.7 m [45 ft] cross-frame spacing and half-pipe connection in isotropic view

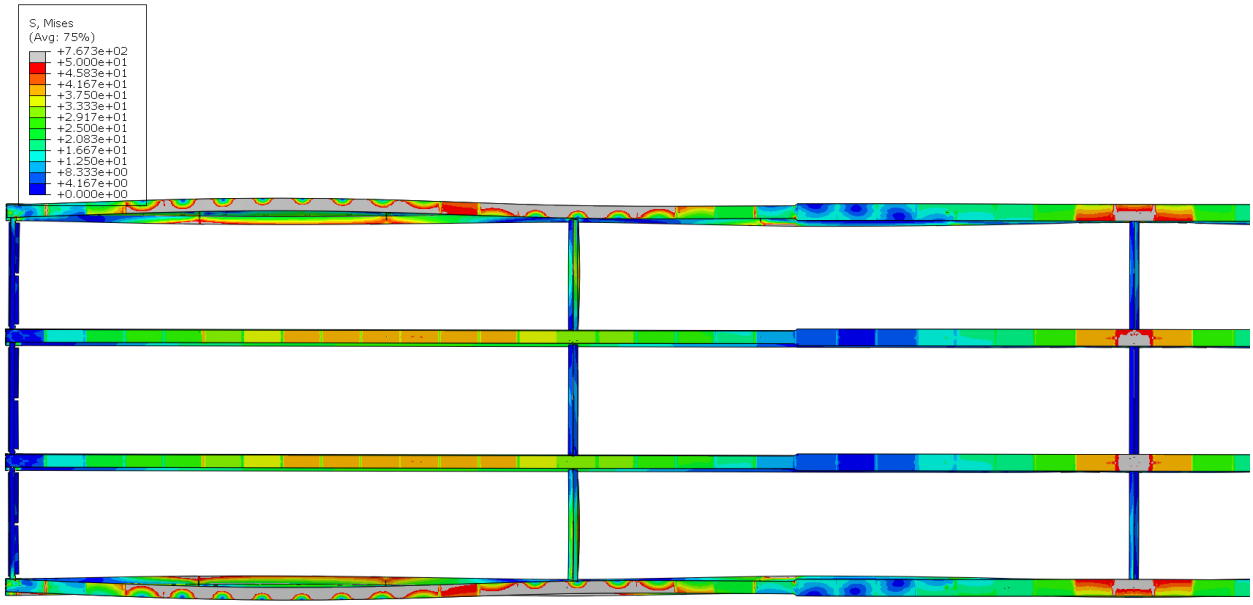

Figure 129 Deformed shape of the non-skewed bridge in Span 1 with 13.7 m [45 ft] cross-frame spacing and half-pipe connection in plan view

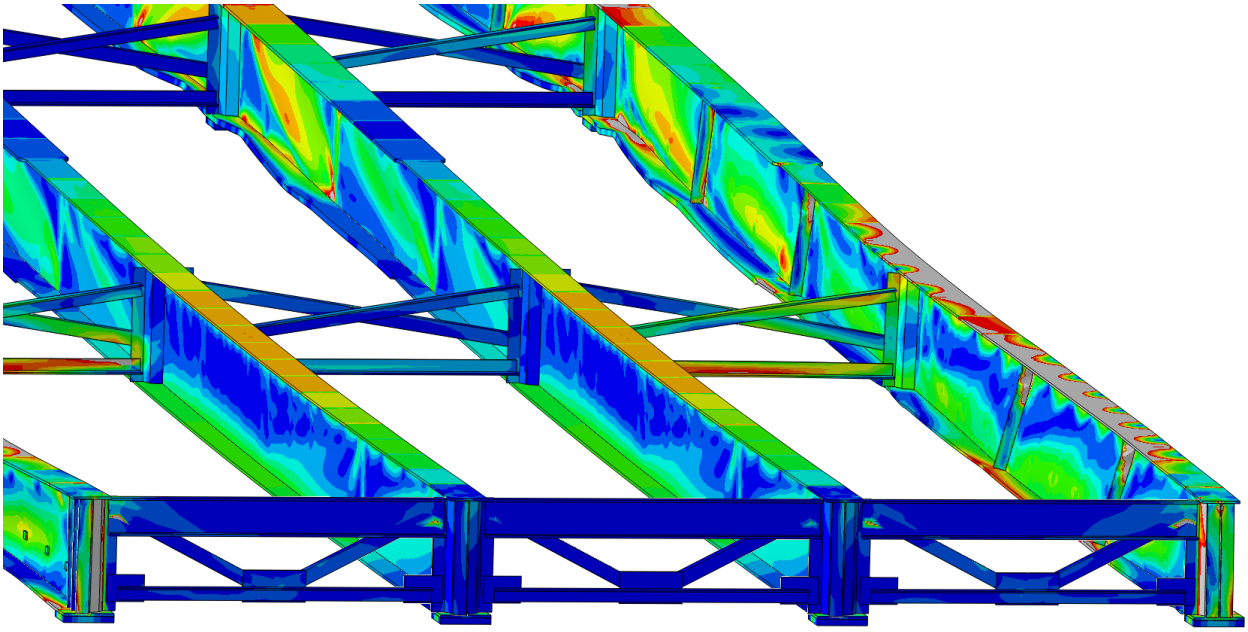

Figure 130 Girder deformation of the non-skewed bridge with 13.7 m [45 ft] cross-frame spacing and half-pipe connection

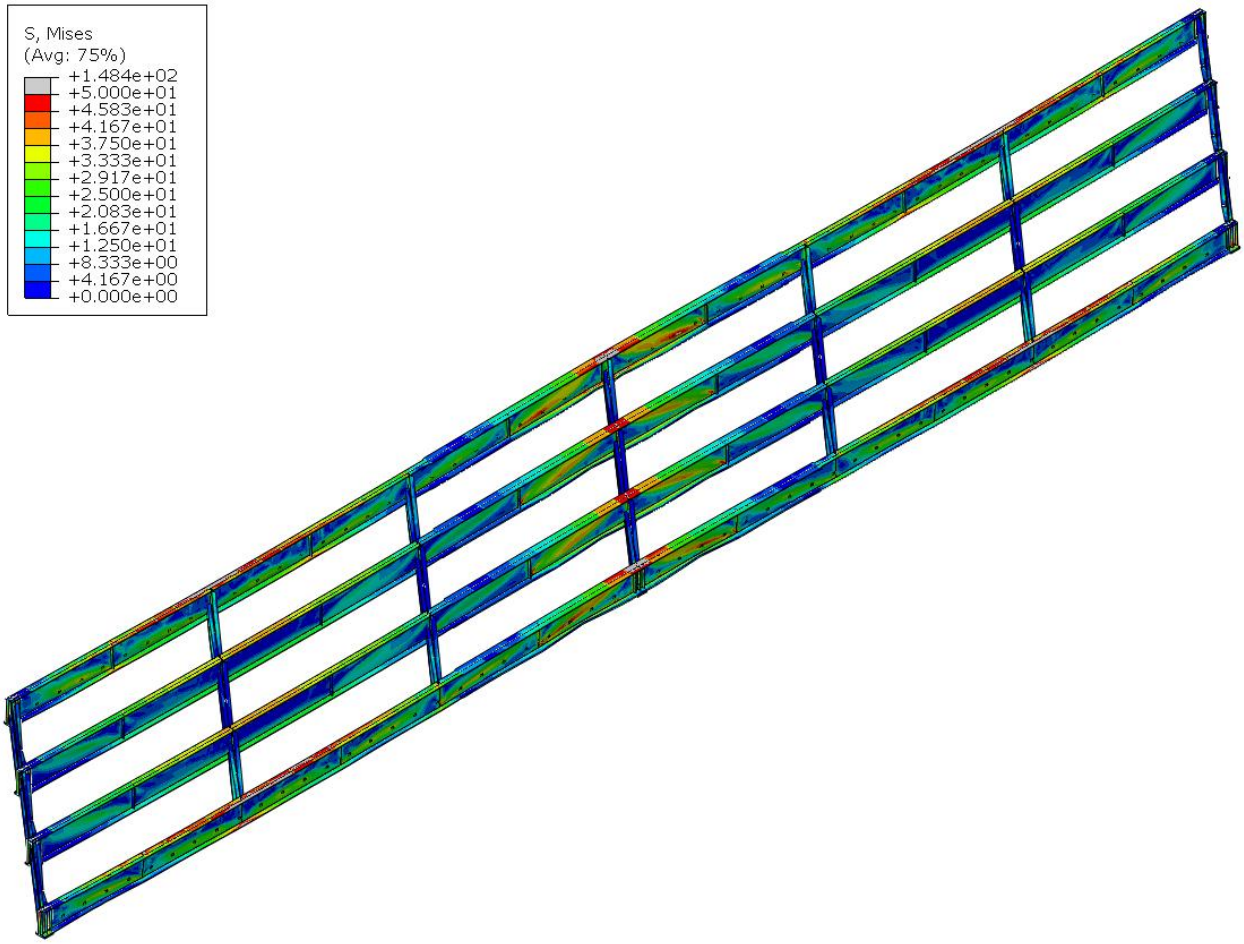

Figure 131 Deformed shaped of the 40° skewed-parallel bridge with 9.14 m [30 ft] cross-frame spacing in isotropic view

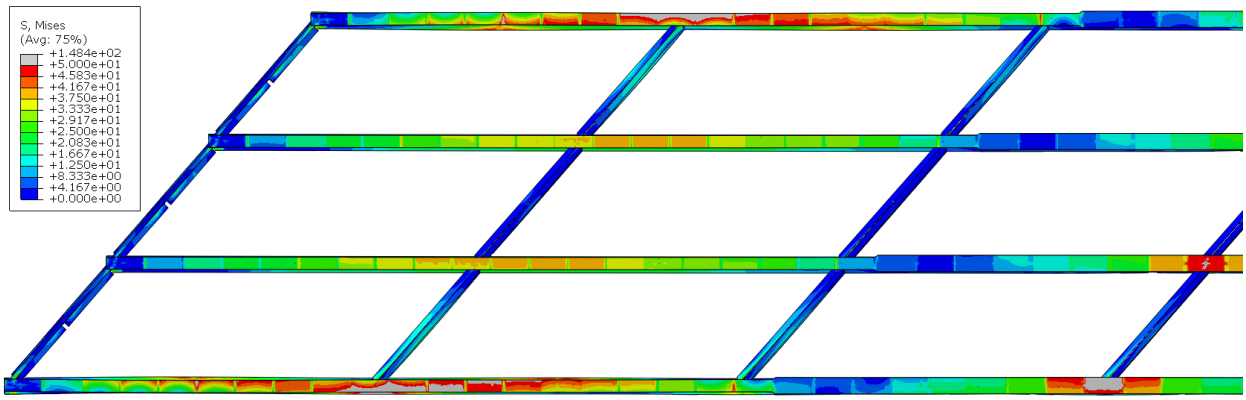

Figure 132 Deformed shape of the 40° skewed-parallel bridge in Span 1 with 9.14 m [30 ft] cross-frame spacing in plan view

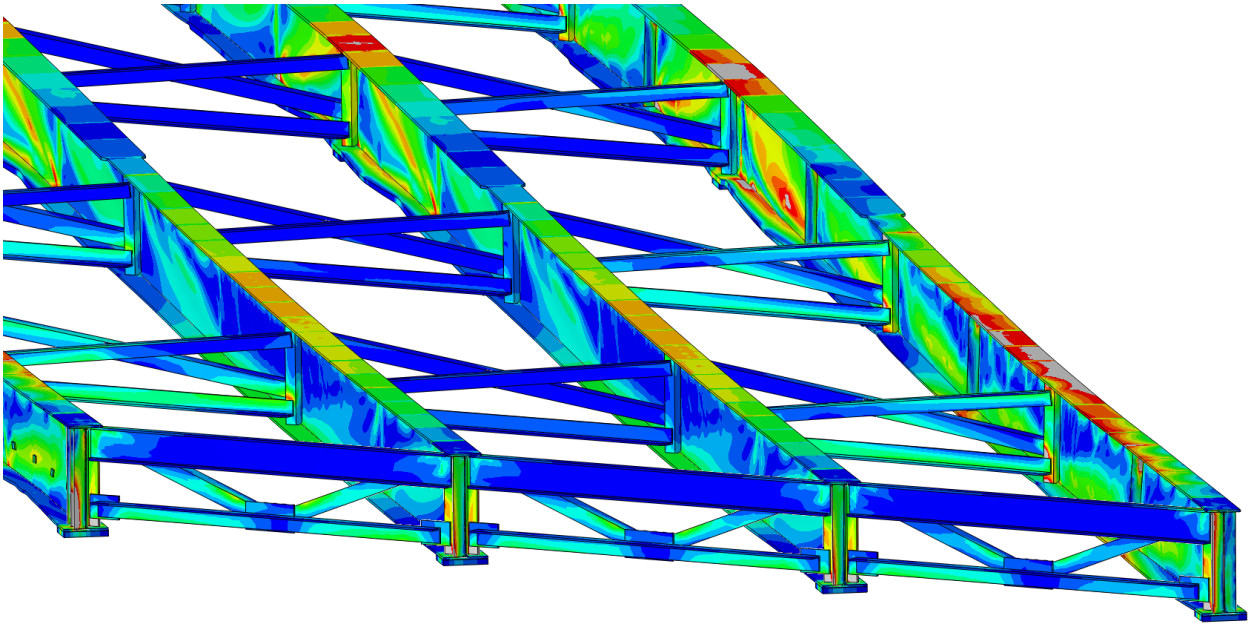

Figure 133 Girder deformation of the 40° skewed-parallel bridge with 9.14 m [30 ft] cross-frame spacing

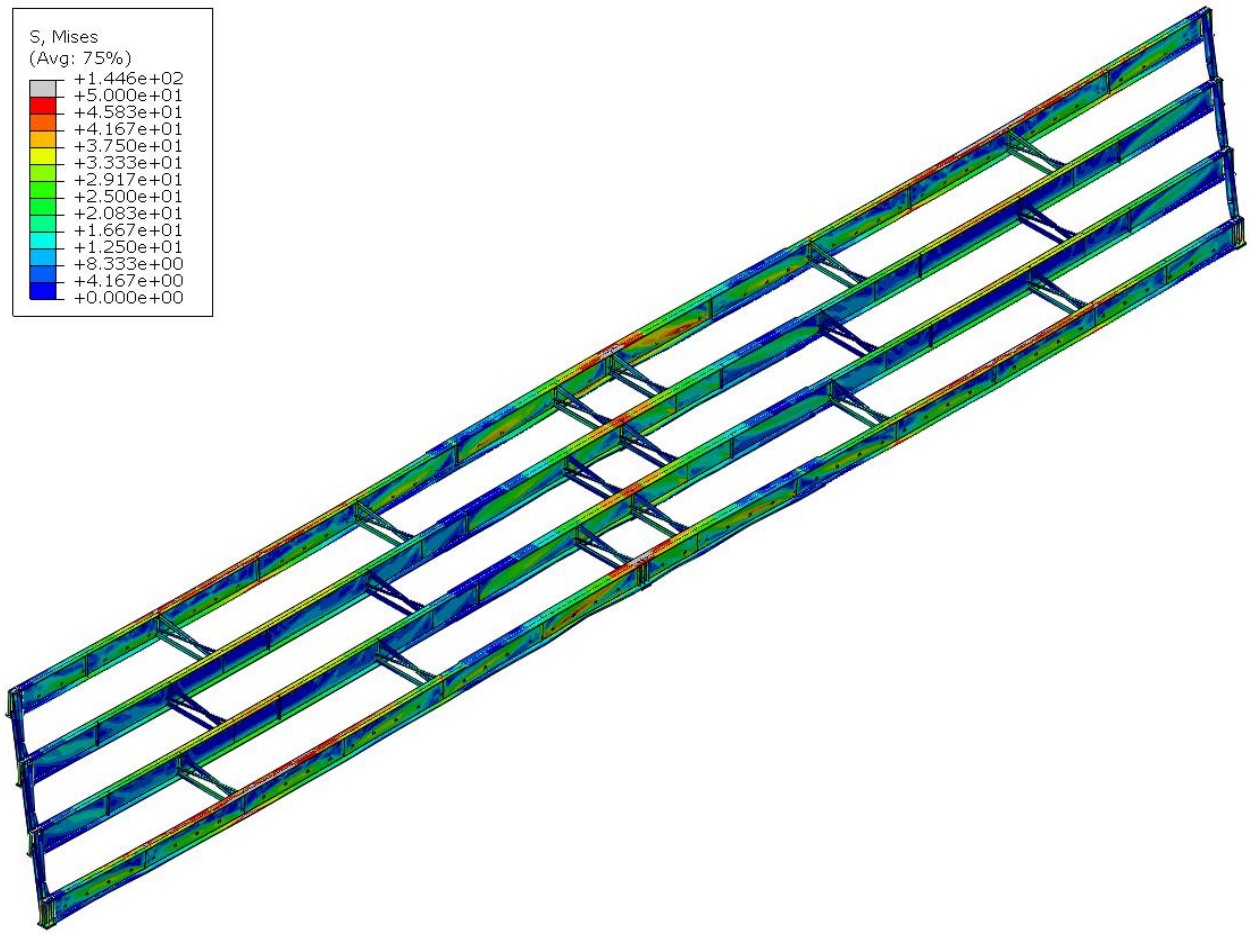

Figure 134 Deformed shaped of the 40° skewed-staggered bridge with 9.14 m [30 ft] cross-frame spacing in isotropic view

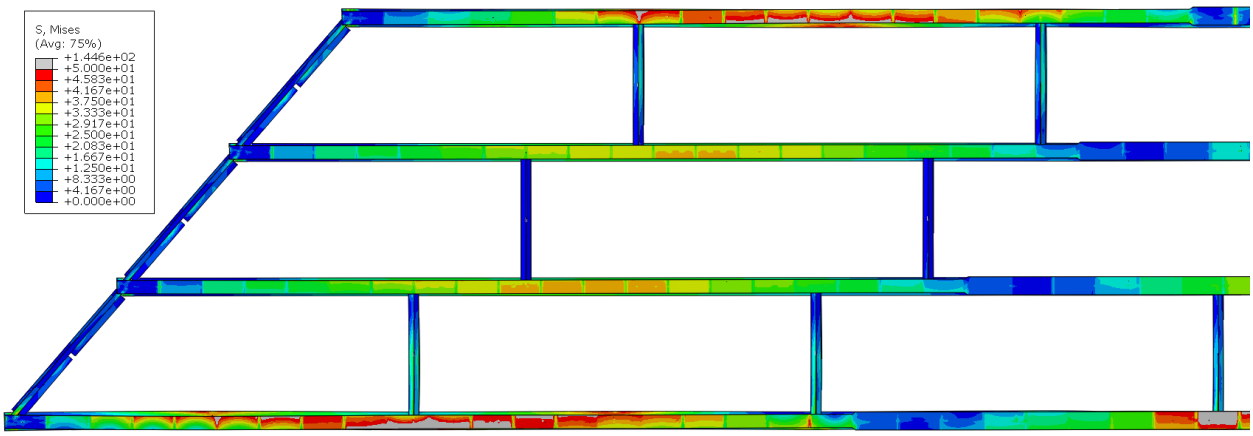

Figure 135 Deformed shape of the 40° skewed-staggered bridge in Span 1 with 9.14 m [30 ft] cross-frame spacing in plan view

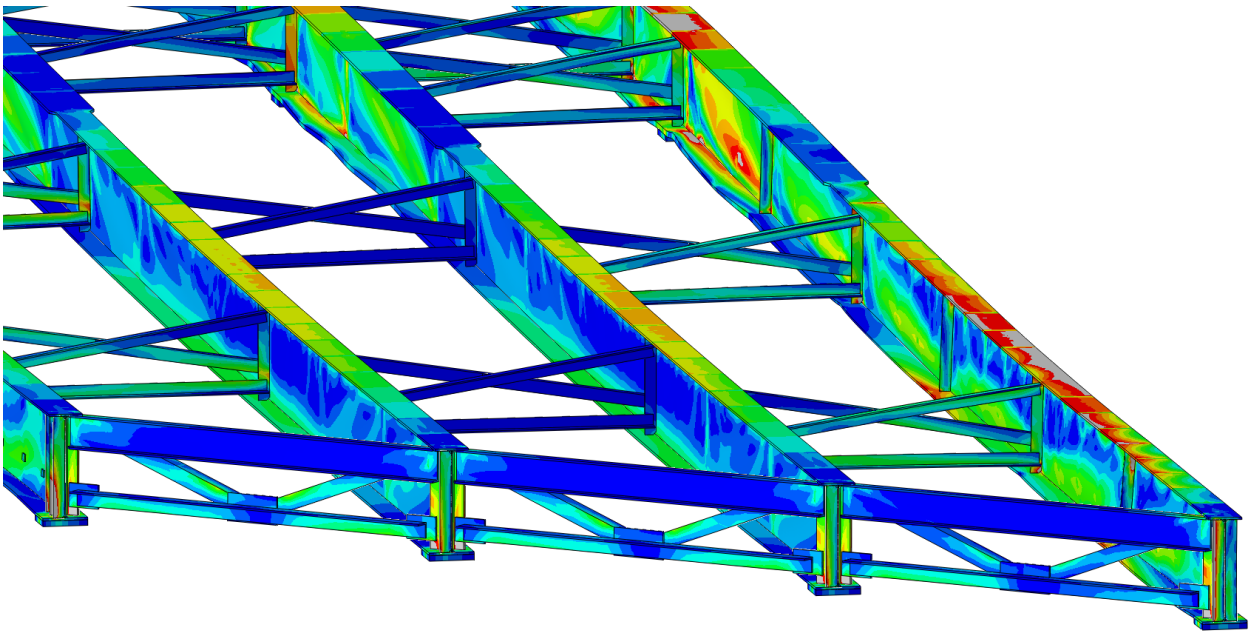

Figure 136 Girder deformation of the 40° skewed-staggered bridge with 9.14 m [30 ft] cross-frame spacing

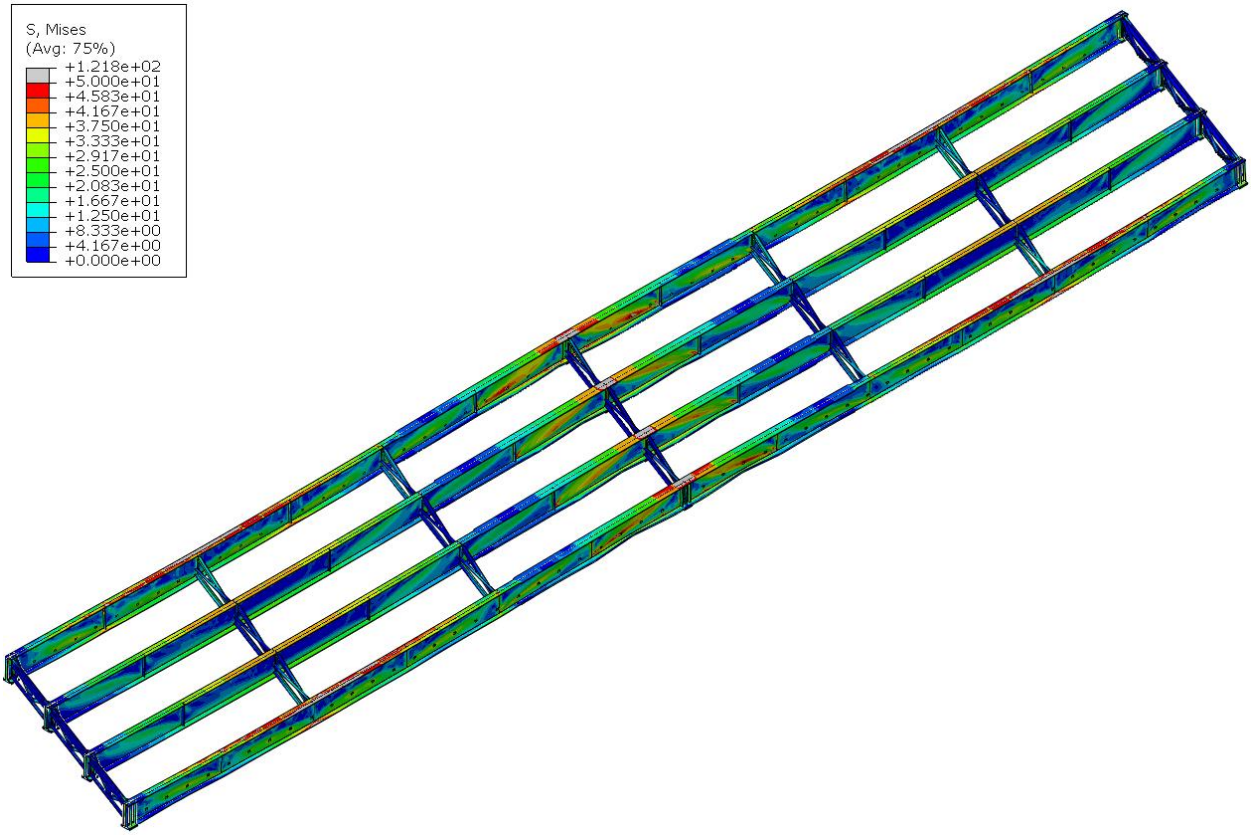

Figure 137 Deformed shaped of the 20° skewed-parallel bridge with 9.14 m [30 ft] cross-frame spacing in isotropic view

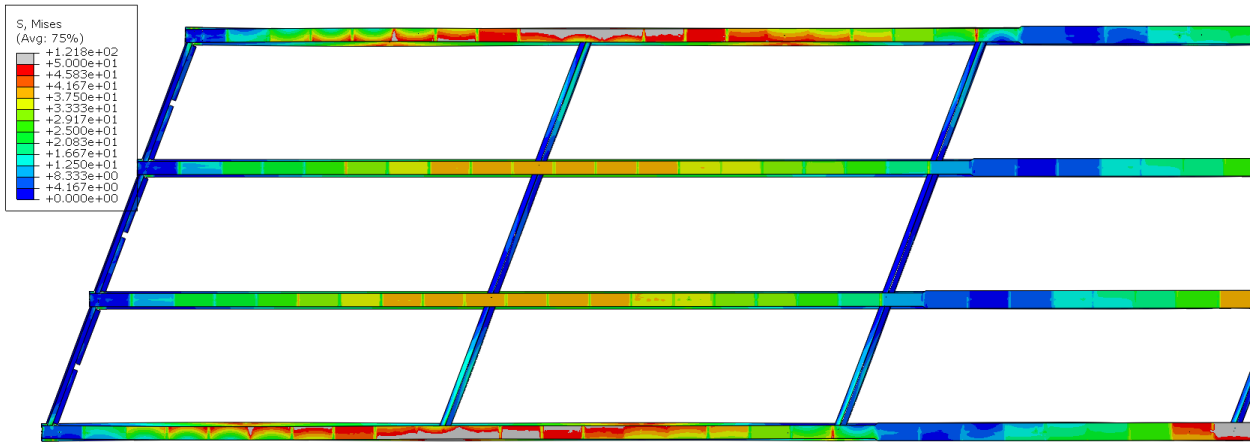

Figure 138 Deformed shape of the 20° skewed-parallel bridge in Span 1 with 9.14 m [30 ft] cross-frame spacing in plan view

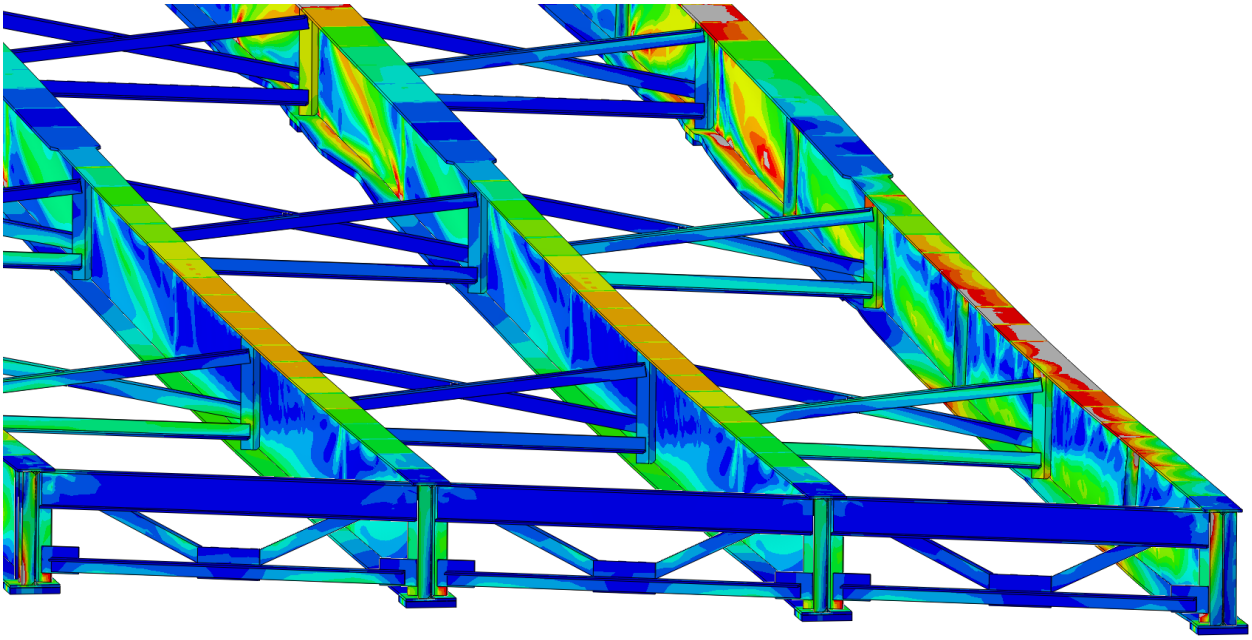

Figure 139 Girder deformation of the 20° skewed-parallel bridge with 9.14 m [30 ft] cross-frame spacing

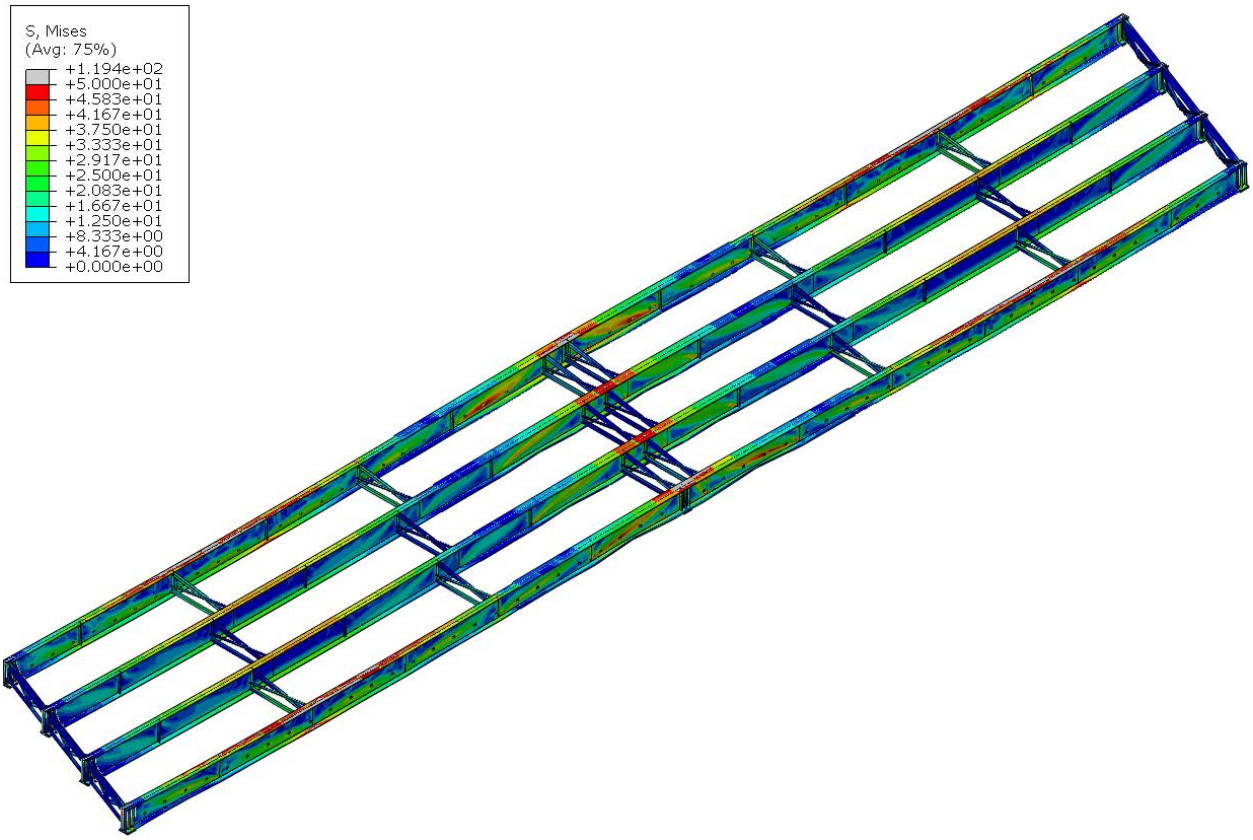

Figure 140 Deformed shaped of the 20° skewed-staggered bridge with 9.14 m [30 ft] cross-frame spacing in isotropic view

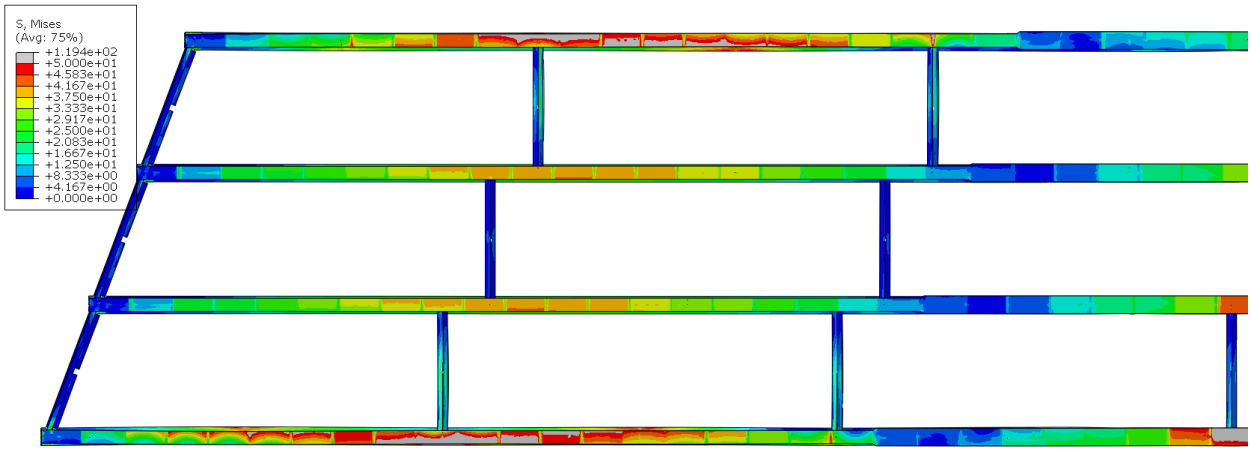

Figure 141 Deformed shape of the 20° skewed-staggered bridge in Span 1 with 9.14 m [30 ft] cross-frame spacing in plan view

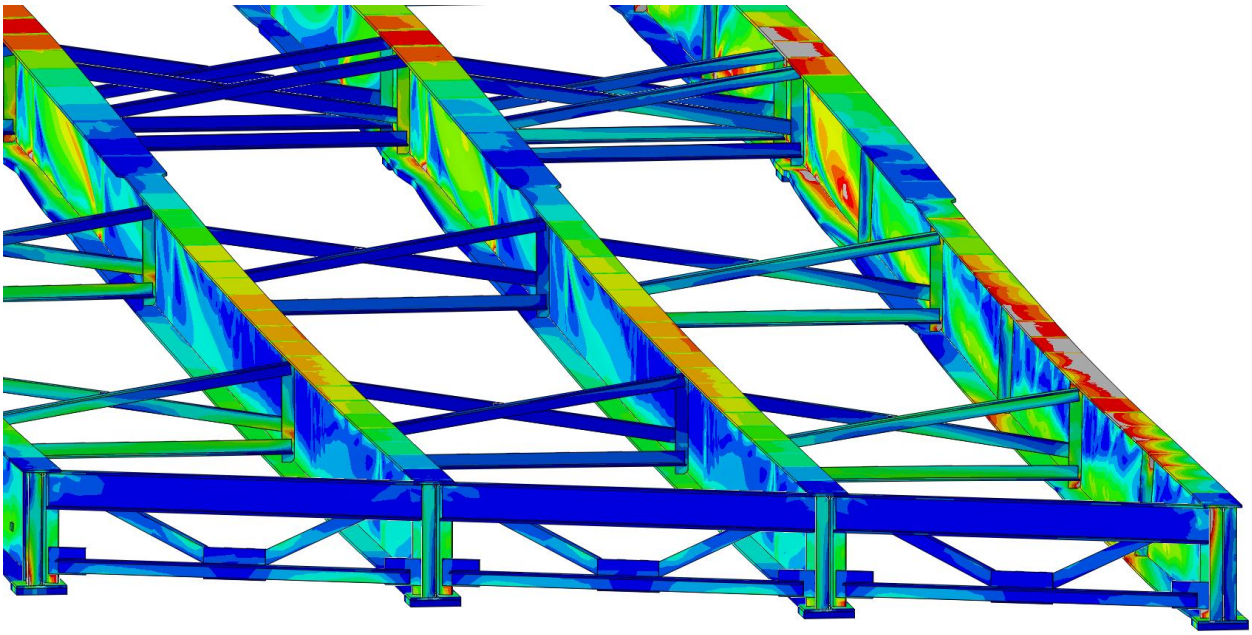

Figure 142 Girder deformation of the 20° skewed-staggered bridge with 9.14 m [30 ft] cross-frame spacing

NON-SKEWED BRIDGE

30 FT CROSS-FRAME SPACING;

3/8" THICK STIFFENERS

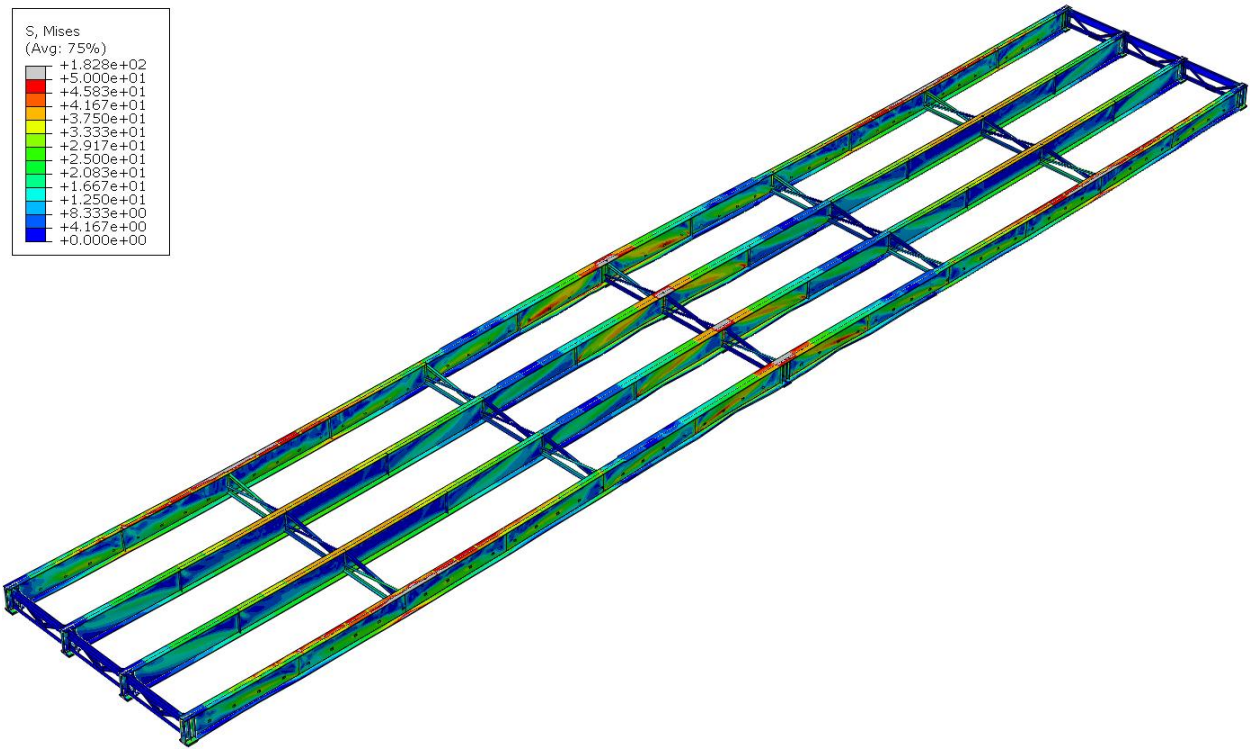

Figure 143 Deformed shaped of the non-skewed bridge with 9.14 m [30 ft] cross-frame spacing in isotropic view

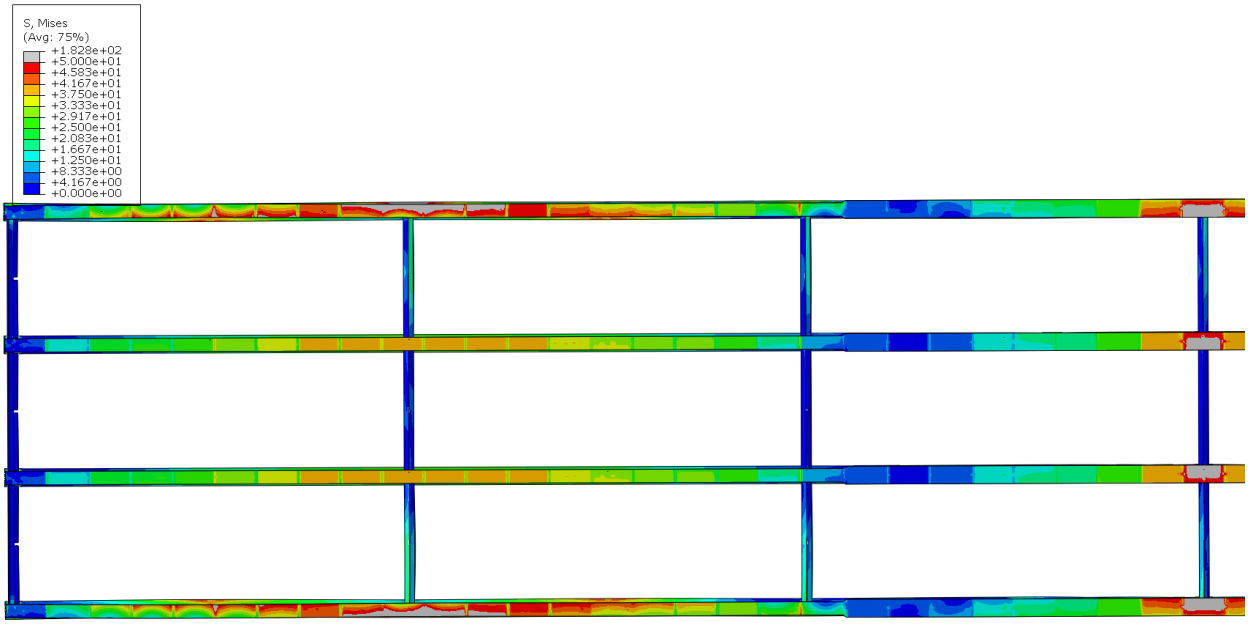

Figure 144 Deformed shape of the non-skewed bridge in Span 1 with 9.14 m [30 ft] cross-frame spacing in plan view

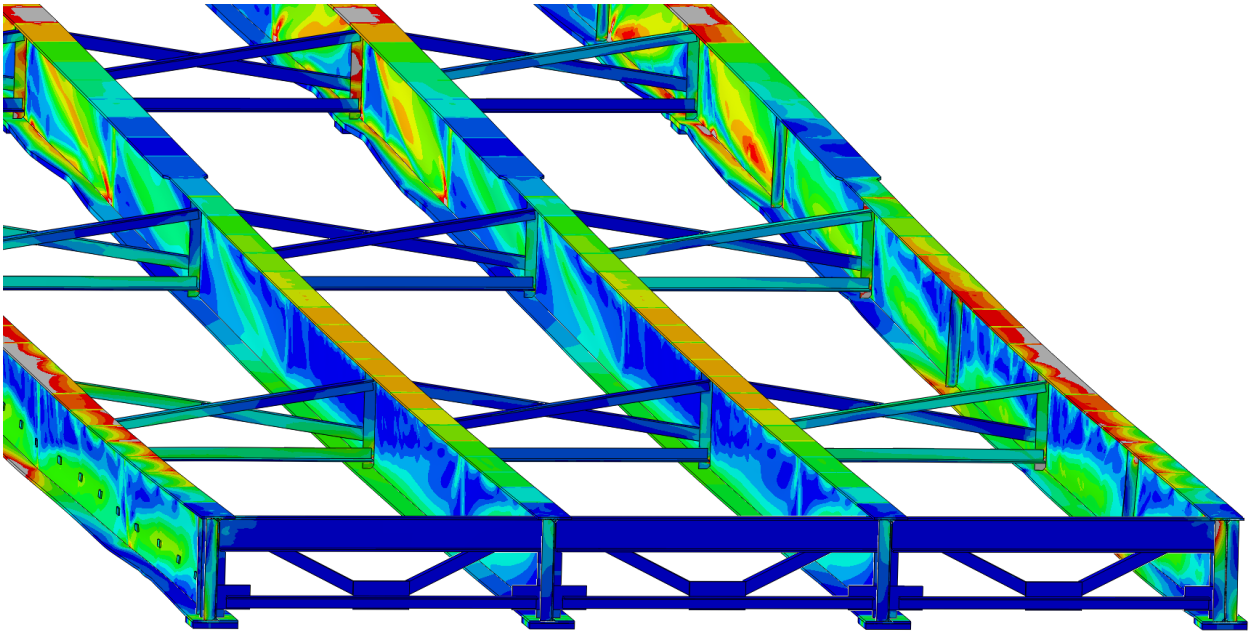

Figure 145 Girder deformation of the non-skewed bridge with 9.14 m [30 ft] cross-frame spacing

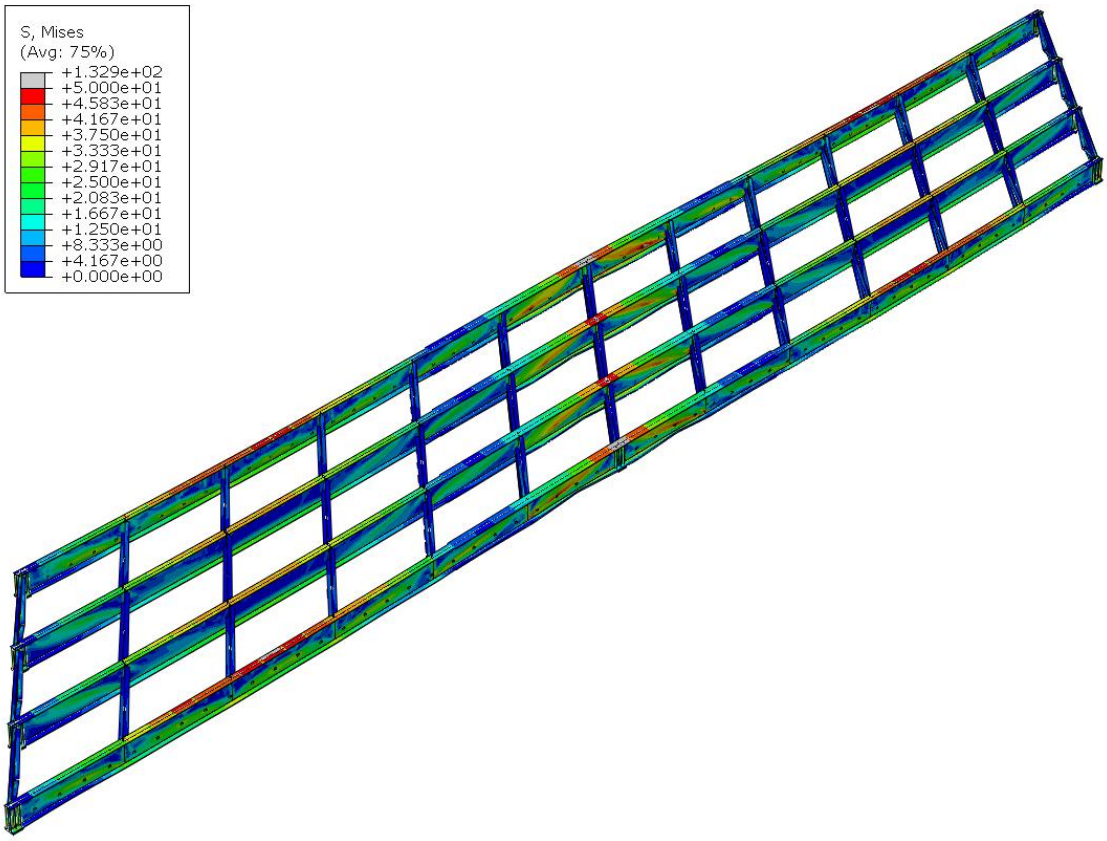

Figure 146 Deformed shaped of the 40° skewed-parallel bridge with 4.6 m [15 ft] cross-frame spacing in isotropic view

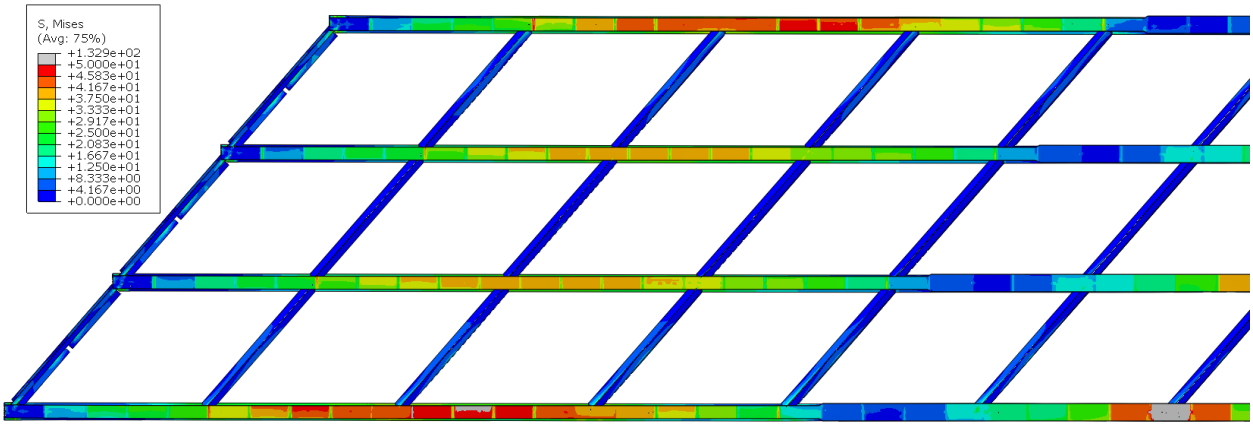

Figure 147 Deformed shape of the 40° skewed-parallel bridge in Span 1 with 4.6 m [15 ft] cross-frame spacing in plan view

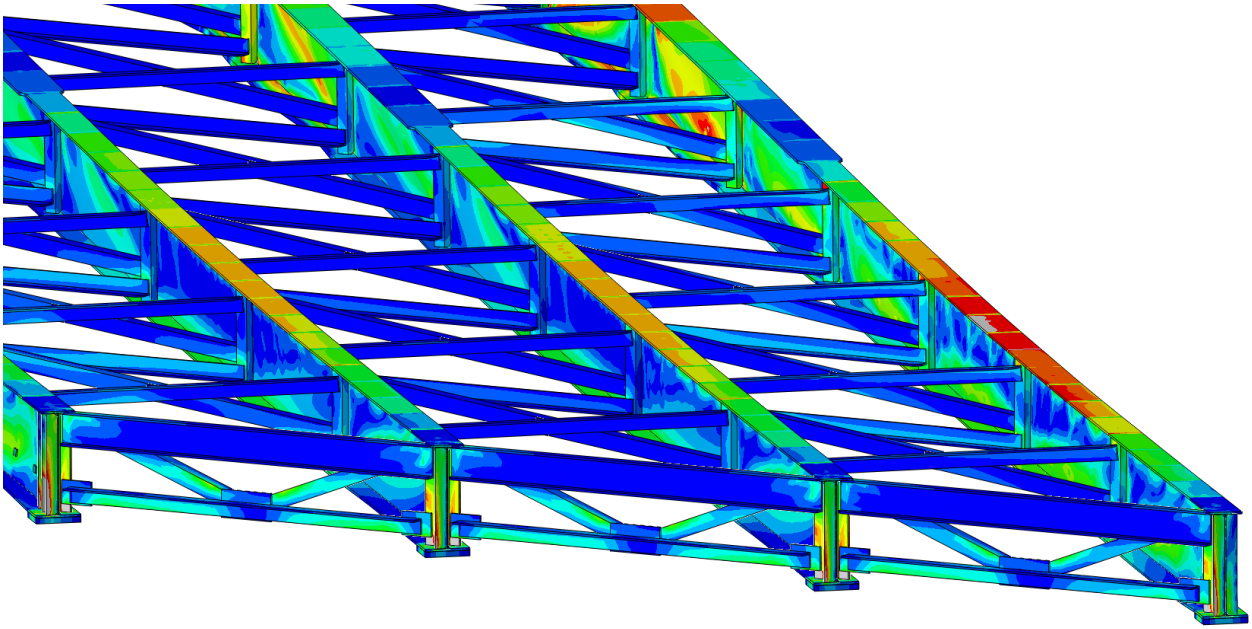

Figure 148 Girder deformation of the 40° skewed-parallel bridge with 4.6 m [15 ft] cross-frame spacing

40° SKEWED-STAGGERED BRIDGE

15 FT CROSS-FRAME SPACING;

3/8" THICK STIFFENERS

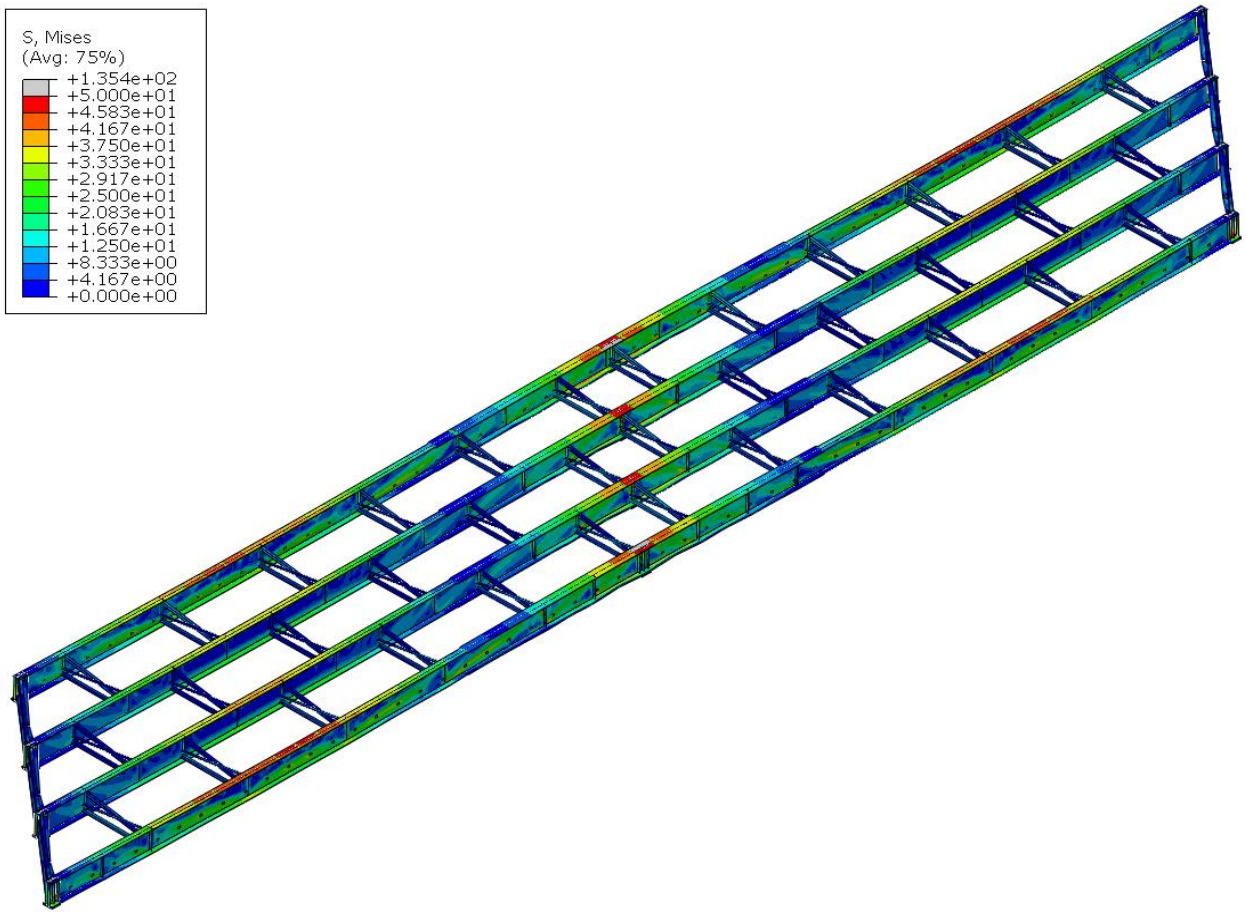

Figure 149 Deformed shaped of the 40° skewed-staggered bridge with 4.6 m [15 ft] cross-frame spacing in isotropic view

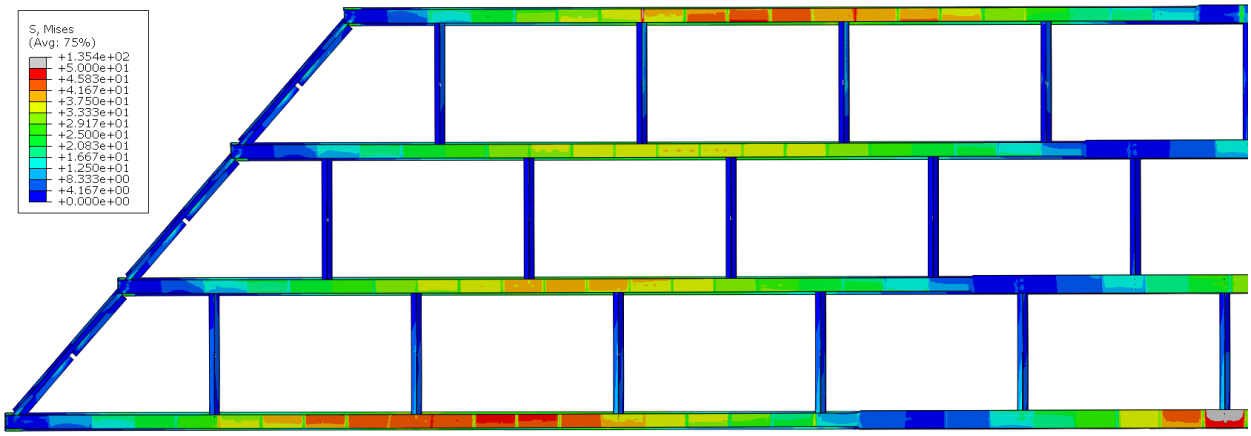

Figure 150 Deformed shape of the 40° skewed-staggered bridge in Span 1 with 4.6 m [15 ft] cross-frame spacing in plan view

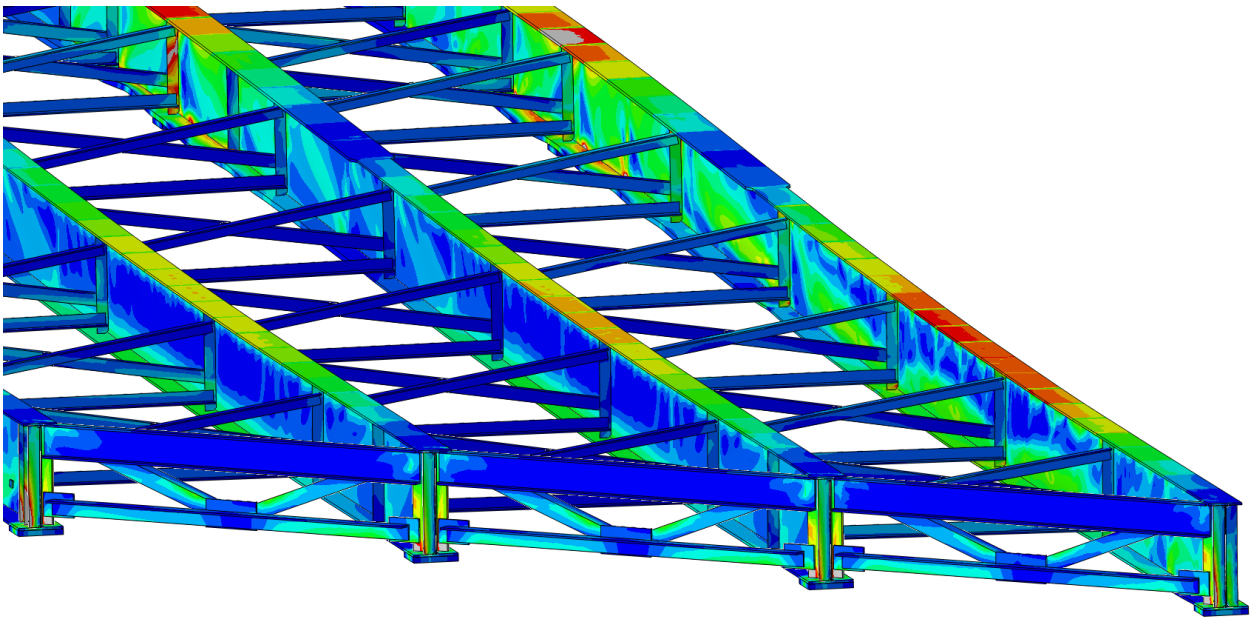

Figure 151 Girder deformation of the 40° skewed-staggered bridge with 4.6 m [15 ft] cross-frame spacing

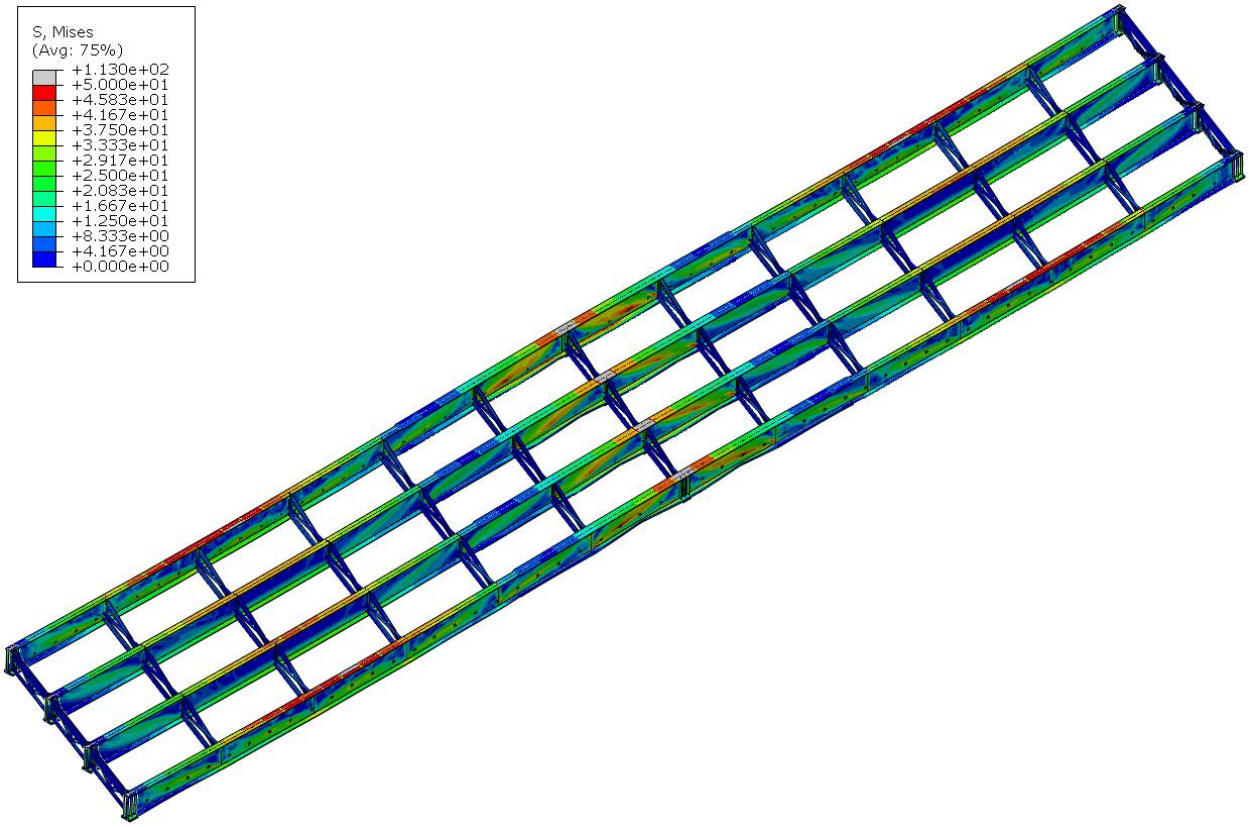

Figure 152 Deformed shaped of the 20° skewed-parallel bridge with 4.6 m [15 ft] cross-frame spacing in isotropic view

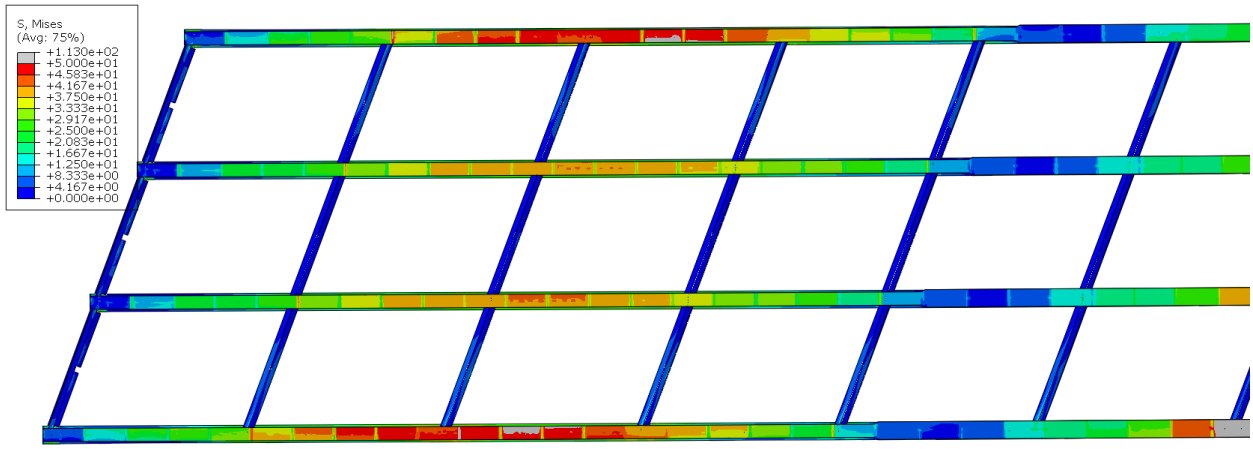

Figure 153 Deformed shape of the 20° skewed-parallel bridge in Span 1 with 4.6 m [15 ft] cross-frame spacing in plan view

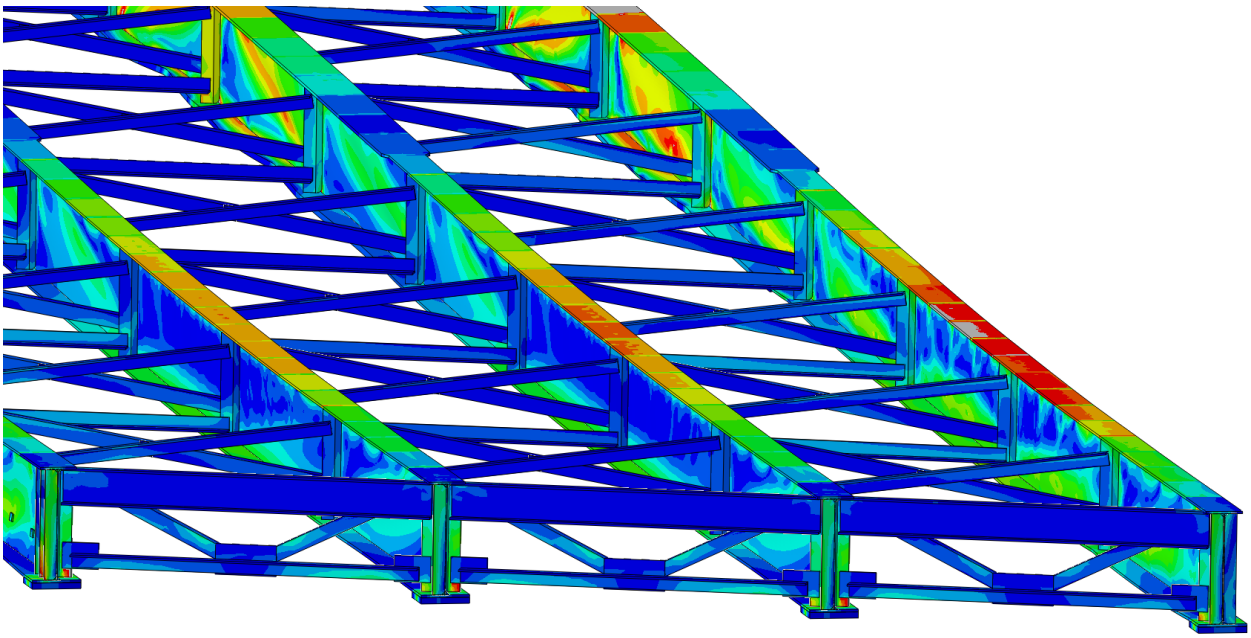

Figure 154 Girder deformation of the 20° skewed-parallel bridge with 4.6 m [15 ft] cross-frame spacing

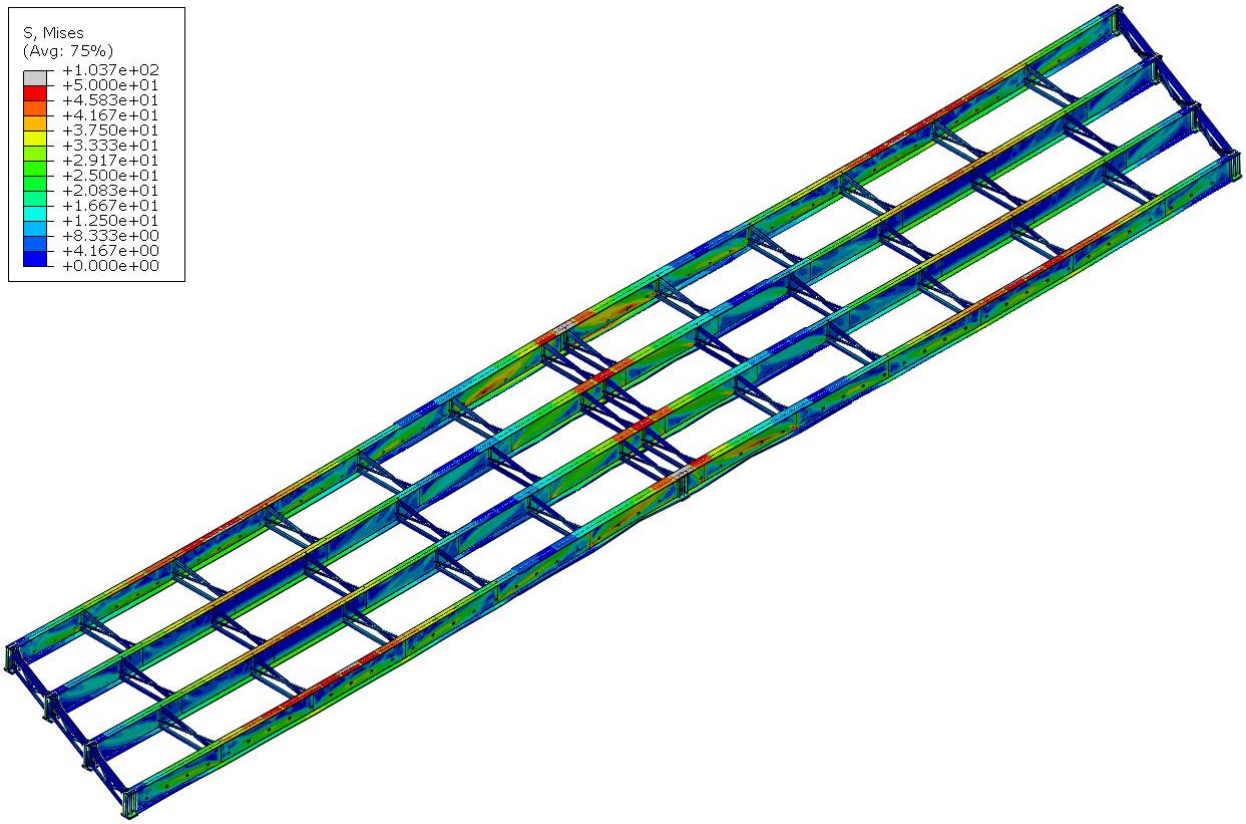

Figure 155 Deformed shaped of the 20° skewed-staggered bridge with 4.6 m [15 ft] cross-frame spacing in isotropic view

.

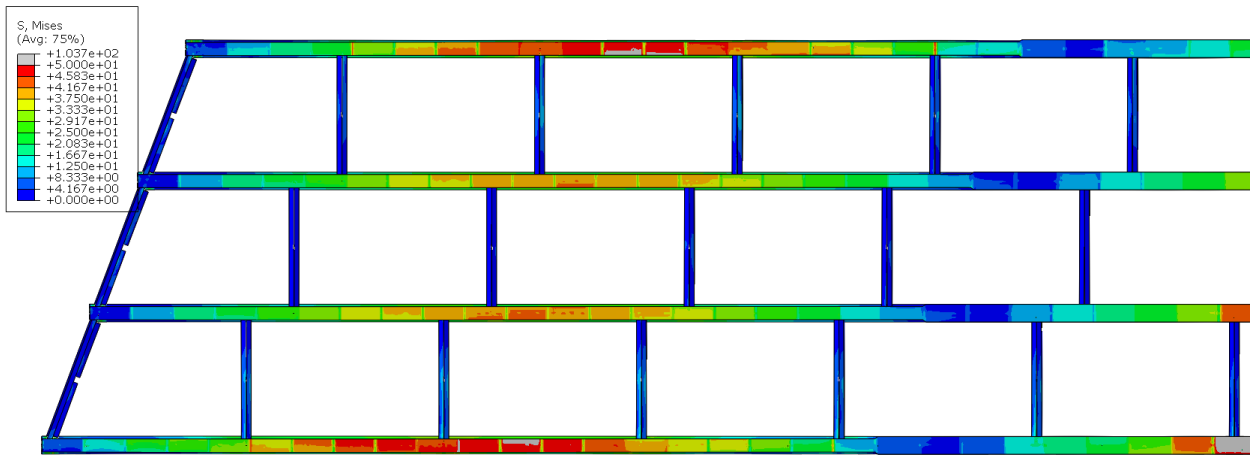

Figure 156 Deformed shape of the 20° skewed-staggered bridge in Span 1 with 4.6 m [15 ft] cross-frame spacing in plan view

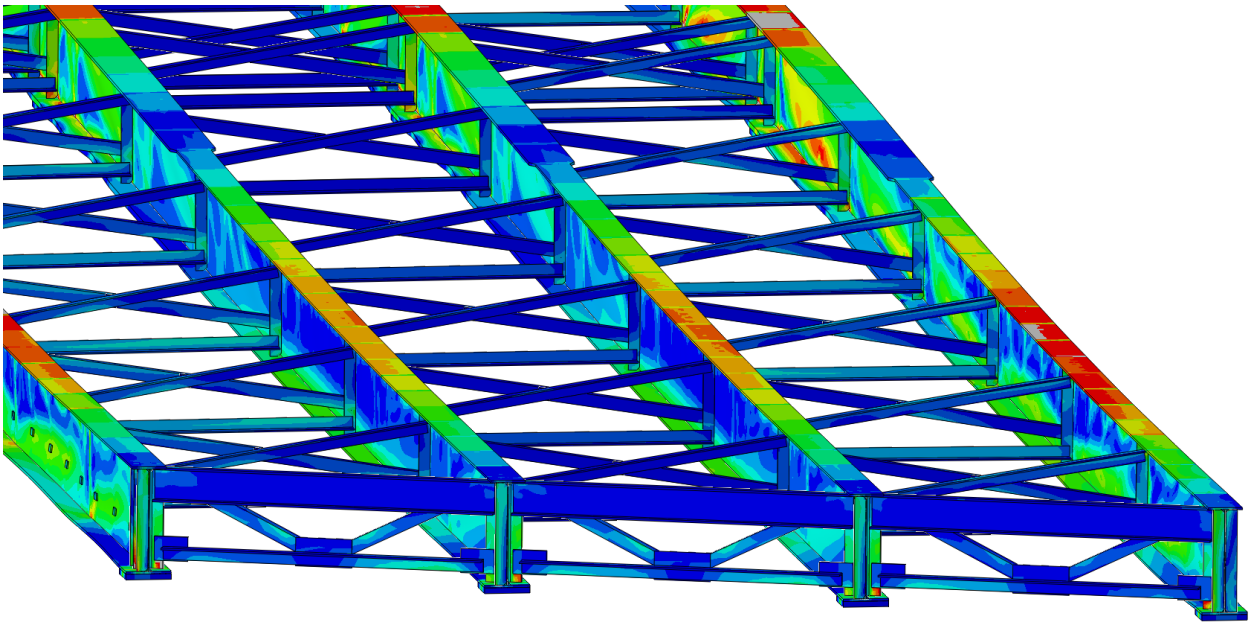

Figure 157 Girder deformation of the 20° skewed-staggered bridge with 4.6 m [15 ft] cross-frame spacing

NON-SKEWED BRIDGE

15 FT CROSS-FRAME SPACING;

3/8" THICK STIFFENERS

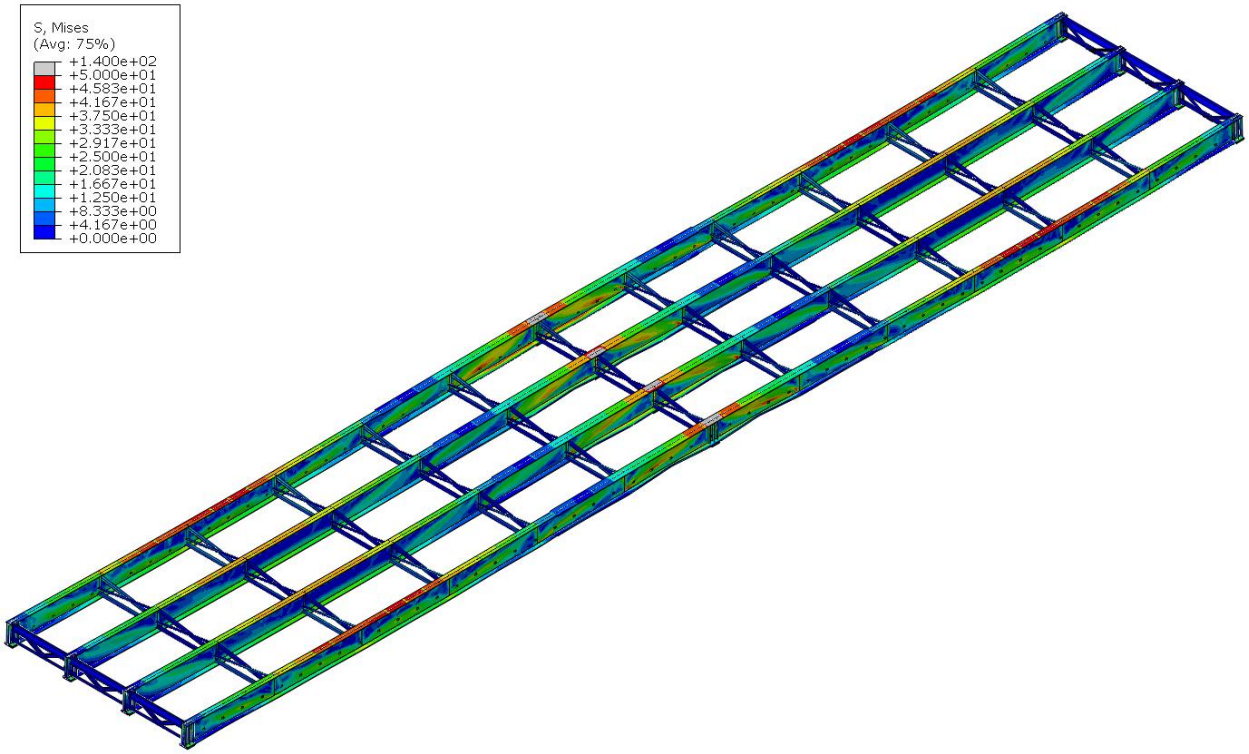

Figure 158 Deformed shaped of the non-skewed bridge with 4.6 m [15 ft] cross-frame spacing in isotropic view

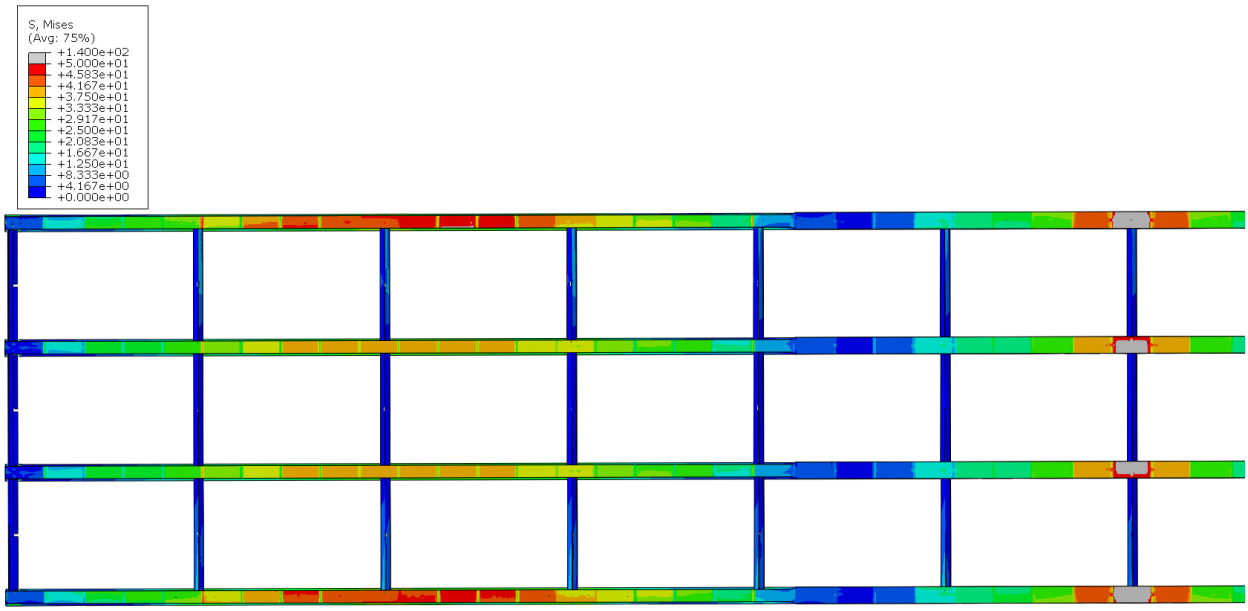

Figure 159 Deformed shape of the non-skewed bridge in Span 1 with 4.6 m [15 ft] cross-frame spacing in plan view

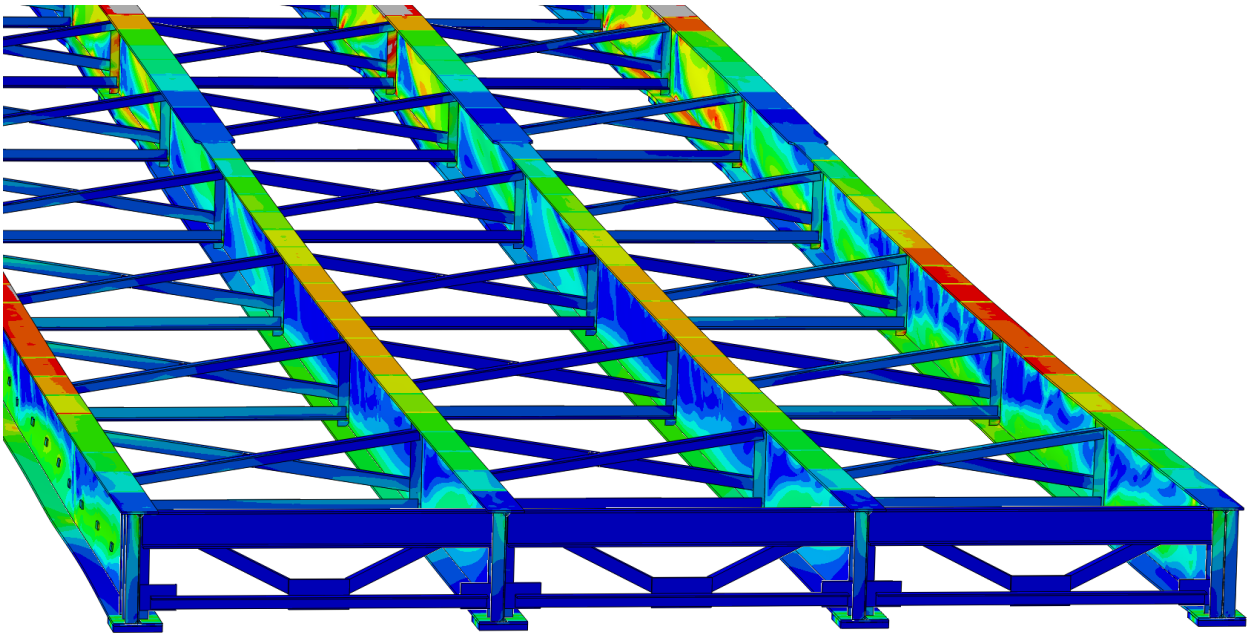

Figure 160 Girder deformation of the non-skewed bridge with 4.6 m [15 ft] cross-frame spacing

APPENDIX B:

AASHTO-Predicted Capacity Calculations

Exterior Girder Check - Positive Flexure Region

b_{fc} = 12”

t_{fc} = 0.75”

D = 36”

t_w = 0.4375”

b_{ft} = 16”

t_{ft} = 0.875”

A = 38.75 in^2

$C_{y,top}$ = 21.145”

$C_{y,bot}$ = 16.48”

I_x = 9278.26 in^4

I_y = 406.92 in^4

S_{xt} = 562.95 in^3

S_{xc} = 438.79 in^3

S_y = 50.86 in^3

r_x = 15.47”

r_y = 3.24”

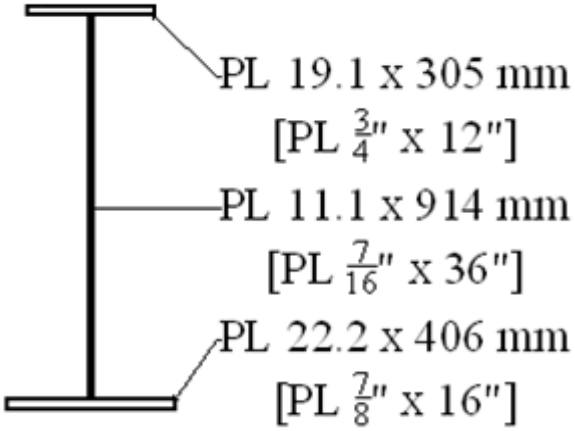

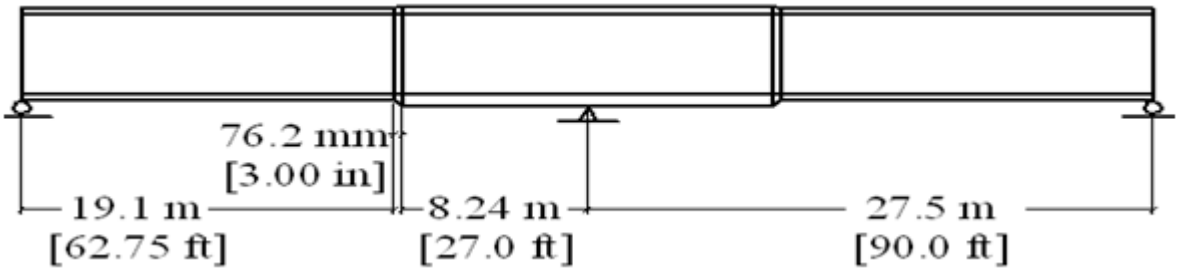

Determine Classification of the Section:

Check $\frac{2D_c}{t_w} \leq 5.7\sqrt{\frac{E}{F_{yc}}}$ *(AASHTO 2010 6.10.6.2.3-1)*

$D_c = D + t_{ft} - C_y = 36 + {}^{7}/_{8}" - 16.48 = 20.40"$

Check $\frac{(2)(19")}{{}^{1}/_{2}"} = 93.23 \leq 5.7\sqrt{\frac{29{,}000\ ksi}{50\ ksi}} = 137.3$ OK, ∴ web is non-slender

Check $\frac{I_{yc}}{I_{yt}} \geq 0.3$

$$I_{yc} = \frac{1}{12}bh^3 + Ad^2$$

$$I_{yc} = \frac{1}{12}(12")(^3/_4")^3 + (9\ in^2)(20.77")^2 = 3{,}883\ in^4$$

$$I_{yt} = \frac{1}{12}(16")(^7/_8")^3 + (14\ in^2)(16.04")^2 = 3{,}604\ in^4$$

Check $\frac{I_{yc}}{I_{yt}} = \frac{3{,}883 in^4}{3{,}604 in^4} = 1.1 \geq 0.3$ OK

<u>Check Compression Flange Local Buckling:</u>

$$\lambda_f = \frac{b_{fc}}{2t_{fc}} = \frac{12"}{(2)(^3/_4")} = 8$$ *(AASHTO 2010 6.10.8.2.2-3)*

$$\lambda_{pf} = 0.38\sqrt{\frac{E}{F_{yc}}} = 0.38\sqrt{\frac{29{,}000\ ksi}{50\ ksi}} = 9.152$$ *(AASHTO 2010 6.10.8.2.2-4)*

$\lambda_f < \lambda_{pf}$ ∴ compact flange

$$F_{nc} = R_b R_h F_{yc}$$ *(AASHTO 2010 6.10.8.2.2-1)*

R_b = 1.0 since web is non-slender

R_h = 1.0 since section is non-hybrid

$$F_{nc} = R_b R_h F_{yc} = (1.0)(1.0)(50\ ksi) = 50\ ksi$$

<u>Check Compression Flange Lateral-Torsional Buckling:</u>

Check unbraced length of the beam, **L_b = 45' = 540"**

$$r_t = \frac{b_{fc}}{\sqrt{12\left(1+\frac{1}{3}\frac{D_c t_w}{b_{fc} t_{fc}}\right)}} = \frac{12}{\sqrt{12\left(1+\frac{1}{3}\frac{(20.395")(^7/_{16}")}{(12")(^3/_4")}\right)}} = 3.003"$$ *(AASHTO 2010 6.10.8.2.3-9)*

$$L_p = 1.0 r_t \sqrt{\frac{E}{F_{yc}}} = (1.0)(3.003")\sqrt{\frac{29{,}000^{ksi}}{50^{ksi}}} = 72.33"$$ *(AASHTO 2010 6.10.8.2.3-4)*

$$F_{yr} = \min\left(0.7F_{yc}, F_{yw}\right) \geq 0.5F_{yc}$$ *(AASHTO 2010 pg6-145)*

$F_{yr} = (0.7)\left(50^{ksi}\right) = 35^{ksi} > 25ksi$

$L_r = \pi r_t \sqrt{\frac{E}{F_{yr}}} = (\pi)(3.003")\sqrt{\frac{29{,}000^{ksi}}{35^{ksi}}} = 271.6"$ *(AASHTO 2010 6.10.8.2.3-5)*

Since $L_p = 72.33" < L_r = 271.6" <$ L_b=540.0", Elastic LTB must be investigated.

$F_{nc} = F_{cr} \leq R_b R_h F_{yc}$ *(AASHTO 2010 6.10.8.2.3-3)*

$F_{cr} = \frac{C_b R_b \pi^2 E}{(\frac{L_b}{r_t})^2}$ *(AASHTO 2010 6.10.8.2.3-8)*

R_b = 1.0 since web is non-slender

R_h = 1.0 since section is non-hybrid

Compute the Moment Gradient Factor, Cb, for the Positive Flexure Critical Segment:

$M_{mid} = 17{,}400^{k-in} \rightarrow f_{mid} = \frac{17{,}400^{k-in}}{438.8\ in^3} = 39.65\ ksi$

$M_2 = 16{,}020^{k-in} \rightarrow f_2 = \frac{16{,}020^{k-in}}{438.8\ in^3} = 36.51\ ksi$

$f_{mid}/f_2 > 1$

$C_b = 1$ *(AASHTO 2010 6.10.8.2.3-6)*

$F_{cr} = \frac{(1.0)(1.0)\pi^2(29{,}000\ ksi)}{(\frac{540"}{3.003})^2} = 8.85\ ksi < 50\ ksi\ max \rightarrow F_{cr} = 8.85\ ksi$

<u>Check Compression Flange Lateral-Torsional Buckling:</u>

Check unbraced length of the beam, **L_b = 30' = 360"**

$r_t = \frac{b_{fc}}{\sqrt{12\left(1+\frac{1}{3}\frac{D_c t_w}{b_{fc} t_{fc}}\right)}} = \frac{12}{\sqrt{12\left(1+\frac{1}{3}\frac{(20.395")(7/16")}{(12")(3/4")}\right)}} = 3.003"$ *(AASHTO 2010 6.10.8.2.3-9)*

$L_p = 1.0 r_t \sqrt{\frac{E}{F_{yc}}} = (1.0)(3.003")\sqrt{\frac{29{,}000^{ksi}}{50^{ksi}}} = 72.33"$ *(AASHTO 2010 6.10.8.2.3-4)*

$F_{yr} = \min\left(0.7F_{yc}, F_{yw}\right) \geq 0.5F_{yc}$ *(AASHTO 2010 pg6-145)*

$F_{yr} = (0.7)\left(50^{ksi}\right) = 35^{ksi} > 25ksi$

$L_r = \pi r_t \sqrt{\frac{E}{F_{yr}}} = (\pi)(3.003")\sqrt{\frac{29{,}000^{ksi}}{35^{ksi}}} = 271.6"$ *(AASHTO 2010 6.10.8.2.3-5)*

Since $L_p = 72.33" < L_r = 271.6" <$ L_b=360.0", Elastic LTB must be investigated.

$F_{nc} = F_{cr} \leq R_b R_h F_{yc}$ *(AASHTO 2010 6.10.8.2.3-3)*

$F_{cr} = \frac{C_b R_b \pi^2 E}{(\frac{L_b}{r_t})^2}$ *(AASHTO 2010 6.10.8.2.3-8)*

R_b = 1.0 since web is non-slender

R_h = 1.0 since section is non-hybrid

Compute the Moment Gradient Factor, Cb, for the Positive Flexure Critical Segment:

$C_b = 1.75 - 1.05\left(\frac{f_1}{f_2}\right) + 0.3\left(\frac{f_1}{f_2}\right)^2 \leq 2.3$ *(AASHTO 2010 6.10.8.2.3-7)*

$M_2 = 17{,}400^{k-in} \rightarrow f_2 = \frac{17{,}400^{k-in}}{438.8\ in^3} = 39.65\ ksi$

$M_0 = 0^{k-in} \rightarrow f_0 = 0\ ksi$

$M_{mid} = 12{,}890^{k-in} \rightarrow f_{mid} = \frac{12{,}890^{k-in}}{438.8\ in^3} = 29.38\ ksi$

Since the bending moment diagram is not concave,

$f_1 = 2f_{mid} - f_2 \geq f_0$ *(AASHTO 2010 6.10.8.2.3-11)*

$(2)(29.38) - (39.65^{ksi}) = 19.11\ ksi \geq 0\ ksi$

$C_b = 1.75 - 1.05\left(\frac{19.11}{39.65}\right) + 0.3\left(\frac{19.11}{39.65}\right)^2 = 1.314 \leq 2.3 \rightarrow C_b = 1.314$

$F_{cr} = \frac{(1.314)(1.0)\pi^2(29{,}000\ ksi)}{(\frac{360"}{3.003})^2} = 26.17\ ksi < 50\ ksi\ max \rightarrow F_{cr} = 26.17\ ksi$

Check Compression Flange Lateral-Torsional Buckling:

Check unbraced length of the beam, $\mathbf{L_b}$ = **15' = 180"**

$$r_t = \frac{b_{fc}}{\sqrt{12\left(1+\frac{1}{3}\frac{D_c t_w}{b_{fc} t_{fc}}\right)}} = \frac{12}{\sqrt{12\left(1+\frac{1}{3}\frac{(20.395")(7/16")}{(12")(3/4")}\right)}} = 3.003"$$ *(AASHTO 2010 6.10.8.2.3-9)*

$$L_p = 1.0 r_t \sqrt{\frac{E}{F_{yc}}} = (1.0)(3.003")\sqrt{\frac{29{,}000^{ksi}}{50^{ksi}}} = 72.33"$$ *(AASHTO 2010 6.10.8.2.3-4)*

$$F_{yr} = \min\left(0.7F_{yc}, F_{yw}\right) \geq 0.5F_{yc}$$ *(AASHTO 2010 pg6-145)*

$$F_{yr} = (0.7)\left(50^{ksi}\right) = 35^{ksi} > 25ksi$$

$$L_r = \pi r_t \sqrt{\frac{E}{F_{yr}}} = (\pi)(3.003")\sqrt{\frac{29{,}000^{ksi}}{35^{ksi}}} = 271.6"$$ *(AASHTO 2010 6.10.8.2.3-5)*

Since $L_p = 72.33" <$ L_b=180.0" $< L_r = 271.6"$, Inelastic LTB must be investigated.

$$F_{nc(LTB)} = C_b\left[1 - \left(1 - \frac{F_{yr}}{R_h F_{yc}}\right)\left(\frac{L_b - L_p}{L_r - L_p}\right)\right]R_b R_h F_{yc} \leq R_b R_h F_{yc}$$ *(AASHTO 2010 6.10.8.2.3-2)*

R_b = 1.0 since web is non-slender

R_h = 1.0 since section is non-hybrid

Compute the Moment Gradient Factor, Cb, for the Abutment Segment:

$$C_b = 1.75 - 1.05\left(\frac{f_1}{f_2}\right) + 0.3\left(\frac{f_1}{f_2}\right)^2 \leq 2.3$$ *(AASHTO 2010 6.10.8.2.3-7)*

$$M_2 = 12{,}890^{k-in} \rightarrow f_2 = \frac{12{,}890^{k-in}}{438.8\ in^3} = 29.38\ ksi$$

$$M_0 = 0^{k-in} \rightarrow f_0 = 0\ ksi$$

$$M_{mid} = 7{,}699^{k-in} \rightarrow f_{mid} = \frac{7{,}699^{k-in}}{438.8\ in^3} = 17.55\ ksi$$

Since the bending moment diagram is not concave,

$$f_1 = 2f_{mid} - f_2 \geq f_0$$ *(AASHTO 2010 6.10.8.2.3-11)*

$$(2)\left(17.55^{ksi}\right) - (29.38^{ksi}) = 5.720^{ksi} \geq 0\ ksi$$

$$C_b = 1.75 - 1.05\left(\frac{5.720}{29.38}\right) + 0.3\left(\frac{5.720}{29.38}\right)^2 = 1.557 \leq 2.3 \;\; \rightarrow C_b = 1.557$$

Compute the Moment Gradient Factor, Cb, for the Mid-span Segment:

$$M_2 = 17{,}400^{k-in} \rightarrow f_2 = \frac{17{,}400^{k-in}}{438.8\ in^3} = 39.65\ ksi$$

$$M_0 = 12{,}890^{k-in} \rightarrow f_0 = \frac{12{,}890^{k-in}}{438.8\ in^3} = 29.38\ ksi$$

$$M_{mid} = 16{,}130^{k-in} \rightarrow f_{mid} = \frac{16{,}130^{k-in}}{438.8\ in^3} = 36.76\ ksi$$

Since the bending moment diagram is not concave,

$f_1 = 2f_{mid} - f_2 \geq f_0$ *(AASHTO 2010 6.10.8.2.3-11)*

$(2)\left(36.76^{ksi}\right) - (39.65^{ksi}) = 33.87^{ksi} \geq f_0 = 29.38 \rightarrow f_1 = 33.87\ ksi$

$C_b = 1.75 - 1.05\left(\frac{33.87}{39.65}\right) + 0.3\left(\frac{33.87}{39.65}\right)^2 = 1.072 \leq 2.3 \;\; \rightarrow C_b = 1.557$ Controls

$$F_{nc(LTB)} = 1.557\left[1 - \left(1 - \frac{35^{ksi}}{(1.00)(50^{ksi})}\right)\left(\frac{180.0" - 72.33"}{271.56" - 72.33"}\right)\right](1.0)(1.0)\left(50^{ksi}\right) \leq (1.0)(1.0)\left(50^{ksi}\right)$$

$F_{nc(LTB)} = 65.23\ ksi \leq 50\ ksi\ max \rightarrow F_{nc(LTB)} = 50\ ksi$

The governing strength for the compression flange is the smaller of $F_{nc(FLB)}\ and\ F_{nc(LTB)}$:

For **L_b = 45'**, $F_{nc(LTB)} = 8.85^{ksi} < F_{nc(FLB)} = 50^{ksi}$, LTB governs the strength of the compression flange.

$F_{nc} = F_{nc(LTB)} = 8.85\ ksi$

$\Phi F_{nc} = (1.0)(8.85) = 8.85\ ksi$ *(AASHTO 2010 6.10.8.1.1-1)*

For **L_b = 30'**, $F_{nc(LTB)} = 26.15^{ksi} < F_{nc(FLB)} = 50^{ksi}$, LTB governs the strength of the compression flange.

$F_{nc} = F_{nc(LTB)} = 26.15\ ksi$

$\Phi F_{nc} = (1.0)(26.15) = 26.15\ ksi$ *(AASHTO 2010 6.10.8.1.1-1)*

For **L_b = 15'**, $F_{nc(LTB)} = F_{nc(FLB)} = 50\ ksi$, yielding governs the strength of the compression flange.

$F_{nc} = F_{yc} = 50\ ksi$

$\Phi F_{nc} = (1.0)\left(50^{ksi}\right) = 50\ ksi$ *(AASHTO 2010 6.10.8.1.1-1)*

Investigate the Strength of the Tension Flange:

$F_{nt} = R_h F_{yt} = (1.0)\left(\ 50^{ksi}\right) = 50^{ksi}$ *(AASHTO 2010 6.10.8.3-1)*

$\Phi F_{nt} = (1.0)\ \left(\ 50^{ksi}\right) = 50^{ksi}$

Exterior Girder Check - Negative Flexure Region

b_{fc} = 16”

t_{fc} = 2.0”

D = 36”

t_w = 0.5”

b_{ft} = 16”

t_{ft} = 1.0”

A = 66 in^2

C_y = 15.27”

I_x = 17510 in^4

I_y = 1024 in^4

S_{xt} = 737.88 in^3

S_{xc} = 1146 in^3

S_y = 128.1 in^3

r_x = 16.29”

r_y = 3.94”

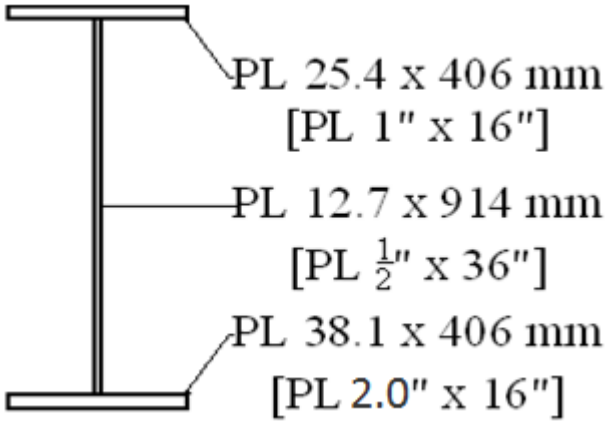

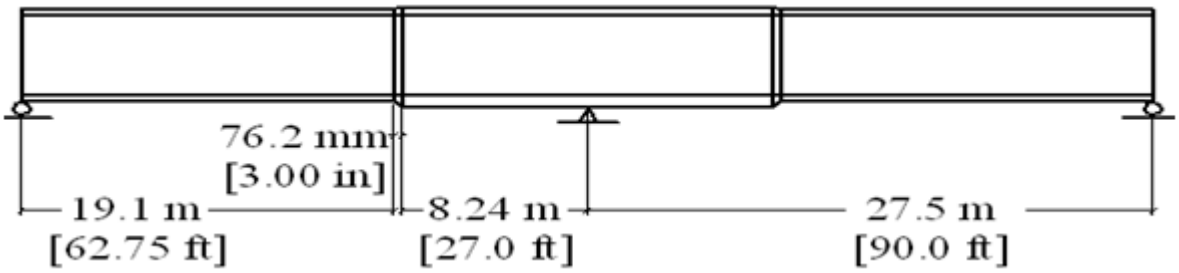

<u>Determine Classification of the Section:</u>

Check $\frac{2D_c}{t_w} \leq 5.7\sqrt{\frac{E}{F_{yc}}}$ *(AASHTO 2010 6.10.6.2.3-1)*

$D_c = C_y - t_{fc} = 15.27 + 2.0" = 13.27"$

Check $\frac{(2)(19")}{1/2"} = 53.08 \leq 5.7\sqrt{\frac{29{,}000\ ksi}{50\ ksi}} = 137.3$ OK, ∴ web is non-slender

Check $\frac{I_{yc}}{I_{yt}} \geq 0.3$

$$I_{yc} = \frac{1}{12}bh^3 + Ad^2$$

$$I_{yc} = \frac{1}{12}(16")(2.0")^3 + (32\ in^2)(14.27")^2 = 6{,}527\ in^4$$

$$I_{yt} = \frac{1}{12}(16")(1.0")^3 + (16\ in^2)(23.23")^2 = 8{,}635\ in^4$$

Check $\frac{I_{yc}}{I_{yt}} = \frac{6{,}527\ in^4}{8{,}635\ in^4} = 0.76 \geq 0.3$ OK

Check Compression Flange Local Buckling:

$$\lambda_f = \frac{b_{fc}}{2t_{fc}} = \frac{16"}{(2)(2.0")} = 4.0$$ *(AASHTO 2010 6.10.8.2.2-3)*

$$\lambda_{pf} = 0.38\sqrt{\frac{E}{F_{yc}}} = 0.38\sqrt{\frac{29{,}000\ ksi}{50\ ksi}} = 9.152$$ *(AASHTO 2010 6.10.8.2.2-4)*

$\lambda_f < \lambda_{pf}$ ∴ compact flange

$$F_{nc} = R_b R_h F_{yc}$$ *(AASHTO 2010 6.10.8.2.2-1)*

R_b = 1.0 since web is non-slender

R_h = 1.0 since section is non-hybrid

$$F_{nc} = R_b R_h F_{yc} = (1.0)(1.0)(50\ ksi) = 50\ ksi$$

Check Compression Flange Lateral-Torsional Buckling:

Check unbraced length of the beam, **L_b = 45' = 540"**

$$r_t = \frac{b_{fc}}{\sqrt{12\left(1+\frac{1}{3}\frac{D_c t_w}{b_{fc} t_{fc}}\right)}} = \frac{16}{\sqrt{12\left(1+\frac{1}{3}\frac{(13.27")(1/2")}{(16")(2.0"}\right)}} = 4.566"$$ *(AASHTO 2010 6.10.8.2.3-9)*

$$L_p = 1.0 r_t \sqrt{\frac{E}{F_{yc}}} = (1.0)(4.566")\sqrt{\frac{29{,}000^{ksi}}{50^{ksi}}} = 110.0"$$ *(AASHTO 2010 6.10.8.2.3-4)*

$$F_{yr} = \min\left(0.7F_{yc}, F_{yw}\right) \geq 0.5F_{yc}$$ *(AASHTO 2010 pg6-145)*

$$F_{yr} = (0.7)\left(50^{ksi}\right) = 35^{ksi} > 25ksi$$

$$L_r = \pi r_t \sqrt{\frac{E}{F_{yr}}} = (\pi)(4.566")\sqrt{\frac{29{,}000^{ksi}}{35^{ksi}}} = 412.9"$$ *(AASHTO 2010 6.10.8.2.3-5)*

Since $L_p = 110.0" < L_r = 412.9" <$ L_b=540.0", Elastic LTB must be investigated.

$$F_{nc} = F_{cr} \leq R_b R_h F_{yc}$$ *(AASHTO 2010 6.10.8.2.3-3)*

$$F_{cr} = \frac{C_b R_b \pi^2 E}{(\frac{L_b}{r_t})^2}$$ *(AASHTO 2010 6.10.8.2.3-8)*

R_b = 1.0 since web is non-slender

R_h = 1.0 since section is non-hybrid

Compute the Moment Gradient Factor, Cb, for the Positive Flexure Critical Segment:

$$C_b = 1.75 - 1.05\left(\frac{f_1}{f_2}\right) + 0.3\left(\frac{f_1}{f_2}\right)^2 \leq 2.3$$ *(AASHTO 2010 6.10.8.2.3-7)*

$$M_{mid} = -5{,}646^{k-in} \rightarrow f_{mid} = \frac{5{,}646^{k-in}}{1{,}146\ in^3} = 4.93\ ksi$$

$$M_2 = -43{,}920^{k-in} \rightarrow f_2 = \frac{43{,}920^{k-in}}{1{,}146\ in^3} = 38.32\ ksi$$

$$M_0 = 0^{k-in} \rightarrow f_0 = 0\ ksi$$

Since the bending moment diagram is concave,

$$f_1 = f_0 = 0\ ksi$$ *(AASHTO 2010 6.10.8.2.3-10)*

$$C_b = 1.75 - 1.05\left(\frac{0}{38.32}\right) + 0.3\left(\frac{0}{38.32}\right)^2 = 1.75 \leq 2.3 \rightarrow C_b = 1.75$$

$$F_{cr} = \frac{(1.75)(1.0)\pi^2(29{,}000\ ksi)}{(\frac{540"}{4.566})^2} = 35.81\ ksi < 50\ ksi\ max \rightarrow F_{cr} = 35.81\ ksi$$

<u>Check Compression Flange Lateral-Torsional Buckling:</u>

Check unbraced length of the beam, **L_b = 30' = 360"**

$$r_t = \frac{b_{fc}}{\sqrt{12\left(1+\frac{1}{3}\frac{D_c t_w}{b_{fc} t_{fc}}\right)}} = \frac{16}{\sqrt{12\left(1+\frac{1}{3}\frac{(13.27")(1/2")}{(16")(2.0"}\right)}} = 4.566"$$ *(AASHTO 2010 6.10.8.2.3-9)*

$$L_p = 1.0 r_t \sqrt{\frac{E}{F_{yc}}} = (1.0)(4.566")\sqrt{\frac{29{,}000^{ksi}}{50^{ksi}}} = 110.0"$$ *(AASHTO 2010 6.10.8.2.3-4)*

$$F_{yr} = \min\left(0.7F_{yc}, F_{yw}\right) \geq 0.5F_{yc}$$ *(AASHTO 2010 pg6-145)*

$$F_{yr} = (0.7)\left(50^{ksi}\right) = 35^{ksi} > 25ksi$$

$$L_r = \pi r_t \sqrt{\frac{E}{F_{yr}}} = (\pi)(4.566")\sqrt{\frac{29{,}000^{ksi}}{35^{ksi}}} = 412.9"$$ *(AASHTO 2010 6.10.8.2.3-5)*

Since $L_p = 110.0" < L_b = 360.0" <$ L_b=412.9", Inelastic LTB must be investigated.

$$F_{nc(LTB)} = C_b[1 - \left(1 - \frac{F_{yr}}{R_h F_{yc}}\right)\left(\frac{L_b - L_p}{L_r - L_p}\right)]R_b R_h F_{yc} \leq R_b R_h F_{yc}$$ *(AASHTO 2010 6.10.8.2.3-2)*

R_b = 1.0 since web is non-slender

R_h = 1.0 since section is non-hybrid

Compute the Moment Gradient Factor, Cb, for the Negative Flexure Critical Segment:

$$C_b = 1.75 - 1.05\left(\frac{f_1}{f_2}\right) + 0.3\left(\frac{f_1}{f_2}\right)^2 \leq 2.3$$ *(AASHTO 2010 6.10.8.2.3-7)*

$$M_2 = -43{,}920^{k-in} \rightarrow f_2 = \frac{43{,}920^{k-in}}{1{,}146\ in^3} = 38.32\ ksi$$

$$M_0 = 0^{k-in} \rightarrow f_0 = 0\ ksi$$

$$M_{mid} = -16{,}290^{k-in} \rightarrow f_{mid} = \frac{16{,}290^{k-in}}{1{,}146\ in^3} = 14.21\ ksi$$

Since the bending moment diagram is concave,

$$f_1 = f_0 = 0\ ksi$$ *(AASHTO 2010 6.10.8.2.3-10)*

$$C_b = 1.75 - 1.05\left(\frac{0}{38.32}\right) + 0.3\left(\frac{0}{38.32}\right)^2 = 1.75 \leq 2.3 \rightarrow C_b = 1.75$$

$$F_{nc(LTB)} = 1.75\left[1 - \left(1 - \frac{35^{ksi}}{(1.00)(50^{ksi})}\right)\left(\frac{360.0" - 110.0"}{412.9" - 110.0"}\right)\right](1.0)(1.0)\left(50^{ksi}\right) \leq (1.0)(1.0)\left(50^{ksi}\right)$$

$$F_{nc(LTB)} = 65.83\ ksi \leq 50\ ksi\ max \rightarrow F_{nc(LTB)} = 50\ ksi$$

Check Compression Flange Lateral-Torsional Buckling:

Check unbraced length of the beam, **L_b = 15' = 180"**

$$r_t = \frac{b_{fc}}{\sqrt{12\left(1+\frac{1}{3}\frac{D_c t_w}{b_{fc} t_{fc}}\right)}} = \frac{16}{\sqrt{12\left(1+\frac{1}{3}\frac{(13.27")(1/2")}{(16")(2.0"}\right)}} = 4.566"$$ *(AASHTO 2010 6.10.8.2.3-9)*

$$L_p = 1.0 r_t \sqrt{\frac{E}{F_{yc}}} = (1.0)(4.566")\sqrt{\frac{29{,}000^{ksi}}{50^{ksi}}} = 110.0"$$ *(AASHTO 2010 6.10.8.2.3-4)*

$$F_{yr} = \min\left(0.7F_{yc}, F_{yw}\right) \geq 0.5F_{yc}$$ *(AASHTO 2010 pg6-145)*

$$F_{yr} = (0.7)\left(50^{ksi}\right) = 35^{ksi} > 25ksi$$

$$L_r = \pi r_t \sqrt{\frac{E}{F_{yr}}} = (\pi)(4.566")\sqrt{\frac{29{,}000^{ksi}}{35^{ksi}}} = 412.9"$$ *(AASHTO 2010 6.10.8.2.3-5)*

Since $L_p = 110.0" < L_b = 180.0" <$ L_b=412.9", Inelastic LTB must be investigated.

$$F_{nc(LTB)} = C_b[1 - \left(1 - \frac{F_{yr}}{R_h F_{yc}}\right)\left(\frac{L_b - L_p}{L_r - L_p}\right)]R_b R_h F_{yc} \leq R_b R_h F_{yc}$$ *(AASHTO 2010 6.10.8.2.3-2)*

R_b = 1.0 since web is non-slender

R_h = 1.0 since section is non-hybrid

Compute the Moment Gradient Factor, Cb, for the Transition Region Segment:

$$C_b = 1.75 - 1.05\left(\frac{f_1}{f_2}\right) + 0.3\left(\frac{f_1}{f_2}\right)^2 \leq 2.3$$ *(AASHTO 2010 6.10.8.2.3-7)*

$$M_2 = -16{,}290^{k-in} \rightarrow f_2 = \frac{16{,}290^{k-in}}{1{,}146\ in^3} = 14.21\ ksi$$

$$M_0 = 0^{k-in} \rightarrow f_0 = 0\ ksi$$

$$M_{mid} = -5{,}646^{k-in} \rightarrow f_{mid} = \frac{5{,}646^{k-in}}{1{,}146\ in^3} = 4.93\ ksi$$

Since the bending moment diagram is concave,

$f_1 = f_0 = 0\ ksi$ *(AASHTO 2010 6.10.8.2.3-10)*

$$C_b = 1.75 - 1.05\left(\frac{0}{14.21}\right) + 0.3\left(\frac{0}{14.21}\right)^2 = 1.75 \leq 2.3 \ \rightarrow C_b = 1.75$$

Compute the Moment Gradient Factor, Cb, for Center Pier Segment:

$$M_2 = -43{,}920^{k-in} \rightarrow f_2 = \frac{43{,}920^{k-in}}{1{,}146\ in^3} = 38.32\ ksi$$

$$M_0 = -16{,}290^{k-in} \rightarrow f_0 = \frac{16{,}290^{k-in}}{1{,}146\ in^3} = 14.21\ ksi$$

$$M_{mid} = -29{,}050^{k-in} \rightarrow f_{mid} = \frac{29{,}050^{k-in}}{1{,}146\ in^3} = 25.35\ ksi$$

Since the bending moment diagram is concave,

$f_1 = f_0 = 14.21\ ksi$ *(AASHTO 2010 6.10.8.2.3-10)*

$$C_b = 1.75 - 1.05\left(\frac{14.21}{38.32}\right) + 0.3\left(\frac{14.21}{38.32}\right)^2 = 1.40 \leq 2.3 \ \rightarrow C_b = 1.75 \text{ Controls}$$

$$F_{nc(LTB)} = 1.75\left[1 - \left(1 - \frac{35^{ksi}}{(1.00)(50^{ksi})}\right)\left(\frac{180.0" - 110.0"}{412.9" - 110.0"}\right)\right](1.0)(1.0)\left(50^{ksi}\right) \leq (1.0)(1.0)\left(50^{ksi}\right)$$

$F_{nc(LTB)} = 81.43\ ksi \leq 50\ ksi\ max \rightarrow F_{nc(LTB)} = 50\ ksi$

The governing strength for the compression flange is the smaller of $F_{nc(FLB)}\ and\ F_{nc(LTB)}$:

For **L_b = 45'**, $F_{nc(LTB)} = 35.81^{ksi} < F_{nc(FLB)} = 50^{ksi}$, LTB governs the strength of the compression flange.

$F_{nc} = F_{nc(LTB)} = 35.81\ ksi$

$\Phi F_{nc} = (1.0)(35.81) = 35.81\ ksi$ *(AASHTO 2010 6.10.8.1.1-1)*

For **L_b = 30'**, $F_{nc(LTB)} = 50^{ksi} < F_{nc(FLB)} = 50^{ksi}$, yielding governs the strength of the compression flange.

$F_{nc} = F_{yc} = 50\ ksi$

$\Phi F_{nc} = (1.0)(50) = 50\ ksi$ *(AASHTO 2010 6.10.8.1.1-1)*

For **L_b = 15'**, $F_{nc(LTB)} = F_{nc(FLB)} = 50\ ksi$, yielding governs the strength of the compression flange.

$F_{nc} = F_{yc} = 50\ ksi$

$\Phi F_{nc} = (1.0)\left(50^{ksi}\right) = 50\ ksi$ *(AASHTO 2010 6.10.8.1.1-1)*

Investigate the Strength of the Tension Flange:

$F_{nt} = R_h F_{yt} = (1.0)\left(50^{ksi}\right) = 50^{ksi}$ *(AASHTO 2010 6.10.8.3-1)*

$\Phi F_{nt} = (1.00)\left(50^{ksi}\right) = 50^{ksi}$

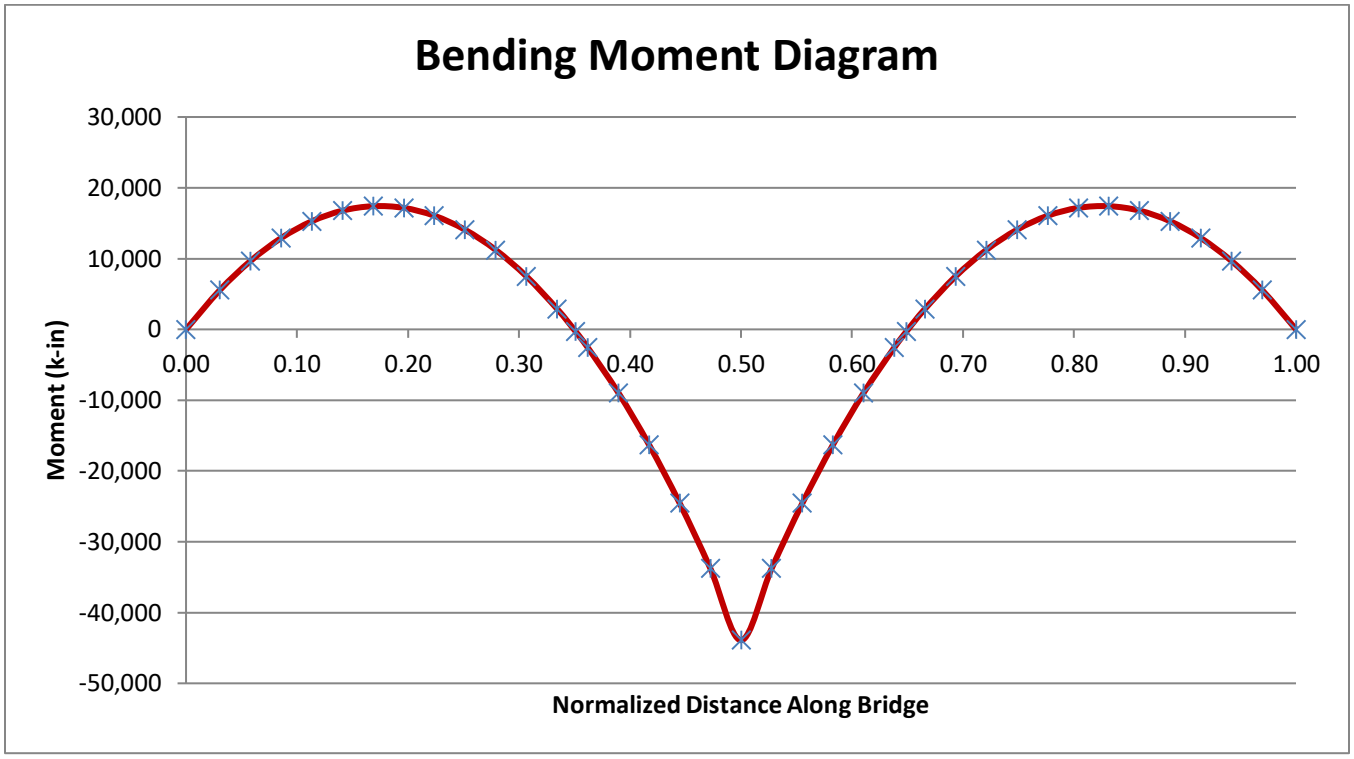
Bending Moment Diagram
30,000
20,000
10,000
0
-10,000
-20,000
-30,000
-40,000
-50,000
0.00
0.10
0.20
0.30
0.40
0.50
0.60
0.70
0.80
0.90
1.00
Moment (k-in)
Normalized Distance Along Bridge

Bending Moment & Stress

Normalized Position	Position (in)	M_z (k-in)	σ_z (ksi)	
0.00	0	0	0.00	
0.03	66	5532.5	9.83	
0.06	126	9647.7	17.14	
0.09	186	12892	22.90	
0.11	246	15266	27.12	
0.14	306	16768	29.78	
0.17	366	17400	30.91	
0.20	426	17161	30.48	
0.22	486	16051	28.51	
0.25	546	14071	24.99	
0.28	606	11219	19.93	
0.31	666	7496.8	13.32	
0.33	726	2903.6	5.16	
0.35	762	-270.35	-0.48	Transition Point
0.36	786	-2565.8	-4.56	
0.39	846	-8960.8	-15.92	
0.42	906	-16293	-28.94	
0.44	966	-24563	-43.63	
0.47	1026	-33771	-59.98	
0.50	1086	-43916	-78.00	
0.53	1146	-33771	-59.98	
0.56	1206	-24563	-43.63	
0.58	1266	-16293	-28.94	
0.61	1326	-8960.8	-15.92	
0.64	1386	-2565.8	-4.56	
0.65	1410	-270.35	-0.48	Transition Point
0.67	1446	2903.6	5.16	
0.69	1506	7496.8	13.32	
0.72	1566	11219	19.93	
0.75	1626	14071	24.99	
0.78	1686	16051	28.51	
0.80	1746	17161	30.48	
0.83	1806	17400	30.91	
0.86	1866	16768	29.78	
0.89	1926	15266	27.12	
0.91	1986	12892	22.90	
0.94	2046	9647.7	17.14	
0.97	2106	5532.5	9.83	
1.00	2172	0	0.00	

Interior Girder Check - Positive Flexure Region

b_{fc} = 12”

t_{fc} = 0.75”

D = 36”

t_w = 0.4375”

b_{ft} = 16”

t_{ft} = 0.875”

A = 38.75 in^2

$C_{y,top}$ = 21.145”

$C_{y,bot}$ = 16.48”

I_x = 9278.26 in^4

I_y = 406.92 in^4

S_{xt} = 562.95 in^3

S_{xc} = 438.79 in^3

S_y = 50.86 in^3

r_x = 15.47”

r_y = 3.24”

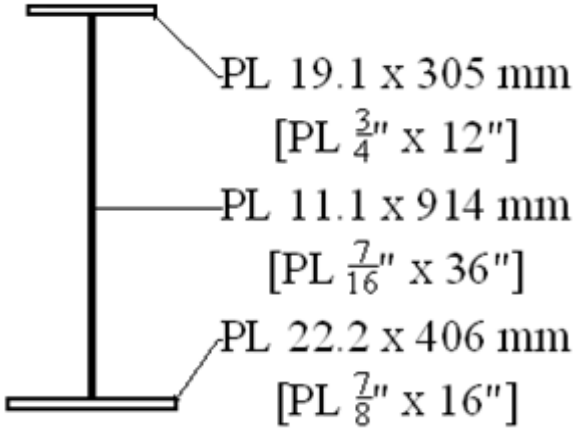

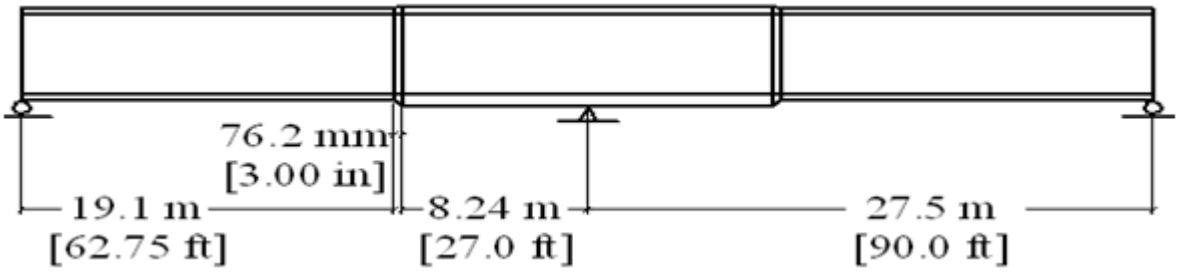

Determine Classification of the Section:

Check $\frac{2D_c}{t_w} \leq 5.7\sqrt{\frac{E}{F_{yc}}}$ *(AASHTO 2010 6.10.6.2.3-1)*

$D_c = D + t_{ft} - C_y = 36 + {}^{7}/_{8}" - 16.48 = 20.40"$

Check $\frac{(2)(19")}{{}^{1}/_{2}"} = 93.23 \leq 5.7\sqrt{\frac{29{,}000\ ksi}{50\ ksi}} = 137.3$ OK, ∴ web is non-slender

Check $\frac{I_{yc}}{I_{yt}} \geq 0.3$

$$I_{yc} = \frac{1}{12}bh^3 + Ad^2$$

$$I_{yc} = \frac{1}{12}(12")(^3/_4")^3 + (9\ in^2)(20.77")^2 = 3{,}883\ in^4$$

$$I_{yt} = \frac{1}{12}(16")(^7/_8")^3 + (14\ in^2)(16.04")^2 = 3{,}604\ in^4$$

Check $\frac{I_{yc}}{I_{yt}} = \frac{3{,}883 in^4}{3{,}604 in^4} = 1.1 \geq 0.3$ OK

Check Compression Flange Local Buckling:

$\lambda_f = \frac{b_{fc}}{2t_{fc}} = \frac{12"}{(2)(^3/_4")} = 8$ *(AASHTO 2010 6.10.8.2.2-3)*

$\lambda_{pf} = 0.38\sqrt{\frac{E}{F_{yc}}} = 0.38\sqrt{\frac{29{,}000\ ksi}{50\ ksi}} = 9.152$ *(AASHTO 2010 6.10.8.2.2-4)*

$\lambda_f < \lambda_{pf}$ ∴ compact flange

$F_{nc} = R_b R_h F_{yc}$ *(AASHTO 2010 6.10.8.2.2-1)*

R_b = 1.0 since web is non-slender

R_h = 1.0 since section is non-hybrid

$F_{nc} = R_b R_h F_{yc} = (1.0)(1.0)(50\ ksi) = 50\ ksi$

Check Compression Flange Lateral-Torsional Buckling:

Check unbraced length of the beam, **L_b = 45' = 540"**

$r_t = \frac{b_{fc}}{\sqrt{12\left(1+\frac{1}{3}\frac{D_c t_w}{b_{fc} t_{fc}}\right)}} = \frac{12}{\sqrt{12\left(1+\frac{1}{3}\frac{(20.395")(^7/_{16}")}{(12")(^3/_4")}\right)}} = 3.003"$ (AASHTO 2010 6.10.8.2.3-9)

$L_p = 1.0 r_t \sqrt{\frac{E}{F_{yc}}} = (1.0)(3.003")\sqrt{\frac{29{,}000^{ksi}}{50^{ksi}}} = 72.33"$ *(AASHTO 2010 6.10.8.2.3-4)*

$F_{yr} = \min(0.7F_{yc}, F_{yw}) \geq 0.5F_{yc}$ *(AASHTO 2010 pg6-145)*

$F_{yr} = (0.7)\left(50^{ksi}\right) = 35^{ksi} > 25ksi$

$L_r = \pi r_t \sqrt{\frac{E}{F_{yr}}} = (\pi)(3.003")\sqrt{\frac{29{,}000^{ksi}}{35^{ksi}}} = 271.6"$ *(AASHTO 2010 6.10.8.2.3-5)*

Since $L_p = 72.33" < L_r = 271.6" <$ L_b=540.0", Elastic LTB must be investigated.

$F_{nc} = F_{cr} \leq R_b R_h F_{yc}$ *(AASHTO 2010 6.10.8.2.3-3)*

$F_{cr} = \frac{C_b R_b \pi^2 E}{(\frac{L_b}{r_t})^2}$ *(AASHTO 2010 6.10.8.2.3-8)*

R_b = 1.0 since web is non-slender

R_h = 1.0 since section is non-hybrid

Compute the Moment Gradient Factor, Cb, for the Positive Flexure Critical Segment:

$M_{mid} = 15{,}323^{k-in} \rightarrow f_{mid} = \frac{15{,}323^{k-in}}{438.8\ in^3} = 34.92\ ksi$

$M_2 = 13{,}432^{k-in} \rightarrow f_2 = \frac{13{,}432^{k-in}}{438.8\ in^3} = 32.07\ ksi$

$f_{mid}/f_2 > 1$

$C_b = 1$ *(AASHTO 2010 6.10.8.2.3-6)*

$F_{cr} = \frac{(1.0)(1.0)\pi^2(29{,}000\ ksi)}{(\frac{540"}{3.003})^2} = 8.85\ ksi < 50\ ksi\ max \rightarrow F_{cr} = 8.85\ ksi$

<u>Check Compression Flange Lateral-Torsional Buckling:</u>

Check unbraced length of the beam, **L_b = 30' = 360"**

$r_t = \frac{b_{fc}}{\sqrt{12\left(1+\frac{1}{3}\frac{D_c t_w}{b_{fc} t_{fc}}\right)}} = \frac{12}{\sqrt{12\left(1+\frac{1}{3}\frac{(20.395")(7/16")}{(12)(3/4")}\right)}} = 3.003"$ *(AASHTO 2010 6.10.8.2.3-9)*

$L_p = 1.0 r_t \sqrt{\frac{E}{F_{yc}}} = (1.0)(3.003")\sqrt{\frac{29{,}000^{ksi}}{50^{ksi}}} = 72.33"$ *(AASHTO 2010 6.10.8.2.3-4)*

$F_{yr} = \min\left(0.7F_{yc}, F_{yw}\right) \geq 0.5F_{yc}$ *(AASHTO 2010 pg6-145)*

$F_{yr} = (0.7)\left(50^{ksi}\right) = 35^{ksi} > 25ksi$

$L_r = \pi r_t \sqrt{\frac{E}{F_{yr}}} = (\pi)(3.003")\sqrt{\frac{29{,}000^{ksi}}{35^{ksi}}} = 271.6"$ *(AASHTO 2010 6.10.8.2.3-5)*

Since $L_p = 72.33" < L_r = 271.6" <$ L_b=360.0", Elastic LTB must be investigated.

$F_{nc} = F_{cr} \leq R_b R_h F_{yc}$ *(AASHTO 2010 6.10.8.2.3-3)*

$F_{cr} = \frac{C_b R_b \pi^2 E}{(\frac{L_b}{r_t})^2}$ *(AASHTO 2010 6.10.8.2.3-8)*

R_b = 1.0 since web is non-slender

R_h = 1.0 since section is non-hybrid

Compute the Moment Gradient Factor, Cb, for the Positive Flexure Critical Segment:

$C_b = 1.75 - 1.05\left(\frac{f_1}{f_2}\right) + 0.3\left(\frac{f_1}{f_2}\right)^2 \leq 2.3$ *(AASHTO 2010 6.10.8.2.3-7)*

$M_2 = 16{,}640^{k-in} \rightarrow f_2 = \frac{16{,}640^{k-in}}{438.8\ in^3} = 37.92\ ksi$

$M_0 = 0^{k-in} \rightarrow f_0 = 0\ ksi$

$M_{mid} = 12{,}340^{k-in} \rightarrow f_{mid} = \frac{12{,}340^{k-in}}{438.8\ in^3} = 28.12\ ksi$

Since the bending moment diagram is not concave,

$f_1 = 2f_{mid} - f_2 \geq f_0$ *(AASHTO 2010 6.10.8.2.3-11)*

$(2)(28.12) - (37.92^{ksi}) = 18.32\ ksi \geq 0\ ksi$

$C_b = 1.75 - 1.05\left(\frac{18.32}{37.92}\right) + 0.3\left(\frac{18.32}{37.92}\right)^2 = 1.313 \leq 2.3 \rightarrow C_b = 1.313$

$F_{cr} = \frac{(1.313)(1.0)\pi^2(29{,}000\ ksi)}{(\frac{360}{3.003})^2} = 26.15\ ksi < 50\ ksi\ max \rightarrow F_{cr} = 26.15\ ksi$

Check Compression Flange Lateral-Torsional Buckling:

Check unbraced length of the beam, **L_b = 15' = 180"**

$$r_t = \frac{b_{fc}}{\sqrt{12\left(1+\frac{1}{3}\frac{D_c t_w}{b_{fc} t_{fc}}\right)}} = \frac{12}{\sqrt{12\left(1+\frac{1}{3}\frac{(20.395")(^7/_{16}")}{(12)(^3/_4")}\right)}} = 3.003"$$ *(AASHTO 2010 6.10.8.2.3-9)*

$$L_p = 1.0 r_t \sqrt{\frac{E}{F_{yc}}} = (1.0)(3.003")\sqrt{\frac{29{,}000^{ksi}}{50^{ksi}}} = 72.33"$$ *(AASHTO 2010 6.10.8.2.3-4)*

$$F_{yr} = \min\left(0.7F_{yc}, F_{yw}\right) \geq 0.5F_{yc}$$ *(AASHTO 2010 pg6-145)*

$$F_{yr} = (0.7)\left(50^{ksi}\right) = 35^{ksi} > 25ksi$$

$$L_r = \pi r_t \sqrt{\frac{E}{F_{yr}}} = (\pi)(3.003")\sqrt{\frac{29{,}000^{ksi}}{35^{ksi}}} = 271.6"$$ *(AASHTO 2010 6.10.8.2.3-5)*

Since $L_p = 72.33" <$ L_b=180.0" $< L_r = 271.6"$, Inelastic LTB must be investigated.

$$F_{nc(LTB)} = C_b[1 - \left(1 - \frac{F_{yr}}{R_h F_{yc}}\right)\left(\frac{L_b - L_p}{L_r - L_p}\right)]R_b R_h F_{yc} \leq R_b R_h F_{yc}$$ *(AASHTO 2010 6.10.8.2.3-2)*

R_b = 1.0 since web is non-slender

R_h = 1.0 since section is non-hybrid

Compute the Moment Gradient Factor, Cb, for the Abutment Segment:

$$C_b = 1.75 - 1.05\left(\frac{f_1}{f_2}\right) + 0.3\left(\frac{f_1}{f_2}\right)^2 \leq 2.3$$ *(AASHTO 2010 6.10.8.2.3-7)*

$$M_2 = 12{,}340^{k-in} \rightarrow f_2 = \frac{12{,}340^{k-in}}{438.8\ in^3} = 28.12\ ksi$$

$$M_0 = 0^{k-in} \rightarrow f_0 = 0\ ksi$$

$$M_{mid} = 7{,}369^{k-in} \rightarrow f_{mid} = \frac{7{,}369^{k-in}}{438.8\ in^3} = 16.79\ ksi$$

Since the bending moment diagram is not concave,

$$f_1 = 2f_{mid} - f_2 \geq f_0$$ *(AASHTO 2010 6.10.8.2.3-11)*

$$(2)\left(16.79^{ksi}\right) - (28.12^{ksi}) = 5.460^{ksi} \geq 0\ ksi$$

$$C_b = 1.75 - 1.05\left(\frac{5.460}{28.12}\right) + 0.3\left(\frac{5.460}{28.12}\right)^2 = 1.557 \leq 2.3 \rightarrow C_b = 1.557$$

Compute the Moment Gradient Factor, Cb, for the Mid-span Segment:

$$M_2 = 16{,}640^{k-in} \rightarrow f_2 = \frac{16{,}640^{k-in}}{438.8\ in^3} = 37.92\ ksi$$

$$M_0 = 12{,}340^{k-in} \rightarrow f_0 = \frac{12{,}340^{k-in}}{438.8\ in^3} = 28.12\ ksi$$

$$M_{mid} = 15{,}430^{k-in} \rightarrow f_{mid} = \frac{15{,}430^{k-in}}{438.8\ in^3} = 35.16\ ksi$$

Since the bending moment diagram is not concave,

$f_1 = 2f_{mid} - f_2 \geq f_0$ *(AASHTO 2010 6.10.8.2.3-11)*

$(2)\left(35.16^{ksi}\right) - (37.92^{ksi}) = 32.41^{ksi} \geq f_0 = 28.12 \rightarrow f_1 = 32.41\ ksi$

$C_b = 1.75 - 1.05\left(\frac{32.41}{37.92}\right) + 0.3\left(\frac{32.41}{37.92}\right)^2 = 1.072 \leq 2.3 \rightarrow C_b = 1.557$ Controls

$$F_{nc(LTB)} = 1.557\left[1 - \left(1 - \frac{35^{ksi}}{(1.00)(50^{ksi})}\right)\left(\frac{180.0" - 72.33"}{271.56" - 72.33"}\right)\right](1.0)(1.0)\left(50^{ksi}\right) \leq (1.0)(1.0)\left(50^{ksi}\right)$$

$F_{nc(LTB)} = 65.23\ ksi \leq 50\ ksi\ max \rightarrow F_{nc(LTB)} = 50\ ksi$

The governing strength for the compression flange is the smaller of $F_{nc(FLB)}\ and\ F_{nc(LTB)}$:

For **L_b = 45'**, $F_{nc(LTB)} = 8.85^{ksi} < F_{nc(FLB)} = 50^{ksi}$, LTB governs the strength of the compression flange.

$F_{nc} = F_{nc(LTB)} = 8.85\ ksi$

$\Phi F_{nc} = (1.0)(8.85) = 8.85\ ksi$ *(AASHTO 2010 6.10.8.1.1-1)*

For **L_b = 30'**, $F_{nc(LTB)} = 26.15^{ksi} < F_{nc(FLB)} = 50^{ksi}$, LTB governs the strength of the compression flange.

$F_{nc} = F_{nc(LTB)} = 26.15\ ksi$

$\Phi F_{nc} = (1.0)(26.15) = 26.15\ ksi$ *(AASHTO 2010 6.10.8.1.1-1)*

For **L_b = 15'**, $F_{nc(LTB)} = F_{nc(FLB)} =$
$50\ ksi$, yielding governs the strength of the compression flange.

$F_{nc} = F_{yc} = 50\ ksi$

$\Phi F_{nc} = (1.0)\left(50^{ksi}\right) = 50\ ksi$ *(AASHTO 2010 6.10.8.1.1-1)*

Investigate the Strength of the Tension Flange:

$F_{nt} = R_h F_{yt} = (1.0)\left(\ 50^{ksi}\right) = 50^{ksi}$ *(AASHTO 2010 6.10.8.3-1)*

$\Phi F_{nt} = (1.0)\ \left(\ 50^{ksi}\right) = 50^{ksi}$

Interior Girder Check - Negative Flexure Region

b_{fc} = 16”

t_{fc} = 2.0”

D = 36”

t_w = 0.5”

b_{ft} = 16”

t_{ft} = 1.0”

A = 66 in^2

C_y = 15.27”

I_x = 17,510 in^4

I_y = 1024 in^4

S_{xt} = 737.88 in^3

S_{xc} = 1146 in^3

S_y = 128.1 in^3

r_x = 16.29”

r_y = 3.94”

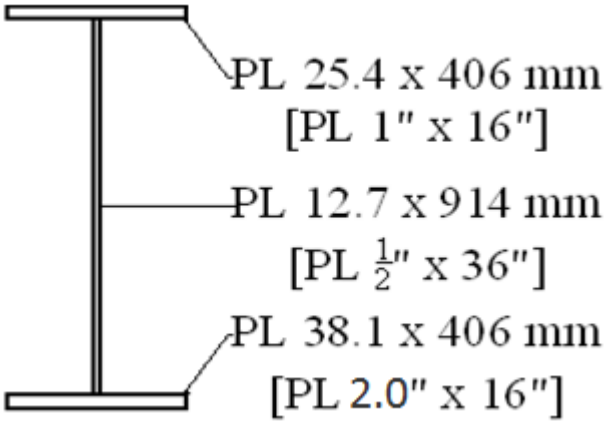

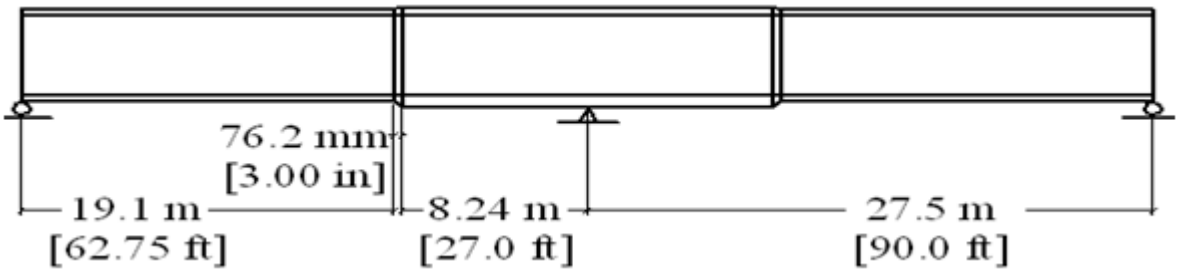

<u>Determine Classification of the Section:</u>

Check $\frac{2D_c}{t_w} \leq 5.7\sqrt{\frac{E}{F_{yc}}}$ *(AASHTO 2010 6.10.6.2.3-1)*

$D_c = C_y - t_{fc} = 15.27 + 2.0" = 13.27"$

Check $\frac{(2)(19")}{1/2"} = 53.08 \leq 5.7\sqrt{\frac{29{,}000\ ksi}{50\ ksi}} = 137.3$ OK, ∴ web is non-slender

Check $\frac{I_{yc}}{I_{yt}} \geq 0.3$

$$I_{yc} = \frac{1}{12}bh^3 + Ad^2$$

$$I_{yc} = \frac{1}{12}(16")(2.0")^3 + (32\ in^2)(14.27")^2 = 6{,}527\ in^4$$

$$I_{yt} = \frac{1}{12}(16")(1.0")^3 + (16\ in^2)(23.23")^2 = 8{,}635\ in^4$$

Check $\frac{I_{yc}}{I_{yt}} = \frac{6{,}527\ in^4}{8{,}635\ in^4} = 0.76 \geq 0.3$ OK

<u>Check Compression Flange Local Buckling:</u>

$$\lambda_f = \frac{b_{fc}}{2t_{fc}} = \frac{16"}{(2)(2.0")} = 4.0$$ *(AASHTO 2010 6.10.8.2.2-3)*

$$\lambda_{pf} = 0.38\sqrt{\frac{E}{F_{yc}}} = 0.38\sqrt{\frac{29{,}000\ ksi}{50\ ksi}} = 9.152$$ *(AASHTO 2010 6.10.8.2.2-4)*

$\lambda_f < \lambda_{pf}$ ∴ compact flange

$$F_{nc} = R_b R_h F_{yc}$$ *(AASHTO 2010 6.10.8.2.2-1)*

R_b = 1.0 since web is non-slender

R_h = 1.0 since section is non-hybrid

$$F_{nc} = R_b R_h F_{yc} = (1.0)(1.0)(50\ ksi) = 50\ ksi$$

<u>Check Compression Flange Lateral-Torsional Buckling:</u>

Check unbraced length of the beam, **L_b = 45' = 540"**

$$r_t = \frac{b_{fc}}{\sqrt{12\left(1+\frac{1}{3}\frac{D_c t_w}{b_{fc} t_{fc}}\right)}} = \frac{16}{\sqrt{12\left(1+\frac{1}{3}\frac{(13.27")(1/2")}{(16)(2.0")}\right)}} = 4.566"$$ *(AASHTO 2010 6.10.8.2.3-9)*

$$L_p = 1.0 r_t\sqrt{\frac{E}{F_{yc}}} = (1.0)(4.566")\sqrt{\frac{29{,}000^{ksi}}{50^{ksi}}} = 110.0"$$ *(AASHTO 2010 6.10.8.2.3-4)*

$$F_{yr} = \min\left(0.7F_{yc}, F_{yw}\right) \geq 0.5F_{yc}$$ *(AASHTO 2010 pg6-145)*

$$F_{yr} = (0.7)\left(50^{ksi}\right) = 35^{ksi} > 25ksi$$

$$L_r = \pi r_t \sqrt{\frac{E}{F_{yr}}} = (\pi)(4.566")\sqrt{\frac{29{,}000^{ksi}}{35^{ksi}}} = 412.9"$$ *(AASHTO 2010 6.10.8.2.3-5)*

Since $L_p = 110.0" < L_r = 412.9" <$ L_b=540.0", Elastic LTB must be investigated.

$$F_{nc} = F_{cr} \leq R_b R_h F_{yc}$$ *(AASHTO 2010 6.10.8.2.3-3)*

$$F_{cr} = \frac{C_b R_b \pi^2 E}{(\frac{L_b}{r_t})^2}$$ *(AASHTO 2010 6.10.8.2.3-8)*

R_b = 1.0 since web is non-slender

R_h = 1.0 since section is non-hybrid

Compute the Moment Gradient Factor, Cb, for the Positive Flexure Critical Segment:

$$C_b = 1.75 - 1.05\left(\frac{f_1}{f_2}\right) + 0.3\left(\frac{f_1}{f_2}\right)^2 \leq 2.3$$ *(AASHTO 2010 6.10.8.2.3-7)*

$$M_{mid} = -7{,}344^{k-in} \rightarrow f_{mid} = \frac{7{,}344^{k-in}}{1{,}146\ in^3} = 6.41\ ksi$$

$$M_2 = -41{,}700^{k-in} \rightarrow f_2 = \frac{41{,}700^{k-in}}{1{,}146\ in^3} = 36.37\ ksi$$

$$M_0 = 0^{k-in} \rightarrow f_0 = 0\ ksi$$

Since the bending moment diagram is concave,

$$f_1 = f_0 = 0\ ksi$$ *(AASHTO 2010 6.10.8.2.3-10)*

$$C_b = 1.75 - 1.05\left(\frac{0}{36.37}\right) + 0.3\left(\frac{0}{36.37}\right)^2 = 1.75 \leq 2.3 \ \rightarrow C_b = 1.75$$

$$F_{cr} = \frac{(1.75)(1.0)\pi^2(29{,}000\ ksi)}{(\frac{540"}{4.566})^2} = 35.81\ ksi < 50\ ksi\ max \rightarrow F_{cr} = 35.81\ ksi$$

<u>Check Compression Flange Lateral-Torsional Buckling:</u>

Check unbraced length of the beam, **L_b = 30' = 360"**

$$r_t = \frac{b_{fc}}{\sqrt{12\left(1+\frac{1}{3}\frac{D_c t_w}{b_{fc} t_{fc}}\right)}} = \frac{16}{\sqrt{12\left(1+\frac{1}{3}\frac{(13.27")(1/2")}{(16)(2.0")}\right)}} = 4.566"$$ *(AASHTO 2010 6.10.8.2.3-9)*

$$L_p = 1.0 r_t \sqrt{\frac{E}{F_{yc}}} = (1.0)(4.566")\sqrt{\frac{29{,}000^{ksi}}{50^{ksi}}} = 110.0"$$ *(AASHTO 2010 6.10.8.2.3-4)*

$$F_{yr} = \min\left(0.7F_{yc}, F_{yw}\right) \geq 0.5F_{yc}$$ *(AASHTO 2010 pg6-145)*

$$F_{yr} = (0.7)\left(50^{ksi}\right) = 35^{ksi} > 25ksi$$

$$L_r = \pi r_t \sqrt{\frac{E}{F_{yr}}} = (\pi)(4.566")\sqrt{\frac{29{,}000^{ksi}}{35^{ksi}}} = 412.9"$$ *(AASHTO 2010 6.10.8.2.3-5)*

Since $L_p = 110.0" < L_b = 360.0" <$ L_b=412.9", Inelastic LTB must be investigated.

$$F_{nc(LTB)} = C_b[1 - \left(1 - \frac{F_{yr}}{R_h F_{yc}}\right)\left(\frac{L_b - L_p}{L_r - L_p}\right)]R_b R_h F_{yc} \leq R_b R_h F_{yc}$$ *(AASHTO 2010 6.10.8.2.3-2)*

R_b = 1.0 since web is non-slender

R_h = 1.0 since section is non-hybrid

Compute the Moment Gradient Factor, Cb, for the Negative Flexure Critical Segment:

$$C_b = 1.75 - 1.05\left(\frac{f_1}{f_2}\right) + 0.3\left(\frac{f_1}{f_2}\right)^2 \leq 2.3$$ *(AASHTO 2010 6.10.8.2.3-7)*

$$M_2 = -41{,}700^{k-in} \rightarrow f_2 = \frac{41{,}700^{k-in}}{1{,}146\ in^3} = 36.37\ ksi$$

$$M_0 = 0^{k-in} \rightarrow f_0 = 0\ ksi$$

$$M_{mid} = -15{,}600^{k-in} \rightarrow f_{mid} = \frac{15{,}600^{k-in}}{1{,}146\ in^3} = 13.61\ ksi$$

Since the bending moment diagram is concave,

$$f_1 = f_0 = 0\ ksi$$ *(AASHTO 2010 6.10.8.2.3-10)*

$$C_b = 1.75 - 1.05\left(\frac{0}{36.37}\right) + 0.3\left(\frac{0}{36.37}\right)^2 = 1.75 \leq 2.3 \rightarrow C_b = 1.75$$

$$F_{nc(LTB)} = 1.75\left[1 - \left(1 - \frac{35^{ksi}}{(1.00)(50^{ksi})}\right)\left(\frac{360.0" - 110.0"}{412.9" - 110.0"}\right)\right](1.0)(1.0)\left(50^{ksi}\right) \leq (1.0)(1.0)\left(50^{ksi}\right)$$

$$F_{nc(LTB)} = 65.83\ ksi \leq 50\ ksi\ max \rightarrow F_{nc(LTB)} = 50\ ksi$$

Check Compression Flange Lateral-Torsional Buckling:

Check unbraced length of the beam, **L_b = 15' = 180"**

$$r_t = \frac{b_{fc}}{\sqrt{12\left(1+\frac{1}{3}\frac{D_c t_w}{b_{fc} t_{fc}}\right)}} = \frac{16}{\sqrt{12\left(1+\frac{1}{3}\frac{(13.27")(1/2")}{(16)(2.0")}\right)}} = 4.566"$$ *(AASHTO 2010 6.10.8.2.3-9)*

$$L_p = 1.0 r_t \sqrt{\frac{E}{F_{yc}}} = (1.0)(4.566")\sqrt{\frac{29{,}000^{ksi}}{50^{ksi}}} = 110.0"$$ *(AASHTO 2010 6.10.8.2.3-4)*

$$F_{yr} = \min\left(0.7F_{yc}, F_{yw}\right) \geq 0.5F_{yc}$$ *(AASHTO 2010 pg6-145)*

$$F_{yr} = (0.7)\left(50^{ksi}\right) = 35^{ksi} > 25ksi$$

$$L_r = \pi r_t \sqrt{\frac{E}{F_{yr}}} = (\pi)(4.566")\sqrt{\frac{29{,}000^{ksi}}{35^{ksi}}} = 412.9"$$ *(AASHTO 2010 6.10.8.2.3-5)*

Since $L_p = 110.0" < L_b = 180.0" <$ L_b=412.9", Inelastic LTB must be investigated.

$$F_{nc(LTB)} = C_b[1 - \left(1 - \frac{F_{yr}}{R_h F_{yc}}\right)\left(\frac{L_b - L_p}{L_r - L_p}\right)]R_b R_h F_{yc} \leq R_b R_h F_{yc}$$ *(AASHTO 2010 6.10.8.2.3-2)*

R_b = 1.0 since web is non-slender

R_h = 1.0 since section is non-hybrid

Compute the Moment Gradient Factor, Cb, for the Transition Region Segment:

$$C_b = 1.75 - 1.05\left(\frac{f_1}{f_2}\right) + 0.3\left(\frac{f_1}{f_2}\right)^2 \leq 2.3$$ *(AASHTO 2010 6.10.8.2.3-7)*

$$M_2 = -15{,}600^{k-in} \rightarrow f_2 = \frac{15{,}600^{k-in}}{1{,}146\ in^3} = 13.61\ ksi$$

$$M_0 = 0^{k-in} \rightarrow f_0 = 0\ ksi$$

$$M_{mid} = -7{,}344^{k-in} \rightarrow f_{mid} = \frac{7{,}344^{k-in}}{1{,}146\ in^3} = 6.41\ ksi$$

Since the bending moment diagram is concave,

$f_1 = f_0 = 0\ ksi$ *(AASHTO 2010 6.10.8.2.3-10)*

$$C_b = 1.75 - 1.05\left(\frac{0}{13.61}\right) + 0.3\left(\frac{0}{13.61}\right)^2 = 1.75 \leq 2.3 \ \rightarrow C_b = 1.75$$

Compute the Moment Gradient Factor, Cb, for Center Pier Segment:

$$M_2 = -41{,}700^{k-in} \rightarrow f_2 = \frac{41{,}700^{k-in}}{1{,}146\ in^3} = 36.37\ ksi$$

$$M_0 = -15{,}600^{k-in} \rightarrow f_0 = \frac{15{,}600^{k-in}}{1{,}146\ in^3} = 13.61\ ksi$$

$$M_{mid} = -27{,}680^{k-in} \rightarrow f_{mid} = \frac{27{,}680^{k-in}}{1{,}146\ in^3} = 24.14\ ksi$$

Since the bending moment diagram is concave,

$f_1 = f_0 = 13.61\ ksi$ *(AASHTO 2010 6.10.8.2.3-10)*

$$C_b = 1.75 - 1.05\left(\frac{13.61}{36.37}\right) + 0.3\left(\frac{13.61}{36.37}\right)^2 = 1.40 \leq 2.3 \ \rightarrow C_b = 1.75 \text{ Controls}$$

$$F_{nc(LTB)} = 1.75\left[1 - \left(1 - \frac{35^{ksi}}{(1.00)(50^{ksi})}\right)\left(\frac{180.0" - 110.0"}{412.9" - 110.0"}\right)\right](1.0)(1.0)\left(50^{ksi}\right) \leq (1.0)(1.0)\left(50^{ksi}\right)$$

$F_{nc(LTB)} = 81.43\ ksi \leq 50\ ksi\ max \rightarrow F_{nc(LTB)} = 50\ ksi$

The governing strength for the compression flange is the smaller of $F_{nc(FLB)}\ and\ F_{nc(LTB)}$:

For **L_b = 45'**, $F_{nc(LTB)} = 35.81^{ksi} < F_{nc(FLB)} = 50^{ksi}$, LTB governs the strength of the compression flange.

$F_{nc} = F_{nc(LTB)} = 35.81\ ksi$

$\Phi F_{nc} = (1.0)(35.81) = 35.81\ ksi$ *(AASHTO 2010 6.10.8.1.1-1)*

For **L_b = 30'**, $F_{nc(LTB)} = 50^{ksi} < F_{nc(FLB)} = 50^{ksi}$, yielding governs the strength of the compression flange.

$F_{nc} = F_{yc} = 50\ ksi$

$\Phi F_{nc} = (1.0)(50) = 50\ ksi$ *(AASHTO 2010 6.10.8.1.1-1)*

For **L_b = 15'**, $F_{nc(LTB)} = F_{nc(FLB)} = 50\ ksi$, yielding governs the strength of the compression flange.

$F_{nc} = F_{yc} = 50\ ksi$

$\Phi F_{nc} = (1.0)\left(50^{ksi}\right) = 50\ ksi$ *(AASHTO 2010 6.10.8.1.1-1)*

Investigate the Strength of the Tension Flange:

$F_{nt} = R_h F_{yt} = (1.0)\left(50^{ksi}\right) = 50^{ksi}$ *(AASHTO 2010 6.10.8.3-1)*

$\Phi F_{nt} = (1.00)\left(50^{ksi}\right) = 50^{ksi}$

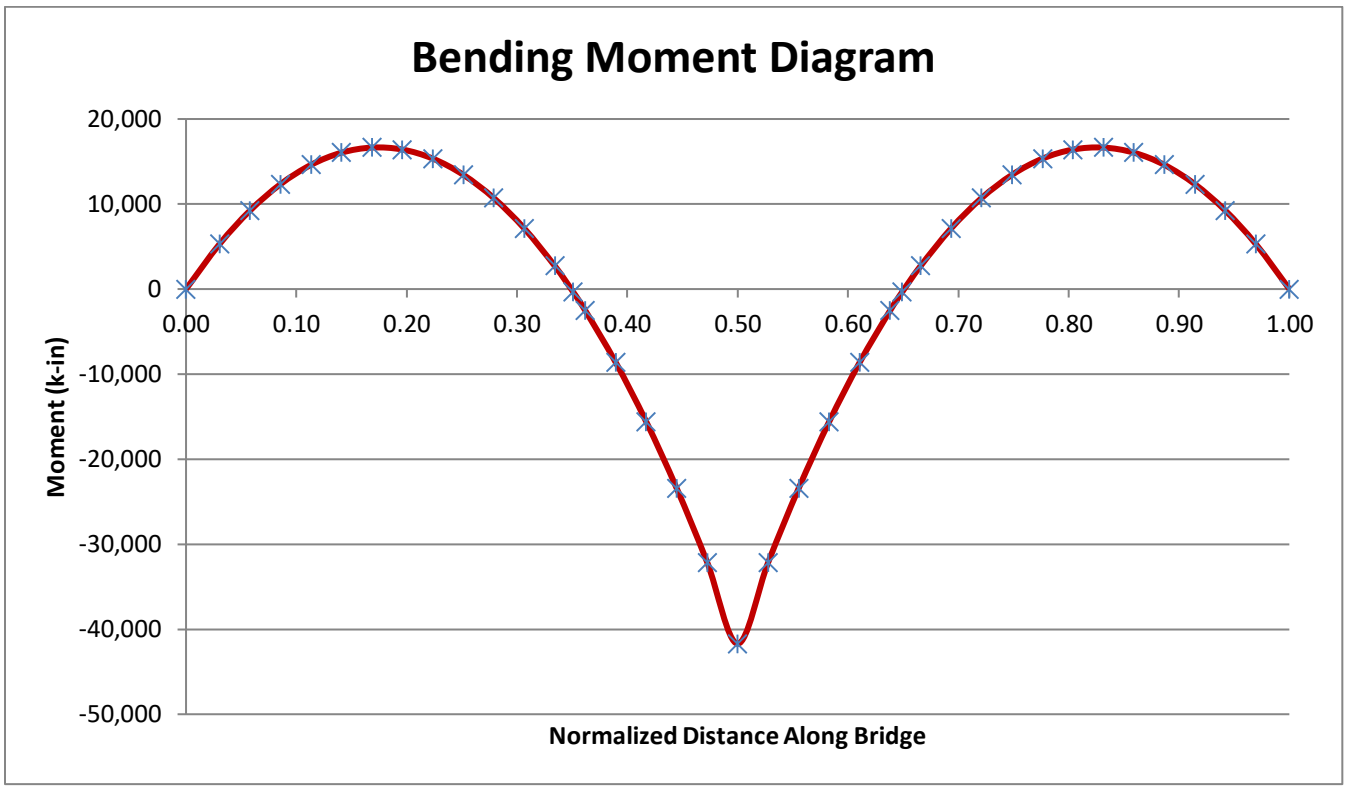
Bending Moment Diagram
20,000
10,000
0
-10,000
-20,000
-30,000
-40,000
-50,000
0.00
0.10
0.20
0.30
0.40
0.50
0.60
0.70
0.80
0.90
1.00
Moment (k-in)
Normalized Distance Along Bridge

Bending Moment & Stress

Normalized Position	Position (in.)	M_z (k-in)	σ_z (ksi)	
0.00	0	0.00	0.00	
0.03	66	5295.5	9.41	
0.06	126	9233.4	16.40	
0.09	186	12337	21.91	
0.11	246	14606	25.94	
0.14	306	16040	28.49	
0.17	366	16640	29.56	
0.20	426	16405	29.14	
0.22	486	15336	27.24	
0.25	546	13432	23.86	
0.28	606	10694	18.99	
0.31	666	7121.6	12.65	
0.33	726	2714.4	4.82	
0.35	762	-330.48	-0.59	← Transition Point
`0.36	786	-2529.8	-4.49	
0.39	846	-8633.8	-15.34	
0.42	906	-15603	-27.71	
0.44	966	-23438	-41.63	
0.47	1026	-32139	-57.09	
0.50	1086	-41704	-74.07	
0.53	1146	-32139	-57.09	
0.56	1206	-23438	-41.63	
0.58	1266	-15603	-27.71	
0.61	1326	-8633.8	-15.34	
0.64	1386	-2529.8	-4.49	
0.65	1410	-330.48	-0.59	← Transition Point
0.67	1446	2714.4	4.82	
0.69	1506	7121.6	12.65	
0.72	1566	10694	18.99	
0.75	1626	13432	23.86	
0.78	1686	15336	27.24	
0.80	1746	16405	29.14	
0.83	1806	16640	29.56	
0.86	1866	16040	28.49	
0.89	1926	14606	25.94	
0.91	1986	12337	21.91	
0.94	2046	9233.4	16.40	
0.97	2106	5295.5	9.41	
1.00	2172	0.00	0.00	